KETOGENIC DIET AND KETONE ESTER SUPPLEMENTATION AS AN ACUTE THERAPEUTIC FOR SPINAL CORD INJURY

by

Kathleen Liisa Kolehmainen

B.Sc., University of Victoria, 2013

A THESIS SUBMITTED IN PARTIAL FULLFILLMENT OF THE REQUIREMENTS OF THE DEGREE OF

DOCTOR OF PHILOSOPHY

in

The Faculty of Graduate and Postdoctoral Studies

(Biochemistry and Molecular Biology)

THE UNIVERSITY OF BRITISH COLUMBIA
(Vancouver)

August 2020

The following individuals certify that they have read, and recommend to the Faculty of Graduate and Postdoctoral Studies for acceptance, the dissertation entitled:

Ketogenic diet and ketone ester supplementation as an acute therapeutic for spinal cord injury

submitted by Kathleen Kolehmainen in partial fulfillment of the requirements for the degree of Doctor of Philosophy

in Biochemistry and Molecular Biology

Examining Committee:

Wolfram Tetzlaff, Zoology
Co-supervisor

Leonard Foster, Biochemistry and Molecular Biology
Co-supervisor

Roger Brownsey, Biochemistry and Molecular Biology
University Examiner

Gerald Krystal, Pathology and Laboratory Medicine
University Examiner

Additional Supervisory Committee Members:

Blair Leavitt, Medical Genetics
Supervisory Committee Member

Robert Boushel, School of Kinesiology
Supervisory Committee Member

Abstract

Spinal cord injury (SCI) is a debilitating condition with no curative treatment. In recent years metabolism has been suggested as a factor that could be altered to enhance recovery after SCI, and research from the Tetzlaff lab showed that a ketogenic diet (KD) can improve recovery after a cervical SCI in rodents. KDs are high fat, low carbohydrate diets that have been successfully used as a treatment for drug-resistant epilepsy in children. KDs produce high levels of the ketone body, beta-hydroxybutyrate (BHB), which can act as an energy source or bind and activate the cell surface receptor, hydroxycarboxylic acid receptor 2 (HCAR2). BHB levels can also be increased by oral ketone ester (KE) supplementation making KE a potential alternative to KD. In Chapter 2, the use of KD on recovery after a cervical forceps crush SCI in mice was assessed. In this injury model KD did not improve recovery of the mice. In Chapter 3, the effect of KD following a more clinically relevant T9 midline contusive SCI was investigated. We observed that KD could reduce pro-inflammatory cytokines CCL3 and CCL4 at 7 days post-injury and a scRNA-sequencing analysis of CD45+ cells at the injury site at 7 days after injury confirmed KD-mediated downregulation of many immune pathways. We also used the T9 contusion injury model with wild type and HCAR2-/- mice to investigate the role of HCAR2 activation on KD-mediated effects. We found that KD could reduce the influx of CD45+CD11b+ myeloid cells into the injury site at 7 days post-injury, which required the HCAR2 receptor. Chapter 4 investigated the use of KE supplementation as a treatment following a C5 hemi-contusive injury in rats. Proteomic analysis at 2 weeks after injury showed that KE and KD appear to impact different cellular pathways. In this model, KE showed only minor improvements in behavioural recovery. Together these results suggest that KD can reduce inflammation at 7 days after injury in mice and that different paradigms of KE supplementation may be needed to see behavioral improvement following SCI in rats.

Lay Summary

Spinal cord injury (SCI) is a traumatic injury with no curative treatment but little research has looked at the impact of diet on recovery. The ketogenic diet (KD) is a high fat, low carbohydrate diet, with sufficient protein. KD produces a measurable increase in beta-hydroxybutyrate (BHB), which can activate a receptor known as HCAR2. After SCI, inflammation at the injury site is detrimental to recovery. KD was previously shown to improve recovery after SCI in rats and could do this by reducing inflammation. After SCI in mice, KD decreased levels of distinct pro-inflammatory cytokines at the injury site. As well, KD reduced specific immune cells and this required the HCAR2 receptor suggesting it may occur through BHB activation of HCAR2. Another method to increase BHB is by ingesting ketone esters (KE), which are broken down into BHB. However, unlike KD, KE did not improve behavioural recovery after SCI in rats.

Preface

All work presented here was approved by the University of British Columbia's Research Ethics Board. The relevant animal care certificates are A14-0350 and A19-0188 (New diet after spinal cord injury) and A18-0015 (Rodent Breeding ICORD Tetzlaff Lab).

I was responsible for writing and assembling this thesis as well as completing all revisions. All animal care was shared responsibility between myself and Dr. Oscar Seira. All surgeries were completed by Dr. Jie Liu except for the C4 DLF crush used in Chapter 2, which was completed by Dr. Seira. Dr. Seira also completed all suturing, while I was responsible for preparing the animals for surgery. I created all images and graphs used in this thesis except Fig 4.7 which was completed entirely by Dr. Seira. I performed all behaviours in Chapter 2. Chapter 4 behaviours were completed jointly between myself and Dr. Seira. Analysis of all behaviours was completed by blinded undergraduate students including but not limited to Ronil Patel, Imara Beattie, and Nima Alaeiilkhchi. I also completed both the proteomics and scRNA-sequencing analyses using modified code provided by Greg Stacey of the Foster Lab and Henry Tung of the Rossi Lab, respectively. The LC/MS/MS experiments and alignment for the proteomics study were completed by Kyung-Mee Moon from the Foster Lab. For the scRNA-sequencing experiment, sorting was completed by Justin Wong at the UBC Flow Core, and library preparation, sequencing, and alignment was completed by the BRC Sequencing Core at UBC.

None of the work presented has been published to date however a manuscript of containing Chapter 4 data is currently being drafted

Table of Contents

List of Tables

List of Figures

List of Abbreviations

Aβ	amyloid beta
AD	Alzheimer's disease
AMPK	5' adenosine monophosphate-activated protein kinase
Arg1	arginase 1
ATP	adenosine triphosphate
BCA	bicinchoninic acid
BHB	beta-hydroxybutyrate
Bl	baseline
BMDM	bone marrow-derived macrophage
bw	body weight
^{o}C	celsius
cAMP	3'5'-cyclic adenosine monophosphate
CCL	C-C Motif Chemokine Ligand
CD	cluster of differentiation
CNS	central nervous system
CoA-SH	coenzyme A
COX2	cyclooxygenase-2 (also known as PTGS2)
CSPG	chondroitin sulfate proteoglycan
CX3CR1	CX3C chemokine receptor 1
DLF	dorsolateral funiculus
DMF	dimethyl fumurate
DNaseI	deoxyribonuclease I
DPI	days post-injury
EAE	experimental allergic encephalomyelitis
EC_{50}	half maximal effective concentration
ECR	eriochrome cyanine R
EDTA	ethylenediaminetetraacetic acid
EGTA	ethylene glycol-bis(2-aminoethylether) – N,N,N'N'-tetraacetic acid
EP2	prostaglandin E2 receptor 2
ERK1/2	extracellular signal-regulated kinases 1 and 2
EODF	every-other-day-fasting
ETS	electron transport system

$FADH_2$	flavin adenine dinucleotide
FBS	fetal bovine serum
Fcgr	Fc gamma receptor
FFA3	free fatty acid receptor 3
FMO	fluorescence minus one
FOXO3a	forkhead box O3
GFAP	glial-fibrillary acidic protein
GO	gene ontology
HCAR2	hydrocarboxylic acid receptor 2 (also known as HCA2)
HDAC	histone deacetylase
hrs	hours
Iba1	ionized calcium binding adaptor molecule 1
IF	immunofluorescence
IFN	interferon
IL	interleukin
iNOS	induced nitric oxide synthase (also known as NOS2)
KD	ketogenic diet
KE	ketone ester (specifically ketone monoester (R)-3-hydroxybutyl (R)-3-hydroxybutyrate)
KEGG	Kyoto encyclopedia of genes and genomes
LC/MS/MS	liquid chromatography tandem mass spectrometry
LPS	lipopolysaccharide
MAG	myelin-associated glycoprotein
MAPK	mitogen-activated protein kinase
MBP	myelin basic protein
MCT	monocarboxylate transporter
MHC-II	major histocompatibility complex Class II
min	minute/minutes
mKi-67	marker of proliferation Ki-67
MMF	monomethyl fumurate
MS	multiple sclerosis
NADH	nicotinamide adenine dinucleotide
NDS	normal donkey serum
NeuN	neuronal nuclear antigen (also known as Fox-3)

NF-κB	nuclear factor kappa-light-chain-enhancer of activated B cells
NK	natural killer
NLRP3	NLR Family Pyrin Domain Containing 3 (also known as NALP3)
NogoA	neurite outgrowth inhibitor
Nrf2	nuclear factor erythroid 2-related factor 2 (also known as NFE2L2)
OMgp	myelin oligodendrocyte glycoprotein
P2ry12	purinergic receptor P2Y12
PAGE	polyacrylamide gel electrophoresis
PBS	phosphate buffered saline
PCA	principal component analysis
PF	paraformaldehyde
PGD_2	prostaglandin D_2
PGE_2	prostaglandin E_2
PI	propidium iodide
PNS	peripheral nervous system
PUMA-G	protein up-regulated in macrophages by IFN-gamma (also known as HCAR2)
RATS	robust automatic threshold selection
RFP	red fluorescent protein
RNA	ribonucleic acid
ROI	region of interest
ROS	reactive oxygen species
rpm	revolutions per minute
SCI	spinal cord injury
SCI-IDS	SCI-induced immune deficiency syndrome
SD	standard diet
SDS	sodium dodecyl sulfate
scRNA	single-cell RNA
siRNA	small interfering RNA
SIRT	sirtuin 1
SOD2	superoxide Dismutase 2
TBI	traumatic brain injury
TBST	tris-buffered saline with Tween-20
TC	tissue culture
Tmem119	transmembrane protein 119

TNFα	tumor necrosis factor alpha
V	volts
WM	white matter
WPI	weeks post-injury
WT	wild type

Acknowledgements

Firstly, I would like to thank my primary supervisor Dr. Wolfram Tetzlaff. He has provided not only a wealth of knowledge, but an amazing lab environment. One of the joys of working in his lab is the opportunity to explore new techniques and ideas, for which I am exceedingly grateful. I also sincerely thank my co-supervisor Dr. Leonard Foster for going above and beyond to provide support throughout my PhD, especially during the extremely stressful process of switching labs. I would also like to thank Dr. Ross MacGillivray for all his support during those stressful months. As well I would like to acknowledge my committee members, Dr. Blair Leavitt, Dr. Robert Boushel, and Dr. Calvin Yip, and thank them very much for all their help and guidance during my graduate studies.

There are so many people in the Tetzlaff lab that I wish I could thank if I had the space. It has been such a wonderful experience to work with so many dedicated and compassionate people. First of all, I am eternally grateful to Dr. Oscar Seira. He has been a pillar of support and knowledge, and every experiment in this thesis is due in some part to his help and expertise. I have thoroughly enjoyed collaborating on this project and cannot thank him enough. I would also like to thank Nicole Janzen, who is the reason for every experiment running smoothly, and who has always been extremely supportive and kind. As well, I thank Dr. Jie Liu for all his surgical help and input, and Dr. Shelly McErlane for her dedication to my animals. I am also extremely appreciative of the non-human members of the Tetzlaff lab: all my mice and rats that I have worked with throughout these years. Despite all the difficult times that are a necessary part of animal experiments, working with these beautiful animals has also been the highlight of my PhD.

I would also like to thank my friends and family. Thank you to my good friends Sai Dharwada and Dr. David Lin, who have been there since the very beginning of my graduate studies. I also could not have made it through this PhD without Dr. Elizabeth Bulaeva, Margarita MacAldaz, and Dr. Davide Pellacani who have been my running buddies and my close friends. I cannot thank enough my brother Matthew Kolehmainen, and mom Bogusława Dobosz, for their constant love and support. As well, I am sincerely grateful to my mom for teaching me that I can do anything and be anything I want. That with hard work, nothing is beyond my reach. Finally, and with all my heart, I would like to thank Colin Hammond. His humour, honesty, love, constant support, cocktail expertise, and R knowledge have, without a doubt, been fundamental to the completion of this PhD. Thank you for celebrating every success and making me smile through every setback.

Dedication

To my mom

Chapter 1. General Introduction

1.1 Introduction and Overview

In this introduction I aim to give a brief overview of the spinal cord and spinal cord injury, paying particular attention to the inflammatory response. Also discussed is an evaluation of the past research into the ketogenic diet, highlighting areas where it could counter some of the secondary deficits of spinal cord injury. As well, I discuss the HCAR2 receptor and its relationship with inflammation. Finally, I will touch upon the use of ketone esters as an alternative to the ketogenic diet. At the end of this Chapter, I outline the hypotheses that follow from the literature and direct the research of Chapters 2, 3, and 4.

1.1.1 The spinal cord

The spinal cord is part of the central nervous system (CNS) and consists of 30 spinal cord nerve segments collected into four regions: cervical, thoracic, lumbar, and sacral. In the human spinal cord, there are 8 cervical spinal nerves (7 cervical vertebrae), 12 thoracic nerves, 5 lumbar nerves, and 5 sacral nerves **(Fig 1.1A)**. The descending spinal nerves of the cervical and lumbar levels rearrange in the so called cervical and lumber plexus to join distinct peripheral nerves that innervate different muscles depending on the region. Cervical nerves carry motor fibres to the muscles of the neck, arms, wrists and fingers, thoracic nerves mediate trunk and abdominal function, while lumbar and sacral nerves control leg and toe function. Ascending nerve fibers have a corresponding regional separation into dermatomes (areas of skin supplied by single spinal nerves) and carry sensory signals – including touch, vibration, pain, temperature and proprioception.

Within the spinal cord, there is white matter and gray matter. The white matter contains axons localized into tracts that convey messages from the brain or brainstem to the periphery (descending tracts) or relay messages from the periphery to the brain/brainstem (ascending tracts) **(Fig 1.1B)**. In addition, many ascending and descending axons connect spinal segments and are confined to the spinal cord (propriospinal). Many axons are covered in a fatty myelin sheath that aids conduction of signals. The gray matter contains multiple neuronal cell types grossly classified as sensory neurons, motor neurons, and interneurons **(Fig 1.1B)**. Within the white and gray matter there are glial cells referred to as oligodendrocytes and astrocytes. Microglia, despite the name glia, are tissue-resident

immune cells that are involved in the surveillance of the CNS microenvironment and protect the CNS from neurotoxic particles such as microbes or dead cell matter. Oligodendrocytes form the myelin sheaths wrapped around axons and aid in the metabolic support of neurons. Astrocytes act to support neurons as well but also have additional roles in CNS immunity. As well, astrocytes become reactive during injury and are a main constituent of the glial scar that forms at the spinal cord lesion epicenter. Additional cells in the CNS include fibroblasts, pericytes, and endothelial cells forming the blood-spinal cord barrier, and epithelial cells which line the central canal of the spinal cord.

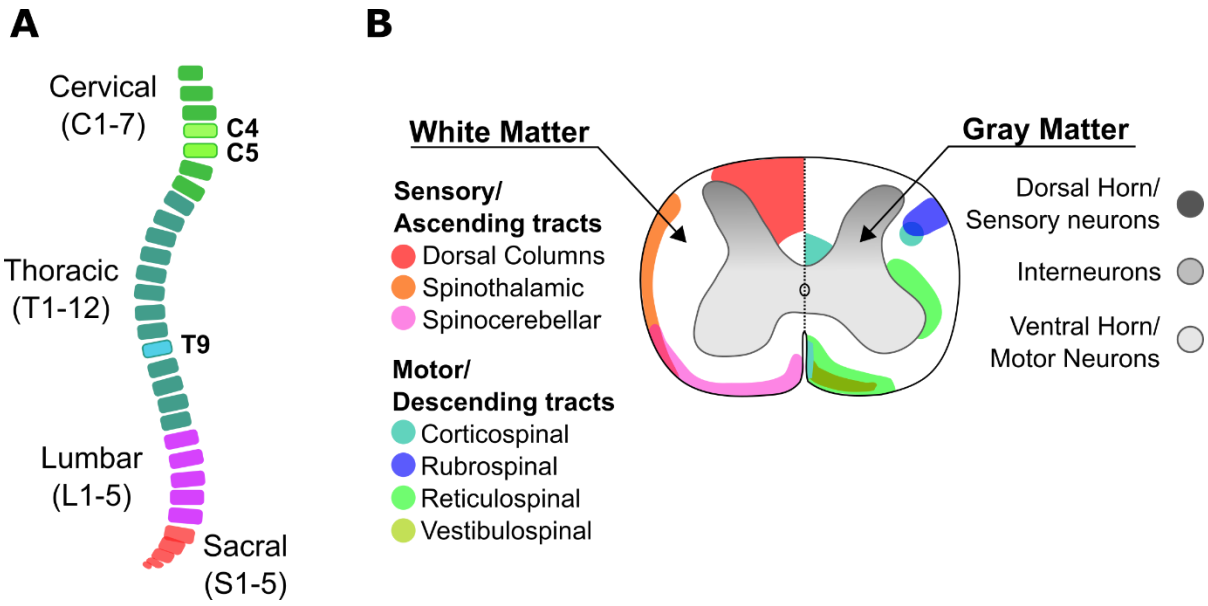

Figure 1.1 Depiction of the spinal cord. **(A)** Representation of spinal cord showing different vertebral segments. C4, C5, and T9 are highlighted as they are injury levels featured in this thesis. **(B)** Cross-section of the rodent spinal cord. The white matter shows sensory (ascending) and motor (descending) tracts on the left and right, respectively. The gray matter is loosely divided into sensory neurons of the dorsal horns, interneurons, and motor neurons of the ventral horns. This image is an adaptation of previously published results on white matter tracts in the rodent spinal cord (Silva et al. 2014; Vogelaar and Estrada 2016)

1.1.2 Spinal Cord Injury

Traumatic spinal cord injury (SCI) is a debilitating injury that affects nearly 1400 people in Canada per year and around 85 000 people in Canada currently live with some type of SCI (Noonan et al. 2012). It is characterized by an initial primary injury followed by a secondary cascade involving further cell death, inflammation, and axonal degeneration. While some spontaneous recovery does occur after injury, it is often limited and the regenerative capacity in the spinal cord remains poor (B.

A. Lee, Leiby, and Marino 2016; Hilton et al. 2016). The best current treatment for enhancing recovery after SCI is rehabilitation paired with electrical stimulation (Behrman, Ardolino, and Harkema 2017; Cho et al. 2019). Early surgical interventions such as decompression have also been shown to have measurable benefit in many pre-clinical and human clinical trials (D. Y. Lee et al. 2018; Fehlings and Perrin 2005). Although research into SCI treatment has been mainly aimed at solving these motor deficits, it's important to note that SCI also leads to multiple systemic problems. Many injuries, even at low lumbar and sacral sections can impact autonomic bowel and bladder movement, and sexual function (Glickman and Kamm 1996; Rabadi and Aston 2015; Benevento and Sipski 2002; Biering-sùrensen and Sùnksen 2001). Many individuals with SCI can also develop mental deficits from a concurrent traumatic brain injury or can develop mental symptoms such as depression and anxiety (Craig et al. 2015; Williams and Murray 2015; Macciocchi et al. 2008). Furthermore, up to 70% of individuals with SCI suffer from chronic pain (Finnerup 2013). Individuals with an SCI at T6 or above can also have a life-threatening syndrome known as autonomic dysreflexia, which is a rapid increase in blood pressure triggered by a stimulus below the level of injury (Lindan et al. 1980; Cragg and Krassioukov 2012). SCI can also increase the risk of a condition known as metabolic syndrome, which is characterized by a variety of symptoms including elevated fasting glucose levels and abdominal obesity (Maruyama et al. 2008; Manns, McCubbin, and Williams 2005). Due to paralysis and mental symptoms such as depression, energy expenditure is significantly diminished after SCI. This leads to disruption in energy balance and widespread metabolic changes (Farkas and Gater 2017; Gorgey et al. 2014). For example, individuals with SCI have increased triglyceride and low-density lipoprotein levels, can develop glucose intolerance or insulin resistance, and may have perturbations in glucose tolerance even with normal glucose fasting levels (Gorgey et al. 2014). Individuals with SCI can also develop immune deficiency, which leads to enhanced infection susceptibility (Brommer et al. 2016; Riegger et al. 2009). Finding a treatment that targets both motor and systemic changes is important for enhancing quality of life after SCI. For this reason, treatments such as diets and exercise, which target multiple systems, are particularly appealing.

1.1.3 Animal models of SCI

In preclinical trials, attempts are made to model the pathology of SCI in humans using rodents and sometimes larger mammals. There are excellent reviews covering the breadth of animal injury models (Hodgetts, Plant, and Harvey 2009); thus, for the purpose of this introduction, I will only describe the injury models that we have employed in our studies. In all these injury models, the injury is delivered under anesthesia and is applied after laminectomy, which is the removal of the back part of the spinal

cord vertebra or lamina. To mimic the blunt trauma seen in most human SCI cases, either contusive or compressive forces can be applied to the spinal cord. In our lab we employ a contusive injury, which is an example of an incomplete injury as white and grey matter is spared at the injury epicenter. The impactor used in contusion can be controlled for force, velocity, or displacement of the impounder and in our case we use the Infinite Horizon impactor (Scheff et al. 2003), which allows us to control the peak force. Most of our injuries employ a mild to moderate contusive force of either 70 kDyn in mice or 120 kDyn in rats. A contusive injury can either be applied midline, that is at the center of the spinal cord, or to just one side, in which case it is called a hemi-contusive injury. Midline contusive injuries can lead to greater behavioural deficits as both sides of the rodent are paralyzed. For this reason, midline contusive injuries are often made at the thoracic level rather than cervical level. For example, a T9 midline contusive injury will significantly impact hindlimb locomotor function (Cao et al. 2005). As well it causes acute impairment in bladder function although partial to full recovery is possible with moderate injuries (B. T. David and Steward 2010). For cervical injuries, a hemi-contusion prevents possible quadriplegia in the rodent and gives an internal control as the injured side can be compared to the non-injured side. In our rat studies we use a C5 hemi-contusion, which produces well-characterized forelimb deficits that can be quantified through tests of skilled and unskilled forelimb usage (Dunham et al. 2010). Another type of injury used in mice is the C4 dorsolateral funiculus (DLF) crush injury, which was previously characterized in the Tetzlaff lab (Hilton et al. 2013). The DLF is a descending pathway that contains both the rubrospinal tract and a small percentage of the corticospinal tract **(Fig 1.1B)**. Injury to the DLF impacts forelimb muscle function (Tie, Sahin, and Sundararajan 2006). A crush injury is another example of an incomplete SCI. Since the customized forceps we use are less than 0.2 mm wide the extent of the lesion is limited and resembles more of a sharp than blunt injury. As well the crush is only applied to one side, limiting impairment to the unilateral forelimb. As with all rodent SCI models, it's important to remember that they are in a controlled environment unlike the traumatic SCI seen in humans, which are highly variable. However, this control has allowed investigation into cellular mechanisms and insight into both the primary and secondary injury processes of SCI.

1.1.4 Response to SCI at the epicenter

The primary injury involves mechanical disruption of neural tissue and blood vessels by the sudden compression of the spinal cord. This is followed by a secondary injury process that includes, hemorrhage, ischemia, production of reactive oxygen species (ROS), metabolic failure, inflammation, widespread cell death, and scarring with variable degrees of cavitation. Inflammation begins very early after injury with production of pro-inflammatory cytokines by microglia and astrocytes (S.

David et al. 2018; Bastien and Lacroix 2014). For example, studies in rodents show that IL-1α, IL-1β, IL-6, and TNFα increase as early as 2 hours after injury. Many of these cytokines have a rapid rise and fall but some, such as IL-1α and IL-1β, remain elevated for at least 24 hours (Stammers, Liu, and Kwon 2012). In rodents, production of ROS is also elevated as early as 4 hours after injury and in response antioxidants such as Catalase and Glutathione are also increased but not until 24 hours post-injury (Azbill et al. 1997). Deficits in mitochondrial metabolic activity are also seen starting 1 hour after injury (Azbill et al. 1997). In the following days, additional inflammatory cells are recruited including neutrophils, macrophages, and T cells. Together, this enhanced inflammatory response, high levels of ROS, accumulation of glutamate and noradrenaline, and perturbations in ATP balance and ionic homeostasis lead to widespread cell death. Over the following days, leakage of the blood-spinal cord barrier continues, and the injury site expands (Dusart & Schwab, 1994). While spontaneous functional recovery does occur, supporting axonal regrowth and sprouting after injury, axons typically do not cross the injury site (Hilton et al. 2016; Kerschensteiner et al. 2005).

What prevents axonal regeneration through the injury site? Contrary to the peripheral nervous system (PNS), poor regeneration is seen in the CNS. This is due to several factors which include both intrinsic differences in the response of severed axons between the PNS and CNS, and the extrinsic generation of an inhibitory environment at the injury site (Filous and Schwab 2018). Lesioned axons in the PNS form growth cones at their tips, however lesioned CNS axons often form swollen, non-regenerative "retraction bulbs" first described by Ramón y Cajal in 1928. Retraction bulbs can occur remarkably early, within just 1 hour after injury, and their formation is driven by microtubule destabilization (Erturk et al. 2007; Kerschensteiner et al. 2005). Further die back of distal axons occurs in a process termed Wallerian degeneration that begins around 12 days after injury in humans (Buss et al. 2004). Although the term Wallerian degeneration was initially coined for the PNS a similar process can occur in the CNS albeit with less efficiency. In the PNS, myelin-producing Schwann cells and recruited macrophages can effectively clear the myelin debris allowing for regeneration of axons (Stoll et al. 1989; Vargas and Barres 2007). However, in the CNS, oligodendrocytes are not adept at fully clearing myelin debris (Stoll et al. 1989), which is one reason for the generation of the inhibitory extracellular environment. CNS myelin proteins such as myelin-associated glycoprotein (MAG), myelin oligodendrocyte glycoprotein (OMgp), and neurite outgrowth inhibitor (NogoA) have all been shown to inhibit neurite growth (McKerracher et al. 1994; Kottis et al. 2002; Chen et al. 2000; K. C. Wang et al. 2002). Furthermore, in humans with inflammatory CNS disorders, autoantibodies are generated against OMgp, and have been shown to be pathogenic in subsequent animal tests (Peschl et al. 2017; Spadaro et al. 2018). Extracellular matrix proteins that

form the glial scar can also limit axonal regeneration (An et al. 1997). In particular, chondroitin sulfate proteoglycans (CSPGs) are highly upregulated after injury and can inhibit axonal growth (Jones et al. 2002; Snow et al. 1990; Cregg et al. 2014). Together, these factors prevent successful regeneration and wound healing at the injury site. Another factor exacerbating secondary damage and enhancing axonal growth inhibition is the persistent inflammatory response that is generated after SCI.

1.2 Inflammation after spinal cord injury

1.2.1 Time course of inflammation after SCI

Following SCI, inflammatory pathways are quickly activated by resident immune cells such as microglia and astrocytes and promote subsequent infiltration of the lesion site by neutrophils, macrophages, T cells, and B cells. Studies in rodents and humans have established a possible timeline for these different immune cell types, which is outlined in **Fig 1.2**.

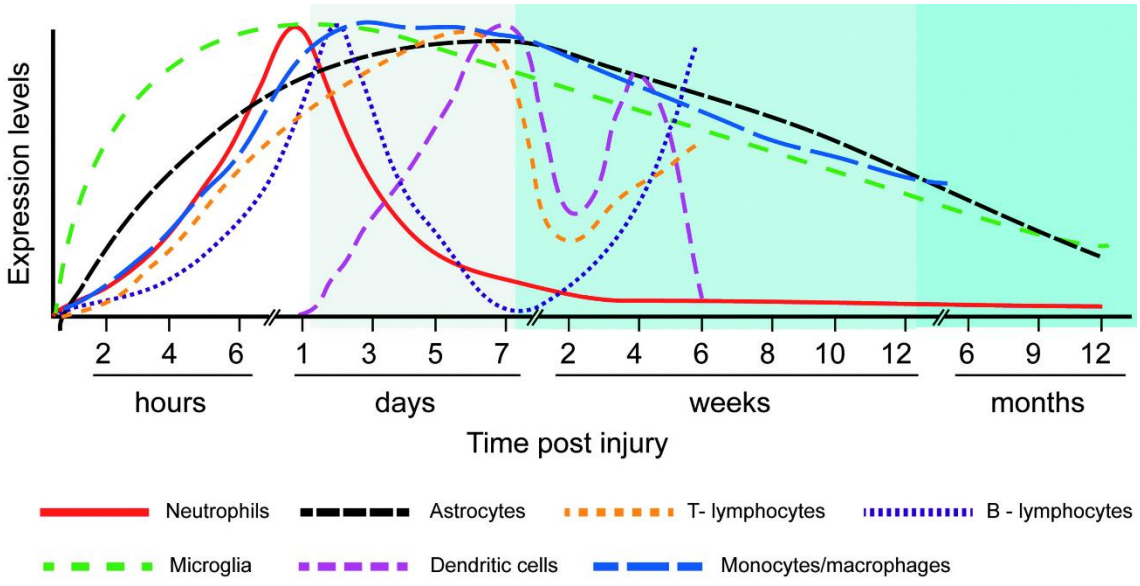

Figure 1.2 Timeline of immune cell infiltration following spinal cord injury reproduced from Bowes & Yip, 2014.

Microglia and astrocytes are the first cells to be activated within the initial hours following injury, leading to production of pro-inflammatory cytokines and recruitment of additional immune cells (Pineau et al. 2010; Pineau and Lacroix 2007). In both humans and rats, neutrophils accumulate

within the blood vessels as early as 3-4 hours after injury and significant infiltration is seen by 12 hours in rats and 24 hours in humans (Beck et al. 2010; Dusart and Schwab 1994; Fleming et al. 2006). Macrophages infiltrate the injury site around 2 days in rats and 5 days in humans, and timeline studies in rats suggest a peak of 7 days post-injury (Dusart and Schwab 1994; Beck et al. 2010; Fleming et al. 2006; Kwiecien et al. 2020). T cells subsequently enter the injury site by around 6 days and peak by 9 days post-injury in rats (Beck et al. 2010). B cell infiltration follows, beginning around 2 weeks post-injury. SCI also triggers extensive B cell proliferation in the spleen with numbers nearly doubling by 2 weeks (Ankeny et al. 2006). Furthermore, circulating antibody levels increase during the first 1 to 2 weeks after injury and remain elevated up to 6 weeks post-injury. These antibodies are autoreactive for CNS components such as myelin basic protein (MBP) and glial-fibrillary acidic protein (GFAP), and can trigger microglial/macrophage activation, glial reactivity, and neuron loss (Ankeny et al. 2006; Arevalo-martin et al. 2018).

All immune cell types can persist in the injury site and even increase in numbers during chronic stages. For example, studies in rats show that despite an initial decline in numbers, neutrophil levels are elevated again by 4 weeks and show a steady increase up to 180 days or about 25 weeks post-injury (Beck et al. 2010). Studies in humans also suggest that infiltration of neutrophils persists for weeks but is fully cleared from the lesion site by around 7 months, although neutrophils are still present in spinal blood vessels (Fleming et al. 2006). In rats, activated microglia/macrophages appear to be cleared from the injury site by 2 weeks, but then re-infiltrate shortly after and peak again at 60 days or around 9 weeks after injury (Beck et al. 2010). Furthermore substantial numbers of activated microglia/macrophages remain in the injury site up to 180 days after injury (Beck et al. 2010). T cells also persist at the injury site with a striking, almost linear increase in numbers during chronic stages of recovery in rats (Beck et al. 2010). In brief, these studies support a timeline of early microglia and astrocyte activation followed by neutrophil then macrophage infiltration. Subsequently T cells enter the injury site followed by B cells. As microglia and macrophages can have both pro- and anti-inflammatory responses after SCI (Kigerl et al. 2009), we were interested in studying these particular cell types further.

1.2.2 Microglia/macrophages after SCI

Activated microglia and macrophages have been suggested to cause cavitation, reduce neuronal survival, and induce production of proteoglycans by astrocytes, which can inhibit axonal regrowth through the injury site (Fitch et al. 1999). However, previous studies were limited in their ability to differentiate between activated microglia and infiltrating macrophages due to the nearly identical

phenotype once activated. Several markers specific to microglia have been identified, however many are downregulated during activation (Bennett et al. 2016). One that appears to remain highly expressed is Transmembrane protein 119 (Tmem119), which was found to distinguish resident microglia from infiltrating macrophages even during models of CNS injury (Bennett et al. 2016). Another method is the use of a tamoxifen inducible Cre reporter mouse line that has a red fluorescent protein (RFP) expressed under the CX3CR1 promoter. CX3CR1 is expressed in both microglia and macrophages, however their different turn-over rates allow for differentiation between the two cell types. Macrophages have a rapid turnover rate and lose their RFP expression quickly, while microglia are long-lived and thus will retain RFP expression for much longer. By carefully timing the induction of the reporter and CNS injury, activated microglia at the injury site will be RFP positive, while infiltrating macrophages will be RFP negative (O'Koren, Mathew, and Saban 2016). This technique was used to show that microglia proliferate extensively within the first week after injury and can form a neuroprotective layer between the astrocytic scar and the immune cell-filled lesion. Furthermore, boosting proliferation of microglia during the first week could enhance recovery while depleting microglia reduced locomotor recovery (Bellver-Landete et al. 2019). As well, recent transcriptomic analyses have identified *HexB* as a new microglia marker that is not diminished in various neurological disorders (Masuda et al. 2020). Further studies with the newly generated transgenic *Hexb*^{tdtomato} mouse line (Masuda et al. 2020) will likely lead to a better understanding of the microglial response following SCI.

Could microglia be beneficial but macrophages harmful after SCI? Not necessarily. In fact, completely blocking macrophage infiltration into the CNS increases microglial inflammation, enhances myelin loss, and reduces locomotor recovery (Greenhalgh et al. 2018). Furthermore, macrophages can directly suppress inflammatory gene expression in microglia through prostaglandin E2 (PGE_2) signalling via the receptor EP2 on the microglia surface (Greenhalgh et al. 2018). This suggests that both microglia and macrophages may be necessary for recovery after SCI. However, macrophages have different inflammatory states and it is possible that altering the inflammatory profile of these cells could promote healing at the injury site.

Macrophage states were originally viewed in terms of a simplistic M1/M2 paradigm as outlined in **Fig 1.3**. M1 macrophages are activated *in vitro* through LPS and/or IFNγ and are considered pro-inflammatory. M2 macrophages are activated *in vitro* by IL-4 or IL-13 and are considered anti-inflammatory. M1 macrophages, classically identified by high levels of intracellular iNOS, produce pro-inflammatory cytokines, ROS, and are bactericidal. On the other hand, M2 macrophages are

involved in tissue remodeling associated with wound healing and are identified by the expression of proteins such as Arginase 1 (Arg1), IL-10 and CD206 (Y. C. Liu et al. 2014).

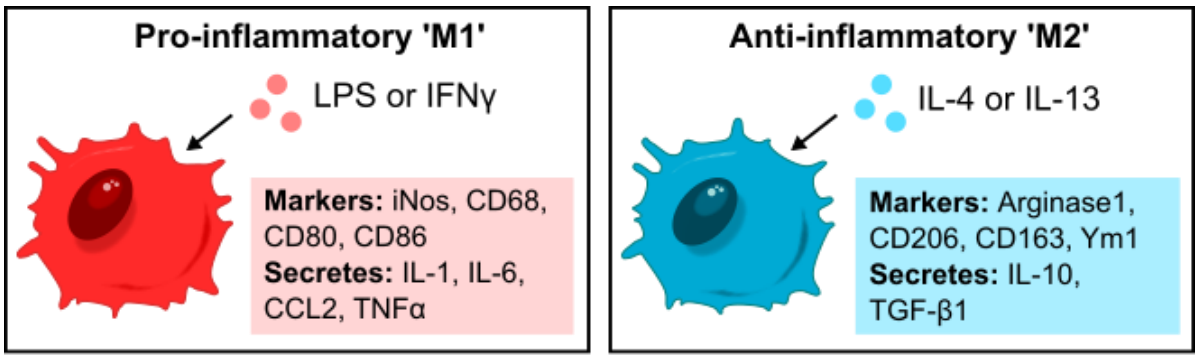

Figure 1.3 M1 and M2 classification showing activating molecules, markers, and cytokines secreted by each subtype. Macrophage illustrations adapted from Krysko, Ravichandran, & Vandenabeele, 2018.

Now it is understood that rather than two states, macrophage activation exists along a spectrum and could be better explained using a function-based phenotypic approach (Mosser and Edwards 2008; Devanney, Stewart, and Gensel 2020). However, until a new classification system is fully developed, M1/M2 classification remains a useful and well characterized definition of macrophage state after injury.

Studies in SCI suggest that activated microglia and/or infiltrating macrophages 1 to 3 days following injury are M1 or M2 in equal numbers. However, by 1 week after injury, M2 markers are largely absent and the M1 phenotype dominates (Kigerl et al. 2009). This suggests that the microglia and macrophages in the injury site during chronic stages could be largely inflammatory and the presence of this M1 state may be partly responsible for the persistent cavitation that is seen after SCI. Indeed, *in vitro* studies show that unlike M1 macrophages, M2 macrophages can enhance axon growth in the context of inhibitory substrates (Kigerl et al. 2009). Furthermore, transplantation of M2 macrophages into the injury site reduced spinal cord lesion volume and pro-inflammatory cytokines IFNγ, IL-6, and TNFα, while increasing anti-inflammatory cytokines IL-10 and IL-13, and improving locomotor function (Ma et al. 2015). Given these promising results, it is possible that a treatment which could promote an increase in M2 macrophages at the injury site could also improve recovery from SCI.

1.2.3 Targeting inflammation for spinal cord recovery

Multiple studies have attempted to improve SCI recovery by reducing inflammation through reduction of pro-inflammatory cytokines, administration of anti-inflammatory cytokines, blocking inflammatory pathways, and depleting immune cells. For example, inhibition of the pro-inflammatory cytokine CCL2 through use of an RNA inhibitory plasmid reduced inflammation and neural cell apoptosis in a rat SCI model (X. Zhang et al. 2015). On the other hand, increasing anti-inflammatory cytokines such as IL-33 in astrocytes reduced inflammation and improved functional recovery after contusive SCI in mice (Pomeshchik et al. 2015). Blocking specific inflammatory pathways has also shown benefits after SCI. For example, inhibition of the p38 mitogen-activated protein kinase (MAPK) pathway in injury-adjacent microglia/macrophages reduced expression of iNOS (indicative of a reduction in M1 macrophages) and enhanced neural survival after spinal cord transection in rats (Xu et al. 2006). Similarly, inhibition of astroglial NF-κB also reduced inflammation, increased axonal sparing, and improved functional recovery following contusive SCI in rats (Brambilla et al. 2005; 2009). Directly targeting immune cells is also a strategy for improving spinal cord recovery. For example, depletion of B cells in mice reduced inflammation and improved motor function after SCI (Casili et al. 2016). Together, these findings show that reducing pro-inflammatory mechanisms can improve recovery after SCI.

1.2.4 Systemic inflammation following SCI

Individuals with SCI are at a higher risk for infectious diseases, particularly septicemia and pneumonia, and immune suppression. This systemic immune dysfunction, also known as SCI-induced immune deficiency syndrome (SCI-IDS), is now understood as a further complication of SCI (Thietje et al. 2011; Brommer et al. 2016; Riegger et al. 2009). As early as 24 hours after injury, circulating lymphocytes (including T cells and B cells), monocytes, and MHC II+ cells are all depleted (Riegger et al. 2009). At 1 week after thoracic contusion in mice, virus-specific CD8 T cell response was also impaired leading to greater susceptibility to infection (Norden, Bethea, and Jiang 2018). Changes in systemic immune function are level dependent as only injuries at or above T4 show such alteration (Campagnolo, Bartlett, and Keller 2000; Brommer et al. 2016). Immune suppression is also long-lasting as reduction in Natural Killer (NK) cells and circulating T cells was seen over 1 year after injury (Herman et al. 2018; Monahan et al. 2015). However, while some immune cells are inhibited, others show elevated levels. For instance granulocyte numbers are nearly doubled by 24 hours (Riegger et al. 2009). Individuals with SCI also show elevated levels of circulating IL-6 and C-reactive protein, a marker of inflammation (Manns, McCubbin, and Williams 2005). As well an activated subset of T cells is also elevated after SCI (Herman et al. 2018; Monahan et al. 2015). It is

not known what causes these changes in systemic immune function, however studies in rodents suggest aberrant nerve signals to the spleen below the level of injury may be responsible (Brommer et al. 2016). While the studies conducted in this thesis do not address systemic immunity, it's important to note that any treatments targeting immune response at the injury site will also need to be studied in context of chronic systemic immunity after SCI.

1.2.5 Comparison of mouse, rat, and human immune systems

While rodents and humans have a similar immune structure, important differences do exist, which must be considered when interpreting rodent SCI results in the context of recovery and treatment of human SCI. For examples, humans have a higher neutrophil/lymphocyte serum ratio than mice (Mestas and Hughes 2004). IFNγ exacerbates multiple sclerosis (MS) in humans but appears protective in the EAE-model of MS in mice (Mestas and Hughes 2004). These differences could influence the immune response after SCI, especially at the injury epicenter. As well, anti-inflammatory strategies in rodents may not work in humans because of these differences in immune response. The immune response also varies between mice and rats. One striking phenotypic difference following SCI is cavitation. In rats, a cystic cavity develops after SCI (similar to the human phenotype) whereas the injury epicenter in mice shows fibrosis, cell infiltration and little cavitation (Sroga et al. 2003). In terms of immune cells at the injury site, T cell infiltration is delayed in mice compared to rats and dendritic cell infiltration appears to be completely absent in mice. Furthermore, infiltration of fibrocytes was only seen in mice but not rats (Sroga et al. 2003). Immune differences between mice and rats have also been investigated in other models of inflammation. For example, administration of high doses of ammonium perfluorooctanoate increased blood neutrophils and monocytes in mice but not rats suggesting a more robust immune response in mice (Loveless et al. 2008). Given that many SCI studies are performed in rodents, these differences should be considered when comparing mice and rat studies. As well they indicate the need for caution when moving from rodent models to the human system.

1.3 Ketogenic diet and its use as a therapeutic in CNS injury

1.3.1 Ketogenic diet and ketone bodies

Ketogenic diet (KD) is a high fat, low carbohydrate diet that was developed by Dr. Russell Morse Wilder at the Mayo Clinic in the 1920s as an alternative to fasting in the treatment of epilepsy (Wilder, 1921). An example of a 3:1 KD is a diet of 75% fat, 20% protein, and 5% carbohydrate by

weight. Fat is broken down in the liver through the process of β-oxidation, which produces molecules of acetyl-CoA. β-oxidation generates energy through production of $FADH_2$ and NADH, which is used to then generate ATP through the electron transport system (ETS). Acetyl-CoA can enter the citric acid cycle, which further produces $FADH_2$ and NADH for ATP production. However, acetyl-CoA can also be used for the generation of ketone bodies through a process known as ketogenesis, which occurs mainly in the liver but can also be carried out by astrocytes in the CNS (Blazquez, Woods, de Ceballos, Carling, & Guzman, 1999; Edmond et al., 1987). There are three ketone bodies produced through ketogenesis: beta-hydroxybutyrate (BHB), acetoacetate, and acetone **(Fig 1.4)**.

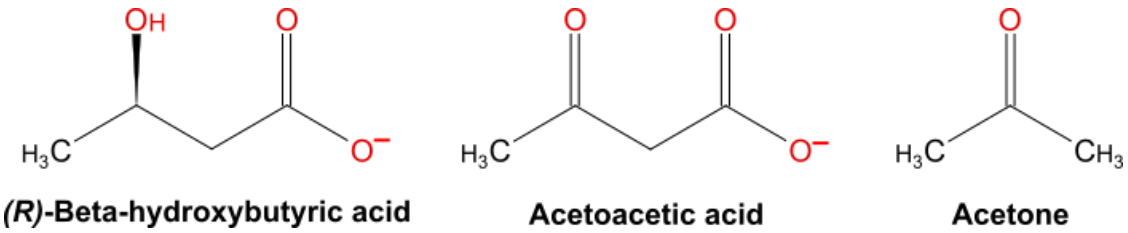

Figure 1.4 The three ketone bodies produced through ketogenesis. The pKa of beta-hydroxybutyrate and acetoacetate are 3.58 and 4.70, respectively. Therefore, they are in their deprotonated forms during blood circulation.

BHB is the most chemically stable, making it the easiest to measure in either blood or urine. BHB (and acetoacetate) can be transported to different tissues through the blood where it's converted back to acetyl-CoA for energy production. Although ketone production primarily occurs in the liver, liver cells do not have the necessary proteins to convert BHB back to acetyl-CoA. This leads to the high circulating levels of BHB seen with starvation or KD. During starvation, glycogen stores are depleted, and fatty acids are released by adipocytes as the body switches from carbohydrate to fatty acid usage. This leads to an increase in fatty acid oxidation in the liver and increased ketone production for extra-hepatic energy (Zauner et al. 2000; Cahill et al. 1966). Due to the high levels of fats and low levels of carbohydrates, KD leads to a similar switch from carbohydrate to fat usage and a measurable increase in circulating BHB levels. These levels can be as high as 5 mmol/L, which is seen in children on a 4:1 KD (Gilbert, Pyzik, and Freeman 2000). This is in comparison to normal circulating levels of BHB which are around 0.2mmol/L (Stubbs et al. 2018). BHB can be circulated to different tissues and enter cells via monocarboxylic acid transporters such as MCT1, MCT2, and MCT4. BHB can also act as an agonist of two receptors: the free fatty acid receptor 3 (FFA3) and the hydroxycarboxylic acid receptor 2 (HCAR2) (Taggart et al. 2005; Won et al. 2013). FFA3, also known as GPR41, can also bind short-chain fatty acids and is expressed by adipocytes (Xiong et al. 2004), pancreatic β-cells

(Veprik et al. 2016), intestinal epithelial cells (M. H. Kim et al. 2013), and sympathetic neurons (Kimura et al. 2011). HCAR2 is expressed in adipocytes (Soga et al. 2003; Tunaru et al. 2003), as well as immune cells such as neutrophils (Kostylina et al. 2008), and monocytes (Knowles et al. 2006) making it a particularly desirable target for studying the mechanism of KD and immune function. As well, the EC_{50} of HCAR2 for BHB is around 0.7mM (Taggart et al. 2005), whereas the EC_{50} for FFA3 is around 2.0mM (Won et al. 2013). In our hands, BHB levels following KD are typically between 1.0-1.5 mM making it likely that the FFA3 receptor is only weakly activated, if at all, under these conditions. As such, we decided to pursue further studies with HCAR2 and this receptor will be discussed in further detail in subsection 1.4.

1.3.2 Use and mechanisms of KD in neurological disorders

KD has been most widely studied in the context of epilepsy. Early studies in epilepsy showed that KD can confer remarkable improvement with at least 30% of KD-fed children becoming seizure-free after treatment and an additional 23% showing significant improvement (Helmholz and Keith 1930). KD is still widely used for clinically refractory epilepsy in children, adults and even infants under 12 months (Mady et al. 2003; Park, Lee, and Lee 2019; Çubukçu, Güzel, and Arslan 2018; Wirrell et al. 2018). In recent years, KD has shown an even greater response rate of around 81% in children with multi drug-resistant epilepsy and the ability to improve cognitive and motor function in conjunction with reduced seizure frequency (Çubukçu, Güzel, and Arslan 2018). Despite its long history of efficacy, the mechanisms behind the anti-epileptic effects of KD are still unclear. The current paradigm is that KD is a multi-targeted approach and can reduce seizures by improving energy levels, mitigating oxidative stress, and reducing inflammation. For example, combination of BHB and acetoacetate can reduce superoxide levels after glutamate exposure in cortical cultures (Maalouf et al. 2007). Furthermore, BHB has been shown to decrease ROS production by increasing NADH and Q/QH_2 oxidation at Complex I (Maalouf et al. 2007; Norwitz, Hu, and Clarke 2019). In rodent hippocampi, KD can also improve mitochondrial numbers and increase proteins involved in mitochondrial biogenesis and uncoupling (Bough et al. 2006; Hasan-olive et al. 2019). BHB has also been shown to improve both redox energy and efficiency of energy usage in the *ex vivo* rat heart (Sato et al. 1995). KD and BHB have also been shown to reduce inflammation. In a mouse model of glaucoma, KD reduced levels of activated Iba1+ microglia, pro-inflammatory markers, and AMPK and NF-κB activation, and increased expression of anti-inflammatory markers (Harun-Or-Rashid and Inman 2018). *In vitro* studies with LPS-primed bone marrow-derived macrophages (BMDMs) from mice, showed that BHB can reduce activation of the NLRP3 inflammasome (Youm et al. 2015). Similar studies with exogenous BHB *in vivo* suggest that it may mediate many of the anti-

inflammatory effects of KD. For example, in a murine diabetes model, BHB administration reduced retinal ER-stress markers, NLRP3 inflammasome activation and pro-inflammatory cytokines IL-1β and IL-18 (Trotta et al. 2019).

KD has also been studied as a treatment for other neurological disorders including Alzheimer's disease (AD), MS, and traumatic brain injury (TBI). KD has been shown to improve motor outcome using a mouse model of AD, although changes were not seen in amyloid-β accumulation, a hallmark of AD (Brownlow et al. 2013; Beckett et al. 2013). However, a separate study using a slightly different mouse AD model was able to show reduction in amyloid deposition although no changes in behavioural outcome were observed (Van der Auwera et al. 2005). In a mouse model of MS, KD was able to reduce inflammatory cytokine and ROS production, reduce hippocampal atrophy, and rescue motor and memory deficits (D. Y. Kim et al. 2012). KD has also shown benefits after TBI in juvenile rats including improvements in brain metabolism, reduction of brain oedema, and better motor function (Z. Hu et al. 2009; Appelberg, Hovda, and Prins 2009; Deng-bryant et al. 2011). Together these results indicate that KD can improve recovery in several rodent models of neurological disorders.

1.3.3 KD as a treatment for SCI

Many of the benefits of KD such as its ability to reduce pro-inflammatory markers and improve mitochondria bioenergetics, suggest that KD is a suitable treatment for SCI. Indeed, previous research in the Tetzlaff lab showed that a 3:1 KD can improve motor function after a C5 hemi-contusive injury in rats (Streijger et al. 2013). KD-fed rats showed improved grooming score and improved usage of the injured paw by 2 weeks post-injury. Importantly, functional improvement was sustained even after switching to a standard diet after 12 weeks. Lesion area was also reduced, and gray matter sparing was increased at 2 weeks post-injury (Streijger et al. 2013). Given these promising results, an important next step will be to further clarify the mechanisms by which KD can improve SCI recovery. Using the same injury model and a 2 week pre-treatment period, KD was shown to reduce ROS production, increase antioxidants catalase and SOD2, and improve acetylation of histone 3 through reduction of histone deacetylases (HDACs) (Kong et al. 2017). As well, KD initiated after a C7 hemi-contusion in rats showed behavioural improvements, reduction of pro-inflammatory cytokines, reduced activation of NF-κB, and increased levels of Nrf2, a regulator of oxidative stress (Lu et al. 2018). Other deficits following SCI may also be treated through KD. For example, transient hyperglycemia is an acute symptom of SCI in humans and improving glycemic control in mice also improved functional outcome (Kobayakawa et al., 2014). Studies in obese mice models show that KD

can indeed improve glucose homeostasis independent of weight loss (Badman, Kennedy, Adams, Pissios, & Maratos-Flier, 2009). Recently a small clinical study also established the safety and feasibility of KD as a treatment for SCI in humans. As well there were promising improvements in motor score although a larger study will be needed to determine efficacy (Yarar-Fisher et al. 2018). As mentioned, KD leads to high levels of circulating BHB which can act as both an energy substrate and signaling molecule. It is tempting to speculate that BHB could be the main compound needed to mediate SCI recovery. In the context of SCI, only one study has looked at use of direct BHB administration. Mice given a T9 contusive injury and continuous BHB administration via subcutaneous pumps showed enhanced histone acetylation, increase levels of the antioxidants FOXO3a, catalase, and SOD2, suppressed NLRP3 inflammasome activation, and reduced levels of pro-inflammatory cytokines IL-1β and IL-18. Furthermore, BHB improved mitochondrial function and locomotor recovery (Qian et al. 2017). Together these studies provide evidence that KD is a feasible treatment for SCI and emphasize the need for further studies on the mechanisms underlying KD, particularly on the role of BHB and its endogenous receptor HCAR2.

1.4 The HCAR2 receptor

1.4.1 Activation of the HCAR2 receptor

HCAR2 (also known as GPR109A, HM74, PUMA-G, and the niacin receptor) is a G_i-protein-coupled receptor that is expressed in multiple tissues and cell types. The highest expression of HCAR2 is found in adipocytes (Tunaru et al. 2003) but it is also expressed by monocytes, neutrophils, Langerhans cells, keratinocytes, and epithelial cells of the retina, intestine, and lungs (Knowles et al. 2006; Kostylina et al. 2008; Trotta et al. 2019; Hanson et al. 2010; F. Liu et al. 2014; Thangaraju et al. 2009). Over the last two decades, multiple agonists of the HCAR2 receptor have been identified including niacin, BHB, butyrate, and monomethyl fumarate (MMF) (Soga et al. 2003; Tunaru et al. 2003; Wise et al. 2003; Taggart et al. 2005; Tang et al. 2008; Thangaraju et al. 2009). The three main agonists that will be discussed, niacin, BHB, and MMF, are shown in **Fig 1.5**, along with the main effects of HCAR2 activation.

A

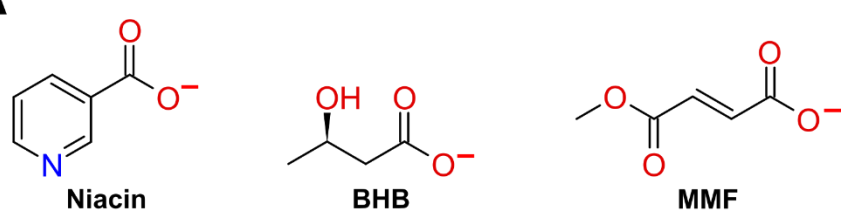

B

	Niacin	BHB	MMF
Metabolic effects:			
Inhibits adipocyte lipolysis	✓	✓	?
Induces subcutaneous flushing	✓	✗	✓
Increases prostaglandin production	✓	?	✓
Increases adiponectin secretion	✓	✓	?
Increases NAD+	?	✓	✓
Anti-inflammatory effects:			
Inhibits neutrophil function	✓	?	✓
Reduces NF-κB activation	✓	✓	✓
Decreases pro-iniflammatory cytokines	✓	?	✓
Inhibits macrophage activation	✓	?	?

Figure 1.5 Key agonists of HCAR2. **(A)** Molecular structure of nicotinate (or niacin), beta-hydroxybutyrate (BHB) and monomethyl fumarate (MMF). **(B)** Metabolic and anti-inflammatory effects mediated by HCAR2. ✓ confirmed with indicated agonist, ✗ does not occur with select agonist, **?** unknown if agonist induces this effect.

Activation of HCAR2 by niacin inhibits adipocyte lipolysis through reduction of intracellular cAMP in adipocytes and can decrease plasma free fatty acid concentrations (Y. Zhang et al. 2005). Niacin-mediated HCAR2 activation also increases COX2-dependent prostaglandin D_2 and E_2 (PGD_2 and PGE_2) production in keratinocytes and skin-resident macrophages known as Langerhans cells. This in turn causes the vasodilation and cutaneous flushing that is seen with niacin treatment (Benyó et al., 2005; Hanson et al., 2010; Maciejewski-Lenoir et al., 2006). Other agonists of HCAR2 have also been shown to have similar effects. For example, MMF can also increase PGD_2 and PGE_2 production via COX-2 in murine keratinocytes (Hanson et al. 2010). To the best of our knowledge, prostaglandin production has not been evaluated with BHB administration, however KD treatment showed no changes in circulating PGE_2 following LPS-induced fever in rats and subcutaneous flushing has not been recorded with BHB or KD (Dupuis et al. 2015). However, like niacin, *in vitro* studies show that

BHB can reduce adipocyte lipolysis through HCAR2 activation (Taggart et al. 2005) supporting the idea that the flushing and anti-lipolytic effects of HCAR2 are separate pathways. Other agonists of HCAR2 have also been designed that are anti-lipolytic yet non-flushing (Richman et al. 2007). *In vitro* studies using HEK-293 cells show that activation of HCAR2 by niacin causes internalization of the receptor and activation of the ERK1/2 signaling pathway (Li et al. 2010). Interestingly agonists of HCAR2 that are non-flushing do not lead to an increase in PGD_2, are not internalized, and do not shown any increase in ERK1/2 phosphorylation (Richman et al. 2007). It is tempting to speculate that BHB activation of HCAR2 may activate similar mechanisms however *in vitro* studies in a murine hypothalamic cell line do show that BHB increases ERK1/2 phosphorylation confusing this interpretation (Fu, Liu, et al. 2015). Clearly more research is needed to determine the outcomes of HCAR2 activation through BHB.

1.4.2 HCAR2-mediated effects on inflammation

Multiple studies have shown that activation of HCAR2, mostly via niacin, is able to reduce inflammation. For example, activation of HCAR2 by niacin accelerates neutrophil apoptosis in a caspase-dependent manner (Kostylina et al. 2008), and can reduce LPS-mediated inflammatory effects in macrophages including expression of pro-inflammatory cytokines IL-6 and IFNβ, NF-κB activation, and macrophage chemotaxis (Zandi-Nejad et al. 2013; Shi et al. 2017; Digby et al. 2010; Subramani et al. 2019). Niacin pre-treatment reduced peritoneal macrophages and liver infiltration of inflammatory cells in a mouse model of sepsis (Shi et al. 2017). The reduction in macrophage numbers and IL-6 levels seen with niacin was subsequently abrogated in HCAR2-/- mice (Shi et al. 2017). Similarly, using a rodent model of hemorrhagic shock, niacin improved survival by reducing inflammatory pathways and improving cellular energetics including ATP levels, NAD+/NADH ratio, and SIRT activity (Subramani et al. 2019). However, survival time was significantly reduced in HCAR2-/- mice pointing to the involvement of this receptor (Subramani et al. 2019). Together these results suggest that activating HCAR2 can reduce inflammation and this could be a mechanism contributing to the effects of KD on inflammation.

1.4.2 Effect of inflammation on HCAR2 expression

As mentioned previously, HCAR2 can mediate the inflammatory response when activated by niacin. Interestingly, HCAR2 expression could itself be regulated by inflammation. Multiple studies have shown that LPS exposure can increase HCAR2 expression (Wanders, Graff, and Judd 2012; Zandi-Nejad et al. 2013; Shi et al. 2017; Feingold et al. 2014). Wanders *et al.* further demonstrated that macrophages exposed to conditioned media from LPS-treated macrophages also increased HCAR2

expression suggesting that secreted factors rather than LPS itself might mediate this upregulation (Wanders, Graff, and Judd 2012). HCAR2 can also be upregulated *in vitro* by IL-6 and IL-1β in macrophages (Shi et al. 2017) and by LPS, TNFα , and IL-1β in adipocytes (Digby et al. 2010; Feingold et al. 2014). Furthermore, HCAR2 expression is also significantly increased in the retina of diabetic mice (Trotta et al. 2019). Endogenous tissue specific BHB levels also increase in instances of inflammation and independently of serum levels. For example, cardiomyocytes accumulate BHB during pressure-induced heart failure without changes in circulating BHB levels (Nagao et al. 2016). It is tempting to speculate that inflammatory signals can trigger a local increase in BHB and HCAR2, which leads to activation of HCAR2 and, in turn, decreases inflammation however further work is needed to understand the changes in BHB expression following inflammation.

1.5 Ketone esters

1.5.1 Ketone esters

One of the issues with KD is that it requires adherence to a non-palatable food regimen rich in fat. As KD leads to high BHB levels, it is possible that supplementation of a normal diet with BHB could show similar benefits. BHB can be given orally as either a ketone salt or ketone ester. A ketone salt consists of BHB bound to a cation such as sodium or calcium, or a positively charged amino acid such as lysine or arginine. However ketone salts only produce a modest increase in circulating levels of BHB (Kephart et al. 2017) and substantially increase salt intake, which in itself is linked to negative health outcomes (de Wardener and MacGregor 2002). For these reasons, using a ketone ester is a preferable method of delivering exogenous BHB. Ketone esters consist of a molecule of BHB bound to a ketone precursor such as butanediol or glycerol through an ester bond. One example is the ketone monoester *(R)*-3-hydroxybutyl *(R)*-3-hydroxybutyrate, which was developed by Dr. Kieran Clarke **(Fig 1.6A)**. This is the ketone ester (hereafter referred to as KE) we chose to use for our studies in SCI as one oral dose could markedly increase circulating BHB levels. As seen in **Fig 1.6B**, oral administration of KE at a dose of 714mg/kg body weight (bw) in humans resulted in an increase in BHB levels to 3.30mM by 1.5-2.5 hours (Clarke, Tchabanenko, Pawlosky, Carter, Todd King, et al. 2012). Repeated administration of KE at 1071 mg/kg bw/day showed only mild gastrointestinal issues in a small number of participants. Furthermore, serum levels of BHB did not exceed 5.5mM, and glucose levels remained between 2.5mM and 22.2mM suggesting that continued dosing with KE is both a safe and effective method to elevate circulating BHB levels (Clarke, Tchabanenko, Pawlosky, Carter, Todd King, et al. 2012). Additionally, administration of KE 3 times daily for 28

days showed no changes to body weight, fasting blood glucose, triglyceride or cholesterol levels, electrolyte concentrations, or kidney function (Soto-Mota et al. 2019).

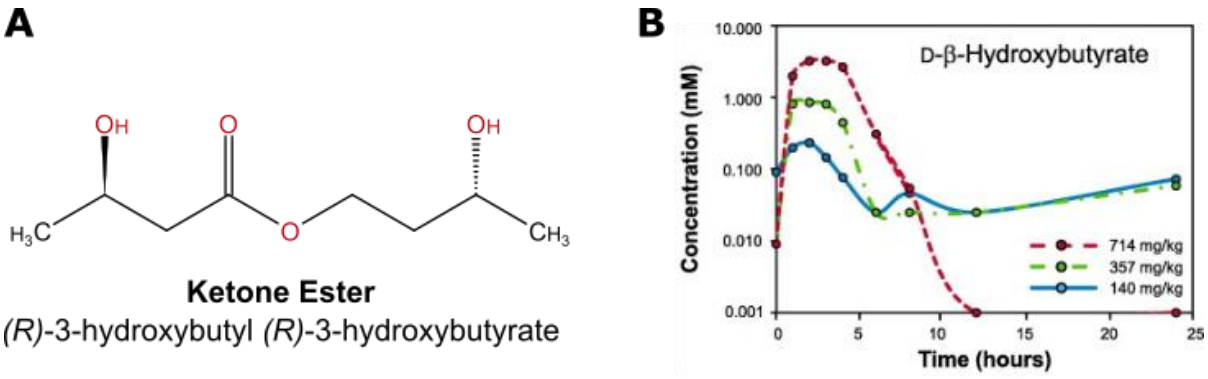

Figure 1.6 Ketone ester. **(A)** Structure of ketone ester (KE) used in study. **(B)** Serum levels of D-β-hydroxybutyrate measured for different concentrations of KE (140, 357, and 714 mg/kg body weight of subject). Figure reproduced from Clarke et al., 2012.

One potential problem with using KE as a treatment is that it has a bitter taste (Stubbs et al. 2017). This is easily remedied for human consumption by adding a sweetener to partially mask the bitter taste, however this does pose a problem for rodent studies where the bitter flavour means voluntary oral consumption can be difficult. One possible solution is the use of oral gavage to administer KE in regular doses. Another is providing KE in the food and masking the bitterness with a sweetener. Oral gavage is more clinically relevant if the KE is to be administered in daily doses, however KE-supplemented food can provide more consistent levels of BHB. Studies in rats show that KE-supplemented food leads to increased circulating ketone levels of around 0.7mM (Kashiwaya et al. 2013). For our studies we decided to administer KE acutely following SCI via oral gavage to circumvent initial problems in eating after SCI surgery in rodents. For longer dosing regimens, KE was then diluted in the daily water with addition of a sweetener.

1.5.2 Effects of KE and use as a treatment

To date, there are no data on KE treatment after SCI, however findings from KE administration under normal conditions show promising results. KE may lower appetite and reduce plasma levels of cholesterol, triglycerides, and glucose suggesting it may help mitigate the risk of metabolic syndrome commonly seen in individuals with SCI (Stubbs et al. 2018; Kashiwaya et al. 2010; Cox et al. 2016). Despite appetite suppression, a prolonged study of ketone administration did not show any weight

changes in humans indicating that excessive weight loss is not a risk (Soto-Mota et al. 2019). In rats, a KE-supplemented diet also increased ATP hydrolysis in the heart and increased cytoplasmic NAD+/NADH in the brain, suggesting it could rescue the energy deficits seen after SCI (Kashiwaya et al. 2010; Cox et al. 2016). Administration of a KE-supplemented diet has also been studied in the context of neurodegenerative diseases such as AD. In a mouse model of AD, KE supplementation improved cognitive performance and reduced Aβ accumulation (Kashiwaya et al. 2013). Given these results, KE appears a promising alternative to KD in treatment of SCI.

1.6 Research Hypotheses and Aims

Stemming from the previous literature, my research had two major objectives: (1) to better understand the mechanisms behind KD treatment of SCI in mice with a focus on its anti-inflammatory effects, and (2) to assess the use of KE as an acute treatment for SCI in rats. These objectives can be broken down into the following 3 hypotheses.

1.6.1 Hypothesis 1

Mice fed KD acutely after a C4 DLF crush injury show reduced markers of injury severity and improved behavioural recovery.

1.6.2 Hypothesis 2

KD can reduce inflammation after SCI in mice through the BHB receptor, HCAR2

1.6.3 Hypothesis 3

KE supplementation can produce similar benefits to KD treatment after SCI in rats

Each chapter will address one of these hypotheses beginning with Chapter 2 where I aim to replicate the previous KD findings in rats following a cervical crush injury in mice.

Chapter 2. KD treatment of mice following a C4 DLF crush injury did not produce long-term behavioural improvements

2.1 Introduction

Despite decades of research, there is still no treatment for spinal cord injury (SCI). This has led to a search for novel methods to stimulate recovery. In particular, the importance of nutrition in recovery has become an important consideration. The ketogenic diet (KD) is a high fat diet with low carbohydrates and sufficient protein levels. A typical KD has a 3:1 ratio of fat to carbohydrates and proteins (by weight). KD leads to high levels of the three ketone bodies: acetone, acetoacetate, and beta-hydroxybutyrate (BHB). KD is known to impact the central nervous system and has been used successfully in treatment of certain types of epilepsy since the 1920s. Multiple mechanisms have been suggested although it is unclear the extent to which these functions are mediated by the ketone bodies, and particularly by activation of the endogenous BHB receptor, HCAR2.

A previous study in the Tetzlaff lab investigated the use of KD as a treatment for SCI. Briefly, Sprague-Dawley rats were fed with KD following a C5 hemi-contusion injury and forelimb recovery was assessed as well as lesion size and grey matter sparing (Streijger et al. 2013). KD improved grooming score, pellet retrieval, and rearing ability suggesting improved forelimb function. As well, KD-fed rats had a reduced lesion area and increased gray matter sparing (Streijger et al. 2013). Together these results show that KD is beneficial following SCI, but the mechanism through which this occurs is unknown.

While there is robust literature on rat SCI models and behavioural tests, there are fewer genetic knockout rat models available. This makes it harder to study the molecular basis of benefits seen with the diet. For this reason, we decided to use a mouse SCI model and the HCAR2-/- mouse line for further studies of the HCAR2 receptor. We chose a C4 dorsolateral funiculus (DLF) crush injury model previously established in the Tetzlaff lab (Hilton et al. 2013) which produces distinct forelimb deficits. This model injures the rubrospinal tract, which descends in the dorsolateral funiculus. In rodents, the rubrospinal tract is involved in the control of skilled movement and locomotion, and plays a significant role in voluntary movement (Kjell and Olson 2016).

Here we assessed the effect of KD on inflammatory parameters at 7 days following a C4 DLF crush. To this end we fixed and sectioned tissue at 7 days post-injury (DPI), then stained for relevant inflammatory markers such as Iba1 for microglia/macrophages, Arg1 for anti-inflammatory M2 macrophages, and phosphorylated p38 MAPK (P-p38) for activation of pro-inflammatory pathways. We also assessed the effect of KD treatment on recovery from the C4 DLF crush injury using several behavioural tests including cylinder rearing, irregular horizontal ladder, and grooming, which were analyzed across 8 weeks starting at 3DPI. Together our results address the effects of KD treatment on inflammation following SCI in mice and assess the use of the C4 DLF crush injury model for further studies in mice.

2.2 Materials and Methods

2.2.1 Mice and diets

All study procedures were completed in accordance with the University of British Columbia Animal Care Committee Protocols #A14-0350 and #A19-0188. For both studies, C57Bl/6 mice were purchased from The Jackson Laboratory (Bar Harbor, Maine, USA) at approximately 8 weeks of age and group-housed on a reverse light-dark cycle. For mice used in the C4 DLF crush study and T9 contusion study, see **Table 2.1**. We lost one mouse from our C4 8WPI cohort due to an accidental injury during routine cage movement that resulted in euthanasia.

Table 2.1 Mice used in Chapter 2 studies. All mice are 8-week-old male C57Bl/6J.

Tissue use	Timepoint	Injury	Diet	N	Mice lost
IF	7DPI	None	SD	4	0
		C4	SD	6	0
		C4	KD	6	0
Behaviour	8WPI	C4	SD	12	0
		C4	KD	12	1

Mice were fed standard chow (Tekland 2020X, Envigo, Indianapolis, Indiana, USA) *ad libitum* until injury. After injury they were either placed on KD (#F5484, Bio-Serv, Flemington, New Jersey USA) or on SD (#F5960, Bio-Serv), which was also supplied *ad libitum* in ceramic bowls within each cage. For diet contents, see **Table 2.2**. Because of the surgery, it is usually about 24-48 hours before the mice are fully eating the new food.

Table 2.2 Composition of SD and KD diets. For calculation of carbohydrates see Streijger et al., 2013

	SD (F5960)	KD (F5848)
Gram % - Macronutrients		
Carbohydrates	**65.4**	**3.0**
Protein	**18.1**	**18.1**
Fat	**5.0**	**65.8**
Gram % - Components		
Casein	20	20
L-methionine	0.3	0.3
Corn Starch	15	0.0
Sucrose	50	0.0
Cellulose	5	5
AIN-76 Mineral Mix	3.5	6.65
Choline Bitartrate	0.2	0.38
AIN-76A Vitamin Mix	1	1.9
Corn Oil	0.72	9.51
Butter	1.26	39.62
Lard	3.02	16.62
Kcal/g		
Carbohydrates	**2.62**	**0.12**
Protein	**0.72**	**0.72**
Fat	**0.45**	**5.92**

2.2.2 C4 DLF crush SCI model

All C4 surgical injuries were performed by Dr. Oscar Seira and follow the surgical procedure outline by Dr. Brett Hilton (Hilton et al. 2013). Briefly, mice were anesthetized using Isoflurane (Fresenius Kabi Canada, Toronto, Ontario, Canada) and the back of the mouse was shaved. Mice received 1mL Lactated-Ringer's solution (Baxter, Deerfield, Illinois, USA) and a single dose of buprenorphine (0.03mg/kg, purchased from McGill University Comparative Medicine Resources). The surgical area was also disinfected with three successive applications of betadine (Bowers Medical Supply, Delta, BC, Canada) then 70% ethanol. A hemilaminectomy was then performed at the C4 spinal cord segment on the left side. Dumont #5 forceps with blades of 200 microns and a 1 mm mark from the tip were inserted into the dorsal horn gray matter such that one blade punctured the spinal cord while the other blade remained outside. They were then closed, and the crush was held for 15 seconds. This was repeated once. The muscles and skin were then sutured, and the mice recovered in a heated incubator before being returned to their home cages. As per protocol, mice received subcutaneous

injections of Lactated-Ringer's solution twice daily and Buprenorphine three times daily for at least 3 days post-surgery.

2.2.3 BHB measurements

Ketone levels were measured from blood obtained by tail prick. Precision Xtra Blood Ketone Test Strips (Diabetes Express, Markham, Ontario, Canada) were used with the Precision Xtra Blood and Ketone Meter (Abbott, Chicago, Illinois, USA) according to manufacturer guidelines.

2.2.4 Immunofluorescent staining

Mice were euthanized by lethal injection of 10% chloral hydrate (MilliporeSigma Canada Co., Oakville, Ontario, Canada) at 7DPI. They were then perfused with ice-cold PBS (NaCl (ThermoFisher Scientific, Waltam, Massachusetts, USA), KCl (MilliporeSigma), Na_2HPO_4 (ThermoFisher Scientific), and KH_2PO_4 (ThermoFisher Scientific) followed by 4% paraformaldehyde (PF; Alfa Aeser, ThermoFisher Scientific). Cervical spinal cords were dissected and placed in 4% PF for at least 24 hours then cryoprotected using 30% sucrose. Subsequently they were cut to 5mm lengthwise (2.5mm each side of injury lesion) and embedded in Tissue Plus® optimal cutting temperature (OCT; VWR, Radnor, Pennsylvania, USA) compound before freezing on dry ice. Embedded cords were then stored at -80ºC until they were cut longitudinally into 20µm sections using a CryoStar™ NX70 cryostat (ThermoFisher Scientific). Cut sections were blocked for 1hr in 10% normal donkey serum (NDS; Jackson ImmunoResearch Laboratories Inc., West Grove, Pennsylvania, USA) then stained overnight with primary antibodies as listed in **Table 2.3**. They were stained the following day with donkey AlexaFluor secondary antibodies (1:500) conjugated to AF594, AF405, AF674, or AF488 (Jackson ImmunoResearch). Images for NeuN, Iba1, and Arg1 analysis were taken with a Zeiss Axio Imager M2 microscope and Fluar 10X/0.50 objective (Carl Zeiss Canada Ltd., Toronto, Ontario, Canada). Images for P-p38 analysis were also taken with the Axio Imager M2 microscope but using a Plan-Neofluar 20X/0.50 Ph2 objective (Carl Zeiss Canada). In all cases, images were captured using an AxioCam HR R3 camera (Carl Zeiss Canada). Images for GFAP analysis were taken with an Axio Observer Z1 microscope using a Plan-Apochromat 20X/0.8 M27 objective. Images were captured with an AxioCam 702 Camera (Carl Zeiss Canada).

Table 2.3 Antibodies used in immunofluorescence (IF) experiments. Novus: Novus Biologicals (Bio-Techne, Oakville, Ontario, Canada). Santa Cruz Biotechnology (Dallas, Texas, USA). CST: Cell Signaling Technology (CST; Danvers, Massachusetts, USA)

Antigen	Host	Dilution	Cat. #	Company
NeuN	Guinea Pig	1:500	ABN90P	MilliporeSigma
GFAP	Chicken	1:500	AB5541	MilliporeSigma
Iba1	Goat	1:500	NB100-1028	Novus
Arg1	Goat	1:500	sc-18351	Santa Cruz Biotechnology
Phospho-P38 MAPK (T180/T182)	Rabbit	1:200	4631	CST

2.2.5 Image analysis

ImageJ v1.52p was used analyze NeuN+ , Arg1, and P-p38 IF. All ImageJ macros can be found in **Appendix A**. For NeuN+ counts, a 0.5 by 1.5mm region of interest (ROI) of the ipsilateral and contralateral sides was selected. Background was then subtracted, and images were manually thresholded. Selected cells were converted to a mask and watershed to separate adjacent cells. Analyze particles was used to count cells. A similar technique was employed to calculate Arg1 area and intensity. However, each image was set to the same threshold (2000-66535) and the mask was also used to create a selection on the original image for intensity analysis. As well, a morphological opening filter and dilation was applied to the mask before watershedding. For P-p38 intensity, background was substracted before all 8-bit images were set to the same threshold (60-210). This threshold was then used to create a selection from which the intensity was measured. Lesion size and Iba1 intensity analyses were completed using Zen 3.1 (blue edition) software (Carl Zeiss Canada). Lesion size was assessed by manually tracing the GFAP reactive lesion border. For Iba1 intensity analysis, ROI of 0.5 by 1mm were selected as indicated in **Fig 2.3A**. The mean fluorescence of each ROI was then quantified. All analyses were performed on images that randomized and renamed for blinding of the researcher using a batch script developed by Jason Faulkner (https://www.howtogeek.com/57661/stupid-geek-tricks-randomly-rename-every-file-in-a-directory/).

2.2.6 Cylinder rearing behavioural test

Mice were accustomed to the plexiglass rearing cylinder for two 15 to 20-minute sessions prior to baseline recordings. For all recordings, mice were filmed for 20 minutes in a lit room without human

presence. Analysis of rearing events was performed by a blinded experimenter and the first 20 spontaneous rearing events were scored. Paw placement was either scored as 'left', 'right', or 'both'. Each or both paws had to be used for weight support during the rear for >0.25 seconds or >7 frames of the video. Additional paw placements were scored as subsequent. When at least one paw returned to the ground, the rearing event was concluded. Percent use of each paw was calculated as a fraction of the total number of paw placements across all 20 grooming sessions.

2.2.7 Horizontal irregular ladder behavioural test

Mice were recorded as they ran across a horizontal ladder with irregular rungs and the number of errors (slip, miss, or drag) that each paw made was counted. Mice were given at least two sessions (one run per mouse) to get acclimatized to the horizontal ladder before baseline recordings were made. At each timepoint, 11 rungs were indiscriminately removed (however never 2 in a row) to provide irregularity. At each time point, the mice were run over the ladder 6 times. During analysis, the run with the most disruptions (e.g. stopping or rearing against the side) was discarded. If no run was deemed a failed attempt, the 6^{th} run was discarded. Errors across the five successful runs were summed to give a cumulative error score.

2.2.8 Grooming behavioural test

Natural grooming during rearing was scored from 0 to 5 using a protocol adapted from Gensel et al. (2006). Grooming was scored as follows: (0) unable to contact any part of the face or head, (1) able to touch underside of chin and/or mouth area, (2) able to contact area between nose and eyes but not eyes, (3) able to contact eyes and area up to, but not including, ears, (4) able to contact front but not back of ears, and (5) able to contact area behind ears. As well an additional 3.5 score could be given as used previously (Streijger et al. 2013). This corresponded to halfway between the eyes and ears. Grooming was analysed by a blinded researcher and top score was recorded as well as the frequency of scores above 3.5 during each grooming session.

2.2.9 Graphing and statistical analysis

Graphs were created using Graphpad Prism 6.01 and edited in Inkscape 0.92. Statistical analysis of data using T-tests and ANOVA with multiple testing corrections (Tukey, Bonferroni, and Sidak) was performed using Graphpad Prism 6.01.

2.3 Results

2.3.1 Weight and BHB after C4 crush SCI

A schematic of the behaviour and timepoints is show in **Fig 2.1A**. The diets were administered immediately following SCI. Mice fed KD or SD after SCI both showed a significant drop in weight compared to non-injured mice on SD (**Fig 2.1B**). KD-fed mice also showed higher weight loss than SD-fed mice at 2 days post-injury (DPI) and 4DPI, however timepoints after this did not show any differences in weight gain between treatments (**Fig 2.1B and 2.1D**). BHB levels were significantly elevated in our KD group with a peak at 1 week post-injury (WPI); however, earlier timepoints were not tested (**Fig 2.1C and 2.1E**). The BHB levels seen (about 1-2mM) are in line with other studies where KD has been tested in mice (Brownlow et al. 2013; Beckett et al. 2013).

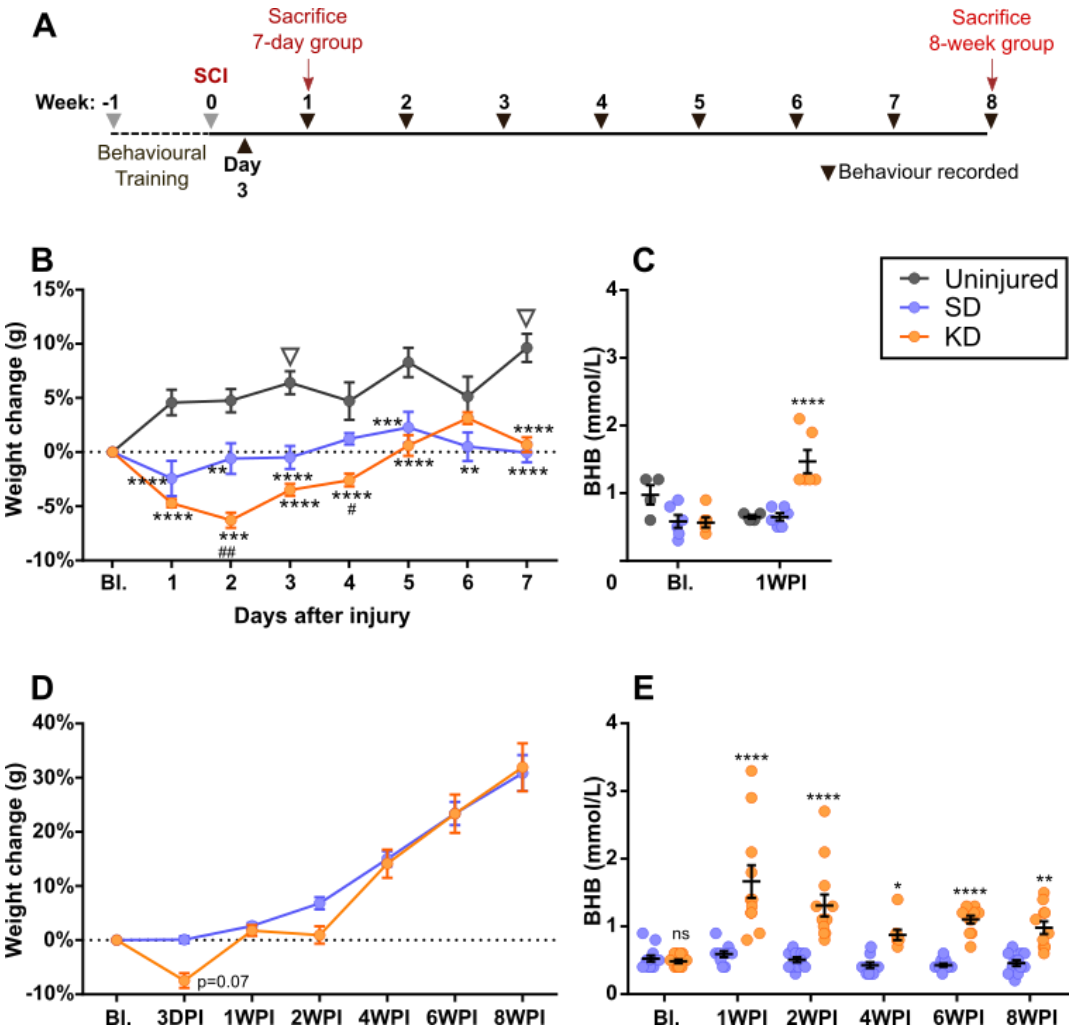

Figure 2.1 Experimental schematic and changes in weight and BHB after injury. **(A)** Experimental outline. Behaviour was only recorded for the 8-week group. **(B)** Change in weight in 7-day group compared to baseline weight. * SD or KD compared to control. # KD compared to SD. Empty triangles show weights recorded over first week for 8-wk group. **(C)** BHB levels measured for 7-day group. **(D)** Changes in weight for 8-wk group compared to baseline weight. **(E)** BHB levels measured for 8-wk group. * or # $p<0.05$, ** or ## $p<0.01$, *** $p<0.001$, **** $p<0.0001$ using Two-way ANOVA with Tukey test for **(B)** and **(C)**, Bonferroni method for **(D)** and Sidak test for **(E)**.

2.3.2 IF analysis of injury site at 7 days after C4 crush SCI

We assessed the injury site at 7DPI. The number of NeuN+ cells in a 0.5 by 1.5mm ROI of the ipsilateral (injured) side was normalized to the same ROI on the contralateral side. However, no differences were seen between KD and SD-fed mice (**Fig 2.2A and B**). We also measured the lesion size based on the GFAP+ scar border (**Fig 2.2D**). Although no significant difference was seen in injury size between KD and SD, a trend towards decreased lesion size in the KD group was evident (**Fig 2.2E**).

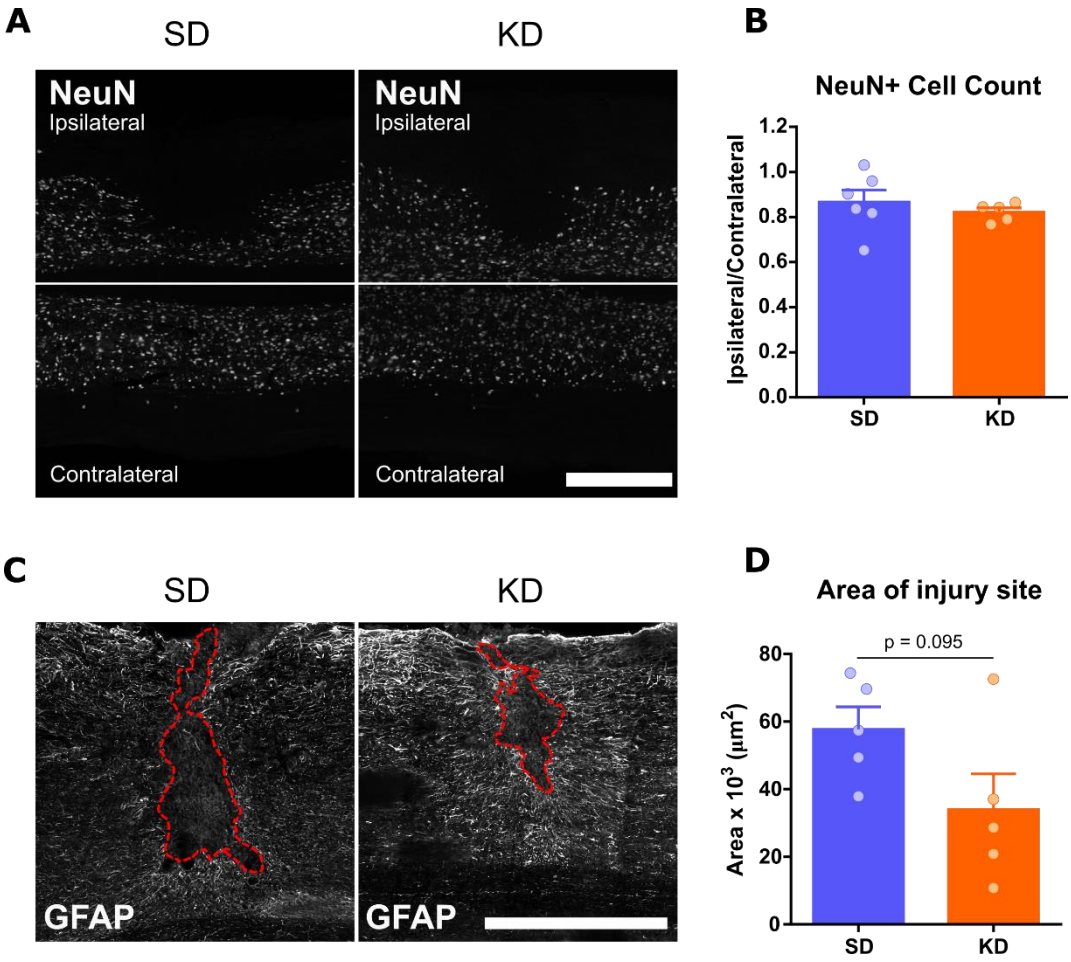

Figure 2.2 IF analysis of NeuN+ cells and lesion size. **(A)** Representative NeuN images of ipsilateral and contralateral sides of the cord. Scale bar = 0.5mm. **(B)** Total NeuN+ cells in ipsilateral side divided by contralateral side. Between 1-4 sections were averaged per animal (sections with tissue defects were discarded while blinded). SD = 6, KD = 5. **(C)** Representative GFAP images of the injury epicenter showing the lesion outline by a dotted red line. Scale bar = 0.5mm. **(D)** Quantification of injury site area. Between 2-4 sections were averaged per animal (sections with tissue defects were discarded while blinded). SD = 5, KD = 5. A Two-sided T-test was used to calculate statistical significance.

2.3.3 IF analysis of inflammation at injury site 7 DPI

Iba1 intensity was quantified at the injury epicenter and 0.5mm and 1.5mM rostral and caudal (**Fig 2.3A**). The intensity in the ipsilateral (injured) side was compared to the contralateral side. No significant differences were seen between SD and KD-fed mice (**Fig 2.3B**).

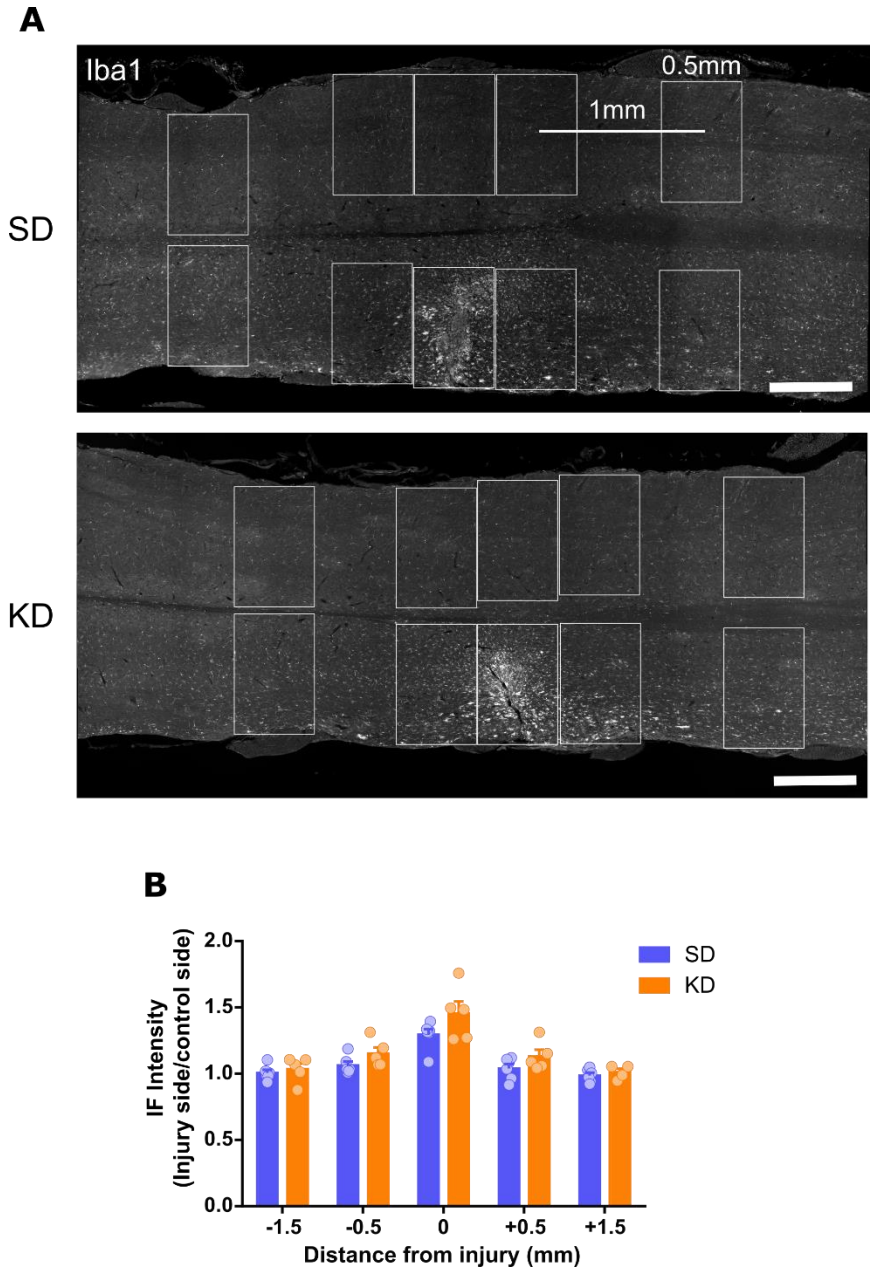

Figure 2.3 IF analysis of Iba1+ cells at the injury site 7DPI. **(A)** Representative images showing longitudinal sections of injured spinal cord with white rectangles showing quantified regions of interest (ROI). Each ROI is 0.5mm by 0.75mm. Scale bar = 0.5mm. **(B)** Quantification of Iba1 intensity of ipsilateral side divided by contralateral side. Between 2-4 sections were averaged per animal (sections with tissue defects were discarded while blinded). SD = 6, KD = 5. A Two-way ANOVA with Sidak correction was used to calculate statistical significance.

Although we did not see changes in macrophage/microglial activation or numbers as indicated through Iba1, KD could still be affecting the polarization of the microglia/macrophages or modulating inflammatory pathways. To look at polarization, we quantified intensity of Arg1, a marker of anti-inflammatory M2 macrophages (**Fig 2.4A**). However, we saw no differences in Arg1+ area or intensity. (**Fig 2.4B**).

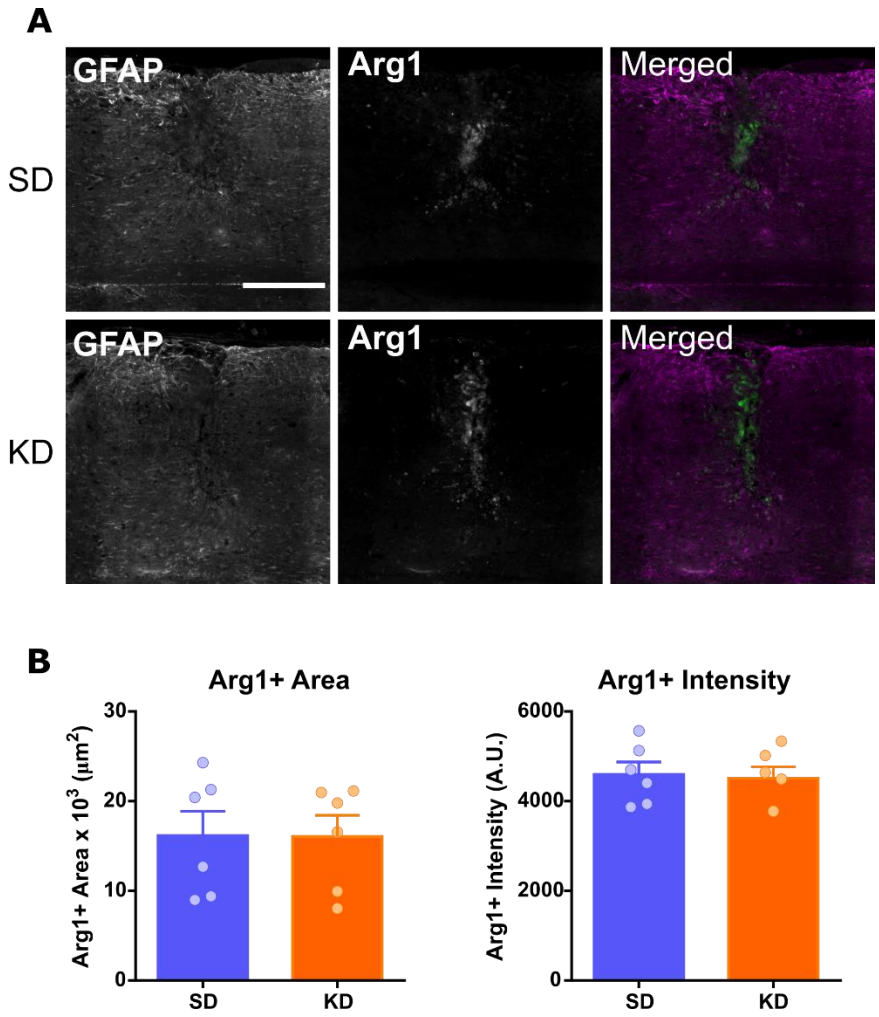

Figure 2.4 IF analysis of Arg1 at the injury site 7DPI. **(A)** Representative images of Arg1 showing localization in the lesion epicenter. Scale bar = 0.2mm. **(B)** Quantification of Arg1+ area and Arg1+ IF intensity.

To look at inflammatory pathways, we quantified P-p38 fluorescence intensity (**Fig 2.5A**). We saw a significant decrease in P-p38 area with KD (**Fig 2.5B**) but no difference in P-p38 intensity (**Fig 2.5C**). As can be seen, at 7DPI, P-p38 is expressed by cells in the injury epicenter (**Fig 2.5D**). Together these results show that, KD could reduce inflammation by specifically targeting activation of pro-inflammatory pathways such as the p38 MAPK pathway.

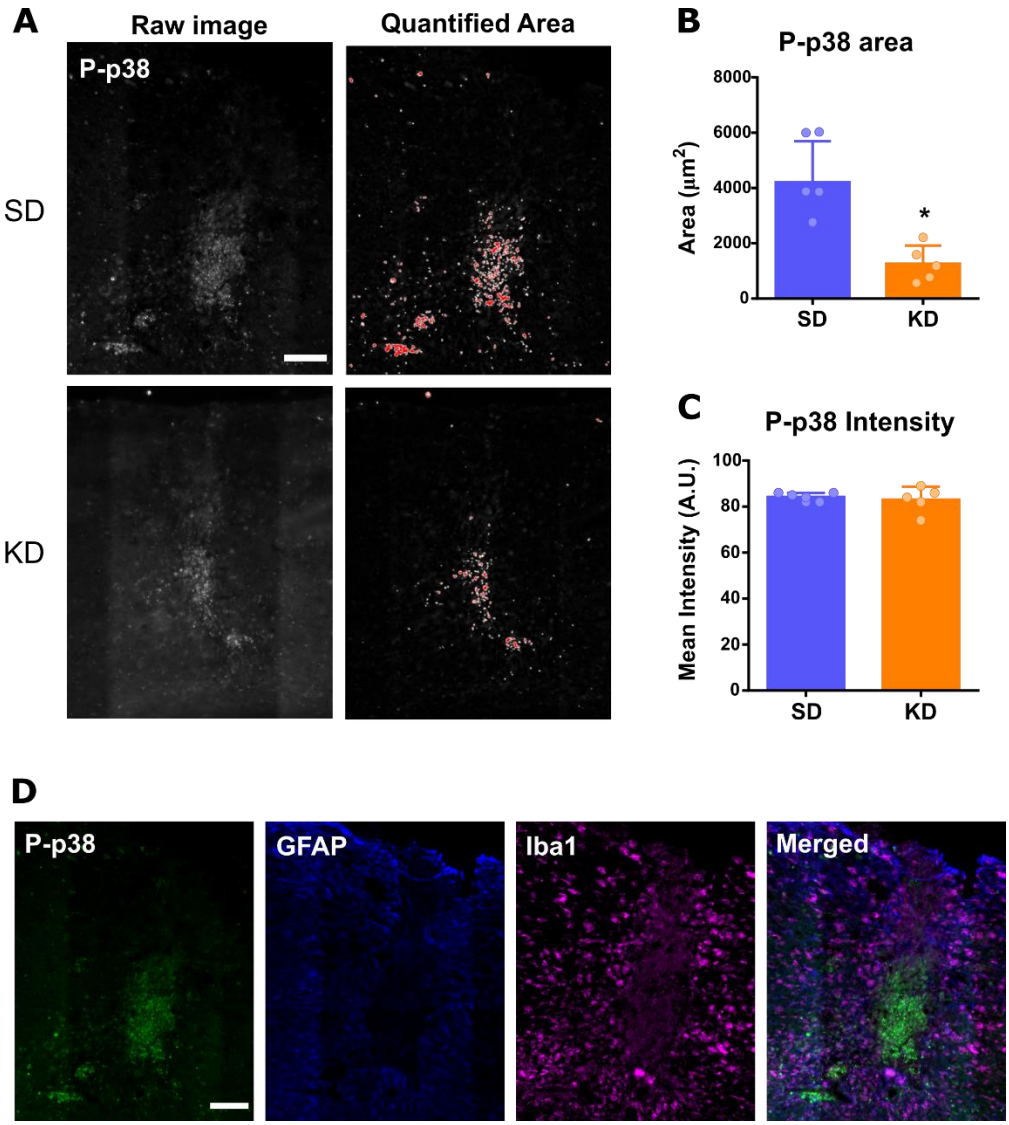

Figure 2.5 IF analysis of P-p38 analysis at the injury site 7DPI. **(A)** Representative images of P-p38 and area of quantified IF. Scale bar = 0.1mm. **(B)** Quantified P-p38+ area. * $p < 0.05$ calculated using a two-sided T-test. **(C)** Quantified P-p38+ intensity. **(D)** Representative image showing P-p38 localization at injury epicenter.

2.3.4 Rearing test for forelimb recovery after C4 crush SCI

The left side was chosen for hemi-lateral crush injury based on previous findings that mice slightly favored use of the left paw during the rearing test (Hilton et al. 2013). Contrary to this we found that use of only the left or right paw was equal during baseline testing (15.1±3.7% and 14.6±4.2%, respectively, for SD-fed mice) (**Fig 2.6A and 2.6B**). After injury, use of either the injured (left) paw or both paws decreased significantly in both groups, while use of the right paw was significantly increased (**Fig 2.6A-H**). KD-fed mice showed a slight improvement in usage of left or both paws, which was significant at 3DPI for combined initial and supplementary scores (**Fig 2.6D and 2.2H**). This corresponded to a significant decrease in use of the right paw for KD-fed mice at 3DPI (combined initial and supplementary scores) (**Fig 2.6F**). However, by 1WPI we did not see a significant difference between SD and KD-fed groups. Although a trend in improvement for the KD-fed group was also seen at 2-6 WPI, it was not significant at any timepoint.

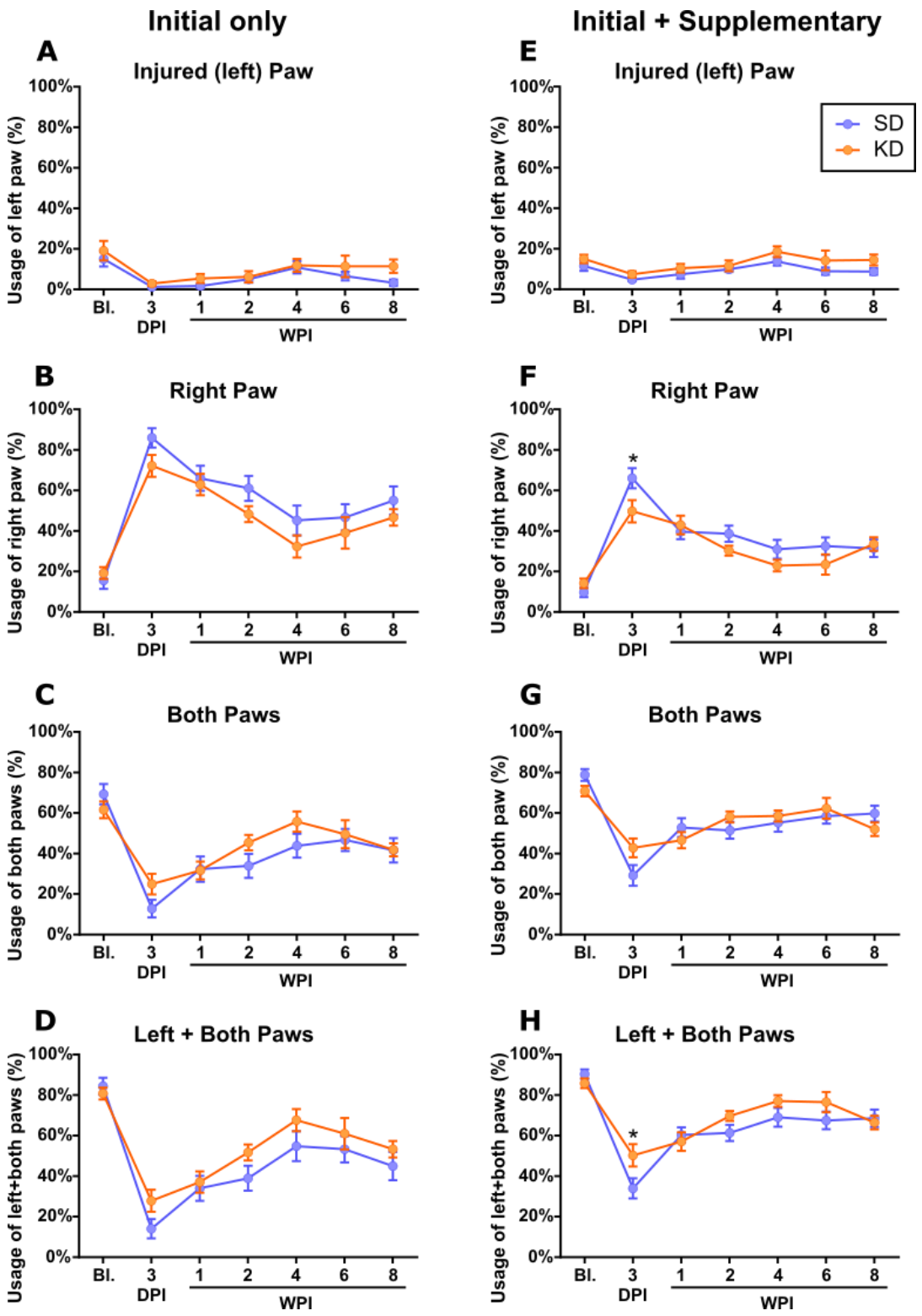

Figure 2.6 Analysis of rearing behaviour. **(A-D)** Percentage of initial paw placements for **(A)** Left paw, **(B)** Right paw, **(C)** Both paws, and **(D)** Combined percentages of left and both paws. **(E-H)** Percentage of initial and supplementary placements for **(E)** Left paw, **(F)** Right paw, **(G)** Both paws,

and **(H)** Combined percentages of left and both paws. * p<0.05 calculated using a Two-way ANOVA with Sidak multiple-testing correction.

2.3.5 Horizontal ladder test for forelimb recovery after C4 crush SCI

We used the horizontal irregular ladder to assess forelimb function after injury. In accordance with previous results (Hilton et al. 2013), we saw a significant increase in left forelimb and left hindlimb errors after injury with a peak at 3DPI (**Fig 2.7A and C**). Interestingly we also saw a significant increase in right forelimb errors, which was not previously observed (**Fig 2.7B**). KD-fed mice showed no significant changes in the number of errors made by the left (injured) forelimb, right forelimb, or left hindlimb. However, we did see a significant increase in errors made by the right hindlimb but only at 3 DPI, and this increase was not sustained at later timepoints (**Fig 2.7D**). It is unclear why such an increase might have occurred; however, it could relate to the lower weight (due to diet aversion) seen in KD-fed animals at this timepoint.

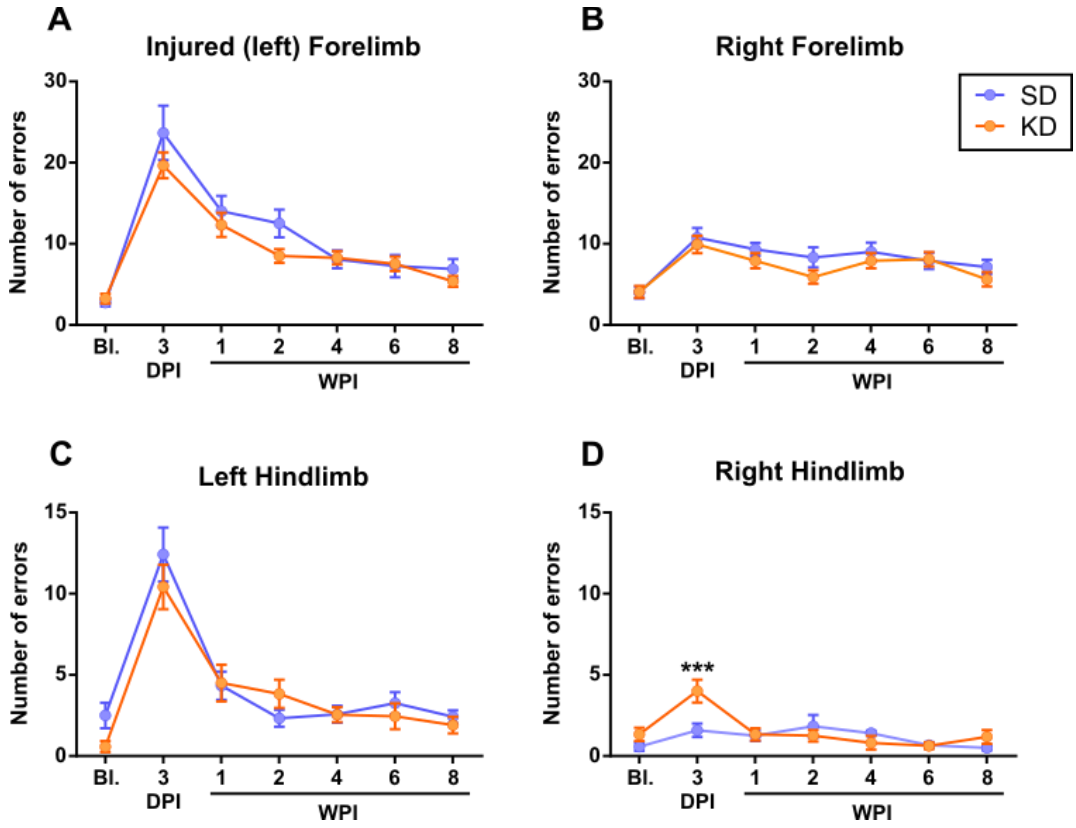

Figure 2.7 Number of errors during irregular horizontal ladder runs. Errors can include slips, misses or drags. Number of errors made by **(A)** left forelimb, **(B)** right forelimb, **(C)** left hindlimb, and **(D)** right hindlimb. *** p<0.001 calculated with a Two-way ANOVA using Sidak correction.

2.3.6 Grooming test for forelimb recovery after C4 crush SCI

We observed normal grooming behaviour that occurred during the rearing behavioural test. Both top score and the frequency of grooming events that reached or exceeded a 3.5 score (paw can reach halfway between the eyes and ears) was quantified. While we saw a significant increase in frequency of 3.5 scores for KD-fed animals at 1WPI and 6WPI, this increase in frequency was seen with both the injured and uninjured paw (**Fig 2.8A**). When we then looked at the ratio of 3.5+ scored grooming events to grooming sessions, we no longer saw a significant increase in the KD group (**Fig 2.8D**). Furthermore, there was no difference in top score between the KD and SD-fed groups (**Fig 2.8E**). Together these results suggest that KD does not improve use of the injured forelimb in grooming behaviour.

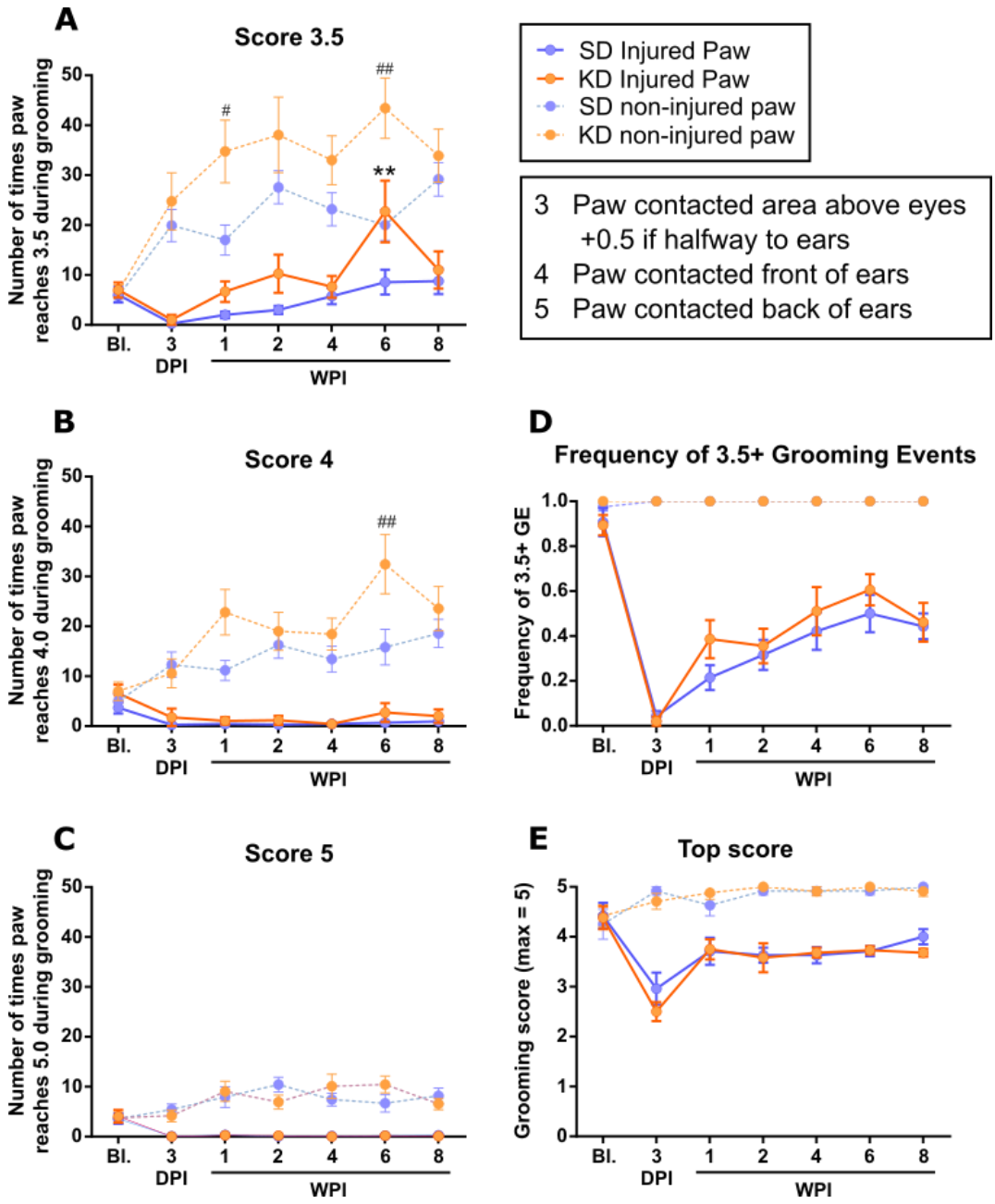

Figure 2.8 Analysis of grooming behaviour and frequency of grooming scores. **(A-C)** Number of individual grooms that reach **(A)** score 3.5, **(B)** score 4, and **(C)** score 5. * KD compared to SD on injured side. # KD compared to SD on uninjured side. **(D)** Number of 3.5 and higher scores normalized to number of grooming events. **(E)** Top grooming score achieved during each session. # $p<0.05$, ** or ## $p<0.01$ calculated using a Two-way ANOVA with Sidak correction.

2.4 Discussion

We chose a cervical injury in mice to mimic the C5 hemi-contusive injury that was previously used to show KD-mediated benefits in rats after SCI (Streijger et al. 2013). Due to the size of the mouse spinal cord compared to the rat spinal cord, a hemi-contusive injury is technically difficult and prone to variability. Therefore, we decided to use a C4 DLF crush injury as it was also a cervical injury and our laboratory has previously reported robust behavioural data using this model (Hilton et al. 2013). As well, it allowed for similar behavioural tests to those that had been used in the previous KD rat study (i.e. rearing and grooming).

In the previous rat study, lesion area was reduced by KD at the injury epicenter (Streijger et al. 2013). We did not see significant reduction in lesion area, although there was a strong trend in the KD group ($p=0.095$) **(Fig 2.2E**). This failure to reach significance may be due to one data point (a Grubb's test failed to classify this as an outlier), while otherwise the lesion area data points of the two groups do not overlap. It is possible that with a larger 'n' in each group, we would have seen a significant difference. However, there was no difference seen in NeuN+ counts around the injury suggesting that KD is not promoting neuronal survival within the spared gray matter itself **(Fig 2.2B)**. KD could be reducing lesion size by mitigating inflammation. Accordingly, we looked at widespread microglia activation and macrophage infiltration using Iba1 as a marker, as well as the presence of anti-inflammatory macrophages using Arg1 as a marker, and activation of inflammatory pathways via P-p38 MAPK presence. We saw no differences in Iba1 or Arg1 fluorescence at the injury site but did see a decrease in P-p38 **(Figs 2.3B, 2.4B, and 2.5B)**. This suggests that KD can impact specific pathways rather than having a global anti-inflammatory effect.

We also aimed to demonstrate in mice similar behavioural effects as seen with the KD in our previous rat study. In rats that were fed KD starting 4 hours after cervical injury, the use of the injured paw in rearing was significantly increased by 2WPI and remained significantly elevated at 3, 5, and 6 WPI (Streijger et al. 2013). Although we saw transient improvements in rearing that were significant at 3DPI, we did not see any sustained effects. Similarly, we saw no sustained improvement on the horizontal ladder or in grooming score. This is not the first time that dietary intervention has been unsuccessful in mice but succeeded in improving behavioural function after SCI in rats. Every-other-day-fasting (EODF) showed behavioural improvements after either a crush of the lateral spinal cord at C4 (hemi-crush) or a T10 midline contusion injury, but mice that received a T10-11 crush injury did not show improvement with EODF (Jeong et al. 2011; Plunet et al. 2008; Streijger et al. 2011).

Furthermore, unlike rats, EODF-treated mice did not show a reduction in lesion size (Streijger et al. 2011; Plunet et al. 2008). Contrary to rats, EODF led to sustained weight loss in mice and lower levels of BHB and glucose acutely after injury (Streijger et al. 2011). Thus, species-specific metabolic differences may underlie the lack of behavioural recovery seen in the mice. Although, we did see comparable BHB levels in our mice after KD to those seen in rats (Streijger et al. 2013), metabolic differences could still contribute to the lack of behavioural recovery. To the best of our knowledge, this is the first study that has looked at behavioural recovery with KD in mice. There are few studies comparing metabolomic profiles of rats and mice, although similar metabolic discrepancies have been observed in studies of sepsis (Zolfaghari et al. 2013). It is also possible that different strains of mice and rats may respond unequally to a given diet/injury strategy.

Another factor in the behavioural differences observed between rats and mice is composition of the lesion epicentre. Rats form a macrophage filled lesion cavity that becomes cystic over time whereas mice have higher fibrosis at the injury site (Sroga et al. 2003) leading to scar contraction. It is conceivable that KD can reduce lesion area in rats by modifying inflammation after contusion injury but not after crush injury in mice which leaves a much smaller lesion filled with myofibroblasts. Of note, administration of BHB alone (leading to serum levels of about 1mM) did improve behavioural recovery after a thoracic contusive injury in mice (Qian et al. 2017).

Compared to a contusive injury, a crush lesion resembles more a sharp transection with small lesion sites severing mostly white matter in the DLF and producing less extensive inflammation. Due to the large size of the contusive injury, both extensive severing of white matter tracts and neuronal losses occur, as well as increased inflammation. It is possible that the C4 crush injury model was not amenable to showing benefits and a more clinically relevant T9 midline contusion would show effects of KD. For this reason, we moved to a T9 injury for further studies in mice.

In conclusion, we show that KD can target the p38 MAPK pathway although this translated only into variable reductions in lesion size that did not reach significance ($p=0.09$) and no behavioural improvements. This was the first study to date to assess KD treatment of mice following SCI and further work using larger cohorts will need to be carried out to address functional recovery in a more clinically relevant contusive model of SCI.

Chapter 3. KD can reduce inflammation at the lesion site after T9 midline SCI by reducing CCL3 and CCL4 production and decreasing infiltrating myeloid cell numbers through HCAR2

3.1 Introduction

Our findings from Chapter 2 show that KD reduces inflammation through the p38 MAPK pathway after a C4 DLF crush injury. However, this is a fairly mild injury and does not elicit as strong an inflammatory response as a contusive injury. For this reason, we chose to move to a moderate 70kdyn T9 midline contusive injury for further studies of inflammation. While we did not see widespread changes in inflammation with the crush injury (as evidenced by similar Iba1 and Arg1 IF between SD and KD-fed mice), we did see a specific reduction in p38 MAPK phosphorylation at the lesion epicenter. Activation of the p38 MAPK pathway leads to induction of multiple pro-inflammatory cytokines including TNFα, IL-1, IL-6, and IL-8 (Schindler, Monahan, and Smith 2007). This result highlights two questions that I aim to answer in Chapter 3: Can KD modulate the production of pro- and anti-inflammatory cytokines? Which cells are being affected? To this end we performed a cytokine analysis at 2- and 7-days post-injury (DPI). As well, we completed a single-cell (sc)RNA-sequencing analysis of CD45+ immune cells isolated from the injury lesion site at 7DPI.

We also aimed to determine if BHB activation of the HCAR2 receptor is required for the anti-inflammatory role of KD. BHB is one of the main ketone bodies produced through breakdown of fats and elevated levels of circulating BHB are characteristic of KD treatment. HCAR2 can be activated by BHB and is found on multiple immune cells including neutrophils, macrophages, and microglia (Taggart et al. 2005; Kostylina et al. 2008; Knowles et al. 2006). Although multiple studies have shown that BHB can reduce inflammation, there is conflicting evidence on whether this occurs through the HCAR2 receptor. For example, in primary rat microglial cells BHB treatment reduced LPS-induced production of IL-1β, TNFα, IL-6, iNOS, and COX-2, and these effects were abrogated with siRNA knock-down of HCAR2 (Fu, Wang, et al. 2015). On the other hand, BHB could reduce NLRP3 activation in LPS-primed BMDMs independently of HCAR2 (Youm et al. 2015). Clearly a better understanding of the mechanisms used by BHB and HCAR2 to target inflammation is needed. To investigate the role of HCAR2, we used several methods to assess inflammatory cells in the injury

epicenter including flow cytometry of CD45+CD11b+ cells, IF of Iba1+ immune cells, and *in vitro* cultures of bone marrow-derived macrophages (BMDMs) collected from wild type (WT) and HCAR2-/- mice. Together, these analyses aimed to provide an expanded understanding of the interplay between KD and HCAR2 in mitigating inflammation following SCI.

3.2 Materials and Methods

3.2.1 Mice

Frozen sperm from HCAR2-/- mice were obtained from the lab of Dr. Stephan Offermanns (Max Planck Institute for Heart and Lung Research, Bad Nauheim, Germany) and rederived on a C57Bl/6 background at the BC Cancer Research Centre (Vancouver, Canada). HCAR2+/- mice were housed in the ICORD vivarium in accordance with the University of British Columbia Animal Care Committee Protocol #A18-0015. This mouse line was generated on the C57Bl/6 background as previously described (Tunaru et al. 2003) and maintained as heterozygotes allowing us to generate HCAR2+/+ and HCAR2-/- for our experiments. Genotyping of each mouse was also performed using the same primers as previously described (Tunaru et al. 2003). For overview of mice used in *in vivo* experiments in Chapter 3 and use of tissue post-euthanasia see **Table 3.1**. We lost one mouse from the T9 7DPI cohort in the cytokine study during bladder squeezing. As well, in the T9 experiment for IF analysis 4 mice were omitted from downstream analyses as they showed a steady decline to over 25% weight loss and high ketone levels indicative of starvation. It is unclear what prompted this as we haven't previously had any issues with the palatability of our standard diet.

Table 3.1 Overview of mice used in SCI experiments. Omitted mice were not used for analyses due to non-compliance with diet. M = male, F = female. SD = standard diet, KD = ketogenic diet.

Tissue use	**Timepoint**	**Injury**	**Strain**	**Diet**	**N** (sex)	**Died (D) or omitted (O)**
Cytokine Levels	2DPI	None	HCAR2+/+	SD	**4** (M)	0
		T9	HCAR2+/+	SD	**8** (M)	0
		T9	HCAR2+/+	KD	**8** (M)	0
	7DPI	None	HCAR2+/+	SD	**4** (M)	0
		T9	HCAR2+/+	SD	**8** (M)	0
		T9	HCAR2+/+	KD	**8** (M)	1 (D)
scRNA-sequencing	7DPI	T9	HCAR2+/+	SD	**2** (M)	0
		T9	HCAR2+/+	KD	**2** (M)	0
Fixed + IF	7DPI	None	HCAR2+/+	SD	**4** (2M/2F)	0
		None	HCAR2-/-	SD	**4** (1M/3F)	0
		T9	HCAR2+/+	SD	**5** (2M/3F)	1 (O)
		T9	HCAR2+/+	SD	**4** (2M/2F)	0
		T9	HCAR2-/-	SD	**5** (2M/3F)	2 (O)
		T9	HCAR2-/-	KD	**6** (2M/4F)	1 (O)
Flow Cytometry	7DPI	T9	HCAR2+/+	SD	**3** (1M/2F)	0
		T9	HCAR2+/+	KD	**4** (1M/3F)	0
		T9	HCAR2-/-	SD	**4** (2M/2F)	0
		T9	HCAR2-/-	KD	**4** (3M/1F)	0

3.2.2 Diets

In all *in vivo* experiments, the diet was administered directly after injury. Mice were given *ad libitum* access to KD (Bio-Serv #F5484) or SD (Bio-Serv #F5960) and usually began eating 24-48 hours after injury as is reflected in the initial drop in weight seen following injury. Both diets were placed in ceramic or plastic dishes in the cage bottom to facilitate access.

3.2.3 T9 midline contusion SCI model

All T9 midline contusion injuries were performed by Dr. Jie Liu using the Infinite Horizon (IH) Impactor (Precision Systems and Instrumentation, LCC, Brimstone, Virginia, USA). Similar to the

C4 DLF crush injury, mice were anesthetized using Isoflurane and the back of the mouse was shaved. Mice received 1mL Lactated-Ringer's solution and a single dose of buprenorphine (0.03mg/kg). The surgical area was also disinfected with three successive applications of betadine then 70% ethanol after which a full dorsal laminectomy at T9-T10 was performed. The vertebral column was stabilized with clamps at T8 and T10, and the mouse was then positioned beneath the IH impactor. A force of 70kDyn was delivered to the spinal cord, then the muscles and skin were sutured. As with the C4 injury, mice were placed in a heated incubator for recovery post-surgery and were given subcutaneous injections of Lactated-Ringer's solution twice daily and Buprenorphine three times daily for at least 3 days post-surgery. As well, bladders were expressed two to three times daily until the mice were able to voluntarily urinate.

3.2.4 BHB measurements

Ketone levels were measured from blood obtained by tail prick. Precision Xtra Blood Ketone Test Strips (Diabetes Express) were used with the Precision Xtra Blood and Ketone Meter (Abbott) according to manufacturer guidelines.

3.2.5 Measurement of cytokine levels

Cytokine levels were measured using the Meso Scale Diagnostics (MSD, Rockville, Maryland, USA) U-PLEX mouse cytokine assay kit. The kit contained antibodies towards the following cytokines: MCP-1 (CCL2), MIP-1α (CCL3), MIP-1β (CCL4), IL-1β, IL-12/IL-23p40, IL-6, TNFα, IFNγ, IL-10, and IL-4. To prepare tissue for cytokine analysis, mice were given a lethal injection of 10% chloral hydrate and perfused with ice-cold PBS. A 5mm segment of thoracic spinal cord around the lesion site was then isolated and flash-frozen on dry-ice. Cords were stored at -80ºC until lysis. Cords were lysed in 0.2-0.3mL cold lysis buffer (50mM HEPES (pH 7.5, Gibco), 150mM NaCl (ThermoFisher Scientific), 1.5mM $MgCl_2$ (BDH, VWR), 1mM EGTA (pH 8.0, MilliporeSigma), 10% Glycerol (VWR), 0.6% Triton X-100 (BDH, VWR), 100mM NaF (ThermoFisher Scientific), 25mM β-glycerophosphate (MilliporeSigma), 10mM Pyrophosphate (ThermoFisher Scientific), 200µM Orthovanadate (ThermoFisher Scientific), and 1X Phosphatase Inhibitors (EMD, VWR)) and mechanically dissociated by Dounce homogenization using a plastic pestle (VWR). Cell debris was pelleted at 14000rpm (Rotor FA-45-18-11; Eppendorf Centrifuge 5418 R, Mississauga, Ontario) for 20min at 4ºC then supernatant was removed to a new tube and stored at -80ºC until further use. A Pierce BCA Protein Assay Kit (ThermoFisher Scientific) was used to determine protein content according to manufacturer's protocol. The U-PLEX plate was run according to MSD protocol and

measured using the MESO QuickPlex SQ 120 (MSD). Cytokine concentrations are per 50µg total protein.

3.2.6 Preparation and single-cell RNA-sequencing of CD45+ cells from the injury epicenter

For experimental outline see **Fig 3.6**. Male HCAR2+/+ and HCAR2-/- mice were given a T9 midline contusive injury then fed with SD or KD *ad libitum*. For numbers used, **see Table 3.1**. At 7DPI, each mouse was perfused with 20mL ice-cold PBS. The injury site (5mm) was harvested and cut into smaller sections using dissection scissors. The cords were then digested using 2mg/mL Collagenase IV (MilliporeSigma) in PBS + 2% FBS (FPBS, Invitrogen, ThermoFisher Scientific) (total volume = 1mL) with 100µg DNAseI (MilliporeSigma) for 40min at 37ºC. At both 20min and the end of the digestion, each dissociated cord was pipetted 15 times using a P1000 Pipette. At this point, dissociated cords from the same diet were combined then strained through 70µm filters into 50mL Falcon tubes and washed with 5mL FPBS. The resulting 6mL solution was moved to a 15mL Falcon with 4mL Percoll (MilliporeSigma) for a final concentration of 40% Percoll. Each sample was mixed and spun at 500Xg for 20min at 4ºC. Pellets were resuspended in 1mL FPBS and filtered through 45µm filter caps into FACS tubes. They were then spun again at 300Xg, 5min, 4ºC and resuspended in 100µL FPBS. Samples were incubated with 1:200 CD45-APC and 1:50 CD16/32 Fc Blocker for 1hr at 4ºC. See **Table 3.2** for more information on the antibodies used. After incubation, samples were washed with 1mL FPBS and spun at 300Xg, 5min, 4ºC. Supernatant was decanted, and the pellet was resuspended in 500µL propidium iodide (PI) solution (1:1000; MilliporeSigma) and 100µg/mL DNAseI in FPBS). Samples were sorted for CD45+ PI- cells using a BD Influx (BD Biosciences, Franklin Lakes, New Jersey, USA) at the UBC Flow core. Through the BRC Sequencing Core at UBC, library preparation was completed using the 10x Genomics Chromium Single Cell Controller (10X Genomics, Pleasanton, California, USA) and sequencing was completed on the Illumina NextSeq 500 (Illumina, San Diego, California, USA).

3.2.7 Analysis of single-cell RNA-sequencing results

Reads were demultiplexed and aligned using Cell Ranger (10X Genomics) by the BRC Sequencing Core at UBC. I carried out subsequent analysis using the Seurat 3.0 package in R (Stuart et al. 2019; Butler et al. 2018). Briefly, individual data sets were filtered for RNA feature counts between 500 and 6000, RNA counts less than 50000, and mitochondrial percentage below 7.5 (**Figure 3.6D-E**). This resulted in filtering out 22% and 28% of cells for KD and SD, respectively. Data were then log normalized and variable features were selected. Anchor identification and integration was performed. PCAs were created and 30 were used for running UMAP and finding neighbours and clusters. Figures

were created in RStudio 1.2.5 and edited with Inkscape 0.92. Graphs were generated using Graphpad Prism V6.01.

3.2.8 Isolation of cells from injury epicenter for flow cytometric analysis

Following a lethal injection of 10% chloral hydrate, mice were perfused with ice-cold PBS. A 5mm section of spinal cord including the injury epicenter was harvested into ice-cold PBS. Tissue was dissociated by Dounce homogenization at 4ºC then passed through an 18.5G needle and 3mL syringe several times. The resulting single-cell suspension was then filtered through a 70µm filter and washed with FPBS. For additional cleaning, the cell pellet was resuspended in 40% ice-cold Percoll and spun at 500Xg for 30min at 4ºC using a previously described protocol (Hammond et al. 2019) then washed again in FPBS. Cells were stained in FPBS and antibody cocktail (total volume of 50uL) for 1hr at 4ºC. The antibody cocktail contained CD45-APC, CD11b-PE, GR1-BV241, and CD16/32 Fc Blocker. For more information, see **Table 3.2**. Following incubation, cells were washed with FPBS and further filtered through 45µm filter caps into new polystyrene FACs tubes. Cells were spun at 300Xg for 5min, 4ºC, and resuspended in 150µL FPBS containing 100µg DNAseI and PI (1:1000). Stained samples were analyzed on a BD Fortessa multicolour analyzer with four lasers (BD Biosciences) and further quantification was performed in FlowJo v10.

Table 3.2 Antibodies used in Chapter 3. BD: BD Biosciences. BioLegend (San Diego, California, USA). Wako (Fujifilm Wako chemicals, Osaka, Osaka, Japan).

	Antibody	**Tag**	**Host**	**Reactivity**	**Dilution**	**Cat. #**	**Company**
Flow Cytometry	CD45	APC	Rat	Mouse	1:200	561018	BD
	CD11b	PE	Rat	Mouse	1:200	561690	BD
	GR1	BV421	Rat	Mouse	1:100	562709	BD
	CD80	BV711	Hamster	Mouse	1:100	740698	BioLegend
	CD86	PECy7	Rat	Mouse	1:100	105013	BioLegend
	CD16/32 Fc Blocker	None	Rat	Mouse	1:50	553141	BD
IF	NeuN	None	Guinea Pig	Mouse	1:500	ABN90P	MilliporeSigma
	Iba1	None	Rabbit	Mouse	1:500	019-19741	Wako
	P-p38	None	Rabbit	Mouse	1:200	4631	CST

3.2.9 IF staining

Mice were processed for IF analysis using the same protocol as outlined in Chapter 2. Primary antibodies used for staining are listed in **Table 3.2**. Donkey AlexaFluor secondary antibodies (1:500; Jackson ImmunoResearch) were used for secondary staining. Images were taken with a Zeiss Axio Imager M2 microscope using a Plan-Apochromat 10X/0.50 objective. Images were captured using an AxioCam HR R3 Camera using Zen 3.1 software. All analyses were performed on images that were randomized and renamed for blinding of the observer using a batch script developed by Jason Faulkner (https://www.howtogeek.com/57661/stupid-geek-tricks-randomly-rename-every-file-in-a-directory/). Analysis was performed using ImageJ 1.52p. Further details are outlined below.

3.2.10 Analysis of inflammatory markers by IF

Injury epicenter was determined by a strong GFAP border and extensive Iba1+ IF. The section that showed the most severe phenotype was denoted as the epicenter and rostal/caudal sections were counted from this section. Images were pre-processed for analysis by tracing the cord and manually removing anything on the slide (e.g. dura mater) around the cord. Robust Automatic Threshold Selection (RATS), which is part of the Segmentation plug-in in ImageJ was used to detect positive fluorescence. The resulting binary image was used to create a selection to measure IF intensity in the original image. Analyze Particles was used to measure area of the binary image and this area was normalized to total cord area by section. To measure the area of the complete cord, a channel of high background was thresholded to capture the entire cord. The MorpholibJ plug-in was used to fill holes and keep the largest section for further analysis. This section was then selected, and area was measured. For analysis of P-p38 IF, a threshold of (3600, 65535) was used to delineate positive P-p38 fluorescence and create a selection for intensity analysis. IF intensity was then normalized to cord size by section. Sections between 2mm rostral and caudal to the injury site were used for both analyses and all macros can be found in **Appendix A**.

3.2.11 Analysis of NeuN+ neurons

Using an ImageJ Macro, TIFF images were analyzed for NeuN+ cell counts. Briefly, using 16-bit images, the macro applied a Gaussian Blur (sigma = 1) and subtracted background (rolling = 30). Each image was then thresholded (20, 65535) and converted to a binary image. A watershed was applied to separate adjacent cells and the Analyze Particles function was used to count any cells that were between 0.01-1µm in size and 0.30-1.00 in circularity. The macro can be found in **Appendix A.**

3.2.12 Eriochrome cyanine staining and analysis

Eriochrome cyanine (ER) staining was used to visualize white matter (WM) and quantify WM sparing. Tissue was prepared and cut as for IF. Slides out of the -80ºC freezer were dried fully before rehydration twice in xylene (ThermoFisher Scientific) (5min each) followed by 100%, 90%, 70%, and 50% ethanol (2min each) then distilled water. Slides were stained with EC (0.16% EC (MilliporeSigma), 0.4% H_2SO_4 (EMD, MilliporeSigma) and 0.4% $FeCl_3$ (MilliporeSigma)) for 10min, rinsed twice with distilled water then differentiated in 0.5% NH_4OH (Ricca Chemical, Arlington, Texas, USA). Slides were again rinsed twice with distilled water then dehydrated using 50%, 70%, 90%, then 100% ethanol (2min each) followed by two immersions in xylene (5min each). Coverslips were attached with SHUR/Mount (VWR) and left to harden in a fume hood overnight. EC stained slides were imaged using Aperio Scan Scope (Leica Biosystems, Concord, Ontario, Canada). at 20X magnification and analyzed using Aperio ImageScope v12.4.0.5043 (Leica Biosystems). For analysis, sections were outlined using the Pen tool and areas to omit within the section (e.g. small areas of folded tissue) were excluded using the Negative Pen tool. The sum of the number of positive signals was used as a measure of white matter sparing and normalized to an average sum calculated from non-injured WT or HCAR2-/- tissue.

3.2.13 *In vitro* BMDM cultures

An adapted version of a previously described protocol (Weischenfeldt and Porse 2008) was used to isolate and culture BMDMs. Briefly, femurs were harvested from mice and crushed in a mortar and pestle with 5mL pre-warmed lymphocyte medium (RPMI-1640 (Gibco, ThermoFisher Scientific) with 10% FBS, 1% Penicillin/Streptomycin (ThermoFisher Scientific), 1X GlutamaxI (ThermoFisher Scientific), and 25mM HEPES) to extract bone marrow. The suspension was filtered through a 70µm strainer and an additional 5mL pre-warmed lymphocyte medium was used to wash the mortar and pestle and strainer. Cells were counted using a hemocytometer then spun at 200Xg for 10min. The pellet was resuspended to a concentration of $2X10^6$ cells/mL in pre-warmed BMM media (Lymphocyte media with 10% L929-conditioned media) then seeded onto non-TC treated wells of a 12-well plate (2mL/well). The media was refreshed at 3 days and changed to treated media at day 7. For treatments and timing, see following sections. For flow cytometric analysis, cells were harvested by adding 0.5mL (12-well plate) Trypsin-EDTA (ThermoFisher Scientific) per well and incubating at 37ºC for 5min. Pre-warmed FPBS was added to quench the trypsin and cells were collected by spinning at 200Xg for 10min.

3.2.14 Activation of BMDMs by LPS

BMDMs were activated to a pro-inflammatory phenotype by treating cultures with 0.1µg/mL LPS (ThermoFisher Scientific) in BMM media for 24 hours at 37ºC, 5% CO_2. LPS treatment for 3 hrs and 72 hrs was also tested. BMDMs were simultaneously treated with 1mM, 4mM, or 8mM BHB for the same time periods. BMDMs were harvested for flow cytometry analysis by incubating cells with 0.5mL (per well) pre-warmed Trypsin-EDTA for 10min (37ºC, 5% CO_2) and pipetting to dislodge cells. The trypsin was quenched with 1mL FPBS and cells were filtered through 0.45µm caps into FACs tubes. The cells were then centrifuged at 200Xg, 10min, 4ºC. BMDMs treated with LPS were incubated with an antibody cocktail (50µL) containing CD45-APC, CD11b-PE, CD80-BV711, CD86-PECy7, and CD16/32 Fc blocker for 1hr at 4ºC. For further information see **Table 3.2**. Unstained, fluorescence minus one (FMO) -CD80, and FMO -CD86 controls were also prepared. After staining, cells were washed with 1mL FPBS and spun at 200Xg for 5min at 4ºC. Cells were resuspended in 150µL PI solution (1:1000 PI, 100µg/mL DNAseI in FPBS (containing Ca^{2+} and Mg^{2+})) and run on a BD Fortessa multicolour analyzer with four lasers (BD Biosciences). Further analysis was completed in FlowJo V10.

3.2.16 Statistical Analyses

Statistical analyses of the data using T-test and Two-way ANOVA with multiple testing correction (Tukey and Sidak) was performed using Graphpad Prism 6.01.

3.3 Results

3.3.1 Cytokine analysis at 2 and 7 days after a T9 contusion SCI

We performed a T9 injury to see if inflammatory changes were more robust using this model. As with the C4 DLF crush injury in Chapter 2, we saw a significant decrease in weight for the injured compared to non-injured mice **(Fig 3.1A and C)**. We also saw a significant difference in weight loss between the KD and SD groups that began around 2-3 days after injury and lasted until 6DPI **(Fig 3.1A and C).** We also checked BHB levels at 2, 4, and 7DPI. BHB levels were highest at 2DPI but also significantly elevated at 4 and 7 DPI, as expected **(Fig 3.1B and D)**.

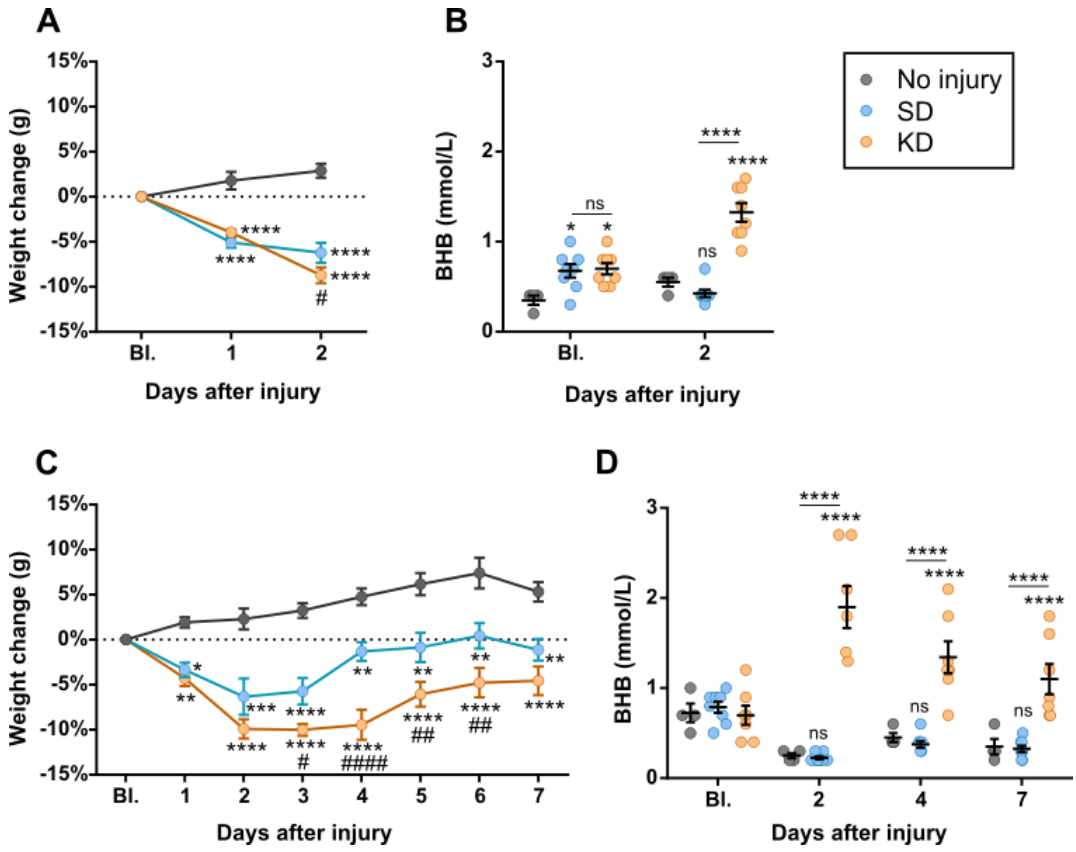

Figure 3.1 Weight and BHB changes up to 2 and 7 days after injury. **(A)** Weight change compared to baseline for mice euthanized at 2DPI. **(B)** Circulating BHB levels of mice euthanized at 2DPI. **(C)** Weight change compared to baseline for mice euthanized at 7DPI. **(D)** Circulating BHB levels of mice euthanized at 7DPI. * SD or KD compared to control, # KD compared to SD. * or # $p<0.05$, ** or ## $p<0.01$, *** $p<0.001$, **** or #### $p<0.0001$ calculated by Two-way ANOVA using Tukey correction.

We compared cytokine levels of uninjured WT mice to injured WT mice fed SD or KD. We analyzed the level of pro-inflammatory cytokines CCL2, CCL3, CCL4, IL-1β, IFNγ, IL-6, TNFα, and IL-12/IL-23p40, and anti-inflammatory cytokines IL-4 and IL-10 at 2DPI and 7DPI. We did not see any differences between SD and KD-fed groups at 2DPI but at 7DPI we saw a significant decrease in CCL3 and CCL4 for KD-fed mice **(Fig 3.2)**. The majority of cytokines also showed differences between the injured mice and uninjured group. The exceptions were IFNγ and IL-4 for both 2 and 7DPI, and IL-1β and IL-6 at 7DPI **(Fig 3.2)**. Together these results further show that KD can reduce inflammation but also suggest that it may be targeting specific pathways as a global decrease in pro-inflammatory cytokine production was not seen.

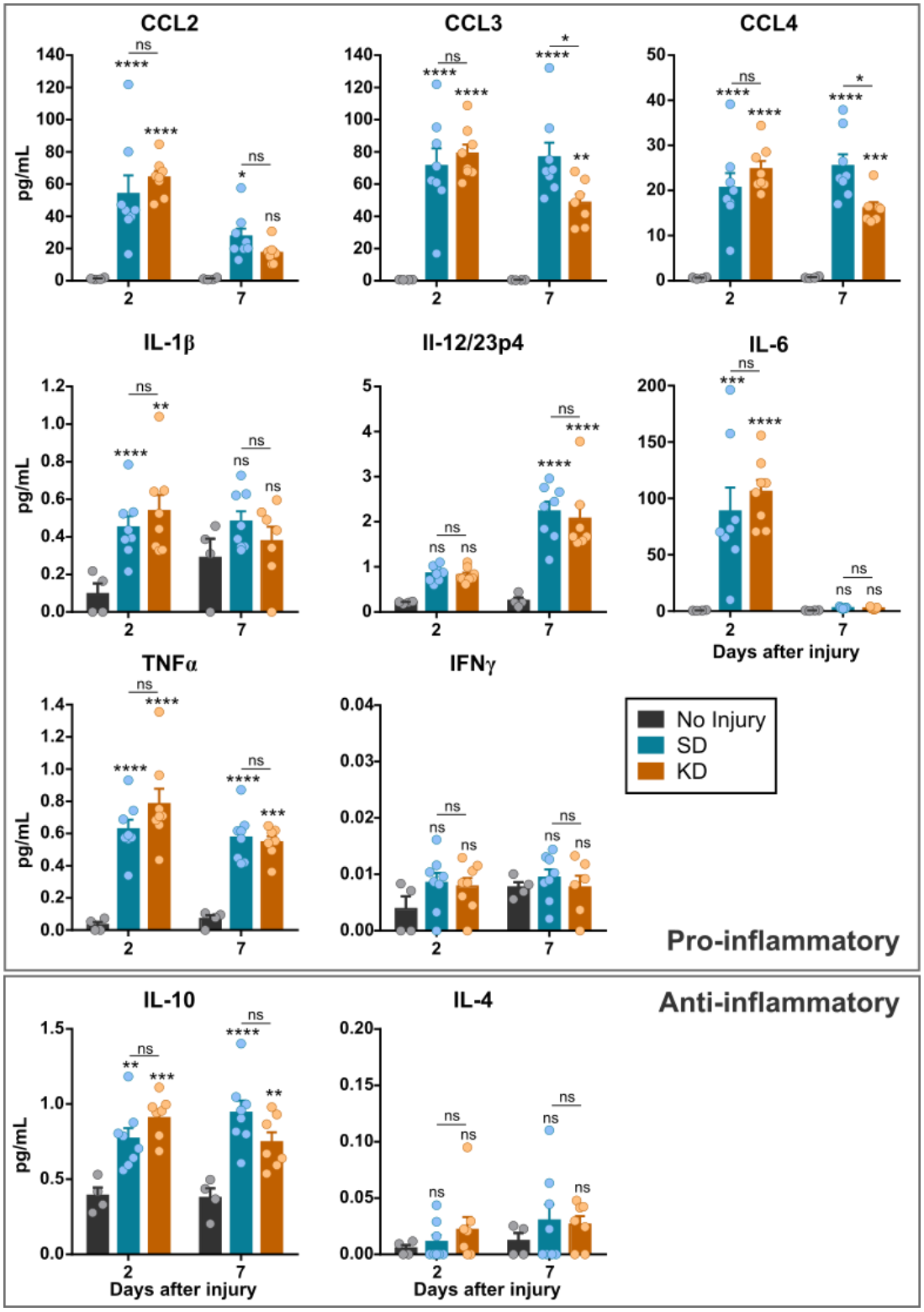

Figure 3.2 Pro- and anti-inflammatory cytokine levels at 2 and 7DPI. Concentration of cytokines (pg/mL) is per 50mg total protein loaded. * p<0.05, ** p<0.01, *** p<0.001, ****p<0.0001 calculated using Two-way ANOVA with Tukey correction. ns = not significant.

3.3.2 Single-cell RNA Sequencing of CD45+ cells from the injury epicenter

While previous studies show that KD can reduce pro-inflammatory cytokines and modulate the p38 MAPK pathway, we do not know if KD is targeting specific immune cells. To this end we decided to perform single-cell (sc)RNA-sequencing of CD45+ cells that were isolated from the injury site at 7DPI. As expected, KD-fed mice trended towards higher weight loss on days 6 and 7 **(Fig 3.3B)** and higher BHB levels by day 7 **(Fig 3.3C)**. **Fig 3.3D and E** show the filtering steps during data analysis, where blue cells were kept while red cells filtered out. As can be seen, there were far fewer cells collected for KD than SD. However, we believe this can be attributed to technical difficulties during the sorting step (sorting into dry tubes) and not the diet.

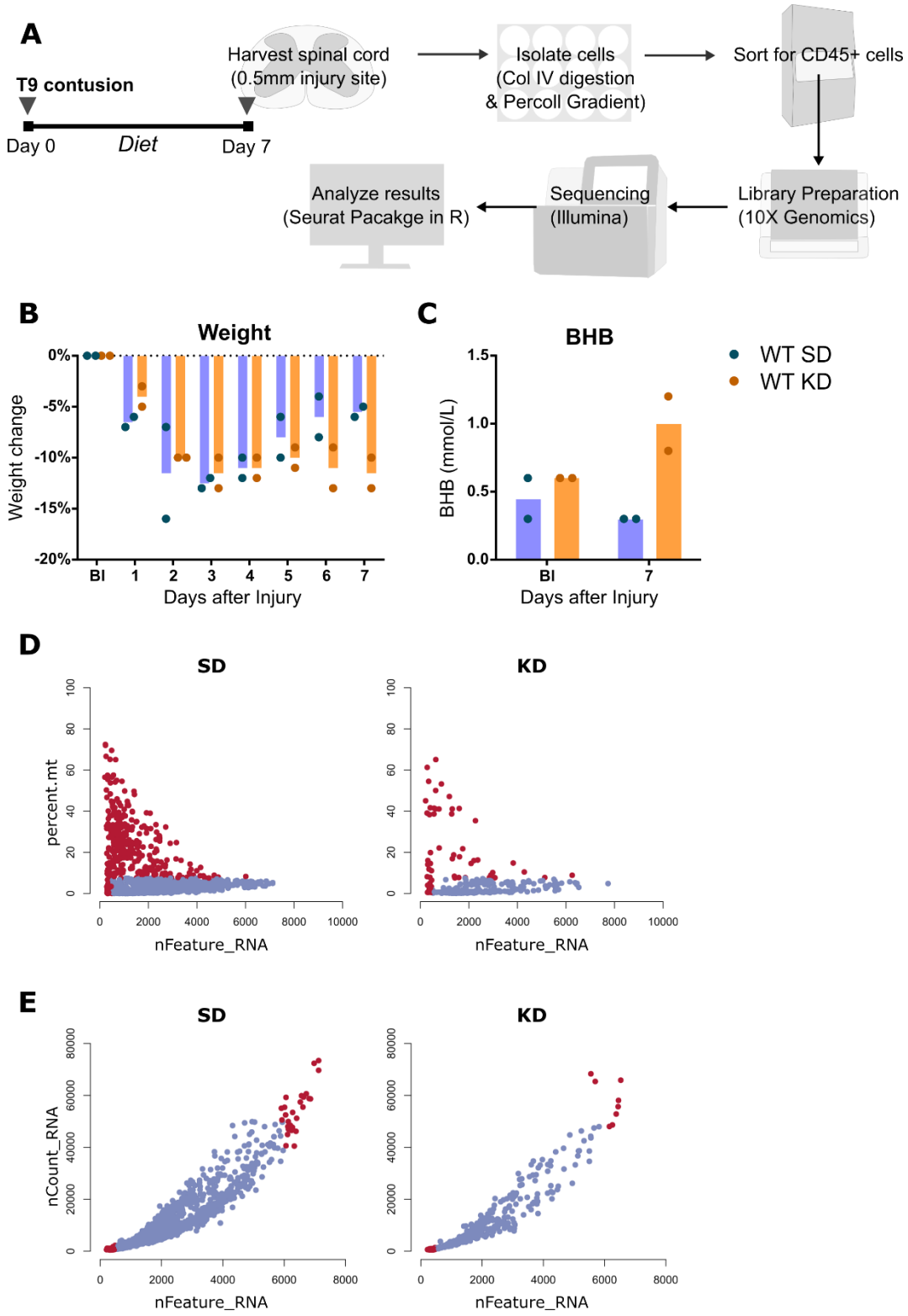

Figure 3.3 scRNA-sequencing of CD45+ cells from mouse spinal cords at 7 days after injury. **(A)** Experimental outline. Diet = KD or SD. **(B)** Percent weight change compared to baseline weight. **(C)** BHB levels at baseline and 7 days after injury. **(D)** Percent mitochondrial counts or **(E)** RNA counts

(total number of counts) vs RNA feature counts (total number of genes) showing filtering steps with cells included in downstream analysis in blue and cells filtered out in red.

For the initial clustering analysis, SD and KD cells were combined. The UMAP (Uniform Manifold Approximation and Projection) visualization shows several immune cell populations present in the spinal cord at 7DPI including myeloid cells (neutrophils and macrophages), microglia, NK cells, and T cells **(Fig 3.4A)**. Designation of these clusters was based on the presence of hallmark genes for each cell type as shown in **Fig 3.4B** and **Supp Fig 1 (Appendix B)**. When microglia become activated, they become almost indistinguishable from macrophages, however we were able to detect bonafide microglia based on the expression of genes such as Tmem119 (Bennett et al. 2016) and P2ry12 (Butovsky et al. 2014) as well as the increased expression of HexB (Masuda et al. 2020). As such, we were able to denote cluster 7 as a mainly microglial cluster. Interestingly, two distinct subsets of T cells were identified by the expression of CD3. We believe that one of these clusters (Cluster 8) is γδ T cells due to their expression of T cell receptor gamma constant 1 (Tcrg-C1) and T cell receptor delta constant (Tdrc), while the other consists of CD4 (Cd4) and CD8 (Cd8b1) T cells (Cluster 4) (**Appendix B: Supp Fig 2**). We also found that cells expressing mKi-67 clustered together to form cluster 6. Clusters 0 and 3 appeared to be mainly neutrophils based on the expression of Ly6g and Cd177 **(Fig 3.4B)**. However, although Cluster 1 also forms part of this super-cluster, it could not be designated as neutrophilic or macrophagic as Cd177 and Cd68 expression were both scarce in this cluster **(Fig 3.4B)**. It is possible this is a cluster of dendritic cells (DC), however we did not see high levels of Cd11c (Itgax) expression nor specific expression of other DC markers in this cluster (**Appendix B: Supp Fig 3**). Alternately, this cluster could denote an immature cell type, such as myeloid precursors. Most immature blood cells are easily defined morphologically such as through Wright-Giemsa staining but do not have well-characterized transcriptomic profiles. As such, we have currently designated Cluster 1 as an unknown myeloid cluster.

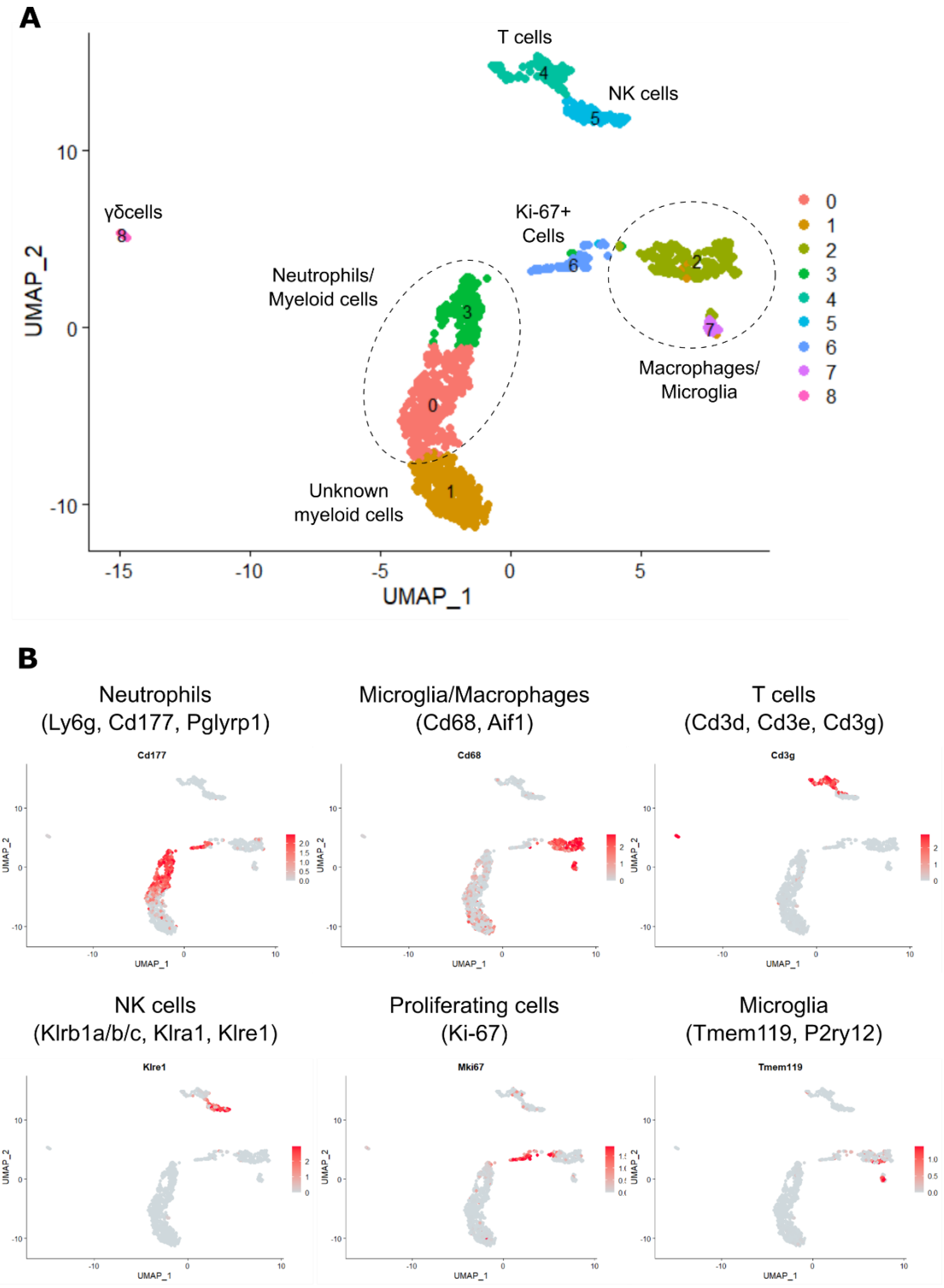

Figure 3.4 UMAP representation of scRNA-sequencing data with cluster identification. **(A)** UMAP representation showing unsupervised clustering of cells that were manually annotated based on markers that defined each cluster. **(B)** UMAP representation of markers used for annotation showing one marker from each list.

We wanted to look more closely at the myeloid cells and therefore limited our analysis to clusters expressing Cd33, a pan-myeloid marker **(Fig 3.5A)**. As I have shown that KD reduced Ccl3 and Ccl4 levels **(Fig 3.2)**, we were interested to see the expression pattern of these two cytokines. Interestingly, Ccl3 and Ccl4 had quite similar expression patterns, with higher levels in Cluster 1 **(Fig 3.5C)**. This can be compared to other cytokines such as Ccl2, which was mostly expressed in the macrophage cluster 6, and showed a distinct expression pattern from Ccl3 and 4 **(Fig 3.5C)**. Hcar2 expression is found in myeloid clusters 0, 1, and 3 but not in the macrophage or microglial clusters **(Fig 3.5D)**. It is important to note that this is mRNA expression data and may not correspond to protein levels. However, it is tempting to speculate that HCAR2 could directly impact CCL3 and 4 expression and may account for the fact that KD was only seen to affect cells expressing these two cytokines.

As well, given that KD could reduce p38 MAPK activation in Chapter 2, we were interested to see which cells expressed p38. We were able to detect 2 out of the 4 isoforms: p38α and p38δ **(Fig 3.5E)**. Expression of p38α was seen in most myeloid cells, however p38δ was not strongly expressed by macrophages or microglia and instead appears to be more highly expressed in the neutrophilic clusters. It should be noted that the antibody used for IF analysis of P-p38 in Chapters 2 and 3 detects phosphorylated versions of all 4 protein isoforms.

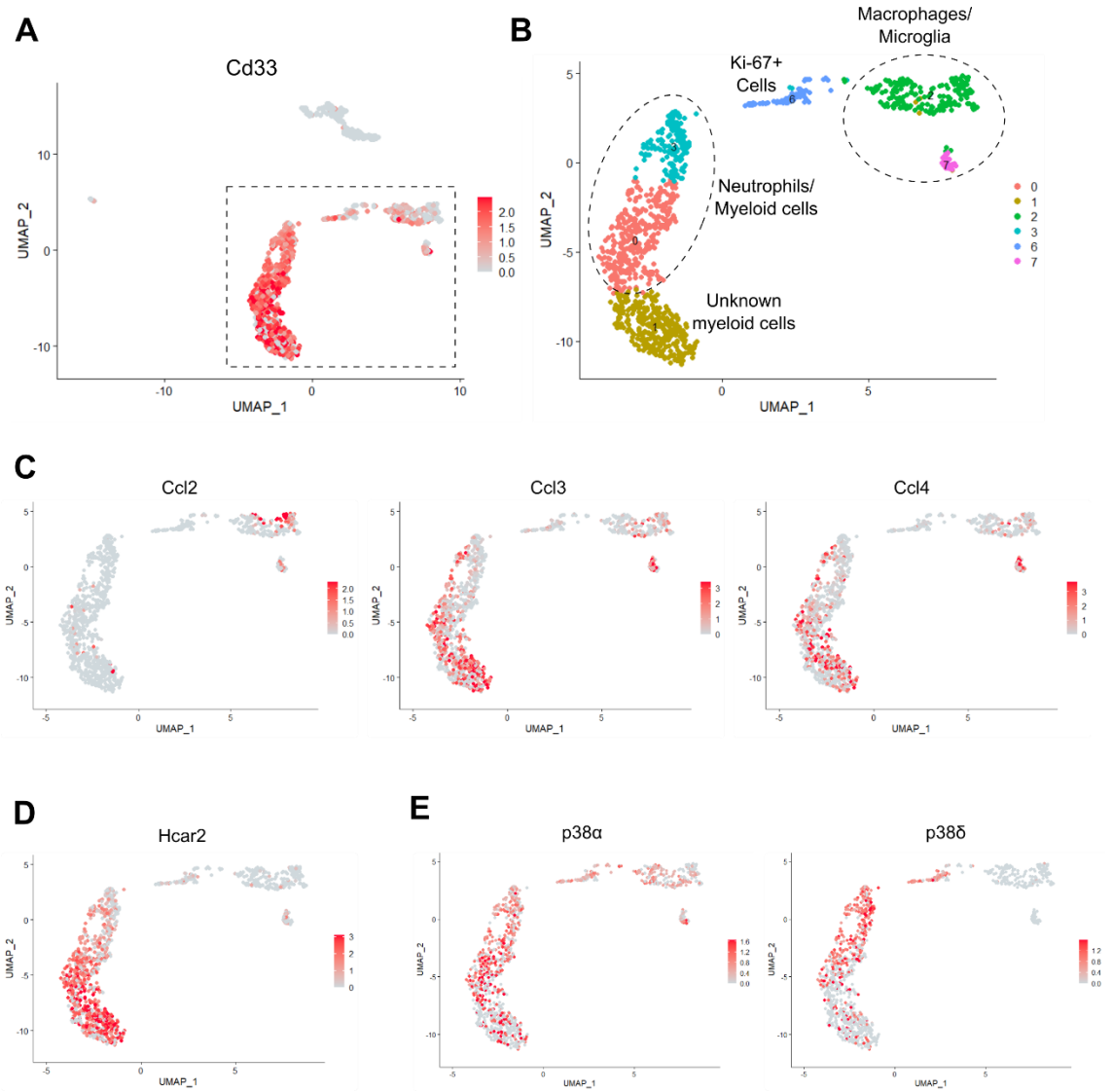

Figure 3.5 Exploration of myeloid (CD33 positive) clusters. **(A)** UMAP representation showing expression of Cd33 to identify myeloid cells. **(B)** UMAP representation of myeloid subset showing classification of clusters. **(C)** UMAP representation of Ccl2, Ccl3, and Ccl4 expression in myeloid subset. **(D)** UMAP representation of Hcar2 expression in myeloid subset. **(E)** UMAP representation of p38α and p38δ MAPK expression.

We also used our scRNA-sequencing data to look at the different sub-types of macrophages present in the injury site at 7DPI. The M1/M2 paradigm has been historically used to classify pro- and anti-inflammatory macrophages, respectively (Kigerl et al. 2009). This classification has been further applied to the injured spinal cord, where a high M1 to M2 ratio was found following injury and M2 macrophages were found to promote regenerative growth (Kigerl et al. 2009). Although the M1/M2

paradigm is understood to be an oversimplification, it is still unclear how different macrophage activations states should be properly characterized (Fernando O Martinez and Gordon 2014; Nahrendorf and Swirski 2016). Unfortunately, we saw little to no expression of the canonical M1 and M2 markers Nos2 (iNos) or Arg1 **(Fig 3.6A and B)**. Furthermore, there was little overlap in expression across different M1 or M2 markers **(Fig 3.6A and B)**. Similar results were seen looking at factors commonly secreted by M1 and M2 macrophages **(Appendix B: Supp Fig 4)**. Again, it's important to remember that these data are for RNA expression, not protein levels. However, this suggests that macrophages cannot be easily classified by M1 or M2 status in our current scRNA-sequencing dataset.

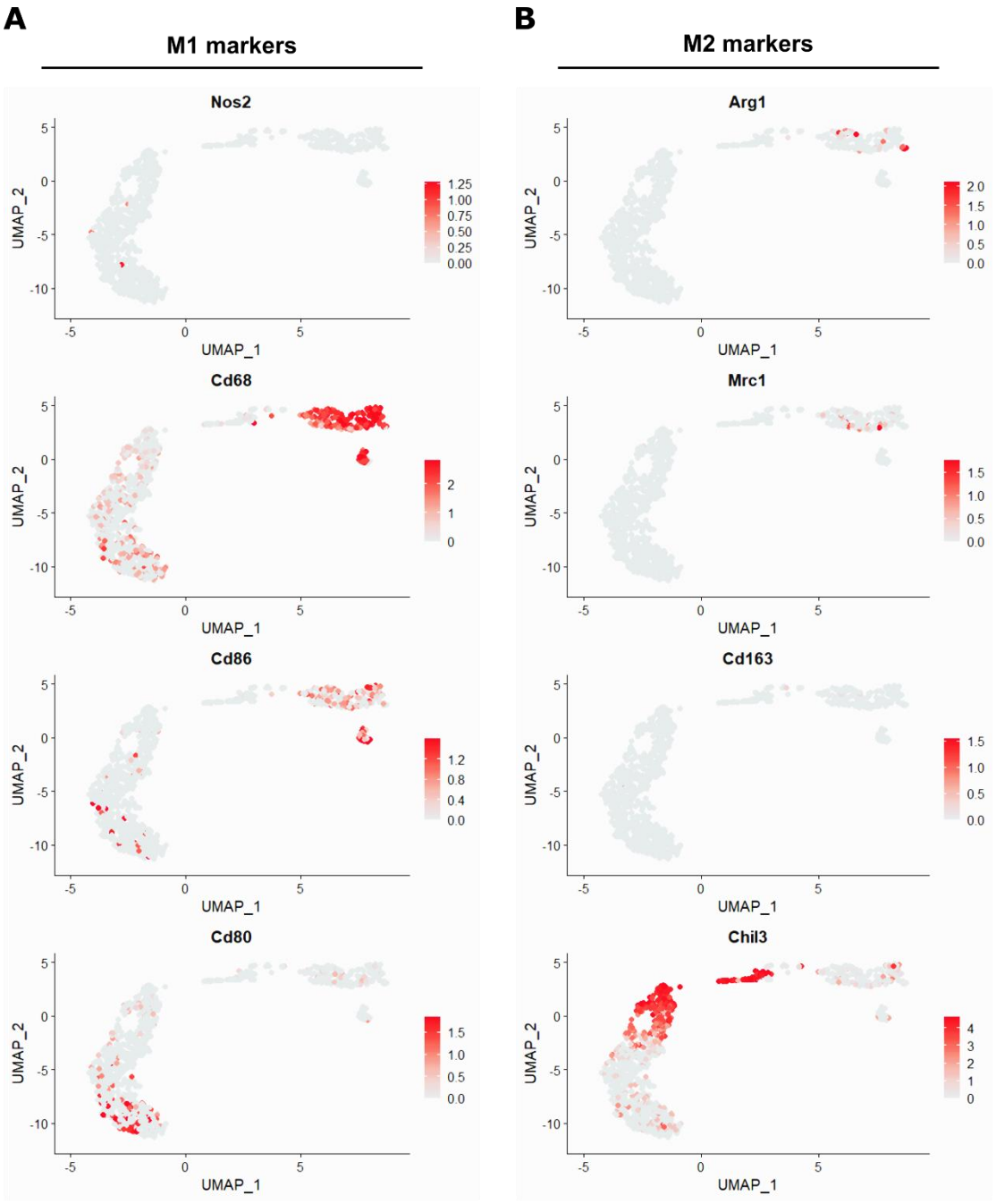

Figure 3.6 M1 and M2 marker expression in myeloid cluster. **(A)** UMAP representation of M1 markers: Nos2 (iNos), Cd68, Cd86, and Cd80. **(B)** UMAP representation of M2 markers: Arg1, Mrc1 (Cd206), Cd163 and Chil3 (Ym1).

We also assessed differences in gene expression between SD and KD-fed mice at 7DPI. A UMAP representation of the SD and KD scRNA-sequencing clusters is shown in **Fig 3.7A.** The lower

number of cells in the KD group can be seen both in the UMAP representation and in cell numbers by cluster **(Fig 3.7B)**. To look at the distribution of each group, we calculated the percentage of cells in each cluster per the total number per group (n=1) **(Fig 3.7B)**. Interestingly the distribution of KD cells led to higher percentages of cells in Cluster 0 and 3, which are a mix of myeloid cells and neutrophils. We also saw a lower percentage of KD cells in clusters 2, 4, and 5, which are macrophages, T cells, and NK cells, respectively.

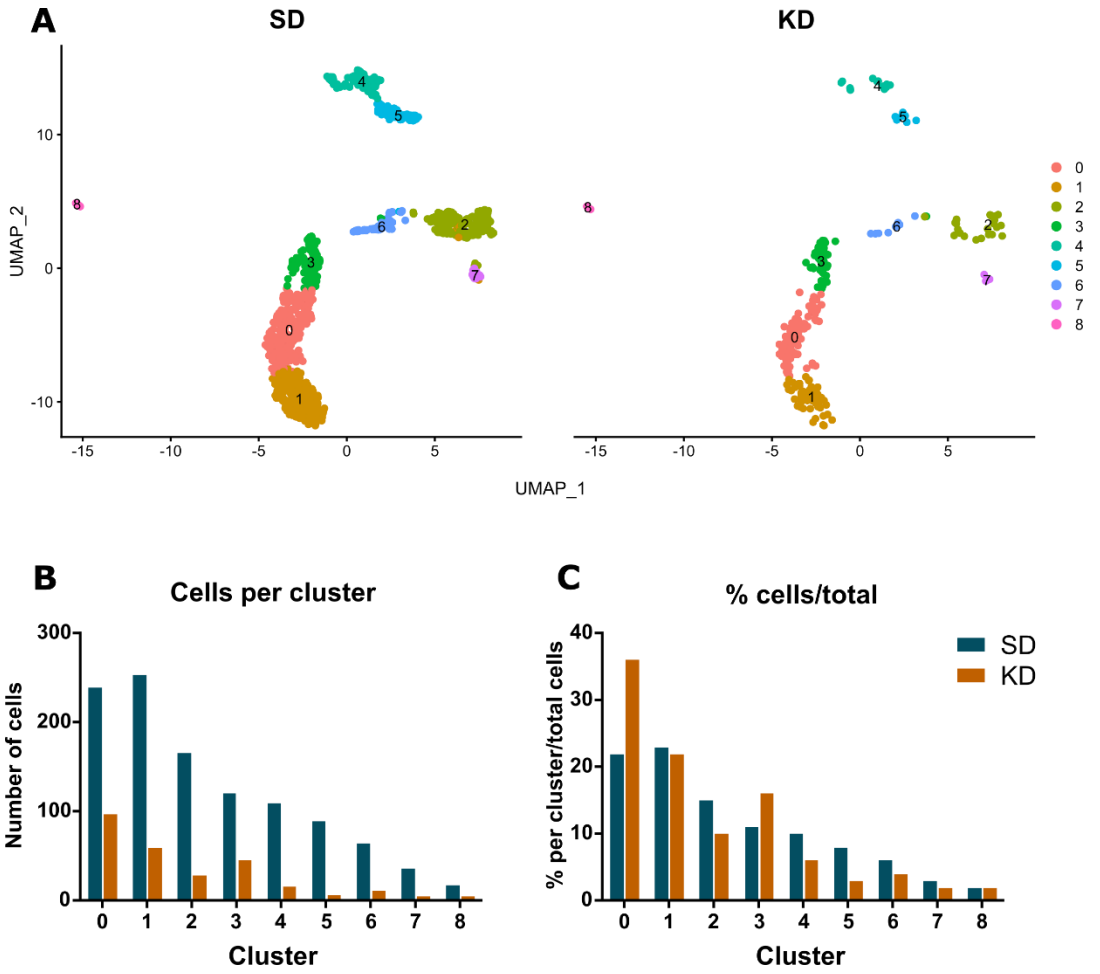

Figure 3.7 Comparison of SD and KD clusters. **(A)** UMAP representation separating cells in SD and KD conditions. **(B)** Graph of number of cells per cluster separated by SD and KD cells. **(C)** Graph of the percent of cells in each cluster divided by the total number of cells in the SD or KD condition.

We also identified genes that showed significantly altered expression in our KD compared to SD group **(Table 3.3)**. Surprisingly, all genes identified were downregulated by KD. Interestingly, this includes Ccl4 **(Table 3.3**), which is in line with our cytokine results **(Fig 3.2**). Ccl3 is also

downregulated but not in the Top 20 genes and thus isn't seen in **Table 3.3**. Some specific cell types also may be downregulated by KD as indicated by the decrease in cell markers, for example: Nkg7 as a marker for NK cells, Elane as a marker for neutrophils, and Cd74, H2-Aa, and H2-Eb1, which are expressed by antigen presenting cells such as macrophages. We also saw multiple ribosomal subunits downregulated by KD **(Table 3.3)**, possibly indicating a global effect of KD on translation. As well, one of the most downregulated genes is Granzyme A (**Table 3.3**). Granzyme A can cause production of ROS (Kiselevsky 2020), suggesting that downregulation of Granzyme A could be one method through which KD can reduce ROS production, which was previously shown (Milder and Patel 2012).

Table 3.3 Top 20 genes differentially regulated by KD with average Log fold change (LogFC) between SD and KD, and the Bonferroni adjusted p-values.

Gene	**Description**	**Average LogFC**	**Adj. p-value**
Gzma	Granzyme A	-1.33	1.02E-51
Cd74	HLA class II histocompatibility gamma chain	-0.85	3.35E-26
Ccl5	Chemokine (C-C motif ligand	-0.85	9.47E-29
H2-Aa	H-2 class II histocompatibility chain	-0.83	0.003
AW112010	Small secreted protein interferon-induced	-0.77	2.11E-09
Elane	Elastase, Neutrophil Expressed	-0.76	1.73E-95
Prtn3	Proteinase 3	-0.74	3.01E-94
H2-Eb1	H-2 class II histocompatibility chain	-0.66	1.62E-09
C1qa	Complement C1q A Chain	-0.58	0.003
Ms4a4b	CD20 homologue in T cells	-0.54	1.19E-04
Nkg7	Natural Killer Cell Granule Protein 7	-0.52	5.11E-16
Rgs1	Regulator of G-protein signaling 1	-0.52	1.55E-08
Rps18	40S ribosomal protein S18	-0.51	0.035
Xcl1	Chemokine (C motif) ligand	-0.51	2.08E-74
Rpl32	60S ribosomal protein L32	-0.50	0.003
Rpl13	60S ribosomal protein L13	-0.50	1.17E-05
Rps19	40S ribosomal protein S19	-0.49	0.007
C1qc	Complement C1q C Chain	-0.49	5.60E-19
Rplp1	Ribosomal Protein Lateral Stalk Subunit P1	-0.49	8.82E-05
Ccl4	Chemokine (C-C motif ligand)	-0.48	6.28E-17

Using the Database for Annotation, Visualization and Integrated Discovery (DAVID), we also identified KEGG pathways that were enriched in our full list of genes downregulated by KD **(Table 3.4)**. Enriched pathways are those for which the gene set in the given list is higher than would be found in the mouse genome by random chance. For example a 10-fold enrichment means 10% of the list of genes are found in this pathway as opposed to only 1% in the mouse genome (Huang, Sherman, and Lempicki 2009b). We found multiple immune pathways enriched in our list of downregulated genes including antigen processing and presentation, NF-kappa B signalling pathway, Toll-like receptor signaling pathway, Chemokine signaling pathway, and Cytokine-cytokine receptor interaction. Ribosomes are also downregulated by KD suggesting a decrease in translation. Together these results support the role of KD in decreasing inflammation and again suggest that this could modulate specific cytokine levels including Ccl3 and Ccl4.

Table 3.4 Select KEGG pathways enriched in KD altered genes.

KEGG Pathway	Fold Enrichment	P-value	Genes
Antigen processing and presentation	14.43	9.58E-07	CTSL, LGMN, H2-EB1, H2-AA, H2-Q7, KLRD1, CD74, HSPA8
Ribosome	14.28	5.70E-12	RPL13, RPL36, RPS15A, RPL39, RPS5, RPS8, RPS18, RPS19, RPS28, RPL32, RPL13A, RPLP0, RPLP1, RPS11
NF-kappa B signaling pathway	6.10	0.026	BCL2A1B, BCL2, CCL4, CD14
Lysosome	6.06	0.008	CTSL, LGMN, CTSC, CTSG, CTSW
Toll-like receptor signaling pathway	5.86	0.029	CCL3, CCL5, CCL4, CD14
Phagosome	4.32	0.026	CTSL, H2-EB1, H2-AA, H2-Q7, CD14
Chemokine signaling pathway	3.77	0.040	CCL3, CCR2, CCL5, XCL1, CCL4
Cytokine-cytokine receptor interaction	3.67	0.021	CCL3, CSF1, CCR2, CCL5, XCL1, CCL4

3.3.3 Weight and BHB levels

Following our experiments looking at inflammation and cell types in WT (HCAR2+/+) mice, we aimed to investigate the role of HCAR2 in KD-mediated inflammatory reduction through use of the HCAR2-/- mouse line. To begin with, we analyzed weight loss, BHB levels, and glucose levels for SD and KD-fed WT and HCAR2-/- mice. Both HCAR2+/+ and HCAR2-/- mice fed either SD or KD showed statistically significant weight loss compared to non-injured animals **(Fig 3.8D**). We also saw statistically significant weight loss in the KD-fed mice compared to SD-fed mice but only in the

HCAR2-/- mice and only at 5 and 6DPI **(Fig 3.8A)**. As well, this was not seen in our 2nd cohort of animals **(Fig 3.8D)** suggesting it may not be a reproducible trend.

Across both experiments we saw an increase in BHB levels by 7DPI for KD-fed animals of either HCAR2+/+ or HCAR2-/- genotype **(Fig 3.8B and E)**. It is interesting to note that the HCAR2-/- animals show more variability in KD levels at this timepoint however the 'n' was fairly low in both experiments. We also tested glucose levels in all groups. At 7DPI there was a trend towards decreased glucose levels in the KD group, which was statistically significant in one cohort (**Fig 3.8C and F**). Again, the low 'n' and differences in significance between the two experiments make it hard to say for certain whether this a reproducible result. Together these data show that WT and HCAR2-/- mice show a similar response after injury.

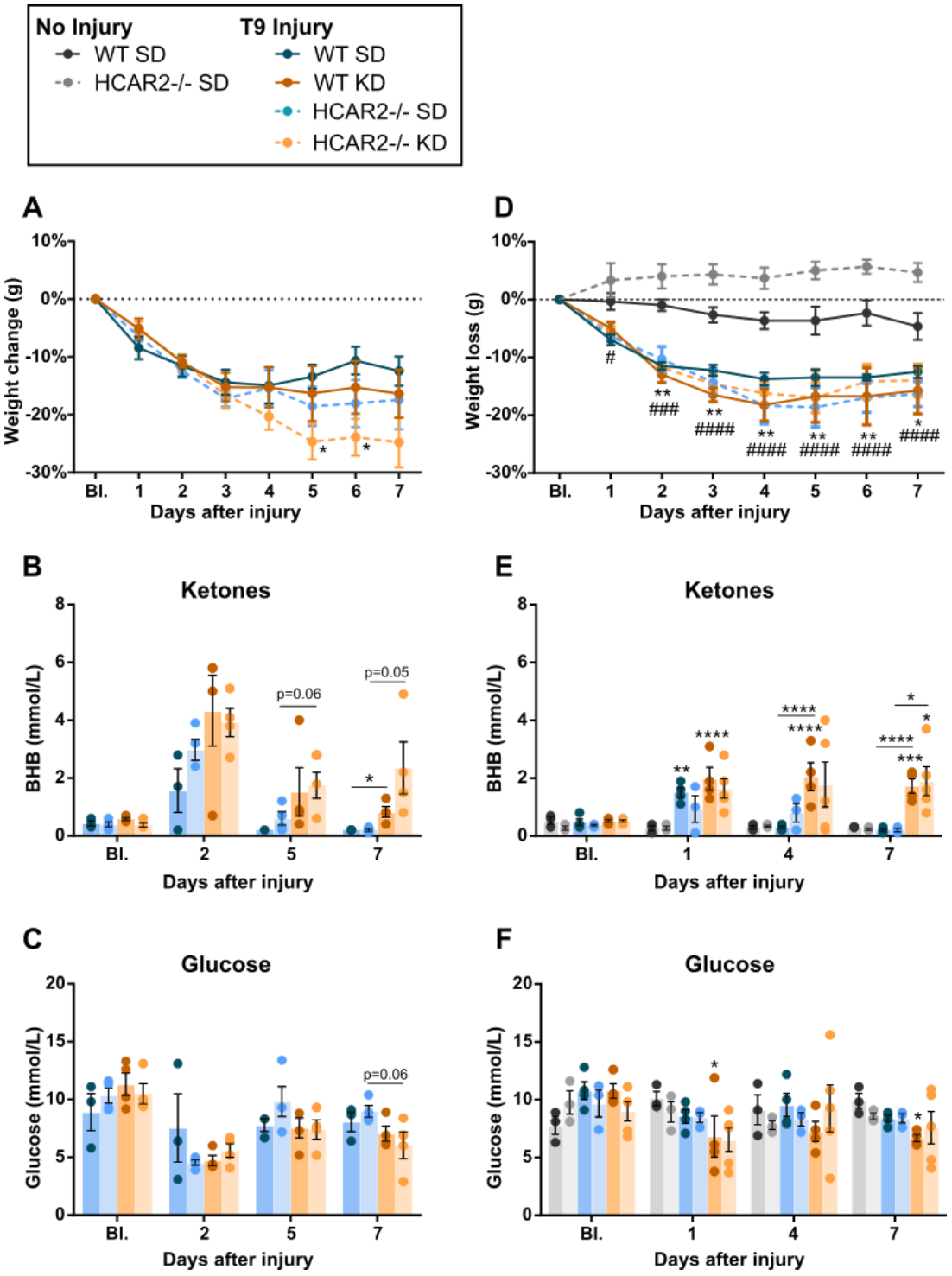

Figure 3.8 Weight, BHB, and glucose levels of mice used in flow Cytometry **(A-C)** and IF **(D-F)** experiments. **(A)** Percent weight change compared to baseline weight. * HCAR2-/- KD compared to HCAR2-/- SD. **(B)** BHB and **(C)** Glucose levels. **(D)** Percent weight change compared to baseline weight. * WT SD/KD vs WT No injury. # HCAR2-/- SD/KD vs HCAR2-/- No injury. **(E)** BHB and **(F)** Glucose levels. Unless otherwise indicated * compares to No Injury of same genotype. * p<0.05,

** p<0.01, *** or ### p<0.001, **** or #### p<0.0001 calculated using Two-way ANOVA with Tukey correction.

3.3.4 Analysis of inflammatory cells at the injury site by flow cytometry

To assess the impact of KD on activated macrophages/microglia at the injury site, we performed flow cytometric analysis from the isolated lesion epicenter **(Fig 3.9A)**. All immune cells in the injury site can be distinguished from other non-immune cells by the presence of CD45, and mature myeloid cells (including neutrophils, macrophages, and microglia) can then be differentiated from lymphoid cells (such as T and B cells) by the expression of CD11b. Neutrophils can also be identified using GR-1, an antibody that detects Ly6C and Ly6G. Thus, $CD45^{+}CD11b^{+}GR\text{-}1^{-}$ cells are myeloid cells encompassing NK cells, macrophages, microglia, and other unknown myeloid cells. We did not see significant differences in $GR\text{-}1^{+}$ myeloid cells (likely neutrophils) between our groups **(Fig 3.9B)**. However, $CD45^{+}CD11b^{+}GR\text{-}1^{-}$ cells showed a significant decrease with KD treatment, which was abrogated by loss of the HCAR2 receptor **(Fig 3.9C)**. It is unclear if this population is infiltrating macrophages or activated microglia, as we do not see any clear $CD45^{lo}$ and $CD45^{hi}$ populations. Together these data indicated that KD can reduce the number of non-neutrophilic myeloid cells at the injury site and that this requires the HCAR2 receptor.

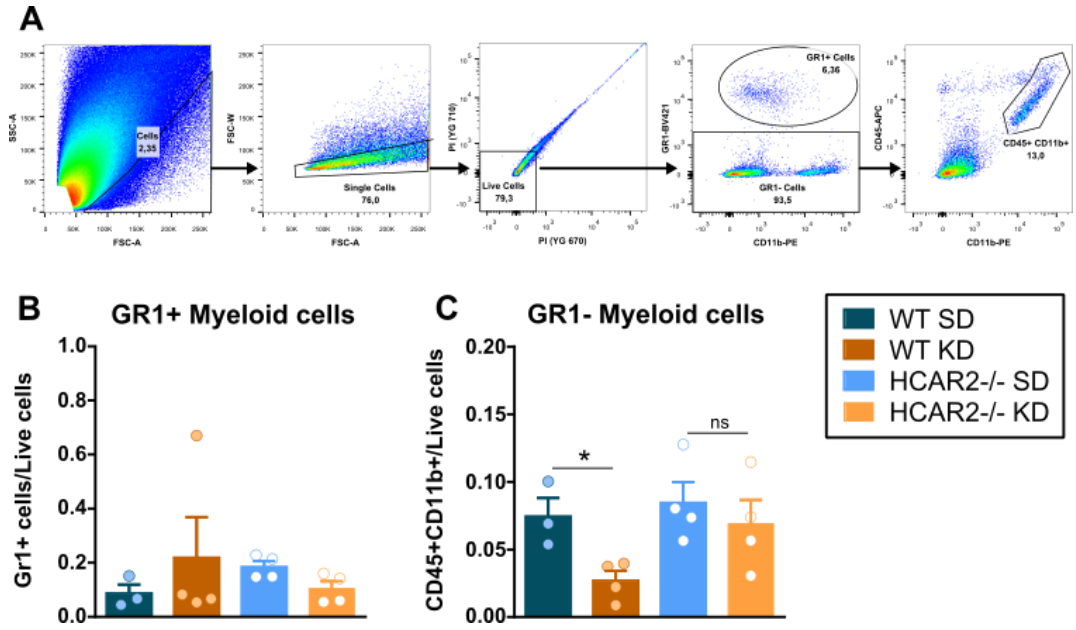

Figure 3.9 Flow cytometry analysis of $CD45^{+}CD11b^{+}$ immune cells at injury epicenter 7 days after injury. **(A)** Flow analysis showing gating strategy to detect macrophages/microglia. **(B)** $Gr1^{+}$ myeloid

cells compared to live cells. **(C)** $CD45^{+}CD11b^{+}GR1^{-}$ myeloid cells compared to live cells. * $p<0.05$ calculated using a T-test.

3.3.5 Analysis of inflammation at the injury site by IF

While flow cytometry analysis indicated that KD could reduce levels of inflammatory cells at the injury site, we wanted to determine how macrophage/activated microglia numbers changed rostral and caudal to the injury site. Iba1 was used as a general marker for macrophages and microglia. As expected, we saw an increase in IF area towards the injury epicenter **(Fig 3.10B)**. However, we saw no significant differences between SD and KD-fed mice regardless of genotype **(Fig 3.10B)**.

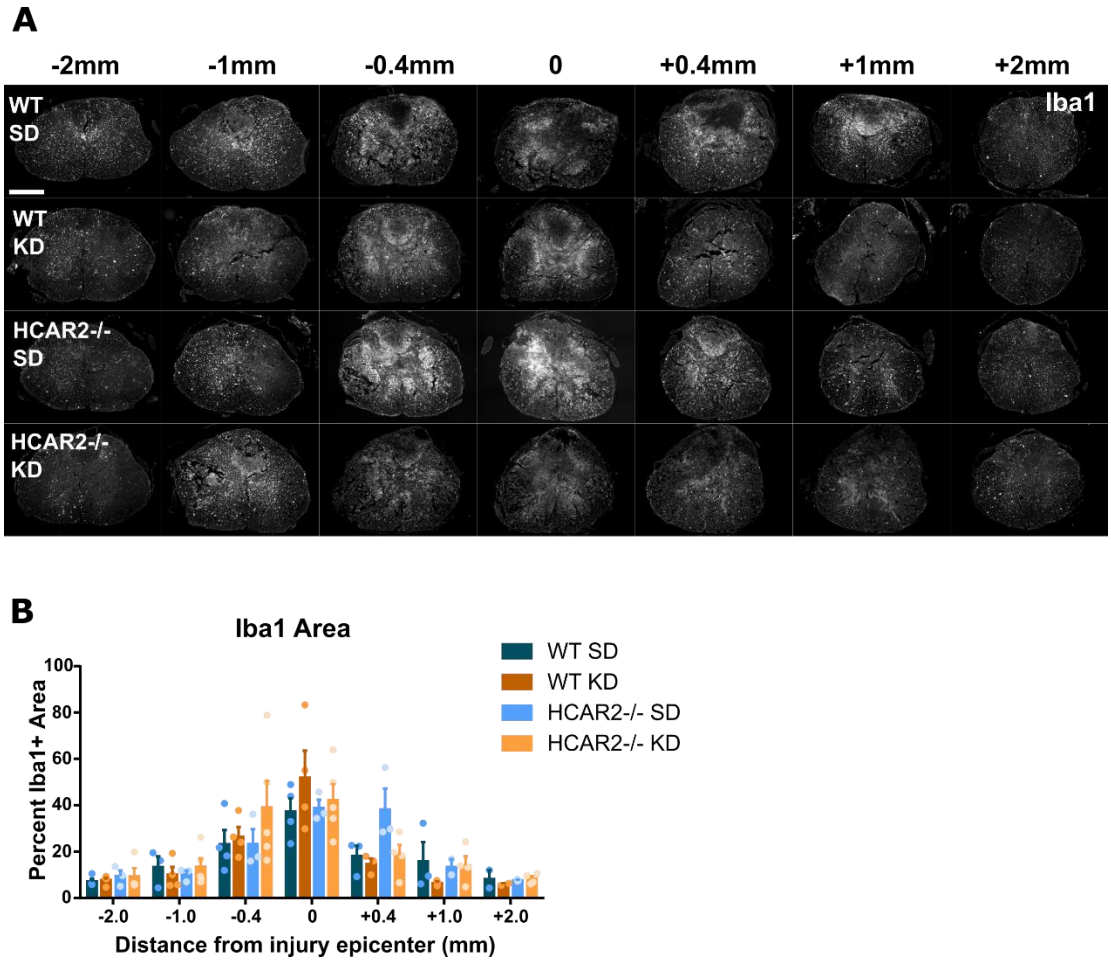

Figure 3.10 Analysis of Iba1 at 7 days after injury. **(A)** Representative sections with Iba1 IF. Scale bar is 0.5mm. **(B)** Percent Iba1+ area compared to cord area for each section (1 section per mouse per timepoint).

As we saw that KD could significantly reduce P-p38 after the C4 DLF crush injury **(Fig 2.5)**, we were interested to see if this required the HCAR2 receptor. Surprisingly, after the T9 contusive injury, we instead saw increased P-p38 at 7DPI with KD **(Fig 3.11A and B)**. As well, this increase was not seen in HCAR2-/- mice suggesting it is mediated by activation of this receptor **(Fig 3.11B)**. Similar increase in P-p38 was seen with KD by Western Blot (data not shown).

We only assessed the epicenter as little to no staining of P-p38 was seen in rostral and caudal sections (data not shown). Together these IF results suggest that KD can increase activation of the p38 MAPK pathway at 7 days following a T9 contusive injury and that this occurs through the HCAR2 receptor.

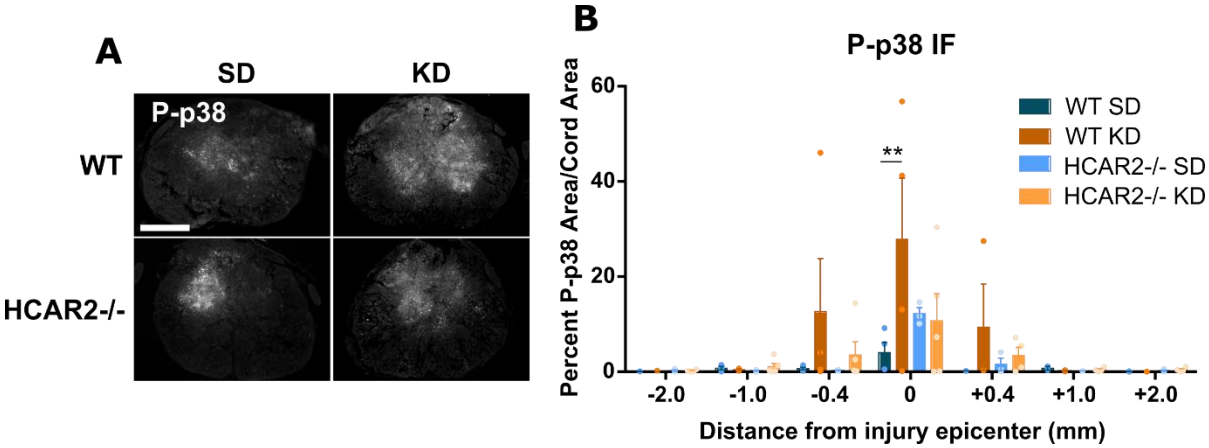

Figure 3.11 Analysis of P-p38 MAPK (P-p38) at 7 days after injury. **(A)** Representative images of P-p38 IF at the injury epicenter. Scale bar = 0.5mm. **(B)** Quantification of percent P-p38 area compared to cord area for each section (1 section per mouse per timepoint). ** $p<0.01$ calculated using a Two-way ANOVA with Sidak correction.

3.3.6 Analysis of white matter sparing and neuronal cells at the injury site

Given our new findings for KD regarding P-p38 MAPK, we were also interested to see if there were any changes in white matter sparing or neuronal counts at this timepoint. We used ECR staining to quantify white matter sparing and compared the white matter in the injured cord to an average of the uninjured cord **(Fig 3.12)**. A ratio closer to 1.0 indicates greater sparing. While we saw a decrease in white matter sparing around the epicenter, as expected, there were no significant differences between groups **(Fig 3.12)**.

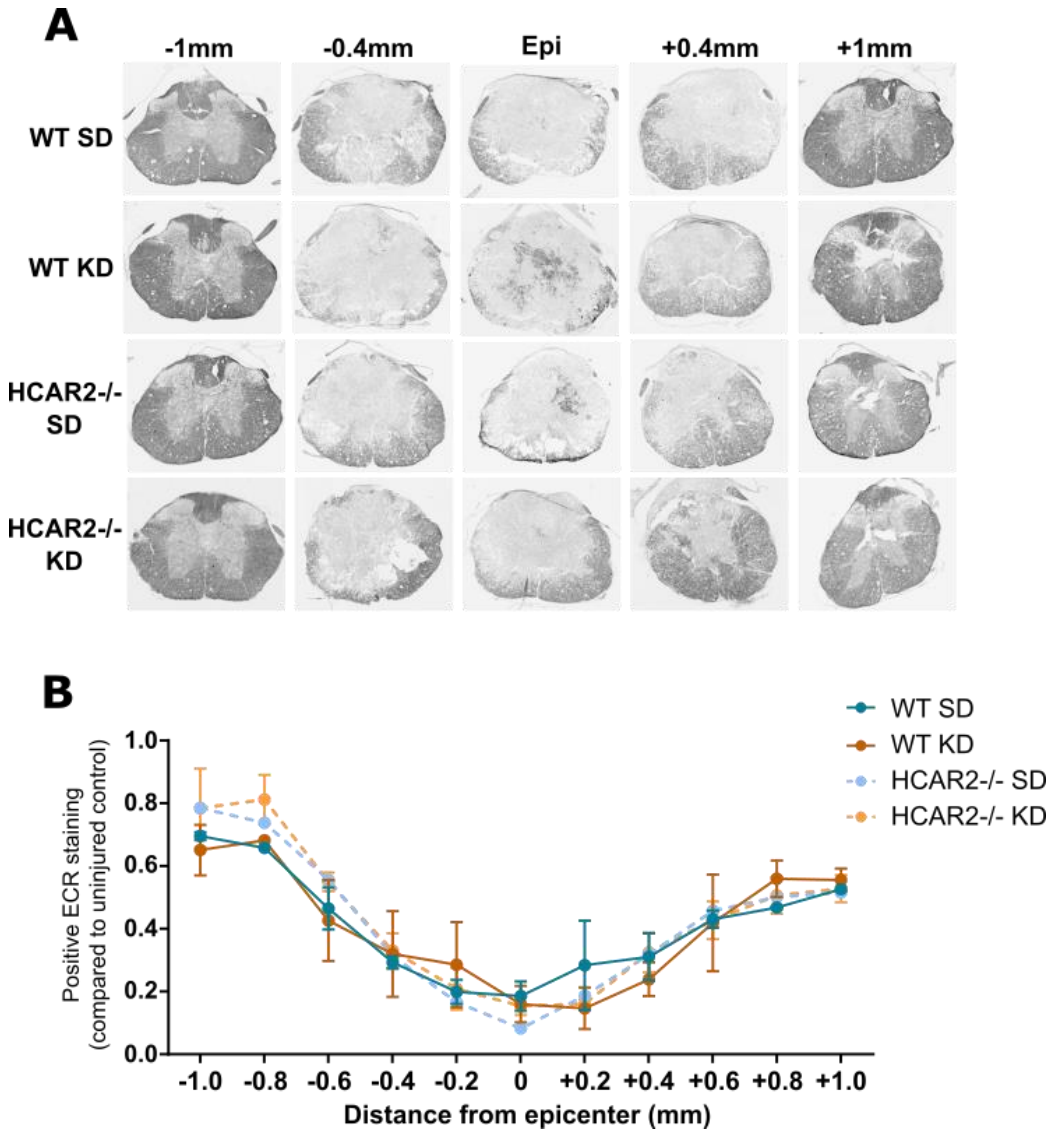

Figure 3.12 Analysis of white matter sparing using ECR stain at 7 days after injury. **(A)** Representative images of ECR stained sections. Animals per condition: WT SD = 3, WT KD = 3, HCAR2-/- SD = 1, HCAR2-/- KD = 3. Note that number of sections varied per position from epicenter as some sections were lost or torn during staining process. **(B)** Quantification of positive ECR staining compared to the average positive score for uninjured tissue (1 section per mouse).

We also counted NeuN+ neurons in each section. We saw a significant decrease at the epicenter for all groups **(Fig 3.13A and B)**. However, we did not see any significant differences between SD and KD at the epicentre or caudal to the injury (**Fig 3.13B)**. Interestingly, at -2mm we saw a marked drop in NeuN+ cells from WT SD mice that was significant compared to HCAR2-/- SD and KD mice but

not WT KD mice **(Fig 3.13B)**. It is unclear why this drop occurred. Together these data provide no evidence that KD promotes white matter or neuronal sparing at this 7-day timepoint in mice.

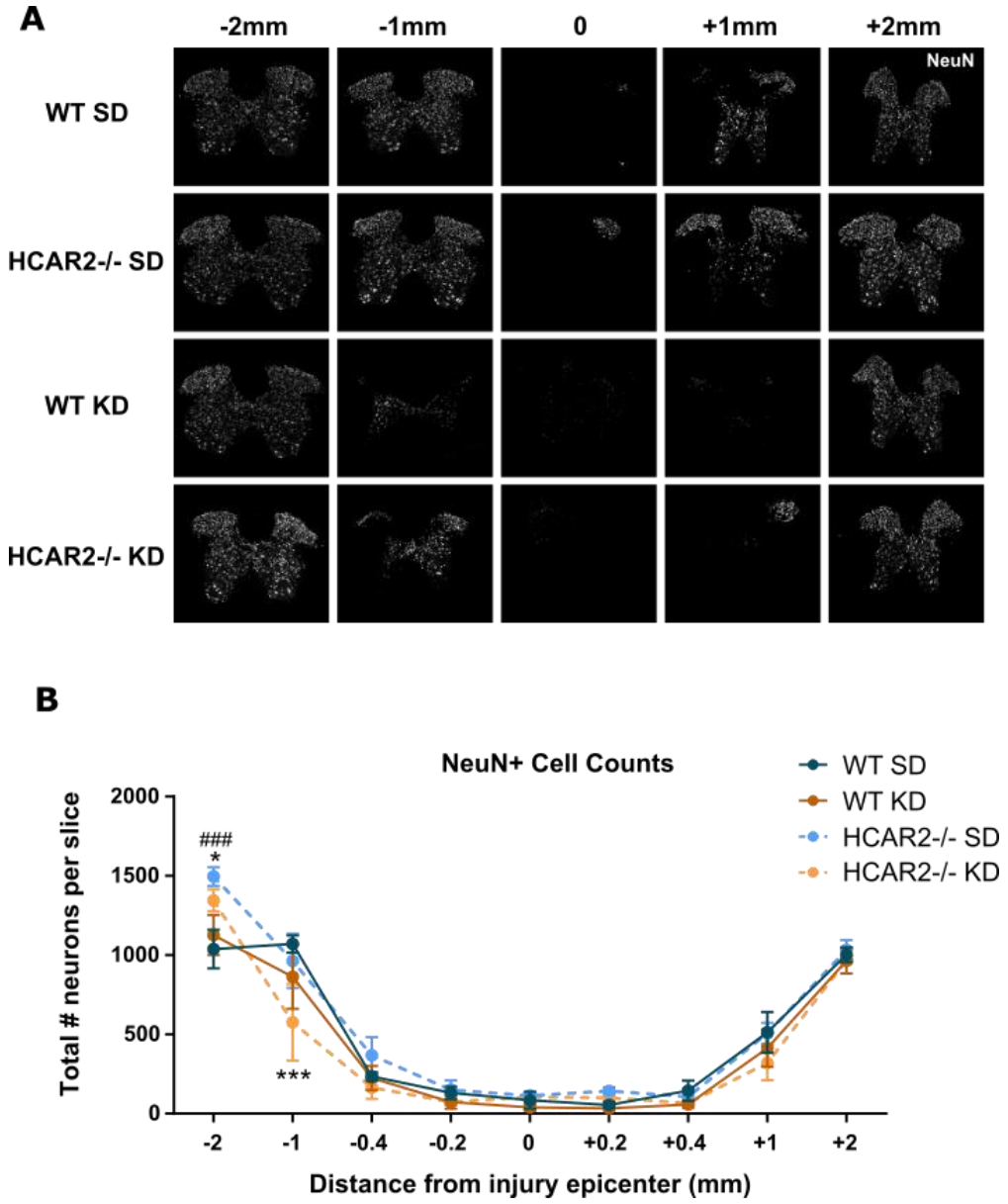

Figure 3.13 Analysis of NeuN+ cells at 7 days after injury. **(A)** Representative images of NeuN+ cells. **(B)** Quantification of NeuN+ cell count. * HCAR2-/- KD vs. WT SD, # HCAR2-/- SD vs WT SD. *p<0.05 and *** or ### p<0.001 calculated using a Two-way ANOVA with Tukey correction.

3.3.7 *In vitro* analysis of HCAR2 and inflammation in BMDMs

KD can reduce inflammation after spinal cord injury and our flow cytometry results suggest this requires the HCAR2 receptor, which is activated by BHB. On the other hand, we also see activation of p38 MAPK through HCAR2 at 7DPI. Given these contradictory results we wanted to assess the effect of BHB on inflammatory markers in BMDMs and this role of the HCAR2 receptor in this *in vitro* system. BMDMs were isolated from the femurs of HCAR2+/+ and HCAR2-/- mice and cultured for 6 days with L292-conditioned media. Mature BMDMs were incubated with 0.1µg/mL LPS and 1, 4, or 8mM BHB for 24 hours *in vitro*. Expression of CD80 and CD86 were then analyzed by flow cytometry. CD80 and CD86 are co-stimulatory molecules that can interact with T cell receptors to activate inflammation. Their presence on the cell surface makes them easy to analyze by flow cytometry. As well, CD80 and CD86 are thought to be markers of M1 macrophages (Fernando Oneissi Martinez et al. 2008). It has been shown that M1 macrophages infiltrate the spinal cord after injury and form the predominant macrophage subtype by 7DPI. If KD is affecting macrophage subtypes through the HCAR2-/- receptor, we would also hypothesize that BHB can reduce expression of M1 markers *in vitro* and that this would require the HCAR2 receptor. Cell-surface CD80 and CD86 increased after 24hr LPS expression but were not affected by BHB concentration **(Fig 3.14A)**. Interestingly, expression of both molecules was significantly lower in HCAR2-/- BMDMs irrespective of BHB presence **(Fig 3.14A).** We decided to repeat the experiment and test CD80/CD86 expression at 3hr, 24hr, and 72hr **(Fig 3.14B)**. Surprisingly, it wasn't until 72hrs that we saw decreased expression of CD80 and CD86 in HCAR2-/- mice. Together these data point to a role of HCAR2 in increasing CD80 and CD86 that is independent of BHB.

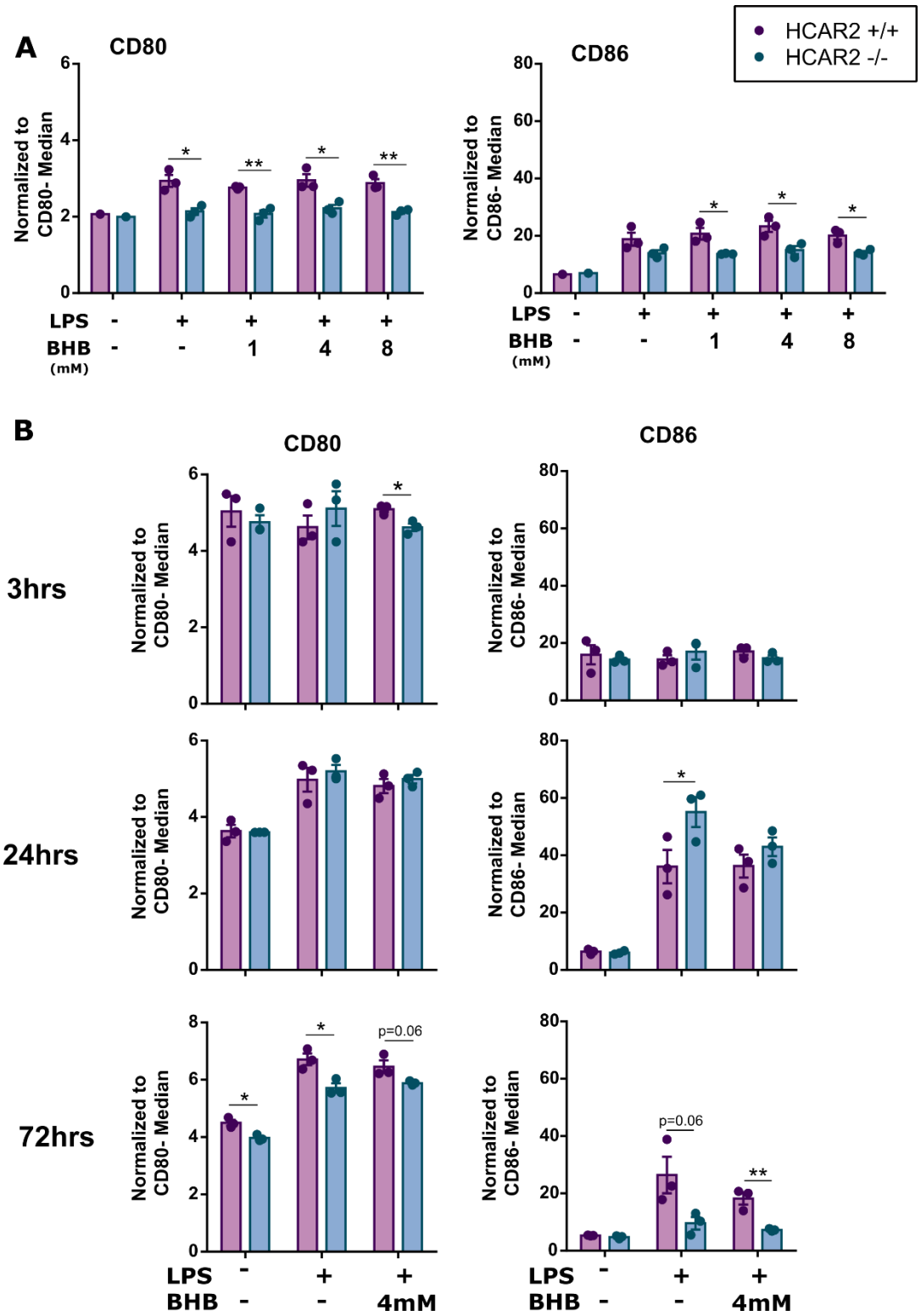

Figure 3.14 BHB treatment of *in vitro* BMDM cultures challenged with LPS. Flow cytometry was used to detect CD80 and CD86 positive fluorescence. **(A)** CD80 and CD86 median positive fluorescence normalized to negative signal after 24-hours treatment with LPS and BHB as indicated.

(B) CD80 and CD86 positive fluorescence compared to negative signal after 3, 24, or 72-hours of treatment with LPS and 4mM BHB as indicated. * $p<0.05$, ** $p<0.01$ calculated by unpaired T-test.

3.4 Discussion

We found that KD can specifically reduce pro-inflammatory cytokines CCL3 and CCL4 after a T9 contusive injury **(Fig 3.2)**. Our scRNA-sequencing data further confirms that KD can downregulate Ccl3 and Ccl4 expression at 7DPI **(Table 3.3)** and that Ccl3 and Ccl4 show very similar expression patterns across cell type (**Fig 3.11C)**. Given that Ccl3, Ccl4 and Hcar2 were expressed in similar clusters **(Fig 3.11D)**, it is tempting to speculate that modulation of these cytokines occurs through BHB activation of HCAR2. For example, a potential mechanism could involve PGE_2. Activation of HCAR2 has been shown to increase PGE_2 (Hanson et al. 2010) and PGE_2, in turn, can inhibit CCL3 and 4 (Jing, Yen, and Ganea 2004). Although this was specifically seen in dendritic cells (Jing, Yen, and Ganea 2004), it could occur in non-dendritic myeloid cells as well. Our single-cell data further suggests that KD can also downregulate NK cells and MHC-II+ cells. Similarly, through flow cytometry we found that KD can reduce $CD45^+CD11b^+Gr\text{-}1^-$ infiltration at 7DPI and that this requires the HCAR2 receptor **(Fig 3.9C)**.

Similar to the effect of KD treatment on white matter sparing and neuronal counts after the C4 DLF crush injury, we did not see improvement in either parameter with KD treatment following a T9 contusive injury **(Figs 3.10 and 3.12)**. As discussed in Chapter 2, metabolic differences between mice and rats may be one reason that we have been unable to recapitulate the KD rat findings in mice. In surprising contrast to Chapter 2, we saw that KD did not decrease levels of P-p38 at the injury epicenter by 7DPI but in fact led to an increase in P-p38 **(Fig 3.11B)**. Furthermore, this increase was not seen in the HCAR2-/- KD-fed mice suggesting that it is mediated by HCAR2. It is unclear why KD would decrease activation of the p38 MAPK pathway after a C4 crush injury but increase activation after a T9 contusive injury. One explanation could be that the impact of KD on this pathway is based on the temporal resolution of inflammation. A moderate T9 contusive injury will lead to a more pronounced inflammatory response indicated by the larger lesion size. Although sections were cut longitudinally after the crush versus cut cross-sectionally following the contusive injury, comparison of the P-p38 MAPK levels **(Fig 2.5A and Fig 3.11A)** leads to the reasonable assumption that the area of positive fluorescence, and thus cells expressing P-p38, is higher after the T9 contusive injury than the crush injury. It is tempting to speculate that the C4 crush injury reaches a plateau state of recovery earlier than the T9 contusive injury and thus may be at a different temporal

state of inflammation by 7DPI. KD could initially increase P-p38 activity during early stages of inflammation leading to compensatory mechanisms that cause more reduction of P-p38 in the KD-fed mice. Indeed, a similar mechanism has been proposed for how KD leads to an overall reduction in ROS following SCI. For example, rats fed KD showed increases in mitochondrial H_2O_2 and 4-hydroxynonenol in the hippocampus at 1 to 3 days following initiation of diet (Milder, Liang, and Patel 2010). However, after 3 weeks of KD, mitochondrial H_2O_2 was significantly decreased while the Nrf2 detoxification pathway and its targets were upregulated (Milder, Liang, and Patel 2010). Interestingly, in addition to inflammation, the p38 MAPK pathway can also be induced by ROS (Son et al. 2011). It is possible that the temporal regulation of KD on ROS and the Nrf2 pathway could induce an initial increase in p38 phosphorylation followed by a compensatory downregulation. However, future experiments will be needed to confirm this mechanism.

To determine if HCAR2 can specifically reduce pro-inflammatory macrophages, we turned to LPS stimulation of BMDMs *in vitro*. CD80 and CD86 are ligands for the T cell receptors CD28 and CD152, which can either stimulate or inhibit the T cell response, respectively (Sansom, Manzotti, and Zheng 2003). Although CD80 and CD86 are co-stimulatory, it's thought that CD80 may activate CD152 in the absence of CD86 leading to inhibition of T cell activation, but together they can activate CD28 instead leading to activation of T cells (Sansom, Manzotti, and Zheng 2003). As there wasn't a clear population of double-positive CD80 CD86 cells, we decided to look at the median fluorescence of each ligand normalized to its negative signal. Interestingly, there was a larger increase in CD86 fluorescence than CD80 following LPS activation of BMDMs that peaked at 24hrs **(Fig 3.14B)**. Unfortunately, we saw no effect of BHB on expression of these markers. However, we did see an effect of the HCAR2 receptor, which appeared to have a temporal role. At 24 hours of LPS treatment, higher CD86 expression was seen in absence of this receptor; however, by 72 hours, there was significantly lower expression of both CD80 and CD86 for HCAR2-/- BMDMs **(Fig 3.14B)**. There was a discrepancy in timing between our initial **(Fig 3.14A)** and secondary experiments **(Fig 3.14B)**, where we looked at titration of BHB and temporal effect of BHB, respectively. In our early experiment, the decrease in CD80 and CD86 with HCAR2-/- BMDMs was seen as early as 24hrs **(Fig 3.14A)**. The first experiment was done with BMDMs collected from 10-wk old female mice while the second experiment was done with BMDMs from 15-wk old male mice. Either the age difference or the sex difference could account for the delayed timing of the HCAR2-mediated decrease in the repeated experiment. Interestingly, at 24hr we saw a substantial increase in CD86 (even higher than previously seen), which was significantly increased in the HCAR2-/- group **(Fig 3.14B)**. It's possible

that the HCAR2 receptor may have a role in prolonging CD80/CD86 expression at the cell surface although further investigation is needed.

Together our findings in Chapter 3 indicate that BHB and HCAR2 can impact inflammation – both in concert, as seen with the flow cytometry and p38 IF experiments, and separately, as seen in our *in vitro* experiments. As well, our *in vitro* CD80/CD86 findings and the difference in P-p38 between Chapter 2 and 3 KD experiments, could point to a temporal response of HCAR2, although further research will be needed to confirm this. Finally, our scRNA-sequencing study identified a novel population of myeloid cells that express Hcar2, which clustered closely with neutrophils and away from macrophages/microglia. Further work is needed to characterize these cells and confirm the expression of HCAR2 at the protein level. As well, an interesting future experiment is the effect of HCAR2 on cytokine production. Given that the scRNA-sequencing data shows that similar myeloid clusters express HCAR2, CCL3, and CCL4, it is possible that HCAR2 is required for KD-mediated decreases in CCL3 and CCL4. Assessing the production of CCL3 and CCL4 in the WT and HCAR2-/- mice fed SD and KD, could establish a causal role of HCAR2 in KD-mediated cytokine reduction.

Chapter 4. KE does not mimic KD treatment after C5 hemi-contusion in rats, KE alone shows modest benefits in grasping, and KD combined with KE is detrimental to acute but not long-term recovery

4.1 Introduction

Although preclinical studies in KD show promising improvements in recovery (Streijger et al. 2013) and clinical pilots show good tolerance of the diet (Yarar-Fisher et al. 2018), adherence to a restrictive diet is still a problem for many individuals. As well, it is difficult to administer a diet early after injury and levels of BHB vary with some being as low as 0.5, which is also below the EC_{50} of HCAR2 (Yarar-Fisher et al. 2018). For these reasons, a pill-in-a-bottle treatment that can produce a robust increase in BHB levels is desirable. Ketone esters are a promising alternative as they can be taken orally and can quickly raise circulating BHB levels. For example, the ketone monoester (KE) created by Dr. Kieran Clarke increases BHB levels to 3.30mM within 1.5-2.5 hrs (Clarke et al., 2012). However, it is still unclear if KE can mimic the improvements seen with KD, particularly after SCI.

To better understand the widespread changes at the injury site that KD and KE can elicit, we used a proteomic approach. 'Omic' methods are a powerful tool to identify pathways altered under specific conditions or treatments. Not only do they produce many biological insights but can be harnessed for generation of additional hypotheses. An additional benefit of proteomics is that it detects translated proteins. Detecting mRNA (via transcriptomics) can tell us about expression levels but does not always correlate with protein levels. We used liquid Chromatography with tandem mass spectrometry (LC/MS/MS) to assess changes in protein levels at the injury site in rats fed KD, KE, or KD+KE. Given that the earliest behavioural improvements with KD were not seen until 2WPI (Streijger et al. 2013), we decided to use a similar time-frame to assess proteomic changes. In particular we were interested to see if KD and KE could produce similar proteomic changes at the injury site. This is addressed in the first part of Chapter 4.

In the second part of Chapter 4, we then looked at the effect of KE on functional and behavioural recovery over 8 weeks of KE or KD+KE treatment that begun 3 hours after injury. Similar to the initial study carried out by Streijger et al. (2013), we assessed white matter sparing, neuroprotection, and behavioural improvements with KD and KD+KE treatment following a C5 hemi-contusive injury in rats. Together, Chapter 4 looks at the feasibility of using KE as an acute SCI therapeutic.

4.2 Material and Methods

4.2.1 Rat housing

A total of 78 male Sprague-Dawley rats (125-150g; approximately 6 weeks) were purchased from Charles River Laboratories (Wilmington, Massachusetts, USA) and group-housed (up to 4 rats per cage) on a reverse light-dark cycle (dark 9-21: light 21-9). Rats were acclimatized to the vivarium and handling during the first week followed by an additional 7 weeks of behavioural training. During this period, the rats were fed an *ad libitum* standard chow diet (Tekland 2020X, Envigo). All study procedures were completed in accordance with the University of British Columbia Animal Care Committee Protocols #A14-0350 and #A19-0188.

4.2.2 Treatment of adverse conditions

Several rats had adverse reactions during the experimental study. Many rats had issues with digestion due to eating of bedding from oral fixation – a known side-effect of buprenorphine. Rats were given an enema and/or gavaged with gas-X to stimulate peristalsis and promote digestion of ingested bedding. Some rats also had gavage-related respiratory issues during the first two weeks of gavage. If respiratory issues were mild (i.e. did not require immediate euthanasia) rats were given access to oxygen for 10-15 min, then placed in a warm incubator for up to 30 min. Using this treatment, respiratory issues were generally alleviated within 2-4 days. Any rats that chewed their forelimb digits (a rare but known occurrence after contusive injury and buprenorphine treatment) and experienced significant blood loss were given a one-time dose of Ensure® or Boost® nutritional drink.

4.2.3 C5 hemi-contusion SCI

Rats were anesthetized using Isoflurane and a unilateral C5 laminectomy was performed. Animals were mounted in a spinal frame with custom designed clamps and C4/C6 dorsal processes were rigidly fixed in a horizontal position (22.5° angle). A contusion force of 120 kdyn was administered

using the Infinite Horizon Impactor with an average velocity of 123 mms/s and an average displacement of 1.3 mm. For behavioural studies, rats were injured on their left or right side depending on the preferred forelimb as identified through training on the Montoya Staircase. Due to the number of animals, surgery was staggered with 4 groups of animals being injured over 4 consecutive days (1 group per day). Rats were given Lactated-Ringer's solution and buprenorphine after surgery as per the University of British Columbia Animal Care Committee Protocol #A14-0350/#A19-0188.

4.2.3 Grouping, diet, and KE administration

Of the 76 rats, the 60 that performed best in the Montoya staircase training were used for an 8-week behavioural experiment while the remaining 16 rats were used in a 2-week proteomics experiment. This selection criterium is unlikely to have introduced bias into the proteomics study as there should be no correlation between ability to learn the Monotoya staircase test and recovery from SCI with treatment. In both cohorts, rats were divided into 3 groups: SD+water, SD+KE, KD+KE. A second 2-week experiment using 18 rats was also completed with rats given SD+water, SD+KE, or KD+water. The number of animals used in each group as well as the animals lost during the experiment are outlined in **Table 4.1**. We primarily lost animals due to complications with the gavage, however one rat in the 2-wk KD+KE group was also found dead over night (a necropsy was not performed). Standard diet (SD; Bio-Serv #F5960) and ketogenic diet (KD; Bio-Serv #F5848) were administered *ad libitum* immediately after surgery. The ΔG® Ketone Ester (KE) was acquired from Dr. Kieran Clarke (University of Oxford). Rats were given 1-1.5mL KE or water by oral gavage from 1-3 times per day over the first 2 weeks for a total of 23 gavages. For more details of the 2-week gavage regimen see **Fig 4.1A**. For our 8-wk cohort, drinking water was substituted with 1:10 KE water (supplemented with 0.1g/mL Stevia in the Raw®) at Day 10 in our SD+KE and KD+KE groups. This was replaced with 1:20 KE water (+ 0.1g/mL Stevia) at Days 21 and 22 and continued till the end of the experiment. As well, the KD+KE group was switched to SD+KE at the beginning of week 7 (day 43) and remained on SD throughout the experiment. An outline of the 8-wk experiment is shown in **Fig 4.4A**.

Table 4.1 Rats used for experiments in Chapter 4. All rats were Sprague-Dawley and between 350 and 405g at the start of each experiment.

Tissue Use	Timepoint	Injury	Diet	Gavage	N	Lost
Proteomics	2WPI	C5	SD	Water	5	0
		C5	SD	KE	6	0
		C5	KD	KE	5	1
Proteomics	2WPI	C5	SD	Water	6	0
		C5	SD	KE	6	1
		C5	KD	Water	6	1
IF / Frozen	8WPI	C5	SD	Water	20	1
		C5	SD	KE	20	1
		C5	KD	KE	20	3

4.2.4 Blood BHB and glucose levels

Ketone and glucose levels were measured from blood obtained by tail prick. Precision Xtra Blood Ketone and Blood Glucose Test Strips (Diabetes Express) were used with the Precision Xtra Blood and Ketone Meter (Abbott) according to manufacturer guidelines.

4.2.5 Protein Lysate Preparation

For 2-week proteomic analysis, rats were euthanized at 14 days post-injury by 10% chloral hydrate injection. Rats were perfused with PBS and injury epicenter (approximately half the cord, 5mm in length) was harvested and flash frozen in dry ice. Protein lysate was prepared using Dounce homogenizers to disrupt tissue in Tris-EDTA SDS lysis buffer (0.01M Tris-HCl (pH 8, VWR)), 1mM EDTA (Ambion, ThermoFisher Scientific) and 0.1% SDS (VWR) with phosphatase inhibitors and protein inhibitor cocktail). Samples were spun at 14000rpm (Rotor FA-45-18-11; Eppendorf Centrifuge 5418 R) and an aliquot of supernatant was taken for LC/MS/MS. Remaining supernatant was re-homogenized with the pellet and Triton X-100 (0.6%, BDH, VWR)) was added. Samples were re-spun and resulting supernatant was then used for Western Blot analysis. Interestingly, a BCA assay of protein concentration showed around a 2-fold increase in concentration with addition of Triton X-100; possibly reflecting dissociation of additional membrane-bound proteins.

4.2.6 LC/MS/MS Proteomics

LC/MS/MS was completed using the Bruker Impact II Ultra-High Resolution Qq-Time of Flight (UHR-QqTOF) (Bruker, Billerica, Massachusetts, USA) coupled to the EASY-nLC 1000 Liquid Chromatograph (ThermoFisher Scientific) and this was carried out by the Core Proteomics Facility at UBC in collaboration with the Foster Lab. 20µg of each sample was run on a 10% SDS-PAGE gel. Samples were then in-gel trypsin digested, dimethylated, and pooled into 5 sets. Each set was fractionated into 6 fractions by basic LC then run on MaxQuant. Groups were labeled as follows: SD+water with Light, SD+KE with Medium, and KD+KE or KD with Heavy. Data from both KE experiments were normalized and combined during analysis. Analysis of normalized ratios was completed in R. Briefly, any proteins that were flagged as 'Only Identified by Site', 'Reverse', or 'Potential Contaminant' were removed. Normalized ratios were changed to log2 form and data was standardized by Z score. Data were then subset based on log2 fold-change mean above 0.5 or below -0.5, and this subset was used for p-value calculation. The FDR-adjusted p-value (Q-value) was also calculated. The Database for Annotation, Visualization and Integrated Discovery (DAVID) 6.8 (Huang, Sherman, and Lempicki 2009b; 2009a) was used to identify GO terms and KEGG pathways enriched in the data sets.

4.2.7 Western Blot

Proteomic samples were prepared for Western blot as described in Section 4.2.5. They were then further processed by combining in a 2:1 ratio with 3X sample buffer (0.2M Tris (pH 6.8), 4% SDS, 40% glycerol (VWR), and 1mg/mL Bromophenol blue (MilliporeSigma)) containing 15% β-mercaptoethanol (Bio-Rad, Hercules, California, USA) and boiled for 5 minutes before loading. Approximately 40µg of protein was loaded per well as calculated using the Pierce BCA assay. Samples were run in 4% separating and 12% resolving gels at 100-130V then transferred to Immobilon-P PVDF membrane (MilliporeSigma) overnight at 40V, 4ºC. Membranes were briefly washed in distilled water then stained with Ponceau S solution (MilliporeSigma) to confirm bands. Membranes were blocked with 3% bovine serum albumin (BSA, MilliporeSigma)) in tris-buffered saline with Tween-20 (MilliporeSigma) (TBST) for 1hr. Membranes were then stained with primary antibodies, listed in **Table 2.2**, for 2 hours in 3% BSA. After washing membranes with TBST 3 times for 10 minutes, membranes were stained for 1 hour with LI-COR secondary antibodies: IRDye® 800CW donkey anti-rabbit (#925-32213, LI-COR Biosciences, Lincoln, Nebraska, USA) and IRDye® donkey anti-mouse (#925-68072, LI-COR Biosciences) at 1:15000. Membranes were washed again with TBST then imaged using the Odyssey Fc Imaging System (LI-COR Biosciences). Images were quantified using Image Studio Lite Ver 5.2 (LI-COR Biosciences).

Table 4.2 Antibodies used in IF and Western Blot experiments. Molecular Probes (ThermoFisher Scientific)

	Antigen	Host	Dilution	Cat. #	Company
WB	Histone 3	Rabbit	1:200	07-690	MilliporeSigma
	Actin	Mouse	1:500	69100	Molecular Probes
IF	NeuN	Guinea Pig	1:500	ABN90P	MilliporeSigma

4.2.8 Tissue processing and IF

Eight weeks after injury, rats were euthanized with 10% chloral hydrate and perfused transcardially with PBS followed by 4% PF. Spinal cords were dissected from a total of 26 animals, post-fixed in 4% PF overnight, and then cryoprotected in 30% sucrose. Thoracic spinal cords (5mm in length surrounding the lesion epicenter) were frozen in Tissue Plus® OCT compound then cut cross-sectionally. Frozen sections were thawed and rehydrated in 10 mM PBS for 10 min, and blocked with 10% normal donkey serum for 30 min. For primary antibodies used, see **Table 2.2**. An AlexaFluor 488-conjugated anti-guinea pig secondary antibody (1:500, Jackson ImmuoResearch) was applied for 2 h at room temperature. Digital images were captured with an Imager M2 microscope (Carl Zeiss Canada). Cut sections were also stained with Eriochrome Cyanine R using an identical protocol to that outlined in chapter 3 (see section 3.2.8).

4.2.9 Montoya staircase behavioural test

The Montoya Staircase assesses the reaching ability of each forelimb (Montoya et al. 1991). All 78 rats were initially trained for 6 weeks and the 60 highest scoring rats were used for further behavioural experiments. To motivate pellet retrieval, rats were fasted for 16 hours prior to testing. Banana-flavoured pellets were loaded onto the staircase apparatus and each rat was placed in the apparatus for 15 min. The number of pellets consumed on either the right or left side was counted. Each step had three color-coded pellets to identify misplacement of pellets between steps.

4.2.10 Cylinder Rearing behavioural test

The cylinder rearing test measured forelimb preference during spontaneous vertical exploration as previously described (Y. Liu et al. 1999). Briefly, rats were placed in a clear plexiglass cylinder and filmed for 20min. Up to 20 spontaneous rearing events were recorded per animal per timepoint. During each event, paw placement on initial contact (left, right, or both) and subsequent contact (left,

right, or both) were noted. If 3 seconds or more elapsed after both paws were removed from the cylinder wall, the event was concluded, and the next rear marked a new event.

4.2.11 Horizontal Ladder behavioural test

A horizontal ladder with irregularly placed but consistent rungs (not changed between timepoints) was used to asses forelimb and hindlimb function, as previously described (Metz and Whishaw 2009). Rats were filmed crossing the ladder 6 separate times and one repetition was excluded for each rat that failed to complete the task properly (e.g. stopped or reared during the run). The total number of errors (slip, miss, or drag) was recorded during each run and summed over all 5 runs. No baseline was taken as the uninjured paw could be used as an internal control.

4.2.12 IBB Forelimb Recovery Score

A modified version of the Irvine, Beatties, and Bresnahan (IBB) Forelimb Recovery Scale was used to assess fine motor function in the forepaws (Irvine et al. 2014). Briefly, each rat was placed in a plexiglass cylinder and given 5 Froot Loops™ cereal pieces. The rat was filmed until all 5 pieces were eaten or for 7 minutes (whichever came first). The following movements were scored: cereal adjustments (none, subtle, or exaggerated), wrist movements (yes or no), non-contact digit movements (digits 2, 3, or 4), contact manipulatory digit movements (digits 2, 3, and/or 4), and grasping method (abnormal, sometimes normal, or predominantly normal). A score was given for each movement with a perfect (non-injured) score being 6. No baseline was taken as the uninjured paw could be used as an internal control.

4.2.13 Digital Extension on Horizontal Ladder

Digital extension during horizontal ladder crossing was also assessed as previously described (Metz and Whishaw 2009). Briefly, the forepaw extension score was recorded when each paw was placed correctly on a rung. The number of correct placements was counted, and both injured and uninjured paws were scored. The degree to which the digits of the forepaw were extended before (or at the moment of) stepping was rated using a three-point scale. The scores were as follows: **(0)** closed paw with no digital extension, **(1)** slightly open paw with slight digital extension (all or only a few digits), and **(2)** open paw with full digital extension. Scores of the first ten steps/paw placements were averaged and used for the analysis. No baseline was taken as the uninjured paw could be used as an internal control.

4.2.14 Statistical analysis

Two-way Anova with multiple testing correction (Tukey) was performed using Graphpad Prism 6.01. All behavioural analyses were performed by blinded researchers.

4.3 Results

4.3.1 Gavage timeline during initial 2WPI

As outlined in **Fig 4.1A**, rats were gavaged repeatedly during a 2-week period, starting 3 hours after the C5 hemi-contusive surgery. Rats were gavaged 3 times per day for the first two days, 2 times per day for an additional four days, and once per day over the last seven days. Rats were either gavaged with 1.5mL KE or 1.5mL water except for 3 gavages during Days 2 and 3, where 1mL was used instead. This change in gavage volume was due to early issues with buprenorphine-induced oral fixation (a known side effect), which led to the rats eating their bedding over the first couple days. The gavage volume was reduced during this time period to prevent respiration problems.

4.3.2 Weight loss and monitoring score over 2 weeks

All groups showed weight loss following injury, however our KE gavaged group showed significantly less weight loss then control group on days 3 and 6 **(Fig 4.1B and D)**. Conversely, our KD+KE group showed much higher weight loss than the control group starting at day 6 **(Fig 4.1D)**. Monitoring score was also assessed during injury. Monitoring score is the sum of individual scores given for weight, physical appearance and signs of pain, behaviour and activity level, clinical signs of poor recovery, lesion infection and autotomy of limbs, and respiration problems after gavage. A higher score is indicative of an animal in worse condition after surgery and may also indicate poorer recovery. A score of 20 is considered humane endpoint unless the animal improves over 48 hours. Monitoring score is usually negatively correlated with weight loss; however, it is also a more thorough indication of health status than weight loss alone. As can be seen in **Fig 4.1C** our KE group showed significantly lower monitoring scores between days 4 and 7 than the control group. Conversely, the KD+KE group showed significantly higher scores that started at 4DPI and was sustained throughout the experiment (**Fig 4.1E**). Together these results suggest that KE given acutely after injury can reduce weight loss and improve health. Our results also show that combining KE and KD is deleterious as it exacerbates weights loss and may negatively impact recovery.

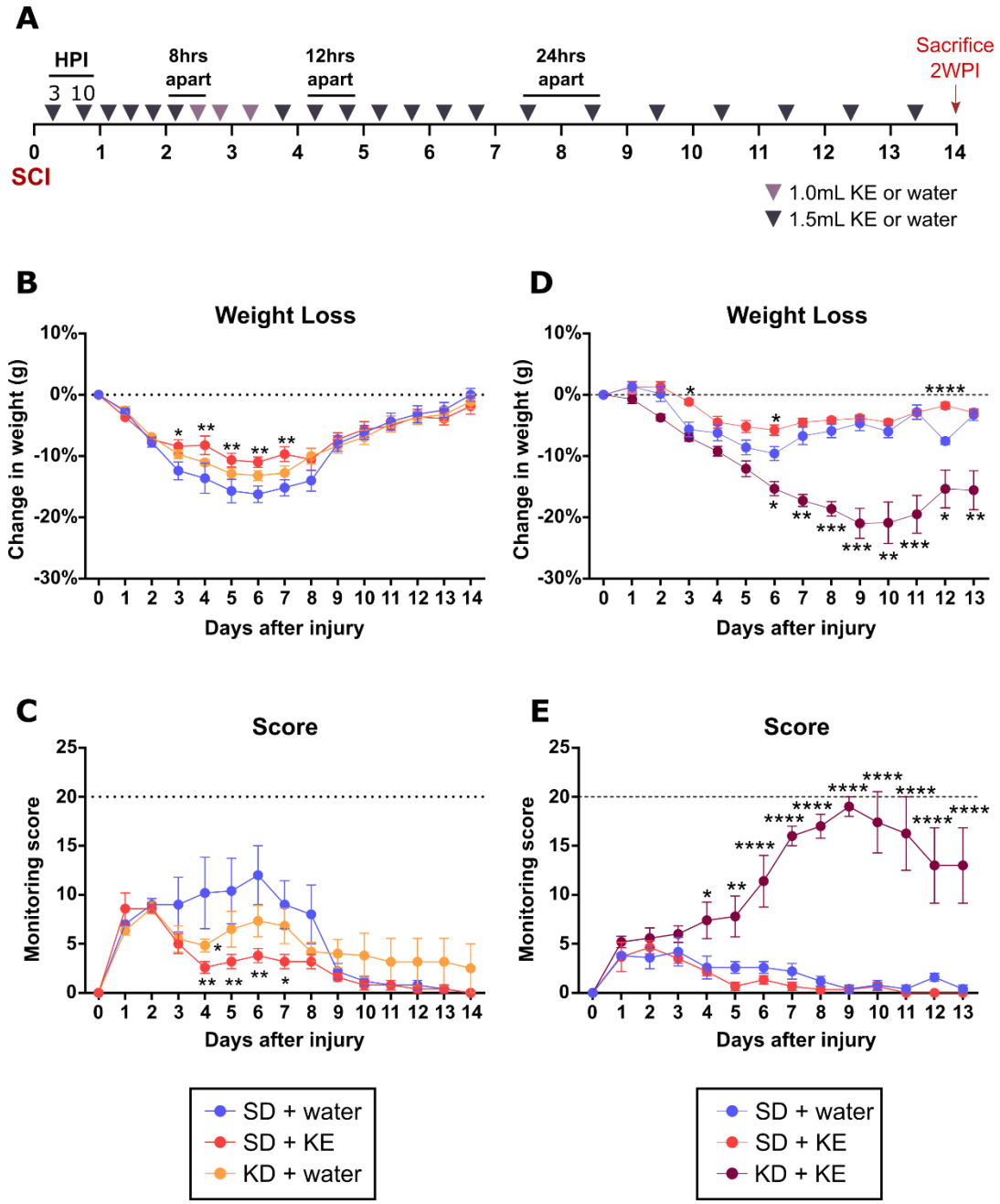

Figure 4.1 Outline of gavage schedule during first 2 weeks, weight loss, and monitoring scores. **(A)** Gavage outline showing time-points of each gavage. Rats were euthanized approximately 24hrs after last gavage on Day 13. **(B)** Change in weight against baseline for rats treated with SD+water (control), KD+water, or SD+KE. *KE compared to control. **(C)** Monitoring score for same rats as in (B). *KE or KD compared to control. **(D)** Change in weight against baseline for rats treated with SD+water (control), SD+KE, or KD+KE. *KE or KD+KE compared to control. **(E)** Monitoring score for same rats as in (D). *KE or KD compared to control. * $p<0.05$, ** $p<0.01$, *** $p<0.001$, **** $p<0.0001$ calculated using a Two-way ANOVA with Tukey correction.

4.3.3 BHB levels during 2-week gavage period

Following injury, BHB and glucose levels were measured at 1, 6, 8 and 12 hours after gavage on days 0, 1, 3, 7, 13, and 14. We saw the highest peak in BHB levels after KE at day 1, one hour after gavage **(Fig 4.2A and C)**. Interestingly, BHB levels taken at the same time-point across days showed a decrease in peak level. For example, unlike day 1, days 13 and 14 did not show a comparable increase in BHB at one-hour post gavage **(Fig 4.2A and C)**. Also, by 8 or 12 hrs post-gavage there was no significant increase in BHB with KE, showing that levels are transient **(Fig 4.2A and C)**. Conversely, the KD+KE group did show sustained levels of BHB as high as 5mmol/L up to 12 hours after gavage **(Fig 4.2C)**. It's important to note that our ketone meter can only read up to 8.0 at which point a reading of "HI" is given. Any rat that measured "HI" was scored 8.1. As can be seen in **Fig 4.2A and C**, many rats scored "HI" throughout the experiment, especially in the KD+KE group. It's possible that the elevated BHB levels may have contributed to high weight loss and monitoring scores in the KD+KE group.

4.3.4 Glucose levels during 2-week gavage period

We also measured glucose levels after gavage to monitor for instances of hypoglycemia (low glucose). As expected, we saw the largest drop in glucose on day 1, one hour after gavage for our KE group **(Fig 4.2B and D)**. However, low levels of glucose were not sustained, nor did they worsen with repeated gavage **(Fig 4.2B)**. Interestingly, KD by itself did not lower glucose levels significantly compared to the SD-fed control group **(Fig 4.2B)**. With combined KD+KE, rats had very low glucose levels that remained significantly lower than the KE or the control group even up to 12 hours after gavage **(Fig 4.2D)**. Glucose levels in all groups also dropped significantly after injury. However, this is unlikely to be a result of the injury but rather an effect of the Isoflurane anesthetic used during baseline measurement (levels are measured during surgery prep), which is known to increase glucose levels (Lattermann et al., 2001). Our BHB and glucose results support the use of SD+KE as an efficient treatment to raise BHB without producing hypoglycemia and argue against the combination of KD+KE.

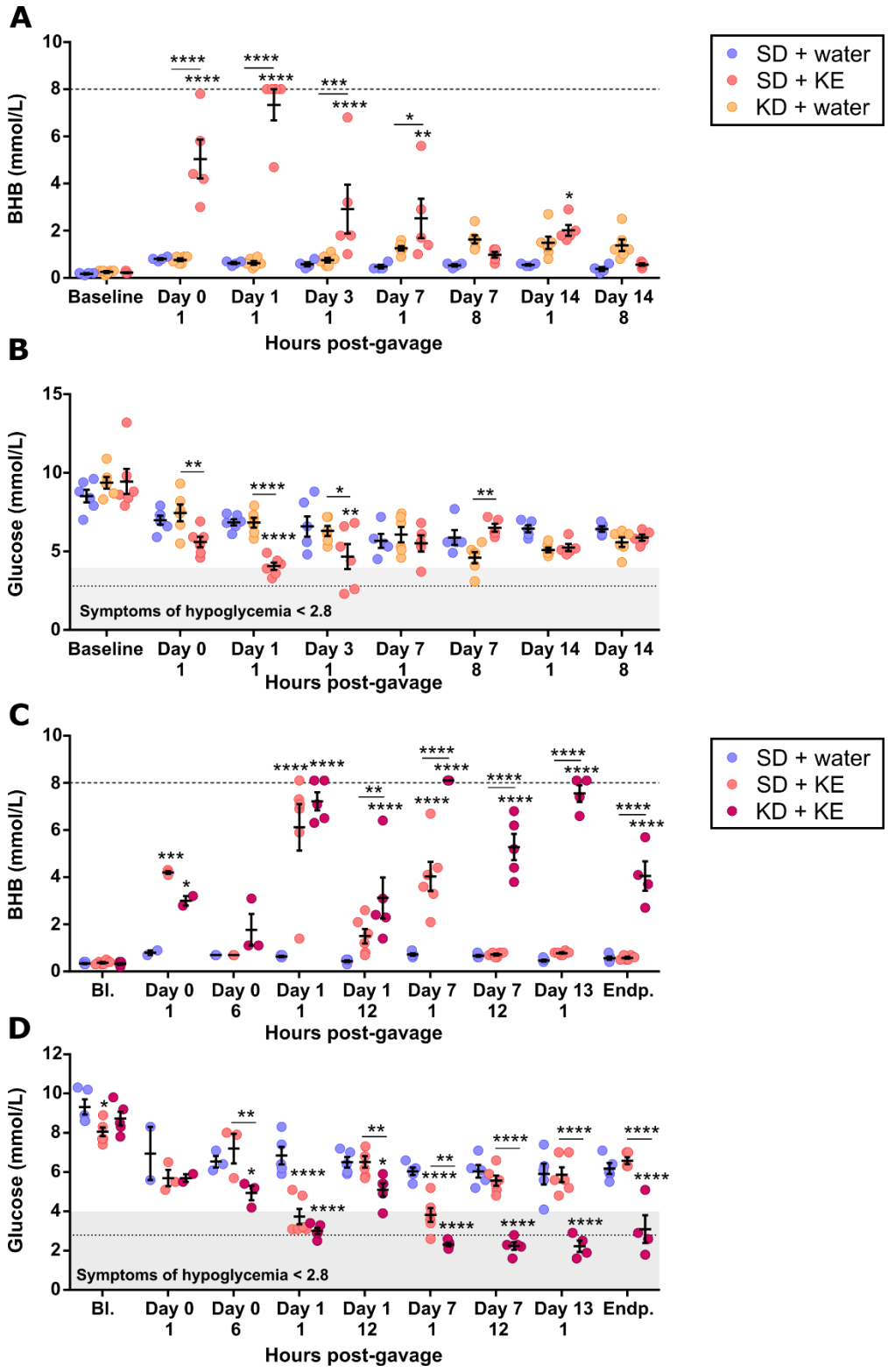

Figure 4.2 BHB and glucose levels over 2-week gavage period. **(A)** BHB levels measured in SD+water, SD+KE, and KD+water groups. Days indicated are post-injury (Day 0 is surgery day) and below are hours post-gavage. BHB levels could only be measured up to 8. Any BHB levels >8

measure as 'HI' and were scored as 8.1. **(B)** Glucose levels measured in SD+water, SD+KE, and KD+water groups. Same days as BHB measurements. Shaded area below 4 mmol/L represents glucose measurements in hypoglycemic range. Dotted line at 2.8 mmol/L indicates glucose concentration below which severe symptoms of hypoglycemia begin. **(C)** Same as in (A) for groups SD+water, SD+KE, and KD+KE. **(D)** Same as (B) for groups SD+water, SD+KE, and KD+KE. * $p<0.05$, ** $p<0.01$, *** $p<0.001$, **** $p<0.0001$ calculated using Two-way ANOVA with Tukey correction.

4.3.5 Proteomic results at 2WPI for KE, KD, and KD+KE

To identify proteomic changes produced by treatment and identify processes targeted by KE and KD, we performed tagged LC/MS/MS analysis of the spinal cord epicenter at 2WPI. The changes in expression were given as normalized ratios comparing KE, KD or KD+KE to the control group (SD+water). The KE vs. control ratios from the two separate experiments (see **Table 4.1**) were combined for analysis after normalization. The number of proteins in each dataset (after quality control steps) were 1482 and 2652. The rat genomes have 23498 protein-coding genes (RGSC Genome Assembly v6.0, https://rgd.mcw.edu/, retrieved Aug. 3, 2020) suggesting our datasets samples approximately 6-11% of the total proteins.

We further identified proteins that were increased or decreased by a log2 fold-change of at least 0.5 and had significance of $p<0.05$. As can be seen in **Fig 4.3**, KD had the highest number of proteins with a fold-change above 0.5 **(Fig 4.3A)**: we found 188 significantly altered proteins in the KD group, compared to 40 for KE and 38 for KD+KE **(Fig 4.3C)**. There was a handful of proteins shared between the different groups, but none shared between all three **(Fig 4.3C)**. These shared proteins are plotted in **Fig 4.3B**. Interestingly most shared proteins show the same direction of change between KE and KD or KE and KD+KE but all shared proteins identified between KD and KD+KE are in the opposite direction **(Fig 4.3B)**. This could be due to the high levels of BHB seen with KE and KD+KE but not with KD.

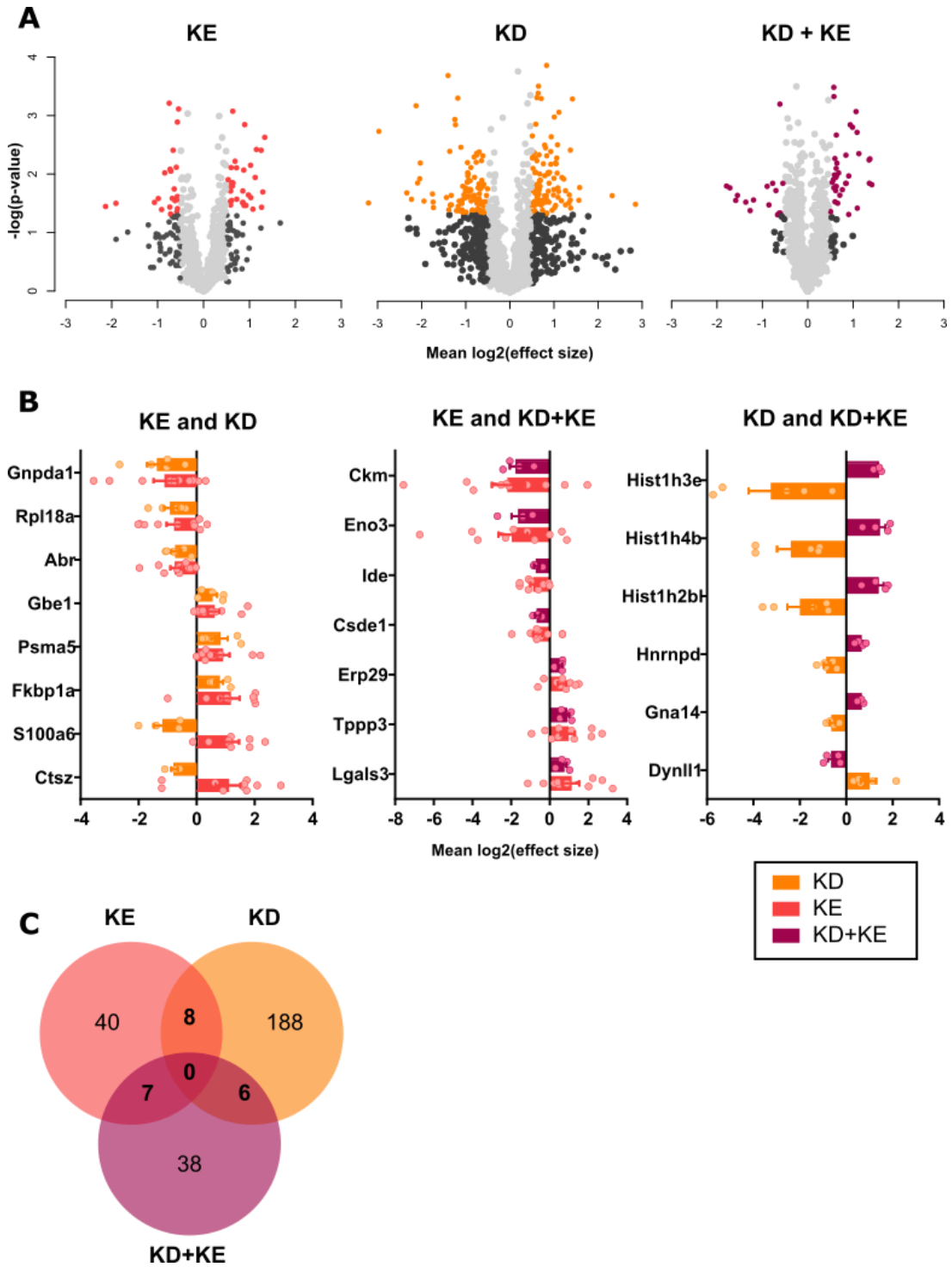

Figure 4.3 Proteomic hits for fold change > 0.5 and p-value < 0.05 showing comparison of three groups. **(A)** Volcano plots of normalized ratios (against control). Dots in grey are proteins below a mean fold-change (log2(effect size)) of 0.5. Dark grey dots are proteins with a mean fold-change above 0.5 but a p-value above 0.05. Coloured dots (pink, orange, or purple) are proteins with a mean fold-change above 0.5 and a p-value below 0.05. **(B)** Shared proteins between different normalized

groups. Each dot is an individual normalized set. **(C)** Venn diagram showing significantly ($p < 0.05$) altered proteins compared to control that have a mean fold-change > 0.5, with overlap showing shared proteins between groups.

KD showed the most protein changes, possibly due to the sustained ketone levels provided by a diet. Interestingly, Aif1 (also known is Iba1) is increased by KD compared to control **(Table 4.3)**. To date, we have not seen any evidence of Iba1 increase by IF or reported in the literature for KD. As can be seen in **Table 4.3**, very few proteins had significant Q-values (that is the P-value adjusted for False Discovery Rate). Therefore, we decided to include proteins with a P-value of 0.05 and complete an exploratory analysis for further hypothesis generation. Of note, multiple histone family members come up as decreased by KD. The largest decrease was seen for Histone 3, with a log2 fold-change of -3.21 in the spinal cord of KD compared to control rats.

Table 4.3 Top 10 mean normalized ratio KD vs. Control proteins hits with Mean Log2 fold-change greater than 1 or less than -1 (shaded grey) and p-values < 0.05. Q-values < 0.05 are bolded.

KD		**Mean**	**P-value**	**Q-value**
Ces1c	Carboxylic ester hydrolase	2.85	0.035	0.111
Dnph1	2-deoxynucleoside 5-phosphate N-hydrolase 1	2.32	0.025	0.107
Rabgap1	Rab GTPase-activating protein 1-like	1.58	0.018	0.106
Plbd2	Putative phospholipase B-like 2	1.56	0.030	0.109
Cryl1	Lambda-crystallin homolog	1.42	0.001	**0.039**
Aif1	Allograft inflammatory factor 1 (Iba1)	1.38	0.040	0.118
Kpna3	Importin subunit alpha	1.37	0.029	0.109
Dynlrb1	Dynein light chain roadblock-type 1	1.35	0.024	0.107
Dclk2	Serine/threonine-protein kinase DCLK2	1.34	0.033	0.110
Csrp1	Cysteine and glycine-rich protein 1	1.26	0.021	0.106
Hist1h3e	Histone H3.1	-3.21	0.033	0.110
Psap	Sulfated glycoprotein 1	-2.97	0.002	0.072
Hist1h4b	Histone H4	-2.34	0.022	0.107
Cbx3	Chromobox 3	-2.23	0.029	0.109
Rnaset2	Ribonuclease T2	-2.13	0.001	**0.045**
Igtp	Interferon gamma induced GTPase	-2.09	0.015	0.106
Hist1h1b	Histone H1.5	-2.04	0.013	0.106
Rps7	40S ribosomal protein S7	-2.03	0.007	0.085
Hist1h2bl	Histone H2B	-1.95	0.031	0.109
Lmna	Prelamin-A/C	-1.76	0.023	0.107

To confirm this finding, we ran a Western blot to look at Histone 3 changes. Similarly, we see a significant decrease in Histone 3 for KD-fed rats that is not seen with either SD or KE **(Fig 4.4)**. The decrease also shows a similar ratio of about -3.5 when compared to SD.

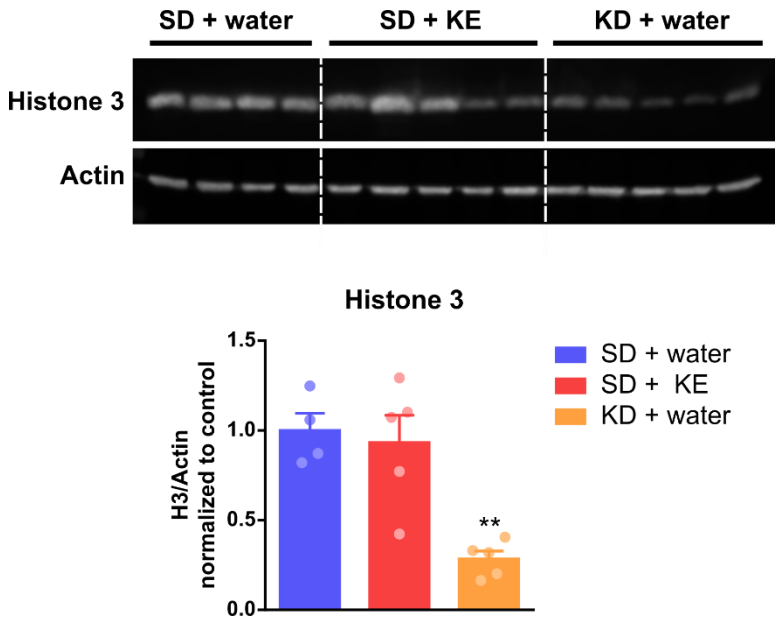

Figure 4.4 Western blot analysis of Histone 3 expression at 2WPI showing stained blot and graph of normalized band density. ** $p<0.01$ calculated using One-way ANOVA with Tukey correction.

KE showed fewer protein changes by proteomic analysis. There is some overlap between KD and KE (compared to control), for example increased Fkbp1a, an isomerase which can bind rapamycin, and decreased Gnpda1, another isomerase involved in sugar metabolism **(Fig 4.3B)**. However, the majority of proteins are unique to KD or KE. Some interesting KE hits, as shown in **Table 4.4**, include elevated Glutathione reductase, which could point to a role in mediating ROS. KE also increases Galectin 3 (Gal-3). Studies looking at the role of Gal-3 after SCI suggest that increased Gal-3 is related to increased neuroinflammation (Mostacada et al. 2015; Pajoohesh-Ganji et al. 2012; Prins, Almeida, and Martinez 2016; Ren et al. 2019). However, other research suggests that Gal-3 may play important roles in axonal branching, oligodendrocyte differentiation, and remyelination (Thomas and Pasquini 2018; Díez-Revuelta et al. 2010).

Table 4.4 Mean normalized ratio of KE vs. Control for hits with Mean > 1 or < -1 (shaded grey) and p-value < 0.05.

KE		Mean	P-value	Q-value
Ftl1	Ferritin light chain 1	1.33	0.002	0.058
Ctsz	Cathepsin Z	1.29	0.020	0.100
Katnal2	Katanin p60 ATPase-containing subunit A-like 2	1.26	0.037	0.109
Gsr	Glutathione reductase	1.25	0.004	0.064
Ostf1	Osteoclast-stimulating factor 1	1.15	0.004	0.064
S100a6	Protein S100	1.12	0.011	0.089
Lgals3	Galectin 3	1.08	0.040	0.113
Fkbp1a	Peptidyl-prolyl cis-trans isomerase FKBP1A	1.03	0.025	0.106
Gns	N-acetylglucosamine-6-sulfatase	1.02	0.007	0.078
Ckm	Creatine kinase M-type	-2.13	0.036	0.109
Eno3	Beta-enolase	-1.91	0.032	0.107
Gnpda1	Glucosamine-6-phosphate isomerase	-1.07	0.030	0.106

KD+KE (compared to control) also showed relatively few hits. However, this is partially due to most of the significant hits being below the 0.5-fold-change cut-off **(Fig 4.3A)**. Interestingly most of the hits (even below 0.5) also had significant Q-values (FDR-adjusted p-values) suggesting tighter grouping of the samples. It is possible that the high and sustained ketone levels achieved through KD+KE, lead to more extreme changes in protein levels in the spinal cord. However, given that the KD+KE group had worse monitoring scores indicating more health problems, it is unclear if these protein changes indicate deleterious shifts or compensatory mechanisms. Of interest is the upregulation of proteins involved in transcription including histones (H2B, H3, and H4), heterogenous nuclear ribonucleoproteins, and the eukaryotic initiation factor 4A-I (**Table 4.5**). As well, many transporters are upregulated including ADP/ATP translocase 1 and 2 and the amino acid transporter Slc1a2. GFAP also stands out as a protein of interest as it is already increased after SCI but appears to be further increased by KD+KE (**Table 4.5**). Two decreased proteins that are unique include Pmp2 and Mpz, members of peripheral myelin (**Table 4.5**). While it's possible that Schwann cell entry into the spinal cord is affected by KD+KE, it is also very likely that the peripheral nerves were not adequately removed from certain samples when harvesting the spinal cord leading to the observed differences.

Table 4.5 Mean normalized ratio of KD+KE vs. Control for hits with Mean > 1 or < -1 (shaded grey) and p-value < 0.05. Significant Q-values are in bold.

KD+KE		Mean	P-value	Q-value
Hist1h4b	Histone H4	1.41	0.014	**0.035**
Hist1h3e	Histone H3	1.37	0.005	**0.029**
Hist1h2bl	Histone H2B	1.36	0.013	**0.035**
Slc25a4	ADP/ATP translocase 1	1.35	0.005	**0.029**
Slc25a3	Phosphate carrier protein, mitochondrial	1.13	0.004	**0.029**
Mog	Myelin-oligodendrocyte glycoprotein	1.09	0.036	0.058
Slc25a5	ADP/ATP translocase 2	1.09	0.002	**0.018**
Slc1a2	Amino acid transporter	1.06	0.001	**0.014**
Ca3	Carbonic anhydrase 3	-1.79	0.015	**0.035**
Ckm	Creatine kinase M-type	-1.72	0.016	**0.035**
Eno3	Beta-enolase	-1.59	0.027	**0.048**
Mpz	Myelin protein P0	-1.55	0.022	**0.041**
Pmp2	Myelin P2 protein	-1.37	0.028	**0.049**
Hp	Haptoglobin	-1.27	0.040	0.063
Cpamd8	Alpha-1-inhibitor 3	-1.20	0.026	**0.048**

Enrichment of GO terms and KEGG pathways for both up- and down-regulated proteins in each group was performed using DAVID analysis. The results are listed in **Tables 4.6** and **4.7**. KE only showed enrichment of the GO term "metabolic process" **(Table 4.6)** and KEGG pathway "glycosaminoglycan degradation" **(Table 4.7)** for proteins increased by KE. Conversely, there were no GO terms or KEGG pathways enriched for the list of decreased protein. Together these results suggest that KE does not cause widespread proteomic changes compared to control rats 2 weeks after SCI. Nevertheless, the glycosaminoglycan degradation pathway is of interest as it mediates degradation of chondroitin sulfate, which is a component of the injury site scar. This could point to a beneficial role of KE in clearing scar tissue, however further research will need to confirm this finding.

Multiple GO terms and KEGG pathways were enriched by KD for both increased (Up) and decreased (Down) proteins. For example, microtubule processes and cytoskeletal organization **(Table 4.6)** and many metabolic and biosynthetic pathways **(Table 4.7)** are enriched in the increased subset of protein. Unexpectedly, the KEGG pathway for fatty acid metabolism appears to be decreased by KD (**Table 4.7)**. Both HADHA and HADHB, which form the Mitochondrial trifunctional protein (MTP) and are involved in β-oxidation, are decreased in the KD group. Intriguingly, translation also appears to be decreased by KD **(Table 4.6)** due to the large number of decreased ribosomal components **(Tables 4.6 and 4.7)**.

KD+KE showed enrichment of GO terms and KEGG pathways for the increased subset of proteins but not for the decreased set. GO terms enriched include sodium ion export, ATP metabolic processes, and axon development **(Table 4.6)**. Multiple redundant pathways were found for ATP1B1, ATP1A3, ATP1A1, and ATP1A2 of which only one is listed in **Table 4.7**. However, its interesting to note that these proteins are also involved in insulin secretion and this pathway was also enriched in KD+KE.

Table 4.6 GO terms from proteomic data (hits with $p<0.05$). *Genes matched to more than one GO term. The GO term with highest enrichment is given. Groups with no enriched GO terms were omitted.

	GO Term	Genes	Fold Enrichment	P-Value
KE Up	metabolic process	ARSB, ASPA, GSTP1	10.03	0.033
KD Up	negative regulation of endocytosis	PACSIN1, PACSIN2*	43.40	0.045
	microtubule-based process	DYNLL1, TUBA4A, TUBA1B, TUBB3	23.37	0.001
	microtubule cytoskeleton organization	MAP1B, DCLK2, TUBA1B	9.91	0.036
KD Down	establishment or maintenance of microtubule cytoskeleton polarity	CKAP5, LMNA	115.15	0.017
	plasma membrane to endosome transport	RAB5B, RAB5C	57.58	0.034
	generation of precursor metabolites and energy	ACOX1, GNPDA1	49.35	0.039
	proteolysis involved in cellular protein catabolic process	PSMB10, CTSZ, PSMB6, CLPP	18.18	0.001
	ribosomal large subunit assembly	RPL6, RPL10, RPL11	16.19	0.014
	translation	RPSA, RPL30, RPS16, RPL18A, RPL6, RPL10, RPL11, RPL4, RPS11, RPS7	5.84	0.000
KD + KE Up	response to glycoside	ATP1A1, ATP1A2*	406.74	0.005
	sodium ion export from cell	ATP1B1, ATP1A3, ATP1A1, ATP1A2*	180.77	0.000
	membrane repolarization	ATP1B1, ATP1A1*	135.58	0.014
	locomotion	ATP1A2, NEFL	116.21	0.017
	axon development	NEFL, GAP43	90.39	0.021
	ATP hydrolysis coupled proton transport	ATP5B, ATP1A3, ATP1A1, ATP5A1, ATP1A2	58.11	0.000
	ATP metabolic process	ATP1B1, ATP1A2	38.74	0.049
	response to drug	SLC1A2, ATP1A3, ATP1A1	17.94	0.011

Table 4.7 KEGG pathways from proteomic data (hits with p<0.05). P-value for enriched KEGG pathways term is given and enriched terms with p>0.05 are italicized. *Genes matched to more than one KEGG term. The KEGG term with highest enrichment is given.

	KEGG Pathways	Genes	Fold Enrichment	P-Value
KE Up	Glycosaminoglycan degradation	GNS, ARSB	39.56	0.047
KD Up	Pyruvate metabolism	HAGH, ACYP2, GLO1, MDH2	10.82	0.006
	Cysteine and methionine metabolism	AHCYL2, MDH2, MPST	9.90	0.035
	Endocrine and other factor-regulated calcium reabsorption	PRKCA, CALB1, DNM1	9.66	0.037
	Biosynthesis of amino acids	PGAM1, ENO2, IDH3B, PFKM	7.22	0.017
	Carbon metabolism	ACADS, PGAM1, ENO2, IDH3B, PFKM, MDH2	6.44	0.002
	Gap junction	PRKCA, MAPK3, TUBA4A, TUBA1B	6.37	0.023
	Sphingolipid signaling pathway	PRKCA, PPP2CA, MAPK3, RHOA, MAPK10	5.83	0.010
	Focal adhesion	PRKCA, TNR, MAPK3, RHOA, MAPK10, CAPN2	3.92	0.016
	Biosynthesis of antibiotics	MVD, PGAM1, ENO2, IDH3B, PFKM, MDH2	3.61	0.023
	Metabolic pathways	MVD, ACADS, PGAM1, IDH3B, PFKM, GMPS, CRYL1, NANS, GBE1, ENO2, ABAT, AHCYL2, PCYT2, MDH2, MPST	1.66	0.046
KD Down	Fatty acid degradation	ACOX1, ALDH3A2, HADHA, HADHB	12.00	0.004
	Vasopressin-regulated water reabsorption	RAB5B, RAB5C, RAB5A	11.44	0.005
	beta-Alanine metabolism	CNDP2, ALDH3A2, HADHA	11.18	0.028
	Proteasome	PSMB10, PSMC6, PSMB6, PSMC2	10.93	0.005
	Fatty acid metabolism	ACOX1, HADHA, HADHB	8.58	0.046
	Amoebiasis	GNA14, RAB5B, RAB5C, RAB5A	5.97	0.009
	Ribosome	RPSA, RPL30, RPS16, RPL18A, RPL6, RPL10, RPL24, RPL4, RPS11, RPS7	4.13	0.001
	Phagosome	RAB5B, RAB5C, RAB5A, ATP6V0D1*	3.87	0.037
	Endocytosis	RAB5B, TSG101, RAB5C, RAB5A, ASAP2, VPS36	3.60	0.011
KD + KE Up	Proximal tubule bicarbonate reclamation	ATP1B1, ATP1A3, ATP1A1, ATP1A2*	61.92	0.000
	Protein digestion and absorption	ATP1B1, SLC3A2, ATP1A3, ATP1A1, ATP1A2	20.94	0.000
	cGMP-PKG signaling pathway	ATP1B1, SLC25A4, SLC25A5, ATP1A3, ATP1A1, ATP1A2	13.96	0.000
	Parkinson's disease	SLC25A4, SLC25A5, ATP5B, ATP5A1*	7.66	0.012

4.3.6 Comparison of proteomics and scRNA-seq data

Although there are multiple differences between the data used for proteomics (rats, C5 hemi-contusion, 2WPI, all cells at lesion epicenter) versus the data used for scRNA-sequencing (mice, T9 midline contusion, 1WPI, CD45+ cells only), we wanted to see if there were any shared hits between the two. Across both sets of data, KD shows downregulation of ribosomal components suggesting decreases in translation **(Table 4.8)**. These ribosomal components also show very similar expression patterns in the scRNA-sequencing data **(Fig 4.5)**. Together these results point to potential targets that are consistently affected by KD within a 1 to 2-week time window regardless of species.

Table 4.8 Shared singificant hits between scRNA-sequencing and proteomics data.

		scRNA-seq		Proteomics	
		Mean	**p-value**	**Mean**	**p-value**
Rpl4	60S ribosomal protein L4	-0.38	2.53E-04	-0.97	0.015
Rpl6	60S ribosomal protein L6	-0.34	1.76E-04	-1.21	0.044
Rps11	40S ribosomal protein S11	-0.40	4.70E-07	-1.36	0.005
Rps6	40S ribosomal protein S6	-0.34	2.64E-04	-1.01	0.027
Rps7	40S ribosomal protein S7	-0.40	1.86E-05	-2.03	0.007
Rpsa	40S ribosomal protein SA	-0.48	7.08E-06	-0.73	0.041

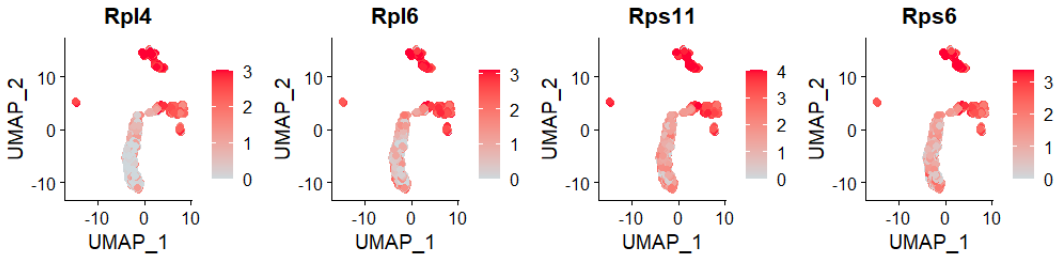

Figure 4.5 UMAP representation of top 4 shared singificant hits between scRNA-sequencing and proteomics data.

4.3.7 Changes in weight and monitoring score during 8-week KE treatment

Following the proteomic results, we turned to an investigation of behavioural improvement. Even though the KD and KE do not share multiple proteome alterations, KE could still be improving recovery. For our 8-week behavioural study, rats were gavaged with KE for the initial two weeks following the timeline shown in **Fig 4.1A** then switched to KE in water at a 1:10-20 dilution for the

following 6 weeks **(Fig 4.6A)**. We decided to reduce the dilution of KE in water as rats were not drinking as much as the controls, which was corrected by switching to the 1:20 dilution. Rats were fed KD or SD for 6 weeks, then all rats were switched to SD to see if any additional benefits conferred by KD+KE were sustained once they were switched to SD+KE. It is important to remember that our SD+KE group maintains the same treatment throughout the experiment – it is only the KD+KE group that is changed to an SD+KE treatment after 6 weeks. This experimental outline is shown in **Fig 4.6A**.

Similar to our two-week study, we saw the most weight loss in our KD+KE group **(Fig 4.6B)**. As well this further points to a KD+KE combination being deleterious for recovery. However, contrary to our initial study, the KE treatment only showed a transient improvement over control animals in terms of weight loss with significantly more weight loss than control animals by 10 days post injury **(Fig 4.6B)**. While KE-gavaged animals also showed a lower monitoring score initially, especially between days 4 and 7, by Day 10 KE-gavaged animals also had a significantly higher monitoring score that persisted until 14DPI **(Fig 4.6C)**. Interestingly, compared to control, KD+KE rats showed improved monitoring score on Days 4 and 5, however by 7DPI, their monitoring scores were significantly worse, and this persisted up to 25DPI (**Fig 4.6C)**. Together these results suggest that KE treatment can acutely reduce weight loss and improve monitoring score but KD+KE is deleterious to acute recovery.

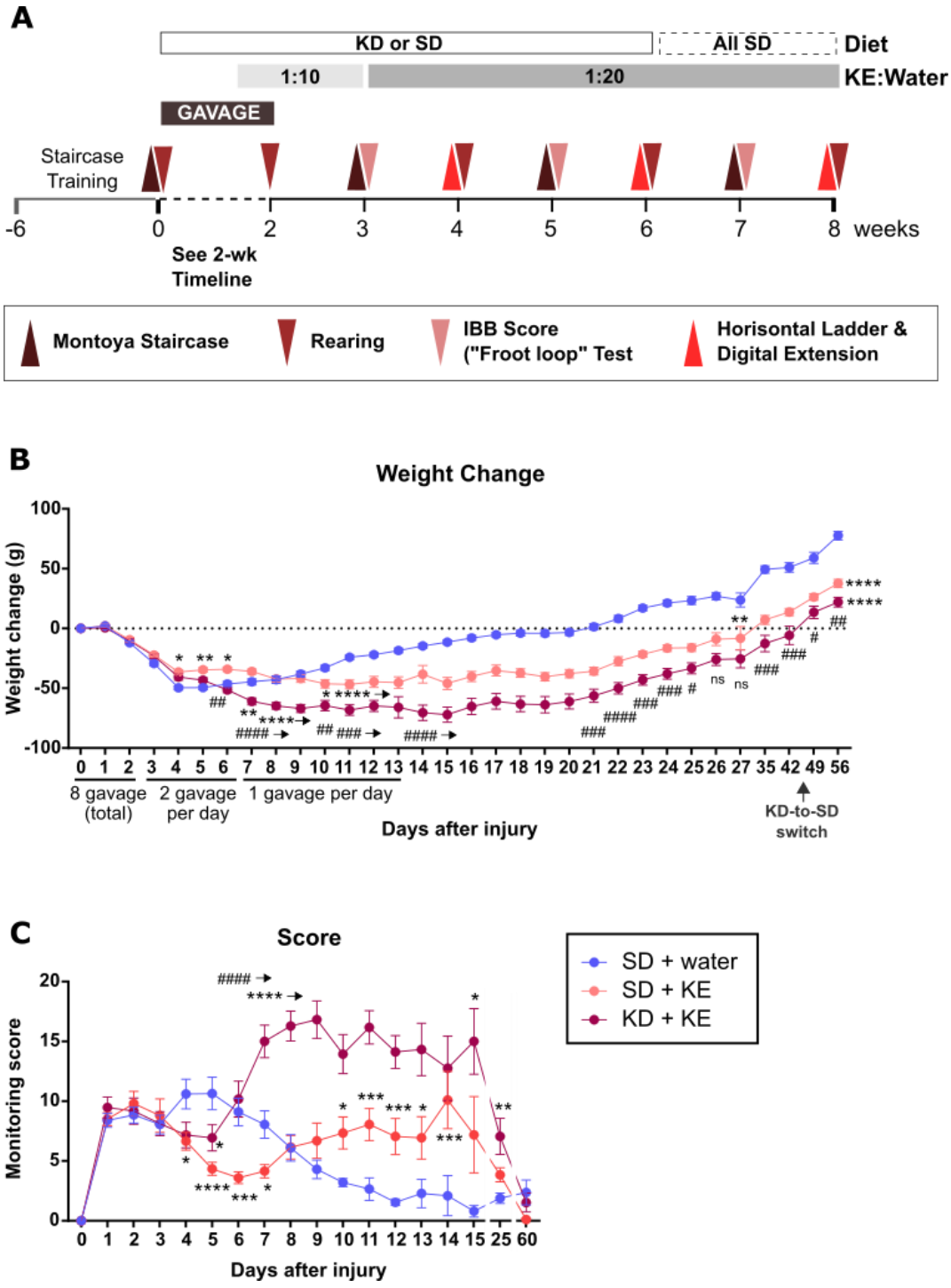

Figure 4.6 Outline of KE and diet administration, and behavioural testing over 8 week experiment. **(A)** Experimental schematic showing diet timeline, KE:water timeline, and behvaioural timepoints. **(B)** Weight change in each group across 8 weeks. KD-to-SD switch for KD+KE group is indicated. * SD+KE or KD+KE compared to SD+water. # SD+KE compared to KD+KE. **(C)** Average monitoring scores for each group. *SD+KE or KD+KE compared to SD+water. Horizontal arrows indicate that

significant is carried on at following timepoints until otherwise specified. * $p<0.05$, ** or ## $p<0.01$, *** or ### $p<0.001$, **** or #### $p<0.0001$ calculated using Two-way ANOVA with Tukey correction.

4.3.8 Changes in BHB levels during 8-week KE treatment

Similar to our 2-week experiments, we saw peaks in BHB levels 1HPG, with the highest peak seen on Day 1 (**Fig 4.7B)**. Interestingly, high levels were sustained even up to 8HPG on Day 1 suggesting that less frequent gavages during the first couple days may be sufficient to maintain high BHB levels **(Fig 4.7B)**. However, SD+KE was no longer significant at 12HPG after 1 week even though a significant increase was seen at 3DPI (**Fig 4.7C and D)**. During weeks 3 to 8, when KE was administered in water, we did not see significantly increased BHB levels in the KE group until week 8 **(Fig 4.7E)**. However, it's important to note that the SD group also has significantly higher BHB levels at 4 and 6WPI compared to 8WPI **(Fig 4.7E)**. Although unclear, this could be partially due to the Montoya staircase behaviour which requires overnight fasting of animals before testing.

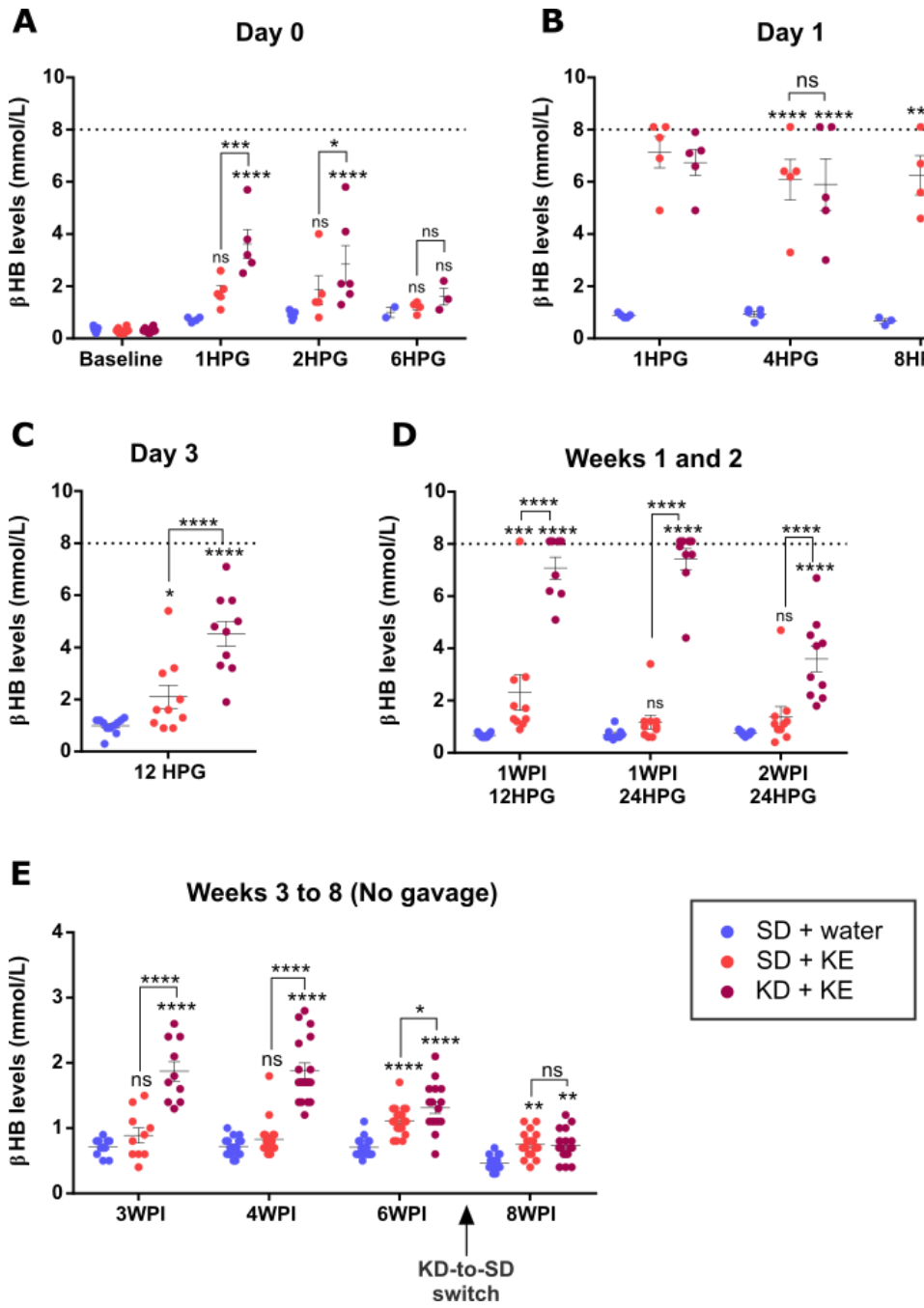

Figure 4.7 BHB levels during 8-week experiment. **(A)** BHB levels on Day 0 at 1, 3, or 6 hours post-gavage (HPG). **(B)** BHB levels on Day 1 and 1, 4, and 8HPG. All BHB readings of HI were plotted as 8.1. **(C)** BHB levels on Day 3 and 12HPG. **(D)** BHB levels at 1 or 2 weeks post-injury (WPI) following 12 or 24HPG. **(E)** BHB levels at 3, 4, 6, or 8WPI with KD-to-SD swtich for KD+KE group indicated. ns = not significant. * p<0.05, ** p<0.01, *** p<0.001, **** p <0.001 calculated using Two-way ANOVA with Tukey correction.

4.3.9 White matter sparing and NeuN+ counts

At 8WPI, tissue was fixed, frozen, sectioned, and stained to quantify white matter sparing and NeuN+ counts rostral and caudal to the injury site. Unfortunately, we did not see any improvement in white matter sparing either rostral, caudal, or at the injury epicenter **(Fig 4.8A and B)**. NeuN+ cells were also counted in sections 1.2mm rostral and caudal to the injury. NeuN+ cells were counted in the dorsal and ventral horn of the ipsilateral (injury) and contralateral sides of the cord. No significant changes were seen rostral to the injury **(Fig 4.8D)**. There was a slight but significant decrease in NeuN+ cells of the ipsilateral dorsal horn for KE-treated rats **(Fig 4.8E)**. This suggests KE may decrease survival of spinal interneurons in the dorsal horn of the ipsilateral side; however further work will need to confirm this finding.

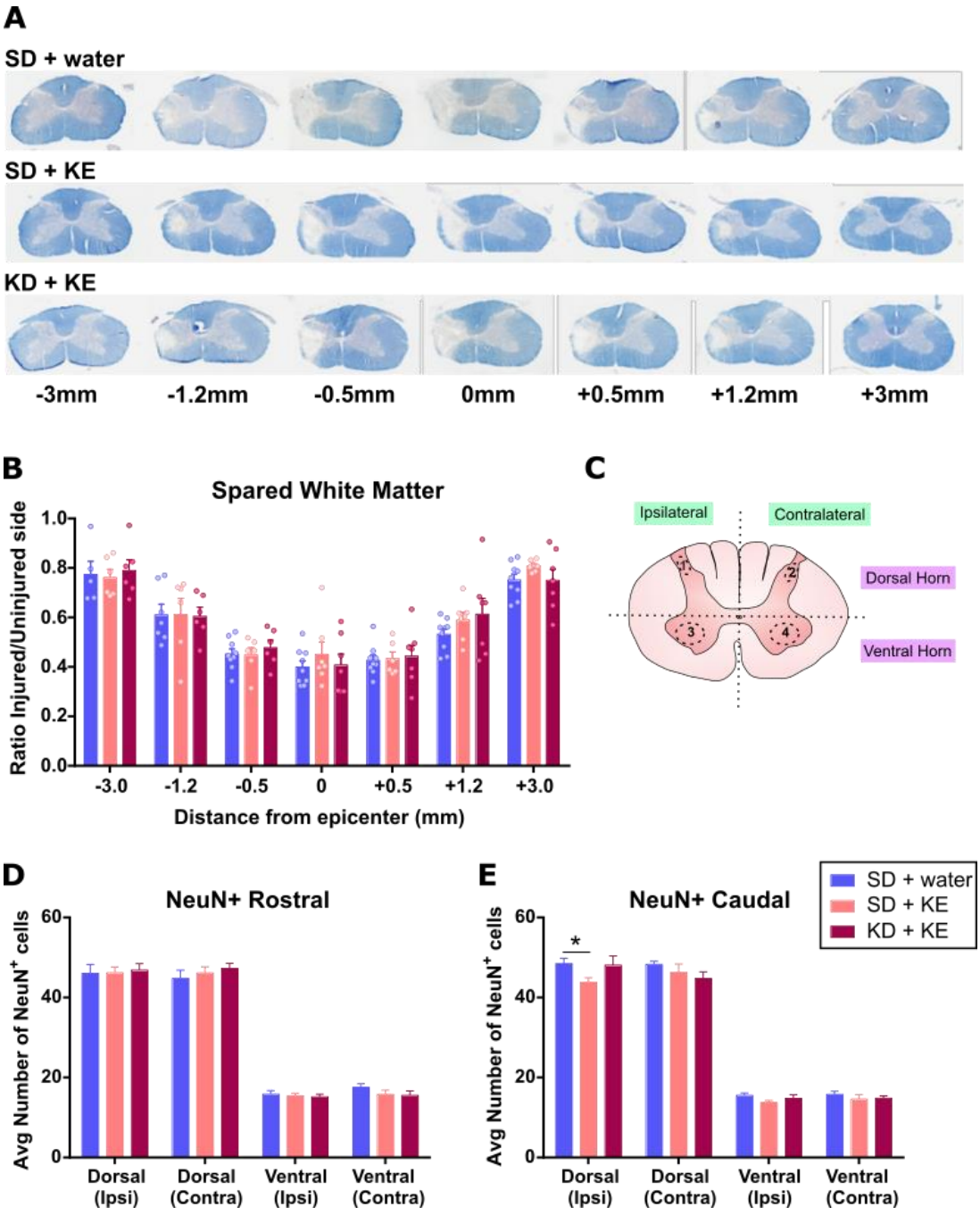

Figure 4.8 White matter sparing and NeuN+ cell counts at 8 WPI. **(A)** Representative images of Eirochrome Cyanine stain for white matter sparing. Deeper blue stain indicates more myelin. **(B)** Quantification of spared white matter comparing injured to uninjured side. **(C)** Schematic of spinal cord showing regions used for NeuN+ counts (dotted circles in ipsilateral and contralateral dises of dorsal and ventral horns). **(D and E)** Quantification of average number of NeuN+ cells per region for ipsilateral (ipsi) and contralateral (contra) regions of dorsal and ventral horns. NeuN+ counts were

performed in Rostral **(D)** or Caudal **(E)** sections. * $p<0.05$ calculated using Two-way ANOVA with Tukey correction.

4.3.10 Behavioural tests for forelimb function: Rearing

To test forelimb function, we used similar tests to those previously introduced in Chapter 2. We tested rearing function and use of the injured paw at 2, 4, 6, and 8 WPI. In this case the injured paw can be either the left or right paw. Each rat's preferred paw was determined during Montoya Staircase training and that side was correspondingly injured. As can be seen in **Fig 4.9**, there was a sharp decrease in use of the injured paw **(Fig 4.9A)** and both paws **(Fig 4.9C)** with a concurrent increase in use of the non-injured paw **(Fig 4.9B)**. In the previous KD study, it was observed that the injured forelimb was used around 3% and 13% for SD- and KD-fed rats respectively by 2 weeks post-injury (Streijger et al. 2013). These levels were sustained throughout the 14-week study. It's important to note that a 150kdyn force was used in the previous study while our present study used a more moderate 120kdyn force. Therefore, we thought it likely that there would be a less severe decrease in injured forelimb usage by 2WPI. However, this was not the case as SD-fed rats still showed around 2% usage of the injured forelimb by 2WPI. Furthermore, we saw no significant improvement in our SD group at later timepoints **(Fig 4.9A)**. As well, we saw no significant improvement in injured paw use with either KE or KD+KE **(Fig 4.9A)**.

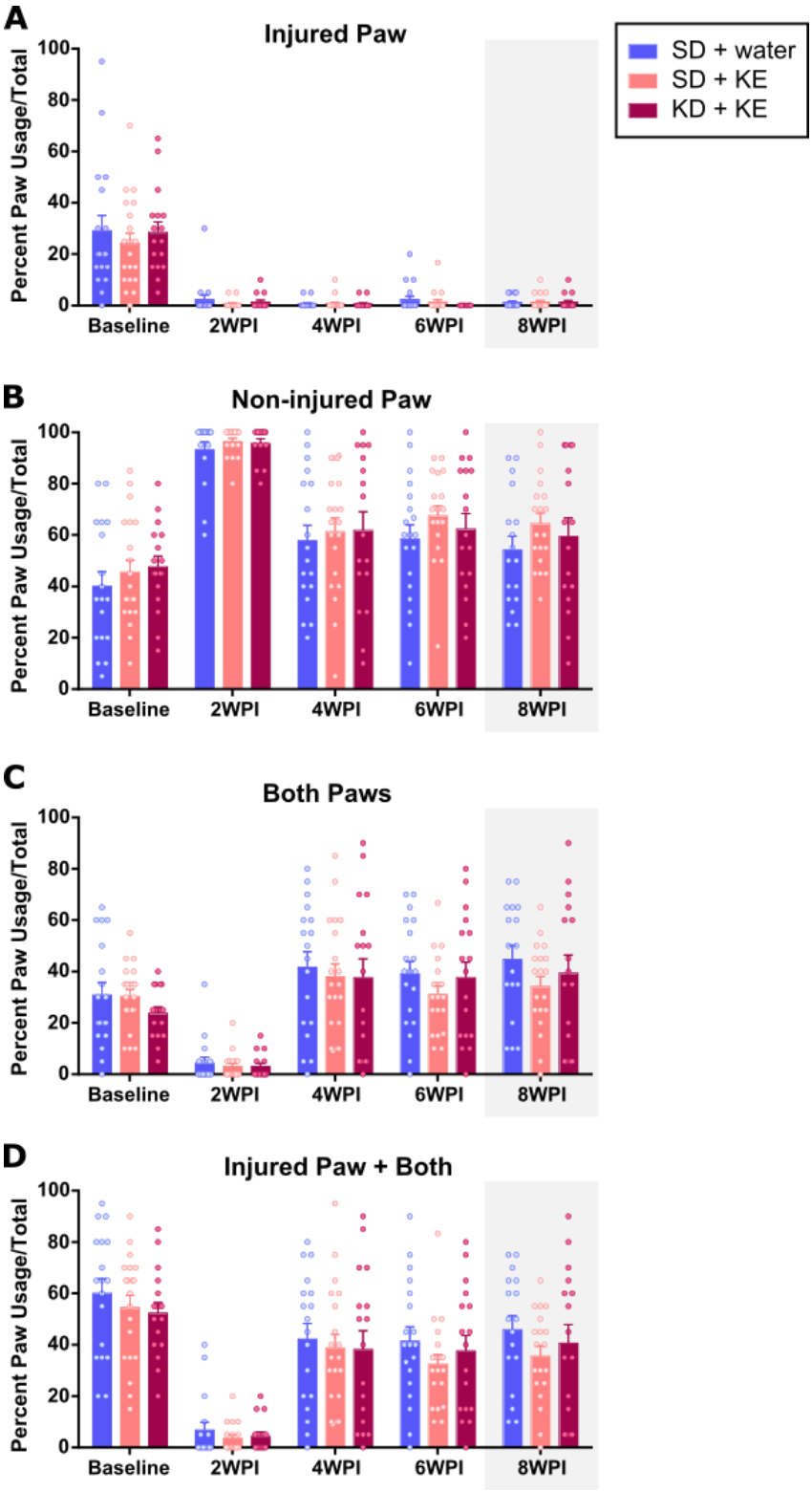

Figure 4.9 Rearing behavioural test showing paw usage during initial rears. Percent paw usage compared to total sum of all paw usage types for **(A)** injured paw, **(B)** non-injured paw, **(C)** both

paws, and **(D)** injured paw combined with both paws. Shaded grey region indicated KD+KE group is on SD at 8WPI.

4.3.11 Behavioural tests for forelimb function: Horizontal Ladder

Another measure of forelimb recovery is the horizontal ladder. This differs slightly from the ladder used with mice in Chapter 2, as although the rungs are irregularly spaced, they are not altered between timepoints. As well, all steps are counted, and errors are given as a percentage of total steps (correct + incorrect). Therefore, a higher percentage indicates more errors and worse behavioural recovery. We did not take a baseline measurement for this behaviour due to time constraints and the internal control of the uninjured paw. However, it is important to note that habituation to the ladder is likely harder once the animals are already injured and this could have led to greater errors in paw placement, both for the injured and non-injured paws. We did not see any significant differences between our 3 groups in use of injured paw at any timepoint **(Fig 4.10)**. Interestingly, we did see differences in % error of the non-injured paw. At 4WPI KD+KE rats showed fewer errors when compared to KE, while at 6WPI both the KE and KD+KE groups showed fewer errors when compared to the control group **(Fig 4.10)**. Its unclear why differences would exist for the non-injured paw, however it could relate to the motivation or speed used to cross the ladder. Regardless, the results of the injured paw indicate that neither KE nor KD+KE improve forelimb function during ladder crossing.

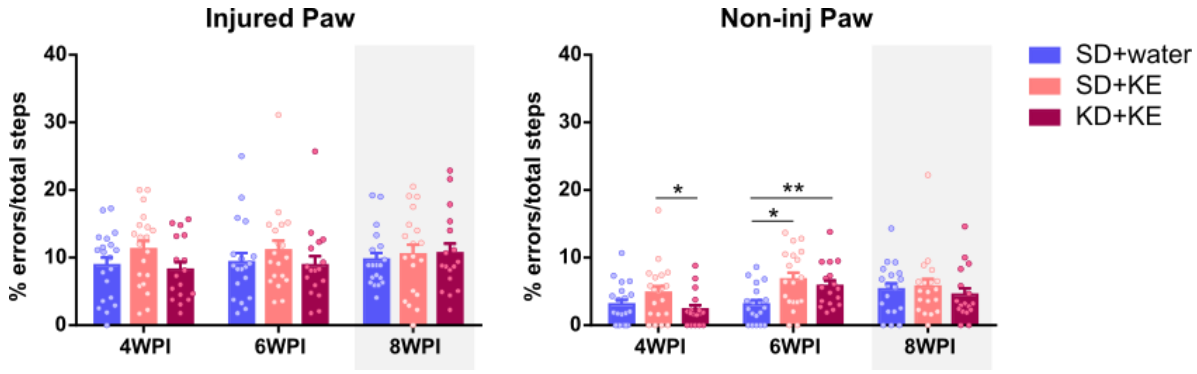

Figure 4.10 Horizontal ladder showing % forelimb errors compared to total steps for injured and non-injured paw. Shaded grey region indicated KD+KE group is on SD at 8WPI. * p<0.05, **p<0.01

4.3.12 Behavioural tests for grasping ability: Montoya Staircase

We also preformed several tests to look at grasping ability. The Montoya staircase test assesses both grasping and forelimb extension and was performed at 3, 5, and 7WPI. In the original KD study (Streijger et al. 2013), improvement of the injured forelimb was seen at 6WPI for the KD-fed group. Although we saw a decrease in percent pellets eaten using the injured paw after injury, we did not see any improvement with KE or KD+KE at any timepoint tested **(Fig 4.11)**. The non-injured paw was used as an internal control and indeed we did not see any changes between baseline and post-injury **(Fig 4.11)**. It is important to address a couple caveats of this behavioural test. For one, rats must be starved overnight to motivate them to eat the pellets. As fasting can also increase BHB levels, this is a confounding variable. As well, KD-fed rats do not get any sugar in their typical diets. As these pellets are high in sugar, KD-fed rats might be more (or less) motivated to eat the pellets. Finally, rats can sometimes move pellets to their mouth using a scooping motion rather than grasping motion. Therefore, the test cannot always perfectly capture improvement in grasping ability. Despite these caveats, our results match those seen with the ladder and rearing tests.

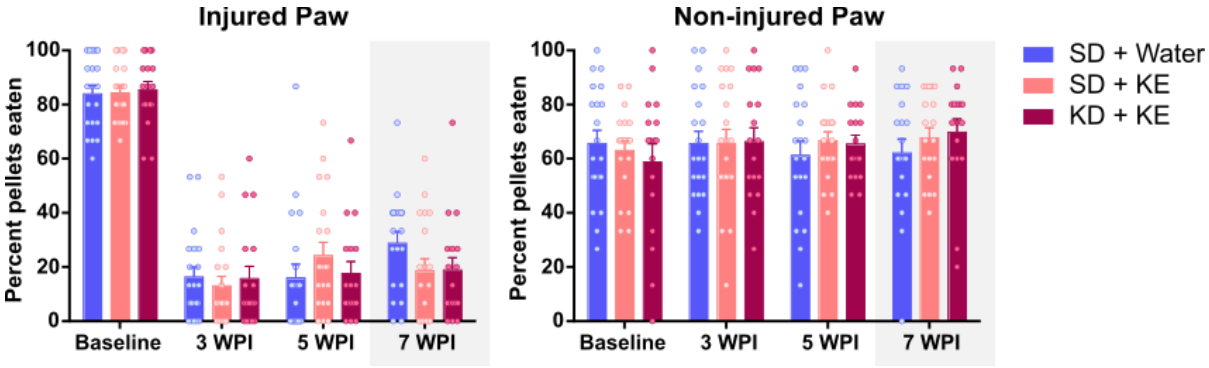

Figure 4.11 Montoya Staircase test of grasping ability by percent pellet eaten using the injured paw or non-injured paw. Shaded grey region indicated KD+KE group is on SD at 7WPI.

4.3.13 Behavioural tests for grasping ability: IBB score

Another measure of grasping improvement is the manipulation of a treat, such as a Froot Loops™ piece, during eating. The use of the forepaw digits during treat manipulation can be scored and summed to produce an IBB score, where the higher score indicates better manipulation and thus improved grasping. Again, we did not record a baseline but assessed behaviour at 3, 5, and 7WPI. Similar to the results of Montoya Staircase, we saw no significant differences between our groups at any time-point **(Fig 4.12)**. However, this behavioural test is also confounded by the use of sugary treats and periods of fasting to motivate eating.

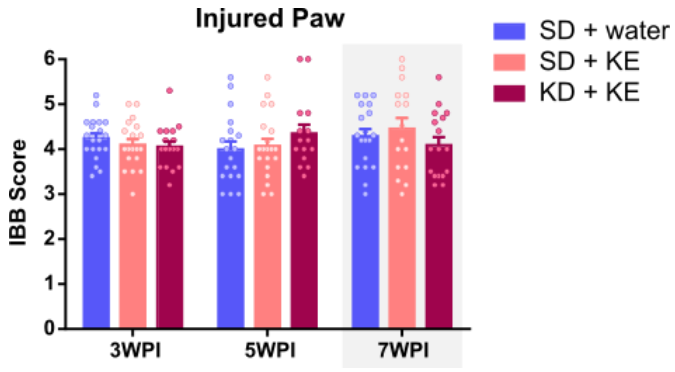

Figure 4.12 IBB score for test of grasping ability by the injured front paw. Shaded grey region indicated KD+KE group is on SD at 7WPI.

4.3.14 Behavioural tests for grasping ability: Digital Extension Score

The third test we used to assess grasping ability was the digital extension score, which is quantified using the horizontal ladder videos. As there is a mirror beneath the ladder, the opening of each paw during grasping of the next rung can be assessed across each ladder run. A perfect digital extension score is 2.0, which is readily achieved in the uninjured paw, as can be seen in **Fig 4.13**. Surprisingly, our KE group showed statistically significant improvement in digital extension score at both 6 and 8WPI **(Fig 4.13)**. Our KD+KE group did not show improvement compared to control and was significantly lower than KE at 8WPI indicating that the switch to SD did not improve recovery **(Fig 4.13)**. Together these results show the KE can improve grasping ability using digital extension as a measure.

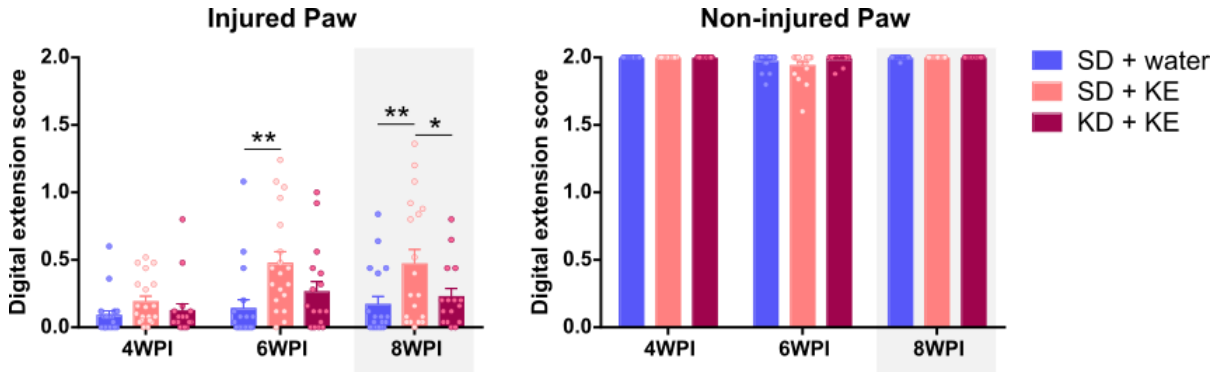

Figure 4.13 Digital Extension score of grasping ability during crossing of horizontal ladder. Digital extension score is shown for both injured and non-injured front paws. Shaded grey region indicated

KD+KE group is on SD at 8WPI. * $p<0.05$, ** $p<0.01$ calculated using Two-way ANOVA with Tukey correction.

4.4 Discussion

In Chapter 4, we aimed to investigate KE as an addition or alternative to KD for treatment of SCI. We took advantage of the exploratory power of proteomics to investigate widespread changes between our three treatments at 2 weeks post-injury and used behavioural tests and IF analysis to assess the potential of KE to improve recovery and tissue sparing following 8 weeks of treatment. Repeated administration of KE in rats and humans has previously been tested showing that continued exposure is safe and feasible (Clarke et al., 2012; Soto-Mota et al., 2019). Based on previous research, we suspected that BHB levels would peak within 1-2 hours after gavage and then decrease back to baseline (Clarke et al., 2012). Indeed, we found that levels were highest at 1 hour after gavage, however we also noted that the highest peak was seen on Day 1 rather than Day 0 **(Fig 4.2A and B, Fig 4.7A and B).** Previous studies reported no significant differences in BHB levels achieved at 30 minutes after gavage throughout a 28-day period (Soto-Mota et al. 2019). However, contrary to these findings we found a noticeable decrease in BHB elevation at 1HPG by 7DPI and an even further decrease by 14DPI **(Fig 4.2A and B).** It is unclear why we saw differences in BHB levels from those previously seen however it's likely due to the different metabolism of rats and/or the perturbations to metabolism after SCI. It is also possible that circulating levels of BHB may not reflect tissue levels of BHB. Future studies could also look at levels of BHB in urine to see if removal of excess BHB occurs as circulating levels of BHB increase. However previous research using a repeated dose of this KE over 5 days in humans did not see any increase in levels of BHB in the urine (Clarke et al., 2012).This suggests that BHB is likely being used by cells rather than being excreted.

Voluntary combination of KD and KE has also been assessed in humans and was not reported to increase BHB levels above those seen with KE alone (Soto-Mota et al. 2019). Contrary to this finding, we saw that KD+KE led to higher spikes in BHB levels that were sustained through the experiment. For example, even at 12 hours after gavage on Day 7, we saw BHB levels of 5.3mM (±0.36) for KD+KE treated rats compared to only 0.72mM (±0.04) in the KE only group **(Fig 4.2B).** In our 8-week experiment these high levels were even sustained up to 24 hours after gavage on Day 7 **(Fig 4.7).** Combined with the impaired weight gain **(Fig 4.1D and 4.5B)**, increased monitoring score **(Fig 4.1E and 4.6C)**, and low glucose levels **(Fig 4.2D)** seen in the KD+KE group, these data

suggests that a KD+KE combination may be deleterious. However, it is important to note that all our observations were after SCI. It is possible that in non-injured rats, we would not see such deficits. Still, these results caution against administering a similar treatment in humans following SCI.

To look at widespread changes in our KE, KD, and KD+KE groups at 2WPI, we performed a proteomic analysis of these groups compared to an injured control. We saw the highest number of significantly altered proteins in our KD group **(Fig 4.3C).** Surprisingly, KD reduced components of the 40S and 60L ribosomal complexes suggesting that KD may decrease translation **(Tables 4.6 and 4.7).** This was also seen in the scRNA-sequencing study from Chapter 3 suggesting it could be a conserved function of KD across species **(Fig 4.5)**. To date no studies of KD have shown this effect, but studies in fasting show that hepatic ribosomes have degradation rates that exceed synthesis of new ribosomes (Hirsch and Hiatt 1966). A similar mechanism could be occurring under KD. Furthermore, given that KD and fasting both generate high levels of ketone bodies, we could speculate that BHB is mediating these effects. However, this does not appear to be the case otherwise we would expect to see similar effects for KE treatment, which we do not. Another set of proteins decreased with KD were the histones including histones 3, 4, H2B, H1.4, and H1.5 **(Table 4.3)**. We confirmed that Histone 3 is decreased in our KD group by Western blot analysis **(Fig 4.4)**. A previous study looking at KD treatment of SCI in rats showed that KD increased acetylation of histone 3 but did not see any changes in total histone 3 levels (X. Wang et al. 2017). It is unclear why this decrease would occur or the effect of such a decrease as very few studies have looked at alteration of total histone levels. However, studies in yeast suggest that histone 3 depletion can lead to a wide-spread increase in gene expression (Gossett and Lieb 2012). This could be one of the reasons that we saw the most proteomic hits in the KD group **(Fig 4.3C)**, however further study is needed to determine the causal nature of these histone changes.

We did not see as many proteins differentially changed by KE or KD+KE **(Fig 4.3)**. Interestingly, for KD+KE there were many proteins significantly altered, however they largely fell below the 0.5 cut-off for fold-change **(Fig 4.3A)**. KE increased Glutathione reductase (Gsr) compared to control **(Table 4.4)**. KD has been shown to increase glutathione levels (Jarrett et al. 2008) and glutathione peroxidase activity (Ziegler et al. 2003). MMF, another agonist of the HCAR2 receptor, has also been shown to upregulate glutathione reductase (Hoffmann et al. 2017). As well BHB could partially rescue the production of glutathione after H_2O_2 stress *in vitro* (Cheng et al. 2013). Given these findings, it is possible that KE could be increasing glutathione reductase through BHB activation of HCAR2. Another protein increased by KE is ferritin light chain 1 (Ftl1) **(Table 4.4)**. Interestingly, upregulation

has been linked to oligodendrocyte biogenesis in the spinal cord (Schonberg et al. 2012). As well, a KEGG pathway analysis of proteins increased by KE shows an enrichment in glycosaminoglycan degradation **(Table 4.7)**. Glycosaminoglycans such as chondroitin sulfate proteoglycans (CSPGs) can inhibit axonal growth after SCI (Jones et al. 2002; Snow et al. 1990), and using chondroitinase to degrade CSPGs has been shown to improve functional recovery after SCI (Bradbury et al. 2002). As such, it is interesting to speculate that KE could also improve recovery by upregulating the glycosaminoglycan degradation pathway. Together our proteomic data suggests that KE and KD do not activate the same pathways and that KD has a more widespread effect on protein levels, possibly through regulation of histone levels.

In the second part of Chapter 4, we assessed changes in behavioural recovery for rats treated with KE or KD+KE compared to the SD control. The previous study showing that KD improves behavioural recovery using the same injury model in rats, showed improved rearing by 2WPI, and improvements on the Monotoya Staircase (Streijger et al. 2013). Using our regimen of KE treatment, we were not able to recapitulate these findings **(Fig 4.9 and Fig 4.11).** Furthermore, we did not see improvements on the horizontal ladder **(Fig 4.10)** or using the 'Froot Loop' test of grasping **(Fig 4.12).** However, we did see improvements in grasping ability using digital extension score **(Fig 4.13).** This test is independent of the rats' desire to eat the provided treat, which could skew both the Montoya staircase and the IBB or 'Froot Loop' test of grasping ability. We postulate that the reason we only saw improvement with the digital extension score is because it was able to detect very subtle changes in grasping ability that were not tied to the motivation of the animal. However, as KE did not show benefits in white matter sparing or NeuN+ cell counts at 8WPI **(Fig 4.8)**, it is unlikely that KE is having a strong effect on recovery - a finding echoed by the largely non-significant behavioural results. However, it is possible that KE alone is not sufficient to improve recovery as it does not target the same mechanisms as KD. Indeed, the proteomics analysis shows little overlap in pathways targeted by KE and KD **(Table 4.7)**. It is possible that this stems largely from the differences in BHB levels between KE and KD. Unlike KD, KE gavage does not provide sustained BHB levels and high spikes can occur with gavage in the first couple days after injury **(Fig 4.7B).** While KE can be incorporated into drinking water as we did after the first 2 weeks **(Fig 4.6)**, the bitter taste means that a high dilution (at least 1:20) is required. Other studies in rats, have incorporated KE in the chow during long-term studies (Clarke, Tchabanenko, Pawlosky, Carter, Knight, et al. 2012). While this allows for sustained BHB levels, it is problematic for administering KE acutely as the rats do not eat for the first 4-5 days after injury. Future studies will likely need to employ a combination of KE administered by gavage and KE administered in food.

In summary we find that KE treatment was not able to produce similar proteomic shifts or improvements in behavioural recovery as seen with KD. Furthermore, we show that a KD+KE combination is deleterious to acute recovery as shown by deficits in weight gain and increased monitoring score, however behavioural function is not significantly impacted. Despite these largely negative results, we still saw improvement in grasping ability with one behavioural test following KE treatment. This hints that manipulation of the treatment model may produce measurable benefits and begs for further studies using different KE treatment paradigms.

Chapter 5. Conclusions and Future Directions

The main goals of this thesis were to better understand the anti-inflammatory potential of KD in mice and to investigate the use of KE as an alternative to KD for acute treatment of SCI. Overall, my findings show that KD can reduce inflammation at 7 days post-injury in mice by reducing production of inflammatory cytokines CCL3 and CCL4 and limiting infiltration of CD45+ CD11b+ non-neutrophilic myeloid cells into the injury site. However, despite these promising findings, I did not see any evidence of neuronal protection or white matter sparing with KD treatment in mice using either a cervical hemi-crush injury or a thoracic midline contusive injury. My research in KE treatment following SCI in rats showed that while KE produced minor behavioural improvements, it did not improve white matter sparing or neuronal protection. As well, the proteomic profiles of KE and KD did not share enriched GO terms or KEGG pathways. Together the KE results suggest that the current paradigm of KE treatment is not sufficient to produce similar benefits to KD. As well, an important finding is that KD+KE is detrimental during acute recovery. In this chapter, I will address the main hypotheses of my thesis, the caveats of my work, and the potential avenues for future research in this field.

5.1 Hypothesis 1

My first hypothesis was that *mice fed KD acutely after a C4 DLF crush injury would show reduced markers of injury severity and improved behavioural recovery*. Previous work in the lab demonstrated that rats fed KD acutely after injury had improved gray matter and white matter sparing, and better behavioural recovery (Streijger et al. 2013). As our work aimed to further study the role of HCAR2 using a HCAR2-/- mouse line, we wanted to see if KD treatment led to similar improvements in mice following a cervical crush injury. Unfortunately, we did not see any sustained behavioural improvement with KD although there was a trend towards decreased lesion size in KD-fed mice at 7DPI. It's important to note that the earlier study in rats looked at the lesion size at 14WPI – a much later time point (Streijger et al. 2013). It is possible we would have seen significant differences at a later time point in mice as well. Although the C4 crush model has been previously characterized using multiple behavioural tests (Hilton et al. 2013), neither cervical nor crush models of SCI are widely used in mouse studies. The most common SCI model is the contusive injury (Sharif-Alhoseini et al. 2017) and a T9 midline contusion is perhaps the most commonly used mouse SCI model. Although

we chose to continue further studies with the T9 SCI model, behavioural testing was not repeated. This was partially due to the fact that we still did not see improved white matter sparing or NeuN+ cell counts with KD in this model. However, to the best of our knowledge no study has looked at KD treatment on behavioural recovery in mice. Therefore, a study evaluating KD in the T9 mouse model is warranted and could also shed light on the role of HCAR2 in mediating any behavioural improvements of KD.

5.2 Hypothesis 2

The second hypothesis I addressed was that *KD can reduce inflammation after SCI in mice through the BHB receptor, HCAR2*. In support of this hypothesis, we found that KD could reduce the presence of $CD45^{+}CD11b^{+}GR\text{-}1^{-}$ cells at the injury site 7DPI and this was dependent on the HCAR2 receptor. We speculated that these cells might be macrophages. On the other hand, we did not see any change in Iba1+ cells at the injury site by IF. As Iba1 is also a marker of macrophages, it is at first unclear why we see different results. However, looking at the data from our scRNA-sequencing experiment may give a clue. As can be seen in **Supp Fig 5 (Appendix B)**, Iba1 (also known as Aif1) is only expressed in Cd68+ macrophages and microglia. On the contrary, Cd11b (or Itgam) and Cd45 (or Ptprc) are expressed by all mature myeloid cells. GR-1 is a mix of Ly6C and Ly6G, and marks neutrophils, which in our scRNA-seq data comprises clusters 0 and 3. If we look at cells that are $CD45^{+}CD11b^{+}GR\text{-}1^{-}$ but not positive for Iba1, this still leaves the unknown myeloid cluster 1. It is possible that this is the subtype of cells affected by KD through HCAR2, especially since we see high expression of Hcar2 in this cluster. An important next step will be to further characterize this cell type at the injury site through IF or flow cytometry using key markers of this cluster (e.g. Csf1, Hdc, Il-1b, Nfkbia, Ptgs2). However it's important to note that RNA expression does not always correlate with protein expression data (Guo et al. 2008). For this reason, the cluster may not be identifiable at a protein level. Another possibility is to use a spatial transcriptomic method to correlate clusters of gene expression to different cells within and surrounding the lesion area. Finally, we only assessed changes in Iba1+ area based on Iba1 IF intensity. It would be worthwhile to assess morphological changes of the macrophages/microglia that are indicative of their activation state (S. David et al. 2018). In particular, are there more rounded, activated macrophages/microglia in the epicenter of SD-fed mice than KD-fed mice? Unfortunately, the 'messiness' of the injury site at early timepoints makes it technically challenging to do this kind of analysis. As such, using flow cytometry to distinguish myeloid cells based on pro-inflammatory cytokine production (especially CCL3 and CCL4), might give a clearer picture of how KD effects pro-inflammatory macrophages/microglia.

To the best of our knowledge, this is the first study to look at the effect of KD on SCI in mice. This makes it hard to compare our results to the literature. However, multiple studies in mice have demonstrated an anti-inflammatory role for KD in other neurodegenerative diseases. For example, KD was shown to reduce Iba1, TNFα, and iNos, while increasing Arg-1 and IL-4, in the optic nerve and retina using a mouse glaucoma model (Harun-Or-Rashid and Inman 2018). Our data did not replicate any of these findings following SCI although we did not specifically look at iNOS. Another study using a mouse experimental autoimmune encephalomyelitis (EAE) model of multiple sclerosis showed that KD reduced infiltration of CD4+ and CD11b+CD45+ cells into brain tissue and decreased production of multiple pro-inflammatory cytokines including IL-1β, IL-6, TNFα, CCL2, CCL3, and CCL4 (D. Y. Kim et al. 2012). They similarly speculate that the CD11b+CD45+ cells could be macrophages or microglia. Although our results likewise show a reduction of CD11b+CD45+ cells and reduction of CCL3 and CCL4, we do not see widespread reduction of multiple pro-inflammatory cytokines. It is important to note that in their study, mice were fed KD before EAE was induced (D. Y. Kim et al. 2012) and thus is a pre-treatment paradigm compared to our KD treatment paradigm where KD is introduced immediately after injury. It is possible that treating mice with KD before SCI would also lead to more extensive cytokine changes as the mice would already be in ketosis at the time of injury. However, this would not be as clinically relevant and as such might reveal results or mechanisms that are not reproducible in human clinical trials.

An important consideration when comparing KD research is that a standardized diet, either for KD or SD, does not exist. For example, in the mouse glaucoma study, they used a KD of 10.4% protein, 0.1% carbohydrate, and 89.5% fat (Harun-Or-Rashid and Inman 2018), while in the EAE study they used a KD of 8.6% protein, 3.2% carbohydrate, and 75.1% fat (D. Y. Kim et al. 2012). In contrast, the KD we use in our studies is 18.1% protein, 3.0% carbohydrate, and 65.8% fat. Although all these diets induce ketosis (increased levels of circulating BHB), it is unclear how the differing macronutrient ratios could affect inflammation. One difference that is readily noticeable between these diets is weight gain. Our diet shows an initial deficit in weight gain with KD following injury; however, by 7 days the difference is no longer statistically significant and both SD and KD-fed mice show comparable weight gain over long term (8-week) experiments. The mouse glaucoma study showed a weight difference of nearly 10g less for KD-fed mice after 8 weeks (Harun-Or-Rashid and Inman 2018). Whereas another study in C57Bl/6 mice showed increased weight in KD-fed mice starting at 38 days (around 5 weeks) after diet initiation (Goldberg et al. 2020). Surprisingly this was found using a seemingly identical KD to that used in the mouse glaucoma study although it could be

explained by the difference in mouse background (DBA/2J in the former study versus C57Bl/6 in the latter). On the other hand, KD may produce differing effects on weight depending on disease or injury models or strain of mice and independent of the macronutrient variation of the diet. While studies have accessed macronutrient variation in non-ketogenic diets (S. Hu et al. 2018), to the best of our knowledge no study has compared different KD in mice. Studies in rats and humans suggest that higher KD ratios (even up to 6:1 in rats) correlate with better seizure control (Wirrell et al. 2018). On the other hand, lower KD ratios were just as efficacious for many patients (Wirrell et al. 2018). Together these studies suggest that further research on the role of macronutrient composition in KD is needed. Especially in the context of neurodegenerative diseases and SCI, altering KD ratio could have significant and unknown effects.

A recent paper looking at KD-fed C57BL/6 mice found that KD decreased pro-inflammatory IL-1β and NLRP3 inflammasome expression in epididymal fat (Efat) at 1 week after KD initiation but led to an increase of both by 4 months on the diet as well as deficits in glucose homeostasis (Goldberg et al. 2020). They attributed these findings, both the initial benefits and eventual deficits, to the population of γδ T cells in the Efat as KD initially increased this pool but ultimately led to a severe reduction of γδ T cells by 4 months (Goldberg et al. 2020). Interestingly we also found a small pool of γδ T-cells (Cluster 8) in our scRNA-sequencing analysis of CD45+ cells from the injured mouse spinal cord at 7DPI. We did not see any change in this cell population between SD and KD, however we may see more infiltration of T cells with a later time-point as, at least in rats, infiltration of T cells peaks around 9DPI (Beck et al. 2010). One question raised by this recent study is: would we see glucose homeostasis deficits and an increase in inflammation had we continued KD longer after SCI? I think it unlikely as we saw no difference in weight gain between our SD and KD-fed mice while the Goldberg study saw significant weight gain in KD-fed mice. However, it will be important to test longer-term KD treatments after SCI to confirm this hypothesis.

Finally, a significant question that arises from Chapter 3 is why we did not see changes in white matter or NeuN+ cell survival with KD despite seeing a reduction in inflammation. It is possible that the time point chosen, 7DPI, is not adequate to show changes in white matter sparing or neuroprotection and a chronic time-point is needed to see the effects of KD. For example, other studies manipulating inflammatory proteins, such as deletion of CX3CR1, assess white matter sparing at 8WPI (Freria et al. 2017). On the other hand, at least in mice, the effects of KD on inflammation may not be sufficient to improve white or gray matter sparing. It is possible combining KD with other

potential SCI treatments, such as rehabilitative strategies, may be needed for reproducible benefits between species.

5.3 Hypothesis 3

Our third hypothesis was that *KE supplementation could produce similar benefits to KD treatment after SCI in rats*. We used a proteomics approach to see if KE and KD regulate similar pathways and also assessed the effect of KE on white matter sparing, NeuN+ cell counts, and behavioural improvement. Ideally we were hoping to replicate the molecular and behavioural improvements seen with KD treatment (Streijger et al. 2013). Unfortunately, we did not see high overlap in proteins altered by KE and KD, nor did we see similar GO terms or KEGG pathways enriched between the treatments. This could be partially due to the small number of proteins that were changed by KE (only 40 with KE versus 188 proteins altered by KD). As well, KE did not improve white matter sparing, NeuN+ cell counts, and there was little to no behavioural recovery with KE treatment compared to the sustained recovery previously seen with KD. Together these data point to marked differences between KE and KD. However, this is the first time that KE has been tested as a treatment for SCI. Although we were able to generate a robust increase in circulating BHB levels, these levels did not show sustained elevation. It is possible that sustained BHB levels are needed after SCI such as can be achieved with KD. On the other hand, KD may be able to activate pathways through other mechanisms than the increased production of BHB. Studies from the epilepsy field looking at KD treatment are mixed on the role of BHB in mediating its effects. Most studies have only shown a mild correlation or non-significant trend between circulating BHB and seizure reduction (van Delft et al. 2010; Gilbert, Pyzik, and Freeman 2000; Buchhalter et al. 2017). This would suggest that KD may be a better therapeutic than KE supplementation for treatment of SCI. On the other hand, continuous delivery of BHB in mice using an osmotic pump that was implanted 6 hours after SCI led to improved behavioural recovery, reduced indication of neuropathic pain, and reduced inflammation (Qian et al. 2017). This finding supports the hypothesis that sustained levels of BHB are needed to see improvements following SCI. Future paradigms of KE treatment could address this point by including KE in the food as has been done before in rat studies (Clarke et al., 2012). While the BHB levels achieved using this strategy were not as high as those achieved with oral gavage, they provided sustained levels around 1.0mmol/L (Murray et al. 2016), which are comparable to levels achievable with KD (Streijger et al. 2013). It would be worth completing further investigation to see if sustained levels of BHB achieved through incorporation of KE into the rats' diet is sufficient to improve behavioural recovery. This could be combined with oral gavage of KE during acute timepoints after

injury (e.g. within the first 24 hours) to further enhance BHB levels. There is also the potential to use KE as a supplement combined with rehabilitative training, which may provide additional benefits.

It's important to stress that we do not know how circulating BHB levels relate to cellular levels of BHB in the spinal cord. However, a strong correlation was found between brain parenchymal and serum BHB levels in pediatric individuals being treated with KD for epilepsy (Wright, Saneto, and Friedman 2018). As well, a recent study using an ^{11}C-AcAc tracer and a PET/CT scan to evaluate whole-body distribution after oral ingestion of BHB showed significant increases in the brain as well as the heart and kidneys (Cuenoud et al. 2020). This would suggest that the BHB from KE breakdown is being transported to the spinal cord after injury although additional studies will be needed to verify this point.

5.4 Conclusion

In summary, the main finding of this thesis is that KD can reduce certain features of inflammation following SCI. My research also highlights the role of HCAR2 in mediating the effect of KD on myeloid cells although further work needs to be completed to determine the pathways that regulate this effect and the specific cell type affected. The scRNA-sequencing analysis of CD45+ cells also identified a novel myeloid cluster. As this cluster was shown to highly express HCAR2, it is worth further characterizing.

Now that KD is being moved into clinical trials as a treatment for SCI (Yarar-Fisher et al. 2018), I am sometimes asked what is the point of my studies in KD? I think that an improved understanding of the cellular and molecular mechanisms involved in the beneficial effects of KD is still very important as it could further inform clinical use of the diet and may identify additional targets for SCI therapy. Especially considering that there have been no treatments proven to effectively improve the acutely injured spinal cord. For example, during the acute stages of SCI, a marked energy deficit occurs. BHB can be used as an energy source but it is difficult to administer KD during the initial 24 hours following injury. KE could be used to increase BHB levels during these acute stages. Even though our data do not yet support use of KE as a treatment for SCI, it is worth pursuing further with different treatment paradigms. Together, the data in this thesis provide evidence of reduced inflammation with KD treatment and promising avenues for further exploration of SCI treatment using KE or KD.

Bibliography

An, R, Stephen J A Davies, Michael T Fitch, and Jerry Silver. 1997. “Regeneration of Adult Axons in White Matter Tracts of the Central Nervous System” 390 (December): 372–75.

Ankeny, Daniel P., Kurt M. Lucin, Virginia M. Sanders, Violeta M. McGaughy, and Phillip G. Popovich. 2006. “Spinal Cord Injury Triggers Systemic Autoimmunity: Evidence for Chronic B Lymphocyte Activation and Lupus-like Autoantibody Synthesis.” *Journal of Neurochemistry* 99 (4): 1073–87. https://doi.org/10.1111/j.1471-4159.2006.04147.x.

Appelberg, K Sofia, David A Hovda, and Mayumi L. Prins. 2009. “The Effects of a Ketogenic Diet on Behavioral Outcome after Controlled Cortical Impact Injury in the Juvenile and Adult Rat” 506 (April): 497–506.

Arevalo-martin, Angel, Lukas Grassner, Daniel Garcia-ovejero, Angela Turrero, Eduardo Vargas, Monica Alcobendas, Carmen Rosell, et al. 2018. “Elevated Autoantibodies in Subacute Human Spinal Cord Injury Are Naturally Occurring Antibodies” 9 (October): 1–18. https://doi.org/10.3389/fimmu.2018.02365.

Auwera, Ingrid Van der, Stefaan Wera, Fred Van Leuven, and Samuel T. Henderson. 2005. “A Ketogenic Diet Reduces Amyloid Beta 40 and 42 in a Mouse Model of Alzheimer’s Disease.” *Nutrition & Metabolism* 2: 28. https://doi.org/10.1186/1743-7075-2-28.

Azbill, Robert D, Xiaojun Mu, Annadora J Bruce-keller, Mark P Mattson, and Joe E Springer. 1997. “Impaired Mitochondrial Function , Oxidative Stress and Altered Antioxidant Enzyme Activities Following Traumatic Spinal Cord Injury.” *Brain Research* 765: 283–90.

Bastien, Dominic, and Steve Lacroix. 2014. “Cytokine Pathways Regulating Glial and Leukocyte Function after Spinal Cord and Peripheral Nerve Injury.” *Experimental Neurology* 258: 62–77. https://doi.org/10.1016/j.expneurol.2014.04.006.

Beck, Kevin D., Hal X. Nguyen, Manuel D. Galvan, Desirée L. Salazar, Trent M. Woodruff, and Aileen J. Anderson. 2010. “Quantitative Analysis of Cellular Inflammation after Traumatic Spinal Cord Injury: Evidence for a Multiphasic Inflammatory Response in the Acute to Chronic Environment.” *Brain* 133 (2): 433–47. https://doi.org/10.1093/brain/awp322.

Beckett, Tina L., Christa M. Studzinski, Jeffrey N. Keller, M. Paul Murphy, and Dana M. Niedowicz. 2013. “A Ketogenic Diet Improves Motor Performance but Does Not Affect B-Amyloid Levels in a Mouse Model of Alzheimer’s Disease.” *Brain Research* 1505: 61–67. https://doi.org/10.1016/j.brainres.2013.01.046.

Behrman, Andrea L., Elizabeth M. Ardolino, and Susan J. Harkema. 2017. “Activity-Based Therapy: From Basic Science to Clinical Application for Recovery after Spinal Cord Injury.” *Journal of Neurologic Physical Therapy* 41 (July 2016): S39–45. https://doi.org/10.1097/NPT.0000000000000184.

Bellver-Landete, Victor, Floriane Bretheau, Benoit Mailhot, Nicolas Vallières, Martine Lessard, Marie Eve Janelle, Nathalie Vernoux, et al. 2019. “Microglia Are an Essential Component of the Neuroprotective Scar That Forms after Spinal Cord Injury.” *Nature Communications* 10 (1). https://doi.org/10.1038/s41467-019-08446-0.

Benevento, Barbara T., and Marca L. Sipski. 2002. “Neurogenic Bladder, Neurogenic Bowel, and Sexual Dysfunction in People With Spinal Cord Injury.” *Physical Therapy* 82 (6): 601–12.

Bennett, Mariko L., F. Chris Bennett, Shane A. Liddelow, Bahareh Ajami, Jennifer L. Zamanian, Nathaniel B. Fernhoff, Sara B. Mulinyawe, et al. 2016. “New Tools for Studying Microglia in the Mouse and Human CNS.” *Proceedings of the National Academy of Sciences* 113 (12): E1738–46. https://doi.org/10.1073/pnas.1525528113.

Biering-sùrensen, Fin, and Jens Sùnksen. 2001. “Review Sexual Function in Spinal Cord Lesioned Men.” *Spinal Cord* 39: 455–70.

Blazquez, Cristina, Angela Woods, Maria L. de Ceballos, David Carling, and Manuel Guzman. 1999. “The AMP-Activated Protein Kinase Is Involved in the Regulation of Ketone Body Production by Astrocytes.” *Journal of Neurochemistry* 73: 1674–82.

Bough, Kristopher J., Jonathon Wetherington, Bjørnar Hassel, Jean Francois Pare, Jeremy W. Gawryluk, James G. Greene, Renee Shaw, Yoland Smith, Jonathan D. Geiger, and Raymond J. Dingledine. 2006. “Mitochondrial Biogenesis in the Anticonvulsant Mechanism of the Ketogenic Diet.” *Annals of Neurology* 60 (2): 223–35. https://doi.org/10.1002/ana.20899.

Bowes, Amy L., and Ping K. Yip. 2014. “Modulating Inflammatory Cell Responses to Spinal Cord Injury: All in Good Time.” *Journal of Neurotrauma* 31 (21): 1753–66. https://doi.org/10.1089/neu.2014.3429.

Bradbury, Elizabeth J., Lawrence D.F. Moon, Reena J. Popat, Von R. King, Gavin S. Bennett, Preena N. Patel, James W. Fawcett, and Stephen B. McMahon. 2002. “Chondroitinase ABC Promotes Functional Recovery after Spinal Cord Injury.” *Nature* 416 (6881): 636–40. https://doi.org/10.1038/416636a.

Brambilla, Roberta, Valerie Bracchi-Ricard, Wen Hui Hu, Beata Frydel, Annmarie Bramwell, Shaffiat Karmally, Edward J. Green, and John R. Bethea. 2005. “Inhibition of Astroglial Nuclear Factor KB Reduces Inflammation and Improves Functional Recovery after Spinal Cord Injury.” *Journal of Experimental Medicine* 202 (1): 145–56. https://doi.org/10.1084/jem.20041918.

Brambilla, Roberta, Andres Hurtado, Trikaldarshi Persaud, Kim Esham, Damien D. Pearse, Martin Oudega, and John R. Bethea. 2009. “Transgenic Inhibition of Astroglial NF-KB Leads to Increased Axonal Sparing and Sprouting Following Spinal Cord Injury.” *Journal of Neurochemistry* 110 (2): 765–78. https://doi.org/10.1111/j.1471-4159.2009.06190.x.

Brommer, Benedikt, Odilo Engel, Marcel A. Kopp, Ralf Watzlawick, Susanne Müller, Harald Prüss, Yuying Chen, et al. 2016. “Spinal Cord Injury-Induced Immune Deficiency Syndrome Enhances Infection Susceptibility Dependent on Lesion Level.” *Brain* 139 (3): 692–707. https://doi.org/10.1093/brain/awv375.

Brownlow, Milene L., Leif Benner, Dominic P. D’Agostino, Marcia N. Gordon, and Dave Morgan. 2013. “Ketogenic Diet Improves Motor Performance but Not Cognition in Two Mouse Models of Alzheimer’s Pathology.” *PLoS ONE* 8 (9): 2–11. https://doi.org/10.1371/journal.pone.0075713.

Buchhalter, Jeffrey R., Sabrina D’Alfonso, Mary Connolly, Ernest Fung, Aspasia Michoulas, David

Sinasac, Rachel Singer, Jacklyn Smith, Narender Singh, and Jong M. Rho. 2017. “The Relationship between D-Beta-Hydroxybutyrate Blood Concentrations and Seizure Control in Children Treated with the Ketogenic Diet for Medically Intractable Epilepsy.” *Epilepsia Open* 2 (3): 317–21. https://doi.org/10.1002/epi4.12058.

Buss, A., G.A. Brook, B. Kakulas, D. Martin, R. Franzen, J. Schoenen, J. Noth, and A.B. Schmitt. 2004. “Gradual Loss of Myelin and Formation of an Astrocytic Scar during Wallerian Degeneration in the Human Spinal Cord.” *Brain* 127 (1): 34–44. https://doi.org/10.1093/brain/awh001.

Butler, Andrew, Paul Hoffman, Peter Smibert, Efthymia Papalexi, and Rahul Satija. 2018. “Integrating Single-Cell Transcriptomic Data across Different Conditions, Technologies, and Species.” *Nature Biotechnology* 36 (5): 411–20. https://doi.org/10.1038/nbt.4096.

Butovsky, Oleg, Mark P. Jedrychowski, Craig S. Moore, Ron Cialic, Amanda J. Lanser, Galina Gabriely, Thomas Koeglsperger, et al. 2014. “Identification of a Unique TGF-β-Dependent Molecular and Functional Signature in Microglia.” *Nature Neuroscience* 17 (1): 131–43. https://doi.org/10.1038/nn.3599.

Cahill, G. F., M. G. Herrera, A. P. Morgan, J. S. Soeldner, J. Steinke, P. L. Levy, G. A. Reichard, and D. M. Kipnis. 1966. “Hormone-Fuel Interrelationships during Fasting.” *The Journal of Clinical Investigation* 45 (11): 1751–69. https://doi.org/10.1172/JCI105481.

Campagnolo, D I, J A Bartlett, and S E Keller. 2000. “Influence of Neurological Level on Immune Function Following Spinal Cord Injury: A Review.” *The Journal of Spinal Cord Medicine* 23 (2): 121–28. https://doi.org/10.1080/10790268.2000.11753519.

Cao, Qilin, Yi Ping Zhang, Christopher Iannotti, William H. DeVries, Xiao-Ming Xu, Christopher B. Shields, and Scott R. Whittemore. 2005. “Functional and Electrophysiological Changes after Graded Traumatic Spinal Cord Injury in Adult Rat.” *Experimental Neurology* 191 (February): S3–16. https://doi.org/10.1016/j.expneurol.2004.08.026.

Casili, Giovanna, Daniela Impellizzeri, Marika Cordaro, Emanuela Esposito, and Salvatore Cuzzocrea. 2016. “B-Cell Depletion with CD20 Antibodies as New Approach in the Treatment of Inflammatory and Immunological Events Associated with Spinal Cord Injury.” *Neurotherapeutics* 13 (4): 880–94. https://doi.org/10.1007/s13311-016-0446-2.

Chen, Maio S., Andrea B. Huber, Marjan E. van der Haar, Marcus Frank, Lisa Schenll, Adrian A. Spillmann, Franziska Christ, and Martin E Schwab. 2000. “Nogo-A Is a Myelin-Associated Neurite Outgrowth Inhibitor and an Antigen for Monoclonal Antibody IN-1.” *Nature* 403: 434–39. https://doi.org/10.1038/35000219.

Cheng, Baohua, Hai Lu, Bo Bai, and Jing Chen. 2013. “D-β-Hydroxybutyrate Inhibited the Apoptosis of PC12 Cells Induced by H2O2 via Inhibiting Oxidative Stress.” *Neurochemistry International* 62 (5): 620–25. https://doi.org/10.1016/j.neuint.2012.09.011.

Cho, Newton, Jordan W. Squair, Jocelyne Bloch, and Grégoire Courtine. 2019. “Neurorestorative Interventions Involving Bioelectronic Implants after Spinal Cord Injury.” *Bioelectronic Medicine* 5 (1): 1–19. https://doi.org/10.1186/s42234-019-0027-x.

Clarke, Kieran, Kirill Tchabanenko, Robert Pawlosky, Emma Carter, Nicholas S. Knight, Andrew J.

Murray, Lowri E. Cochlin, et al. 2012. “Oral 28-Day and Developmental Toxicity Studies of (R)-3-Hydroxybutyl (R)-3-Hydroxybutyrate.” *Regulatory Toxicology and Pharmacology* 63 (2): 196–208. https://doi.org/10.1016/j.yrtph.2012.04.001.

Clarke, Kieran, Kirill Tchabanenko, Robert Pawlosky, Emma Carter, M. Todd King, Kathy Musa-Veloso, Manki Ho, et al. 2012. “Kinetics, Safety and Tolerability of (R)-3-Hydroxybutyl (R)-3-Hydroxybutyrate in Healthy Adult Subjects.” *Regulatory Toxicology and Pharmacology* 63 (3): 401–8. https://doi.org/10.1016/j.yrtph.2012.04.008.

Cox, Pete J., Tom Kirk, Tom Ashmore, Kristof Willerton, Rhys Evans, Alan Smith, Andrew J. Murray, et al. 2016. “Nutritional Ketosis Alters Fuel Preference and Thereby Endurance Performance in Athletes.” *Cell Metabolism* 24 (2): 256–68. https://doi.org/10.1016/j.cmet.2016.07.010.

Cragg, Jacquelyn, and Andrei V. Krassioukov. 2012. “Autonomic Dysreflexia.” *Cmaj* 184 (1): 66. https://doi.org/10.1503/cmaj.110859.

Craig, Ashley, Kathryn Nicholson Perry, Rebecca Guest, Yvonne Tran, Annalisa Dezarnaulds, Alison Hales, Catherine Ephraums, and James Middleton. 2015. “Prospective Study of the Occurrence of Psychological Disorders and Comorbidities after Spinal Cord Injury.” *Archives of Physical Medicine and Rehabilitation* 96 (8): 1426–34. https://doi.org/10.1016/j.apmr.2015.02.027.

Cregg, Jared M., Marc A. DePaul, Angela R. Filous, Bradley T. Lang, Amanda Tran, and Jerry Silver. 2014. “Functional Regeneration beyond the Glial Scar.” *Experimental Neurology* 253 (1): 197–207. https://doi.org/10.1016/j.expneurol.2013.12.024.

Çubukçu, Duygu, Orkide Güzel, and Nur Arslan. 2018. “Effect of Ketogenic Diet on Motor Functions and Daily Living Activities of Children With Multidrug-Resistant Epilepsy: A Prospective Study.” *Journal of Child Neurology* 33 (11): 718–23. https://doi.org/10.1177/0883073818786558.

Cuenoud, Bernard, Mickaël Hartweg, Jean Philippe Godin, Etienne Croteau, Mathieu Maltais, Christian Alexandre Castellano, André C. Carpentier, and Stephen C. Cunnane. 2020. “Metabolism of Exogenous D-Beta-Hydroxybutyrate, an Energy Substrate Avidly Consumed by the Heart and Kidney.” *Frontiers in Nutrition* 7 (February): 1–9. https://doi.org/10.3389/fnut.2020.00013.

David, Brian T., and Oswald Steward. 2010. “Deficits in Bladder Function Following Spinal Cord Injury Vary Depending on the Level of the Injury.” *Experimental Neurology* 226 (1): 128–35. https://doi.org/10.1016/j.expneurol.2010.08.014.

David, Samuel, Antje Kroner, Andrew D. Greenhalgh, Juan G. Zarruk, and Rubén López-Vales. 2018. “Myeloid Cell Responses after Spinal Cord Injury.” *Journal of Neuroimmunology* 321 (March): 97–108. https://doi.org/10.1016/j.jneuroim.2018.06.003.

Delft, Renske van, Danielle Lambrechts, Pauline Verschuure, Jacques Hulsman, and Marian Majoie. 2010. “Blood Beta-Hydroxybutyrate Correlates Better with Seizure Reduction Due to Ketogenic Diet than Do Ketones in the Urine.” *Seizure* 19 (1): 36–39. https://doi.org/10.1016/j.seizure.2009.10.009.

Deng-bryant, Ying, Mayumi L. Prins, David A Hovda, and Neil G Harris. 2011. “Ketogenic Diet

Prevents Alterations in Brain Metabolism in Young but Not Adult Rats after Traumatic Brain Injury" 1825 (September): 1813–25. https://doi.org/10.1089/neu.2011.1822.

Devanney, Nicholas A., Andrew N. Stewart, and John C. Gensel. 2020. "Microglia and Macrophage Metabolism in CNS Injury and Disease: The Role of Immunometabolism in Neurodegeneration and Neurotrauma." *Experimental Neurology* 329 (April): 113310. https://doi.org/10.1016/j.expneurol.2020.113310.

Díez-Revuelta, Natalia, Silvia Velasco, Sabine André, Herbert Kaltner, Dieter Kübler, Hans Joachim Gabius, and José Abad-Rodríguez. 2010. "Phosphorylation of Adhesion- and Growth-Regulatory Human Galectin-3 Leads to the Induction of Axonal Branching by Local Membrane L1 and ERM Redistribution." *Journal of Cell Science* 123 (5): 671–81. https://doi.org/10.1242/jcs.058198.

Digby, Janet E., Eileen McNeill, Oliver J. Dyar, Vincent Lam, David R. Greaves, and Robin P. Choudhury. 2010. "Anti-Inflammatory Effects of Nicotinic Acid in Adipocytes Demonstrated by Suppression of Fractalkine, RANTES, and MCP-1 and Upregulation of Adiponectin." *Atherosclerosis* 209 (1): 89–95. https://doi.org/10.1016/j.atherosclerosis.2009.08.045.

Dunham, Kelly A, Akkradate Siriphorn, Supin Chompoopong, and Candace L Floyd. 2010. "Characterization of a Graded Cervical Hemicontusion Spinal Cord Injury Model in Adult Male Rats" 2106 (November): 2091–2106. https://doi.org/10.1089/neu.2010.1424.

Dupuis, Nina, Niccolo Curatolo, Jean-Francois Benoist, and Stephane Auvin. 2015. "Ketogenic Diet Exhibits Anti-Inflammatory Properties." *Epilepsia* 56 (7): e95–98. https://doi.org/10.1111/epi.13038.

Dusart, I., and Martin E Schwab. 1994. "Secondary Cell Death and the Inflammatory Reaction After Dorsal Hemisection of the Rat Spinal Cord." *European Journal of Neuroscience* 6 (5): 712–24. https://doi.org/10.1111/j.1460-9568.1994.tb00983.x.

Erturk, A., Farida Hellal, Joana Enes, and Frank Bradke. 2007. "Disorganized Microtubules Underlie the Formation of Retraction Bulbs and the Failure of Axonal Regeneration." *Journal of Neuroscience* 27 (34): 9169–80. https://doi.org/10.1523/JNEUROSCI.0612-07.2007.

Farkas, Gary J., and David R. Gater. 2017. "Neurogenic Obesity and Systemic Inflammation Following Spinal Cord Injury: A Review." *The Journal of Spinal Cord Medicine* 0 (0): 1–10. https://doi.org/10.1080/10790268.2017.1357104.

Fehlings, Michael G., and Richard G. Perrin. 2005. "The Role and Timing of Early Decompression for Cervical Spinal Cord Injury: Update with a Review of Recent Clinical Evidence." *Injury* 36 (SUPPL. 2): S13–26. https://doi.org/10.1016/j.injury.2005.06.011.

Feingold, Kenneth R., Arthur Moser, Judy K. Shigenaga, and Carl Grunfeld. 2014. "Inflammation Stimulates Niacin Receptor (GPR109A/HCA2) Expression in Adipose Tissue and Macrophages." *Journal of Lipid Research* 55 (12): 1–43. https://doi.org/10.1194/jlr.M050955.

Filous, Angela R., and Jan M. Schwab. 2018. "Determinants of Axon Growth, Plasticity, and Regeneration in the Context of Spinal Cord Injury." *American Journal of Pathology* 188 (1): 53–62. https://doi.org/10.1016/j.ajpath.2017.09.005.

Finnerup, Nanna Brix. 2013. “Pain in Patients with Spinal Cord Injury.” *Pain* 154: S71–76. https://doi.org/10.1016/j.pain.2012.12.007.

Fitch, Michael T, Catherine Doller, Colin K Combs, Gary E Landreth, and Jerry Silver. 1999. “Cellular and Molecular Mechanisms of Glial Scarring and Progressive Cavitation: In Vivo and in Vitro Analysis of Inflammation-Induced Secondary Injury after CNS Trauma.” *The Journal of Neuroscience : The Official Journal of the Society for Neuroscience* 19 (19): 8182–98. https://doi.org/10.1523/jneurosci.2488-08.2008.

Fleming, Jennifer C., Michael D. Norenberg, David A. Ramsay, Gregory A. Dekaban, Alexander E. Marcillo, Alvaro D. Saenz, Melissa Pasquale-Styles, W. Dalton Dietrich, and Lynne C. Weaver. 2006. “The Cellular Inflammatory Response in Human Spinal Cords after Injury.” *Brain* 129 (12): 3249–69. https://doi.org/10.1093/brain/awl296.

Freria, Camila M., Jodie C.E. Hall, Ping Wei, Zhen Guan, Dana M. McTigue, and Phillip G. Popovich. 2017. “Deletion of the Fractalkine Receptor, CX3CR1, Improves Endogenous Repair, Axon Sprouting, and Synaptogenesis after Spinal Cord Injury in Mice.” *Journal of Neuroscience* 37 (13): 3568–87. https://doi.org/10.1523/JNEUROSCI.2841-16.2017.

Fu, Shou Peng, B.-R. Liu, J.-F. Wang, W.-J. Xue, H.-M. Liu, Y.-L. Zeng, B.-X. Huang, et al. 2015. “β-Hydroxybutyric Acid Inhibits Growth Hormone-Releasing Hormone Synthesis and Secretion Through the GPR109A/Extracellular Signal-Regulated 1/2 Signalling Pathway in the Hypothalamus.” *Journal of Neuroendocrinology* 27 (3): 212–22. https://doi.org/10.1111/jne.12256.

Fu, Shou Peng, Jian Fa Wang, Wen Jing Xue, Hong Mei Liu, Bing run Liu, Ya Long Zeng, Su Nan Li, et al. 2015. “Anti-Inflammatory Effects of BHBA in Both in Vivo and in Vitro Parkinson’s Disease Models Are Mediated by GPR109A-Dependent Mechanisms.” *Journal of Neuroinflammation* 12 (1): 1–14. https://doi.org/10.1186/s12974-014-0230-3.

Gilbert, D. L., Paula L. Pyzik, and J. M. Freeman. 2000. “The Ketogenic Diet: Seizure Control Correlates Better with Serum β-Hydroxybutyrate than with Urine Ketones.” *Journal of Child Neurology* 15 (12): 787–90. https://doi.org/10.1177/088307380001501203.

Glickman, Scott, and Michael A Kamm. 1996. “Bowel Dysfunction in Spinal-Cord-Injury Patients.” *Lancet* 347: 1651–53.

Goldberg, Emily L., Irina Shchukina, Jennifer L. Asher, Sviatoslav Sidorov, Maxim N. Artyomov, and Vishwa Deep Dixit. 2020. “Ketogenesis Activates Metabolically Protective Γδ T Cells in Visceral Adipose Tissue.” *Nature Metabolism* 2 (1): 50–61. https://doi.org/10.1038/s42255-019-0160-6.

Gorgey, A S, David R. Dolbow, J D Dolbow, R K Khalil, C Castillo, and D R Gater. 2014. “Effects of Spinal Cord Injury on Body Composition and Metabolic Profile – Part I.” *The Journal of Spinal Cord Medicine* 37 (6): 693–702. https://doi.org/10.1179/2045772314Y.0000000245.

Gossett, Andrea J., and Jason D. Lieb. 2012. “In Vivo Effects of Histone H3 Depletion on Nucleosome Occupancy and Position in Saccharomyces Cerevisiae.” *PLoS Genetics* 8 (6). https://doi.org/10.1371/journal.pgen.1002771.

Greenhalgh, Andrew D., Juan G. Zarruk, Luke M. Healy, Sam J. Baskar Jesudasan, Priya Jhelum,

Christopher K. Salmon, Albert Formanek, et al. 2018. “Peripherally Derived Macrophages Modulate Microglial Function to Reduce Inflammation after CNS Injury.” *PLoS Biology* 16 (10): e2005264. https://doi.org/10.1371/journal.pbio.2005264.

Guo, Yanfang, Peng Xiao, Shufeng Lei, Feiyan Deng, Gary Guishan Xiao, Yaozhong Liu, Xiangding Chen, et al. 2008. “How Is MRNA Expression Predictive for Protein Expression? A Correlation Study on Human Circulating Monocytes.” *Acta Biochimica et Biophysica Sinica* 40 (5): 426–36. https://doi.org/10.1111/j.1745-7270.2008.00418.x.

Hammond, Timothy R., Connor Dufort, Lasse Dissing-Olesen, Stefanie Giera, Adam Young, Alec Wysoker, Alec J. Walker, et al. 2019. “Single-Cell RNA Sequencing of Microglia throughout the Mouse Lifespan and in the Injured Brain Reveals Complex Cell-State Changes.” *Immunity* 50 (1): 253-271.e6. https://doi.org/10.1016/j.immuni.2018.11.004.

Hanson, Julien, Andreas Gille, Sabrina Zwykiel, Martina Lukasova, Björn E. Clausen, Kashan Ahmed, Sorin Tunaru, Angela Wirth, and Stefan Offermanns. 2010. “Nicotinic Acid- and Monomethyl Fumarate-Induced Flushing Involves GPR109A Expressed by Keratinocytes and COX-2-Dependent Prostanoid Formation in Mice.” *Journal of Clinical Investigation* 120 (8): 2910–19. https://doi.org/10.1172/JCI42273.

Harun-Or-Rashid, Mohammad, and Denise M. Inman. 2018. “Reduced AMPK Activation and Increased HCAR Activation Drive Anti-Inflammatory Response and Neuroprotection in Glaucoma.” *Journal of Neuroinflammation* 15 (1): 313. https://doi.org/10.1186/s12974-018-1346-7.

Hasan-olive, Mahdi, Knut H. Lauritzen, Mohammad Ali, Lene Juel Rasmussen, Jon Storm-Mathisen, and Linda H. Bergersen. 2019. “A Ketogenic Diet Improves Mitochondrial Biogenesis and Bioenergetics via the PGC1α-SIRT3-UCP2 Axis.” *Neurochemical Research* 44 (1): 22–37. https://doi.org/10.1007/s11064-018-2588-6.

Helmholz, Henry F., and Haddow M. Keith. 1930. “Eight Years’ Experience with the Ketogenic Diet in the Treatment of Epilepsy.” *JAMA: The Journal of the American Medical Association* 95 (10): 707. https://doi.org/10.1001/jama.1930.02720100005002.

Herman, Paige, Adam B. Stein, Katie Gibbs, Ilya Korsunsky, Peter Gregersen, and Ona Bloom. 2018. “Persons with Chronic Spinal Cord Injury Have Decreased NK Cell and Increased TLR/Inflammatory Gene Expression.” *Journal of Neurotrauma* 11: neu.2017.5519. https://doi.org/10.1089/neu.2017.5519.

Hilton, Brett J., Eitan Anenberg, Thomas C Harrison, Jamie D Boyd, Timothy H Murphy, and Wolfram Tetzlaff. 2016. “Re-Establishment of Cortical Motor Output Maps and Spontaneous Functional Recovery via Spared Dorsolaterally Projecting Corticospinal Neurons after Dorsal Column Spinal Cord Injury in Adult Mice.” *The Journal of Neuorscience* 36 (14): 4080–92. https://doi.org/10.1523/JNEUROSCI.3386-15.2016.

Hilton, Brett J., Peggy Assinck, Greg J Duncan, Daniel Lu, Stephanie Lo, and Wolfram Tetzlaff. 2013. “Dorsolateral Funiculus Lesioning of the Mouse Cervical Spinal Cord at C4 but Not at C6 Results in Sustained Forelimb Motor Deficits.” *Journal of Neurotrauma* 30 (12): 1070–83. https://doi.org/10.1089/neu.2012.2734.

Hirsch, C. A., and H. H. Hiatt. 1966. “Turnover of Liver Ribosomes in Fed and in Fasted Rats.”

Journal of Biological Chemistry 241 (24): 5936–40.

Hodgetts, Stuart I, Giles W Plant, and Alan R Harvey. 2009. "Spinal Cord Injury: Experimental Animal Models and Relation to Human Therapy." In *The Spinal Cord*, 209–37. Elsevier. https://doi.org/10.1016/B978-0-12-374247-6.50018-3.

Hoffmann, Christina, Michael Dietrich, Ann Kathrin Herrmann, Teresa Schacht, Philipp Albrecht, and Axel Methner. 2017. "Dimethyl Fumarate Induces Glutathione Recycling by Upregulation of Glutathione Reductase." *Oxidative Medicine and Cellular Longevity* 2017: 1–9. https://doi.org/10.1155/2017/6093903.

Hu, Sumei, Lu Wang, Dengbao Yang, Li Li, Jacques Togo, Yingga Wu, Quansheng Liu, et al. 2018. "Dietary Fat, but Not Protein or Carbohydrate, Regulates Energy Intake and Causes Adiposity in Mice." *Cell Metabolism* 28 (3): 415-431.e4. https://doi.org/10.1016/j.cmet.2018.06.010.

Hu, Zhi-gang, Han-dong Wang, Liang Qiao, Wei Yan, Qi-fu Tan, and Hong-Xia Yin. 2009. "The Protective Effect of the Ketogenic Diet on Traumatic Brain Injury-Induced Cell Death in Juvenile Rats." *Brain Injury* 23 (5): 459–65. https://doi.org/10.1080/02699050902788469.

Huang, Da Wei, Brad T Sherman, and Richard A Lempicki. 2009a. "Bioinformatics Enrichment Tools: Paths toward the Comprehensive Functional Analysis of Large Gene Lists." *Nucleic Acids Research* 37 (1): 1–13. https://doi.org/10.1093/nar/gkn923.

Huang, Da Wei, Brad T SHerman, and Richard A Lempicki. 2009b. "Systematic and Integrative Analysis of Large Gene Lists Using DAVID Bioinformatics Resources." *Nature Protocols* 4 (1): 44–57. https://doi.org/10.1038/nprot.2008.211.

Irvine, Karen Amanda, Adam R. Ferguson, Kathleen D. Mitchell, Stephanie B. Beattie, Amity Lin, Ellen D. Stuck, J. Russell Huie, et al. 2014. "The Irvine, Beatties, and Bresnahan (IBB) Forelimb Recovery Scale: An Assessment of Reliability and Validity." *Frontiers in Neurology* 5 JUL (July): 1–19. https://doi.org/10.3389/fneur.2014.00116.

Jarrett, Stuart G., Julie B. Milder, Li Ping Liang, and Manisha Patel. 2008. "The Ketogenic Diet Increases Mitochondrial Glutathione Levels." *Journal of Neurochemistry* 106 (3): 1044–51. https://doi.org/10.1111/j.1471-4159.2008.05460.x.

Jeong, Mi-ae, Ward T. Plunet, Femke Streijger, Jae H.T. Lee, Jason R Plemel, Sophia Park, Clarrie K Lam, Jie Liu, and Wolfram Tetzlaff. 2011. "Intermittent Fasting Improves Functional Recovery after Rat Thoracic Contusion Spinal Cord Injury." *Journal of Neurotrauma* 28 (3): 479–92. https://doi.org/10.1089/neu.2010.1609.

Jing, Huie, Jui Hung Yen, and Doina Ganea. 2004. "A Novel Signaling Pathway Mediates the Inhibition of CCL3/4 Expression by Prostaglandin E2." *Journal of Biological Chemistry* 279 (53): 55176–86. https://doi.org/10.1074/jbc.M409816200.

Jones, Leonard L, Yu Yamaguchi, William B Stallcup, and Mark H Tuszynski. 2002. "NG2 Is a Major Chondroitin Sulfate Proteoglycan Produced after Spinal Cord Injury and Is Expressed by Macrophages and Oligodendrocyte Progenitors." *The Journal of Neuorscience* 22 (7): 2792–2803.

Kashiwaya, Yoshihiro, Christian Bergman, Jong Hwan Lee, Ruiqian Wan, Michael Todd King,

Mohamed R. Mughal, Eitan Okun, Kieran Clarke, Mark P. Mattson, and Richard L. Veech. 2013. “A Ketone Ester Diet Exhibits Anxiolytic and Cognition-Sparing Properties, and Lessens Amyloid and Tau Pathologies in a Mouse Model of Alcheimer’s Disease.” *Neurobiology of Aging* 34 (6): 1530–39. https://doi.org/10.1016/j.neurobiolaging.2012.11.023.

Kashiwaya, Yoshihiro, Robert Pawlosky, William Markis, M. Todd King, Christian Bergman, Shireesh Srivastava, Andrew Murray, Kieran Clarke, and Richard L. Veech. 2010. “A Ketone Ester Diet Increases Brain Malonyl-CoA and Uncoupling Proteins 4 and 5 While Decreasing Food Intake in the Normal Wistar Rat.” *Journal of Biological Chemistry* 285 (34): 25950–56. https://doi.org/10.1074/jbc.M110.138198.

Kephart, Wesley C., Petey W. Mumford, Xuansong Mao, Matthew A. Romero, Hayden W. Hyatt, Yufeng Zhang, Christopher B. Mobley, et al. 2017. “The 1-Week and 8-Month Effects of a Ketogenic Diet or Ketone Salt Supplementation on Multi-Organ Markers of Oxidative Stress and Mitochondrial Function in Rats.” *Nutrients* 9 (9). https://doi.org/10.3390/nu9091019.

Kerschensteiner, Martin, Martin E Schwab, Jeff W Lichtman, and Thomas Misgeld. 2005. “In Vivo Imaging of Axonal Degeneration and Regeneration in the Injured Spinal Cord.” *Nature Medicine* 11 (5): 572–77.

Kigerl, Kristina A., John C. Gensel, Daniel P. Ankeny, Jessica K. Alexander, Dustin J. Donnelly, and Phillip G. Popovich. 2009. “Identification of Two Distinct Macrophage Subsets with Divergent Effects Causing Either Neurotoxicity or Regeneration in the Injured Mouse Spinal Cord.” *Journal of Neuroscience* 29 (43): 13435–44. https://doi.org/10.1523/JNEUROSCI.3257-09.2009.

Kim, Do Young, Junwei Hao, Ruolan Liu, Gregory Turner, Fu Dong Shi, and Jong M. Rho. 2012. “Inflammation-Mediated Memory Dysfunction and Effects of a Ketogenic Diet in a Murine Model of Multiple Sclerosis.” *PLoS ONE* 7 (5). https://doi.org/10.1371/journal.pone.0035476.

Kim, Myung H, Seung G Kang, Jeong H Park, Masashi Yanagisawa, and Chang H Kim. 2013. “Short-Chain Fatty Acids Activate GPR41 and GPR43 on Intestinal Epithelial Cells to Promote Inflammatory Responses in Mice.” *Gastroenterology* 145 (2): 396-406.e10. https://doi.org/10.1053/j.gastro.2013.04.056.

Kimura, I., D. Inoue, T. Maeda, T. Hara, A. Ichimura, S. Miyauchi, M. Kobayashi, A. Hirasawa, and G. Tsujimoto. 2011. “Short-Chain Fatty Acids and Ketones Directly Regulate Sympathetic Nervous System via G Protein-Coupled Receptor 41 (GPR41).” *Proceedings of the National Academy of Sciences* 108 (19): 8030–35. https://doi.org/10.1073/pnas.1016088108.

Kiselevsky, D. B. 2020. “Granzymes and Mitochondria.” *Biochemistry (Moscow)* 85 (2): 131–39. https://doi.org/10.1134/S0006297920020017.

Kjell, Jacob, and Lars Olson. 2016. “Rat Models of Spinal Cord Injury: From Pathology to Potential Therapies.” *DMM Disease Models and Mechanisms* 9 (10): 1125–37. https://doi.org/10.1242/dmm.025833.

Knowles, Helen J., Robert Te Poole, Paul Workman, and Adrian L. Harris. 2006. “Niacin Induces PPARy Expression and Transcriptional Activation in Macrophages via HM74 and HM74a-Mediated Induction of Prostaglandin Synthesis Pathways.” *Biochemical Pharmacology* 71 (5): 646–56. https://doi.org/10.1016/j.bcp.2005.11.019.

Kong, Ganggang, Z Huang, Wei Ji, Xiaomeng Wang, Junhao Liu, Xiuhua Wu, Zhiping Huang, Rong Li, and Qingan Zhu. 2017. “The Ketone Metabolite β-Hydroxybutyrate Attenuates Oxidative Stress in Spinal Cord Injury by Suppression of Class I Histone Deacetylases.” *Journal of Neurotrauma* 11 (18): neu.2017.5192. https://doi.org/10.1089/neu.2017.5192.

Kostylina, G, D Simon, M F Fey, S Yousefi, and H U Simon. 2008. “Neutrophil Apoptosis Mediated by Nicotinic Acid Receptors (GPR109A).” *Cell Death and Differentiation* 15 (1): 134–42. https://doi.org/10.1038/sj.cdd.4402238.

Kottis, Vicky, Pierre Thibault, Daniel Mikol, Zhi-cheng Xiao, Rulin Zhang, Pauline Dergham, and Peter E Braun. 2002. “Oligodendrocyte-Myelin Glycoprotein (OMgp) Is an Inhibitor of Neurite Outgrowth.” *Journal of Neurochemistry* 82: 1566–69.

Krysko, Dmitri V., Kodi S. Ravichandran, and Peter Vandenabeele. 2018. “Macrophages Regulate the Clearance of Living Cells by Calreticulin.” *Nature Communications* 9 (1): 9–11. https://doi.org/10.1038/s41467-018-06807-9.

Kwiecien, Jacek M., Wojciech Dabrowski, Beata Dąbrowska-Bouta, Grzegorz Sulkowski, Wendy Oakden, Christian J. Kwiecien-Delaney, Jordan R. Yaron, et al. 2020. “Prolonged Inflammation Leads to Ongoing Damage after Spinal Cord Injury.” *PLoS ONE* 15 (3): 1–22. https://doi.org/10.1371/journal.pone.0226584.

Lattermann, Ralph, Thomas Schricker, Ulrich Wachter, Michael Georgieff, and Axel Goertz. 2001. “Understanding the Mechanisms by Which Isoflurane Modifies the Hyperglycemic Response to Surgery.” *Anesthesia & Analgesia* 93: 121–27.

Lee, Brian A., Benjamin E. Leiby, and Ralph J. Marino. 2016. “Neurological and Functional Recovery after Thoracic Spinal Cord Injury.” *Journal of Spinal Cord Medicine* 39 (1): 67–76. https://doi.org/10.1179/2045772314Y.0000000280.

Lee, Dong Yeong, Young Jin Park, Sang Youn Song, Sun Chul Hwang, Kun Tae Kim, and Dong Hee Kim. 2018. “The Importance of Early Surgical Decompression for Acute Traumatic Spinal Cord Injury.” *CiOS Clinics in Orthopedic Surgery* 10 (4): 448–54. https://doi.org/10.4055/cios.2018.10.4.448.

Li, Guo, Ying Shi, Haishan Huang, Yaping Zhang, Kuangpei Wu, Jiansong Luo, Yi Sun, Jianxin Lu, Jeffrey L. Benovic, and Naiming Zhou. 2010. “Internalization of the Human Nicotinic Acid Receptor GPR109A Is Regulated by Gi, GRK2, and Arrestin3.” *Journal of Biological Chemistry* 285 (29): 22605–18. https://doi.org/10.1074/jbc.M109.087213.

Lindan, R., E. Joiner, A.A. Freehafer, and C. Hazie. 1980. “Incidence and Clinical Features of Autonomic Dysreflexia in Patients with Spinal Cord Injury.” *Paraplegia*, 285–92.

Liu, Fengxiu, Yucai Fu, Chiju Wei, Yongru Chen, Shuhua Ma, and Wencan Xu. 2014. “The Expression of GPR109A , NF-KB and IL-1 β in Peripheral Blood Leukocytes from Patients with Type 2 Diabetes.” *Annals of Clinical and Laboratory Science* 44 (4).

Liu, Yan Cun, Xian Biao Zou, Yan Fen Chai, and Yong Ming Yao. 2014. “Macrophage Polarization in Inflammatory Diseases.” *International Journal of Biological Sciences* 10 (5): 520–29. https://doi.org/10.7150/ijbs.8879.

Liu, Yi, Duckhyun Kim, B Timothy Himes, Stella Y Chow, Timothy Schallert, Marion Murray, Alan Tessler, and Itzhak Fischer. 1999. “Transplants of Fibroblasts Genetically Modified to Express BDNF Promote Regeneration of Adult Rat Rubrospinal Axons and Recovery of Forelimb Function.” *The Journal of Neuroscience* 19 (11): 4370–87.

Loveless, Scott E., Denise Hoban, Greg Sykes, Steven R. Frame, and Nancy E. Everds. 2008. “Evaluation of the Immune System in Rats and Mice Administered Linear Ammonium Perfluorooctanoate.” *Toxicological Sciences* 105 (1): 86–96. https://doi.org/10.1093/toxsci/kfn113.

Lu, Yao, Yan Yan Yang, Mou Wang Zhou, Nan Liu, Hua Yi Xing, Xiao Xie Liu, and Fang Li. 2018. “Ketogenic Diet Attenuates Oxidative Stress and Inflammation after Spinal Cord Injury by Activating Nrf2 and Suppressing the NF-KB Signaling Pathways.” *Neuroscience Letters* 683 (May): 13–18. https://doi.org/10.1016/j.neulet.2018.06.016.

Ma, Shan Feng, Yue Juan Chen, Jing Xing Zhang, Lin Shen, Rui Wang, Jian Sheng Zhou, Jian Guo Hu, and He Zuo Lü. 2015. “Adoptive Transfer of M2 Macrophages Promotes Locomotor Recovery in Adult Rats after Spinal Cord Injury.” *Brain, Behavior, and Immunity* 45: 157–70. https://doi.org/10.1016/j.bbi.2014.11.007.

Maalouf, Marwan, Patrick G. Sullivan, Laurie Davis, Do Young Kim, and Jong M. Rho. 2007. “Ketones Inhibit Mitochondrial Production of Reactive Oxygen Species Production Following Glutamate Excitotoxicity by Increasing NADH Oxidation.” *Neuroscience* 145 (1): 256–64. https://doi.org/10.1002/ajmg.c.30169.

Macciocchi, Stephen, Ronald T Seel, Nicole Thompson, Rashida Byams, and Brock Bowman. 2008. “Spinal Cord Injury and Co-Occurring Traumatic Brain Injury: Assessment and Incidence.” *Archives of Physical Medicine and Rehabilitation* 89 (7): 1350–57. https://doi.org/10.1016/j.apmr.2007.11.055.

Mady, Mackenzie A., Eric H. Kossoff, Amy L. McGregor, James W. Wheless, Paula L. Pyzik, and John M. Freeman. 2003. “The Ketogenic Diet: Adolescents Can Do It, Too.” *Epilepsia* 44 (6): 847–51. https://doi.org/10.1046/j.1528-1157.2003.57002.x.

Manns, Patricia J., Jeffrey A. McCubbin, and Daniel P. Williams. 2005. “Fitness, Inflammation, and the Metabolic Syndrome in Men with Paraplegia.” *Archives of Physical Medicine and Rehabilitation* 86 (6): 1176–81. https://doi.org/10.1016/j.apmr.2004.11.020.

Martinez, Fernando O, and Siamon Gordon. 2014. “The M1 and M2 Paradigm of Macrophage Activation: Time for Reassessment.” *F1000prime Reports* 6 (March): 13. https://doi.org/10.12703/P6-13.

Martinez, Fernando Oneissi, Antonio Sica, Alberto Mantovani, and Massimo Locati. 2008. “Macrophage Activation and Polarization.” *Frontiers of Bioscience* 13: 453–61. https://doi.org/10.2741/2692.

Maruyama, Y., M. Mizuguchi, T. Yaginuma, M. Kusaka, H. Yoshida, K. Yokoyama, Y. Kasahara, and T. Hosoya. 2008. “Serum Leptin, Abdominal Obesity and the Metabolic Syndrome in Individuals with Chronic Spinal Cord Injury.” *Spinal Cord* 46 (7): 494–99. https://doi.org/10.1038/sj.sc.3102171.

Masuda, Takahiro, Lukas Amann, Roman Sankowski, Ori Staszewski, Maximilian Lenz, Paolo d´Errico, Nicolas Snaidero, et al. 2020. “Novel Hexb-Based Tools for Studying Microglia in the CNS.” *Nature Immunology* 21 (7): 802–15. https://doi.org/10.1038/s41590-020-0707-4.

McKerracher, L., S. David, D.L. Jackson, V. Kottis, R.J. Dunn, and P.E. Braunt. 1994. “Identification of Myelin-Associated G Lycoprotein as a Major Myelin-Berived Inhibitor of Neurite Growth.” *Neuron* 13: 805–11.

Mestas, Javier, and Christopher C. W. Hughes. 2004. “Of Mice and Not Men: Differences between Mouse and Human Immunology.” *The Journal of Immunology* 172 (5): 2731–38. https://doi.org/10.4049/jimmunol.172.5.2731.

Metz, Gerlinde A, and Ian Q Whishaw. 2009. “The Ladder Rung Walking Task: A Scoring System and Its Practical Application.” *Journal of Visualized Experiments*, no. 28 (June): 2–5. https://doi.org/10.3791/1204.

Milder, Julie B., Li-Ping Ping Liang, and Manisha Patel. 2010. “Acute Oxidative Stress and Systemic Nrf2 Activation by the Ketogenic Diet.” *Neurobiology of Disease* 40 (1): 238–44. https://doi.org/10.1016/j.nbd.2010.05.030.

Milder, Julie B, and Manisha Patel. 2012. “Modulation of Oxidative Stress and Mitochondrial Function by the Ketogenic Diet.” *Epilepsy Research* 100 (3): 295–303. https://doi.org/10.1016/j.eplepsyres.2011.09.021.Modulation.

Monahan, Rachel, Adam B. Stein, Katie Gibbs, Matthew Bank, and Ona Bloom. 2015. “Circulating T Cell Subsets Are Altered in Individuals with Chronic Spinal Cord Injury.” *Immunologic Research* 63 (1–3): 3–10. https://doi.org/10.1007/s12026-015-8698-1.

Montoya, C.P., L.J. Cambell-Hope, K.D. Pemberton, and S.B. Dunnett. 1991. “The " Staircase Test " " a Measure of Independent Forelimb Reaching and Grasping Abilities in Rats.” *Journal of Neuroscience Methods* 36: 219–28.

Mosser, David M., and Justin P. Edwards. 2008. “Exploring the Full Spectrum of Macrophage Activation.” *Nature Reviews Immunology* 8 (12): 958–69. https://doi.org/10.1038/nri2448.

Mostacada, Klauss, Felipe L. Oliveira, Déa M.S. Villa-Verde, and Ana Maria Blanco Martinez. 2015. “Lack of Galectin-3 Improves the Functional Outcome and Tissue Sparing by Modulating Inflammatory Response after a Compressive Spinal Cord Injury.” *Experimental Neurology* 271: 390–400. https://doi.org/10.1016/j.expneurol.2015.07.006.

Murray, Andrew J., Nicholas S. Knight, Mark A. Cole, Lowri E. Cochlin, Emma Carter, Kirill Tchabanenko, Tica Pichulik, et al. 2016. “Novel Ketone Diet Enhances Physical and Cognitive Performance.” *FASEB Journal* 30 (12): 4021–32. https://doi.org/10.1096/fj.201600773R.

Nagao, Manabu, Ryuji Toh, Yasuhiro Irino, Takeshige Mori, Hideto Nakajima, Tetsuya Hara, Tomoyuki Honjo, et al. 2016. “β-Hydroxybutyrate Elevation as a Compensatory Response against Oxidative Stress in Cardiomyocytes.” *Biochemical and Biophysical Research Communications* 475 (4): 322–28. https://doi.org/10.1016/j.bbrc.2016.05.097.

Nahrendorf, Matthias, and Filip K. Swirski. 2016. “Abandoning M1/M2 for a Network Model of Macrophage Function.” *Circulation Research* 119 (3): 414–17.

https://doi.org/10.1161/CIRCRESAHA.116.309194.

Noonan, Vanessa K, Matthew Fingas, Angela Farry, David Baxter, Anoushka Singh, Michael G. Fehlings, and Marcel F. Dvorak. 2012. “Incidence and Prevalence of Spinal Cord Injury in Canada: A National Perspective.” *Neuroepidemiology* 38 (4): 219–26. https://doi.org/10.1159/000336014.

Norden, Diana M., John R. Bethea, and Jiu Jiang. 2018. “Impaired CD8 T Cell Antiviral Immunity Following Acute Spinal Cord Injury.” *Journal of Neuroinflammation* 15 (1): 1–11. https://doi.org/10.1186/s12974-018-1191-8.

Norwitz, Nicholas G., Michele T. Hu, and Kieran Clarke. 2019. “The Mechanisms by Which the Ketone Body D-β-Hydroxybutyrate May Improve the Multiple Cellular Pathologies of Parkinson’s Disease.” *Frontiers in Nutrition* 6 (May): 1–8. https://doi.org/10.3389/fnut.2019.00063.

O’Koren, E. G., R. Mathew, and D. R. Saban. 2016. “Fate Mapping Reveals That Microglia and Recruited Monocyte-Derived Macrophages Are Definitively Distinguishable by Phenotype in the Retina.” *Scientific Reports* 6 (October 2015): 1–12. https://doi.org/10.1038/srep20636.

Pajoohesh-Ganji, Ahdeah, Susan M. Knoblach, Alan I. Faden, and Kimberly R. Byrnes. 2012. “Characterization of Inflammatory Gene Expression and Galectin-3 Function after Spinal Cord Injury in Mice.” *Brain Research* 1475: 96–105. https://doi.org/10.1016/j.brainres.2012.07.058.

Park, Eu Gene, Jiwon Lee, and Jeehun Lee. 2019. “The Ketogenic Diet for Super-Refractory Status Epilepticus Patients in Intensive Care Units.” *Brain and Development* 41 (5): 420–27. https://doi.org/10.1016/j.braindev.2018.12.007.

Peschl, Patrick, Kathrin Schanda, Bleranda Zeka, Katherine Given, Denise Böhm, Klemens Ruprecht, Albert Saiz, et al. 2017. “Human Antibodies against the Myelin Oligodendrocyte Glycoprotein Can Cause Complement-Dependent Demyelination.” *Journal of Neuroinflammation* 14 (1): 208. https://doi.org/10.1186/s12974-017-0984-5.

Pineau, Isabelle, and Steve Lacroix. 2007. “Proinflammatory Cytokine Synthesis in the Injured Mouse Spinal Cord: Multiphasic Expression Pattern and Identification of the Cell Types Involved.” *The Journal of Comparative Neurology* 500 (2): 267–85. https://doi.org/10.1002/cne.21149.

Pineau, Isabelle, Libo Sun, Dominic Bastien, and Steve Lacroix. 2010. “Astrocytes Initiate Inflammation in the Injured Mouse Spinal Cord by Promoting the Entry of Neutrophils and Inflammatory Monocytes in an IL-1 Receptor/MyD88-Dependent Fashion.” *Brain, Behavior, and Immunity* 24 (4): 540–53. https://doi.org/10.1016/j.bbi.2009.11.007.

Plunet, Ward T., Femke Streijger, Clarrie K. Lam, Jae H.T. Lee, Jie Liu, and Wolfram Tetzlaff. 2008. “Dietary Restriction Started after Spinal Cord Injury Improves Functional Recovery.” *Experimental Neurology* 213 (1): 28–35. https://doi.org/10.1016/j.expneurol.2008.04.011.

Pomeshchik, Yuriy, Iurii Kidin, Paula Korhonen, Ekaterina Savchenko, Merja Jaronen, Sarka Lehtonen, Sara Wojciechowski, Katja Kanninen, Jari Koistinaho, and Tarja Malm. 2015. “Interleukin-33 Treatment Reduces Secondary Injury and Improves Functional Recovery after Contusion Spinal Cord Injury.” *Brain, Behavior, and Immunity* 44: 68–81.

https://doi.org/10.1016/j.bbi.2014.08.002.

Prins, Caio Andrade, Fernanda Martins Almeida, and Ana Maria Blanco Martinez. 2016. “Absence of Galectin-3 Attenuates Neuroinflammation Improving Functional Recovery after Spinal Cord Injury.” *Neural Regeneration Research* 11 (1): 92–93. https://doi.org/10.4103/1673-5374.175051.

Qian, Jiao, Wenjun Zhu, Ming Lu, Bin Ni, and Jun Yang. 2017. “D-β-Hydroxybutyrate Promotes Functional Recovery and Relieves Pain Hypersensitivity in Mice with Spinal Cord Injury.” *British Journal of Pharmacology* 174 (13): 1961–71. https://doi.org/10.1111/bph.13788.

Rabadi, M H, and C Aston. 2015. “Complications and Urologic Risks of Neurogenic Bladder in Veterans with Traumatic Spinal Cord Injury.” *Spinal Cord* 53 (3): 200–203. https://doi.org/10.1038/sc.2014.205.

Ren, Zhouliang, Weidong Liang, Jun Sheng, Chuanhui Xun, Tao Xu, Rui Cao, and Weibin Sheng. 2019. “Gal-3 Is a Potential Biomarker for Spinal Cord Injury and Gal-3 Deficiency Attenuates Neuroinflammation through ROS/TXNIP/NLRP3 Signaling Pathway.” *Bioscience Reports* 39 (12): 1–12. https://doi.org/10.1042/BSR20192368.

Richman, Jeremy G., Martha Kanemitsu-Parks, Ibragim Gaidarov, Jill S. Cameron, Peter Griffin, Hong Zheng, Nuvia C. Guerra, et al. 2007. “Nicotinic Acid Receptor Agonists Differentially Activate Downstream Effectors.” *Journal of Biological Chemistry* 282 (25): 18028–36. https://doi.org/10.1074/jbc.M701866200.

Riegger, T., S. Conrad, Hermann J. Schluesener, H. P. Kaps, A. Badke, C. Baron, J. Gerstein, K. Dietz, M. Abdizahdeh, and Jan M. Schwab. 2009. “Immune Depression Syndrome Following Human Spinal Cord Injury (SCI): A Pilot Study.” *Neuroscience* 158 (3): 1194–99. https://doi.org/10.1016/j.neuroscience.2008.08.021.

Sansom, David M., Claire N. Manzotti, and Yong Zheng. 2003. “What’s the Difference between CD80 and CD86?” *Trends in Immunology* 24 (6): 313–18. https://doi.org/10.1016/S1471-4906(03)00111-X.

Sato, Kazunori, Y. Kashiwaya, C. A. Keon, N. Tsuchiya, M. T. King, G. K. Radda, B. Chance, Kieran Clarke, and Richard L. Veech. 1995. “Insulin, Ketone Bodies, and Mitochondrial Energy Transduction.” *FASEB Journal* 9 (8): 651–58.

Scheff, Stephen W, Alexander G Rabchevsky, Isabella Fugaccia, John a Main, and James E Lumpp. 2003. “Experimental Modeling of Spinal Cord Injury: Characterization of a Force-Defined Injury Device.” *Journal of Neurotrauma* 20 (2): 179–93. https://doi.org/10.1089/08977150360547099.

Schindler, J F, J B Monahan, and W G Smith. 2007. “P38 Pathway Kinases as Anti-Inflammatory Drug Targets.” *J Dent Res* 86 (9): 800–811. https://doi.org/10.1177/154405910708600902.

Schonberg, David L., Evan Z. Goldstein, Fatma Rezan Sahinkaya, Ping Wei, Phillip G. Popovich, and Dana M. McTigue. 2012. “Ferritin Stimulates Oligodendrocyte Genesis in the Adult Spinal Cord and Can Be Transferred from Macrophages to NG2 Cells in Vivo.” *Journal of Neuroscience* 32 (16): 5374–84. https://doi.org/10.1523/JNEUROSCI.3517-11.2012.

Sharif-Alhoseini, M., M. Khormali, M. Rezaei, M. Safdarian, A. Hajighadery, M. M. Khalatbari, M. Safdarian, et al. 2017. “Animal Models of Spinal Cord Injury: A Systematic Review.” *Spinal Cord* 55 (November 2016): 1–8. https://doi.org/10.1038/sc.2016.187.

Shi, Ying, Xiangru Lai, Lingyan Ye, Keqiang Chen, Zheng Cao, Wanghua Gong, and Lili Jin. 2017. “Activated Niacin Receptor HCA2 Inhibits Chemoattractant- Mediated Macrophage Migration via G Bγ / PKC / ERK1 / 2 Pathway and Heterologous Receptor Desensitization.” *Nature Publishing Group*, no. January: 1–14. https://doi.org/10.1038/srep42279.

Silva, Nuno A., Nuno Sousa, Rui L. Reis, and António J. Salgado. 2014. “From Basics to Clinical: A Comprehensive Review on Spinal Cord Injury.” *Progress in Neurobiology* 114: 25–57. https://doi.org/10.1016/j.pneurobio.2013.11.002.

Snow, Diane M, Vance Lemmon, David A Carrino, Arnold I Caplan, and Jerry Silver. 1990. “Sulfated Proteoglycans in Astroglial Barriers Inhibit Neurite Outgrowth in Vitro.” *Experimental Neurology* 109: 111–30.

Soga, Takatoshi, Masazumi Kamohara, Jun Takasaki, Shun Ichiro Matsumoto, Tetsu Saito, Takahide Ohishi, Hideki Hiyama, Ayako Matsuo, Hitoshi Matsushime, and Kiyoshi Furuichi. 2003. “Molecular Identification of Nicotinic Acid Receptor.” *Biochemical and Biophysical Research Communications* 303 (1): 364–69. https://doi.org/10.1016/S0006-291X(03)00342-5.

Son, Yong, Yong-Kwan Cheong, Nam-Ho Kim, Hun-Taeg Chung, Dae Gill Kang, and Hyun-Ock Pae. 2011. “Mitogen-Activated Protein Kinases and Reactive Oxygen Species: How Can ROS Activate MAPK Pathways?” *Journal of Signal Transduction* 2011: 1–6. https://doi.org/10.1155/2011/792639.

Soto-Mota, Adrian, Hannah Vansant, Rhys D. Evans, and Kieran Clarke. 2019. “Safety and Tolerability of Sustained Exogenous Ketosis Using Ketone Monoester Drinks for 28 Days in Healthy Adults.” *Regulatory Toxicology and Pharmacology* 109 (October): 104506. https://doi.org/10.1016/j.yrtph.2019.104506.

Spadaro, Melania, Stephan Winklmeier, Eduardo Beltrán, Caterina Macrini, Romana Höftberger, Elisabeth Schuh, Franziska S Thaler, et al. 2018. “Pathogenicity of Human Antibodies against Myelin Oligodendrocyte Glycoprotein.” *Annals of Neurology* 84 (2): 315–28. https://doi.org/10.1002/ana.25291.

Sroga, Julie M., T. Bucky Jones, Kristina A. Kigerl, Violeta M. McGaughy, and Phillip G. Popovich. 2003. “Rats and Mice Exhibit Distinct Inflammatory Reactions after Spinal Cord Injury.” *Journal of Comparative Neurology* 462 (2): 223–40. https://doi.org/10.1002/cne.10736.

Stammers, A. T., J. Liu, and Brian K. Kwon. 2012. “Expression of Inflammatory Cytokines Following Acute Spinal Cord Injury in a Rodent Model.” *Journal of Neuroscience Research* 90 (4): 782–90. https://doi.org/10.1002/jnr.22820.

Stoll, G., J.W. Griffin, C.Y. Li, and B.D. Trapp. 1989. “Wallerian Degeneration in the Peripheral Nervous System: Participation of Both Schwann Cells and Macrophages in Myelin Degradation.” *Journal of Neurocytology* 18: 671–83.

Streijger, Femke, Ward T. Plunet, Jae H.T. Lee, Jie Liu, Clarrie K. Lam, Soeyun Park, Brett J. Hilton, et al. 2013. “Ketogenic Diet Improves Forelimb Motor Function after Spinal Cord Injury in

Rodents." *PLoS ONE* 8 (11): 1–19. https://doi.org/10.1371/journal.pone.0078765.

Streijger, Femke, Ward T. Plunet, Jason Ryan Plemel, Clarrie K Lam, Jie Liu, and Wolfram Tetzlaff. 2011. "Intermittent Fasting in Mice Does Not Improve Hindlimb Motor Performance after Spinal Cord Injury." *Journal of Neurotrauma* 28 (6): 1051–61. https://doi.org/10.1089/neu.2010.1715.

Stuart, Tim, Andrew Butler, Paul Hoffman, Christoph Hafemeister, Efthymia Papalexi, William M. Mauck, Yuhan Hao, Marlon Stoeckius, Peter Smibert, and Rahul Satija. 2019. "Comprehensive Integration of Single-Cell Data." *Cell* 177 (7): 1888-1902.e21. https://doi.org/10.1016/j.cell.2019.05.031.

Stubbs, Brianna J., Pete J. Cox, Rhys D. Evans, Malgorzata Cyranka, Kieran Clarke, and Heidi de Wet. 2018. "A Ketone Ester Drink Lowers Human Ghrelin and Appetite." *Obesity* 26 (2): 269–73. https://doi.org/10.1002/oby.22051.

Stubbs, Brianna J., Pete J. Cox, Rhys D. Evans, Peter Santer, Jack J. Miller, Olivia K. Faull, Snapper Magor-Elliott, Satoshi Hiyama, Matthew Stirling, and Kieran Clarke. 2017. "On the Metabolism of Exogenous Ketones in Humans." *Frontiers in Physiology* 8 (OCT): 1–13. https://doi.org/10.3389/fphys.2017.00848.

Subramani, Kumar, Xiaogang Chu, Marie Warren, Mariah Lee, Sumin Lu, Nagendra Singh, and Raghavan Raju. 2019. "Deficiency of Metabolite Sensing Receptor HCA2 Impairs the Salutary Effect of Niacin in Hemorrhagic Shock." *Biochimica et Biophysica Acta - Molecular Basis of Disease* 1865 (3): 688–95. https://doi.org/10.1016/j.bbadis.2019.01.009.

Taggart, Andrew K.P., Jukka Kero, Xiaodong Gan, Tian-quan Quan Cai, Kang Cheng, Marc Ippolito, Ning Ren, et al. 2005. "(D)-Beta-Hydroxybutyrate Inhibits Adipocyte Lipolysis via the Nicotinic Acid Receptor PUMA-G." *The Journal of Biological Chemistry* 280 (29): 26649–53. https://doi.org/10.1074/jbc.C500213200.

Tang, Hua, Jenny Ying Lin Lu, Xiaomu Zheng, Yuhua Yang, and Jeff D. Reagan. 2008. "The Psoriasis Drug Monomethylfumarate Is a Potent Nicotinic Acid Receptor Agonist." *Biochemical and Biophysical Research Communications* 375 (4): 562–65. https://doi.org/10.1016/j.bbrc.2008.08.041.

Thangaraju, Muthusamy, Gail A Cresci, Kebin Liu, Sudha Ananth, Jaya P Gnanaprakasam, Darren D Browning, John D Mellinger, et al. 2009. "GPR109A Is a G-Protein-Coupled Receptor for the Bacterial Fermentation Product Butyrate and Functions as a Tumor Suppressor in Colon." *Cancer Research* 69 (7): 2826–32. https://doi.org/10.1158/0008-5472.CAN-08-4466.

Thietje, Roland, M. H. Pouw, A. P. Schulz, B. Kienast, and Sven Hirschfeld. 2011. "Mortality in Patients with Traumatic Spinal Cord Injury: Descriptive Analysis of 62 Deceased Subjects." *Journal of Spinal Cord Medicine* 34 (5): 482–87. https://doi.org/10.1179/2045772311Y.0000000022.

Thomas, Laura, and Laura Andrea Pasquini. 2018. "Galectin-3-Mediated Glial Crosstalk Drives Oligodendrocyte Differentiation and (Re)Myelination." *Frontiers in Cellular Neuroscience* 12 (September): 1–16. https://doi.org/10.3389/fncel.2018.00297.

Tie, Yanmei, Mesut Sahin, and Nappinnai Sundararajan. 2006. "Organization in the Descending

Tracts of the Dorsolateral Funiculus in the Cat." *Brain Research* 1117 (1): 61–68. https://doi.org/10.1016/j.brainres.2006.08.040.

Trotta, Maria Consiglia, Rosa Maisto, Francesca Guida, Serena Boccella, Livio Luongo, Cornel Balta, Giovanbattista D'Amico, et al. 2019. "The Activation of Retinal HCA2 Receptors by Systemic Beta-Hydroxybutyrate Inhibits Diabetic Retinal Damage through Reduction of Endoplasmic Reticulum Stress and the NLRP3 Inflammasome." *PLoS ONE* 14 (1): 1–16. https://doi.org/10.1371/journal.pone.0211005.

Tunaru, Sorin, Jukka Kero, Annette Schaub, Christian Wufka, Andree Blaukat, Klaus Pfeffer, and Stefan Offermanns. 2003. "PUMA-G and HM74 Are Receptors for Nicotinic Acid and Mediate Its Anti-Lipolytic Effect." *Nature Medicine* 9 (3): 352–55. https://doi.org/10.1038/nm824.

Vargas, Mauricio E, and Ben A. Barres. 2007. "Why Is Wallerian Degeneration in the CNS So Slow?" *Annual Review of Neuroscience* 30 (1): 153–79. https://doi.org/10.1146/annurev.neuro.30.051606.094354.

Veprik, Anna, Dana Laufer, Sara Weiss, Nir Rubins, and Michael D Walker. 2016. "GPR41 Modulates Insulin Secretion and Gene Expression in Pancreatic B-cells and Modifies Metabolic Homeostasis in Fed and Fasting States." *The FASEB Journal* 30 (11): 3860–69. https://doi.org/10.1096/fj.201500030R.

Vogelaar, Christina F, and Veronica Estrada. 2016. "Experimental Spinal Cord Injury Models in Rodents: Anatomical Correlations and Assessment of Motor Recovery." In *Recovery of Motor Function Following Spinal Cord Injury*, 1–35. InTech. https://doi.org/10.5772/62947.

Wanders, Desiree, Emily C. Graff, and Robert L. Judd. 2012. "Effects of High Fat Diet on GPR109A and GPR81 Gene Expression." *Biochemical and Biophysical Research Communications* 425 (2): 278–83. https://doi.org/10.1016/j.bbrc.2012.07.082.

Wang, Kevin C., Vuk Koprivica, Jieun A. Kim, Rajeev Sivasankaran, Yong Guo, Rachel L. Neve, and Zhigang He. 2002. "Oligodendrocyte-Myelin Glycoprotein Is a Nogo Receptor Ligand That Inhibits Neurite Outgrowth." *Nature* 417 (6892): 941–44. https://doi.org/10.1038/nature00867.

Wang, Xiaomeng, Xiaoliang Wu, Qi Liu, Ganggang Kong, Jian Zhou, Jie Jiang, Xiuhua Wu, Zhiping Huang, Wanhan Su, and Qingan Zhu. 2017. "Ketogenic Metabolism Inhibits Histone Deacetylase (HDAC) and Reduces Oxidative Stress after Spinal Cord Injury in Rats." *Neuroscience* 366: 36–43. https://doi.org/10.1016/j.neuroscience.2017.09.056.

Wardener, HE de, and GA MacGregor. 2002. "Harmful Effects of Dietary Salt in Addition to Hypertension." *Journal of Human Hypertension* 16: 213–23. https://doi.org/10.1038/sj/jhh/1001374.

Weischenfeldt, Joachim, and Bo Porse. 2008. "Bone Marrow-Derived Macrophages (BMM): Isolation and Applications." *Cold Spring Harbor Protocols* 3 (12): 1–7. https://doi.org/10.1101/pdb.prot5080.

Williams, Ryan, and Adrian Murray. 2015. "Prevalence of Depression after Spinal Cord Injury: A Meta-Analysis." *Archives of Physical Medicine and Rehabilitation* 96 (1): 133–40. https://doi.org/10.1016/j.apmr.2014.08.016.

Wirrell, Elaine, Susan Eckert, Lily Wong-Kisiel, Eric Payne, and Katherine Nickels. 2018. "Ketogenic Diet Therapy in Infants: Efficacy and Tolerability." *Pediatric Neurology* 82: 13–18. https://doi.org/10.1016/j.pediatrneurol.2017.10.018.

Wise, Alan, Steven M. Foord, Neil J. Fraser, Ashley A. Barnes, Nabil Elshourbagy, Michelle Eilert, Diane M. Ignar, et al. 2003. "Molecular Identification of High and Low Affinity Receptors for Nicotinic Acid." *Journal of Biological Chemistry* 278 (11): 9869–74. https://doi.org/10.1074/jbc.M210695200.

Won, Y.-J., V. B. Lu, H. L. Puhl, and S. R. Ikeda. 2013. "B-Hydroxybutyrate Modulates N-Type Calcium Channels in Rat Sympathetic Neurons by Acting as an Agonist for the G-Protein-Coupled Receptor FFA3." *Journal of Neuroscience* 33 (49): 19314–25. https://doi.org/10.1523/JNEUROSCI.3102-13.2013.

Wright, J. N., R. P. Saneto, and S. D. Friedman. 2018. "Hydroxybutyrate Detection with Proton MR Spectroscopy in Children with Drug-Resistant Epilepsy on the Ketogenic Diet." *American Journal of Neuroradiology* 39 (7): 1336–40. https://doi.org/10.3174/ajnr.A5648.

Xiong, Yumei, Norimasa Miyamoto, Kenji Shibata, Mark A Valasek, Toshiyuki Motoike, Rafal M Kedzierski, and Masashi Yanagisawa. 2004. "Short-Chain Fatty Acids Stimulate Leptin Production in Adipocytes through the G Protein-Coupled Receptor GPR41." *Proceedings of the National Academy of Sciences* 101 (4): 1045–50. https://doi.org/10.1073/pnas.2637002100.

Xu, Zhen, Bai Ren Wang, Xi Wang, Fang Kuang, Xiao Li Duan, Xi Ying Jiao, and Gong Ju. 2006. "ERK1/2 and P38 Mitogen-Activated Protein Kinase Mediate INOS-Induced Spinal Neuron Degeneration after Acute Traumatic Spinal Cord Injury." *Life Sciences* 79 (20): 1895–1905. https://doi.org/10.1016/j.lfs.2006.06.023.

Yarar-Fisher, Ceren, Adarsh Kulkarni, Jia Li, Paige Farley, Cassandra Renfro, Hammad Aslam, Patrick Bosarge, Landon Wilson, and Stephen Barnes. 2018. "Evaluation of a Ketogenic Diet for Improvement of Neurological Recovery in Individuals with Acute Spinal Cord Injury: A Pilot, Randomized Safety and Feasibility Trial." *Spinal Cord Series and Cases* 4 (1): 1–13. https://doi.org/10.1038/s41394-018-0121-4.

Youm, Yun-hee, Kim Y Nguyen, Ryan W Grant, Emily L Goldberg, Monica Bodogai, Seokwon Kang, Tamas L Horvath, et al. 2015. "Ketone Body Beta-Hydroxybutyrate Blocks the NLRP3 Inflammasome-Mediated Inflammatory Disease." *Nature Medicine* 21 (3): 263–69. https://doi.org/10.1038/nm.3804.Ketone.

Zandi-Nejad, Kambiz, Ayumi Takakura, Mollie Jurewicz, Anil K. Chandraker, Stefan Offermanns, David Mount, and Reza Abdi. 2013. "The Role of HCA2 (GPR109A) in Regulating Macrophage Function." *FASEB Journal* 27 (11): 4366–74. https://doi.org/10.1096/fj.12-223933.

Zauner, Christian, Bruno Schneeweiss, Alexander Kranz, Christian Madl, Klaus Ratheiser, Ludwig Kramer, Erich Roth, Barbara Schneider, and Kurt Lenz. 2000. "Resting Energy Expenditure in Short-Term Starvation Is Increased as a Result of an Increase in Serum Norepinephrine." *American Journal of Clinical Nutrition* 71 (6): 1511–15. https://doi.org/10.1093/ajcn/71.6.1511.

Zhang, Xuelian, Xuesong Zhang, Chao Chen, Shengzhong Ma, Yan Wang, and Xiaojing Su. 2015. "Inhibition of Monocyte Chemoattractant Peptide-1 Decreases Secondary Spinal Cord Injury." *Molecular Medicine Reports* 11 (6): 4262–66. https://doi.org/10.3892/mmr.2015.3330.

Zhang, Youyan, Robert J. Schmidt, Patricia Foxworthy, Renee Emkey, Jennifer K. Oler, Thomas H. Large, He Wang, et al. 2005. “Niacin Mediates Lipolysis in Adipose Tissue through Its G-Protein Coupled Receptor HM74A.” *Biochemical and Biophysical Research Communications* 334 (2): 729–32. https://doi.org/10.1016/j.bbrc.2005.06.141.

Ziegler, Denize R, Leticia C Ribeiro, Martine Hagenn, R Siqueira, Emeli Araújo, Iracy L S Torres, Carmem Gottfried, Carlos Alexandre Netto, and Carlos-alberto Gonçalves. 2003. “Ketogenic Diet Increases Glutathione Peroxidase Activity in Rat Hippocampus.” *Neurochemical Research* 28 (12): 1793–97.

Zolfaghari, Parjam S, Bernardo Pinto, Alex Dyson, and Mervyn Singer. 2013. “The Metabolic Phenotype of Rodent Sepsis: Cause for Concern?” *Intensive Care Medicine Experimental* 1 (1): 6. https://doi.org/10.1186/2197-425x-1-6.

Appendices

Appendix A: ImageJ Macros used for IF quantification

C4 DLF Crush NeuN+ Count:

```
run("Set Scale...", "distance=1000 known=645 pixel=1 unit=micron");
run("Duplicate...", " ");
run("Grays");
run("Subtract Background...", "rolling=50 sliding");
setAutoThreshold("Default dark");
waitForUser("select threshold")
setOption("BlackBackground", true);
run("Convert to Mask");
run("Watershed");
run("Analyze Particles...", "size=20-Infinity show=Overlay exclude clear include summarize");
```

C4 DLF crush Arg1 IF Intensity:

```
originalTitle = getTitle();
run("Duplicate...", " ");
run("Subtract Background...", "rolling=100 sliding");
setAutoThreshold("Default dark");
setThreshold(2000, 65535);
setOption("BlackBackground", true);
run("Convert to Mask");
run("Morphological Filters", "operation=Opening element=Square radius=1");
run("Dilate");
run("Watershed");
run("Analyze Particles...", "  show=Overlay exclude clear include summarize");
run("Create Selection");
roiManager("Add");
selectWindow(originalTitle);
roiManager("Measure");
```

C4 DLF crush P-p38 IF intensity:

```
run("Set Scale...", "distance=160.5 known=50 pixel=1 unit=um");
run("16-bit");
setOption("ScaleConversions", true);
run("8-bit");
run("Subtract Background...", "rolling=100");
setThreshold(60, 210);
run("Create Selection");
run("Set Measurements...", "area mean min display redirect=None decimal=0");
run("Measure");
```

T9 Iba1+ IF:

```
run("Set Scale...", "distance=1.5504 known=1 pixel=1 unit=micron");
originalTitle = getTitle()
rename("current");
run("Robust Automatic Threshold Selection", "noise=100 lambda=3 min=800");
run("Create Selection");
roiManager("Add");
rename(originalTitle);
run("Analyze Particles...", "include summarize");
selectWindow("current");
rename(originalTitle);
roiManager("Select", 0);
roiManager("Measure");
roiManager("Deselect");
roiManager("Delete")
```

T9 P-p38+ IF:

```
originalTitle = getTitle()
rename("current");
run("Split Channels");
selectWindow("C2-current");
run("Duplicate...", " ");
selectWindow("C2-current-1");
setThreshold(3600, 65535);
waitForUser("adjust");
//removed any dura or nerves by clearing outside
setOption("BlackBackground", true);
run("Convert to Mask");
run("Create Selection");
roiManager("Add");
selectWindow("C2-current");
rename(originalTitle);
roiManager("Select", 0);
roiManager("Measure");
roiManager("Delete");
run("Close All")
```

T9 NeuN+:

```
waitForUser("Subset if necessary")
run("16-bit");
run("Gaussian Blur...", "sigma=1");
run("Subtract Background...", "rolling=30");
setAutoThreshold("Default dark");
setThreshold(20, 65535);
setOption("BlackBackground", true);
run("Convert to Mask");
run("Make Binary");
run("Watershed");
run("Analyze Particles...", "size=0.01-1 circularity=0.30-1.00 show=[Overlay Masks] exclude clear
summarize");
```

T9 Cord Area:

```
originalTitle = getTitle();
run("Split Channels");
selectWindow(originalTitle + " (blue)");
run("Subtract Background...", "rolling=200");
setThreshold(1, 255);
setOption("BlackBackground", true);
run("Convert to Mask");
run("Fill Holes");
run("Keep Largest Region");
run("Create Selection");
run("Set Measurements...", "area redirect=None decimal=2");
run("Measure");
saveAs("Tiff", output + filename);
```

Appendix B: Supplementary Figures

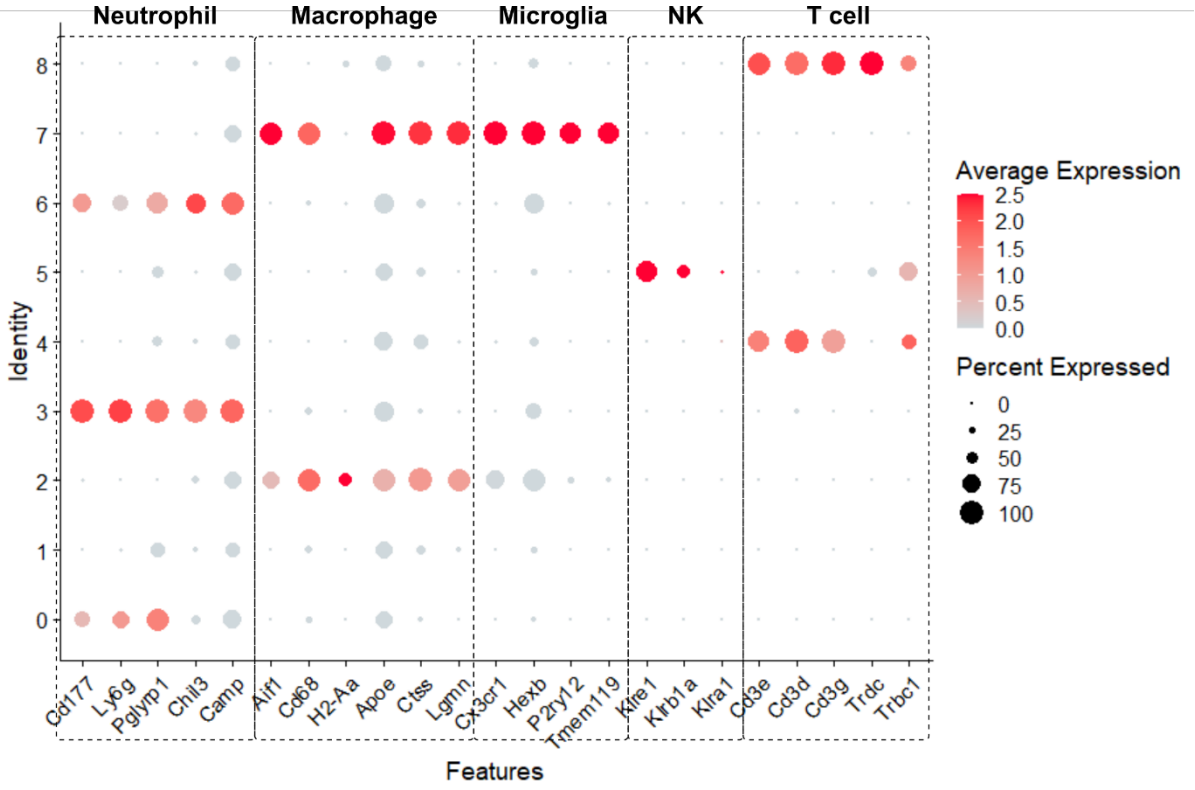

Supplementary Figure 1. Dotplot showing genes used to identify different clusters and the type of cell predominantly expressing each set of genes. Some genes such as Chil3 and Camp for neutrophils, and Ctss and Lgmn for macrophages/microglia or not canonical markers but were found to be predominantly expressed by these cell types.

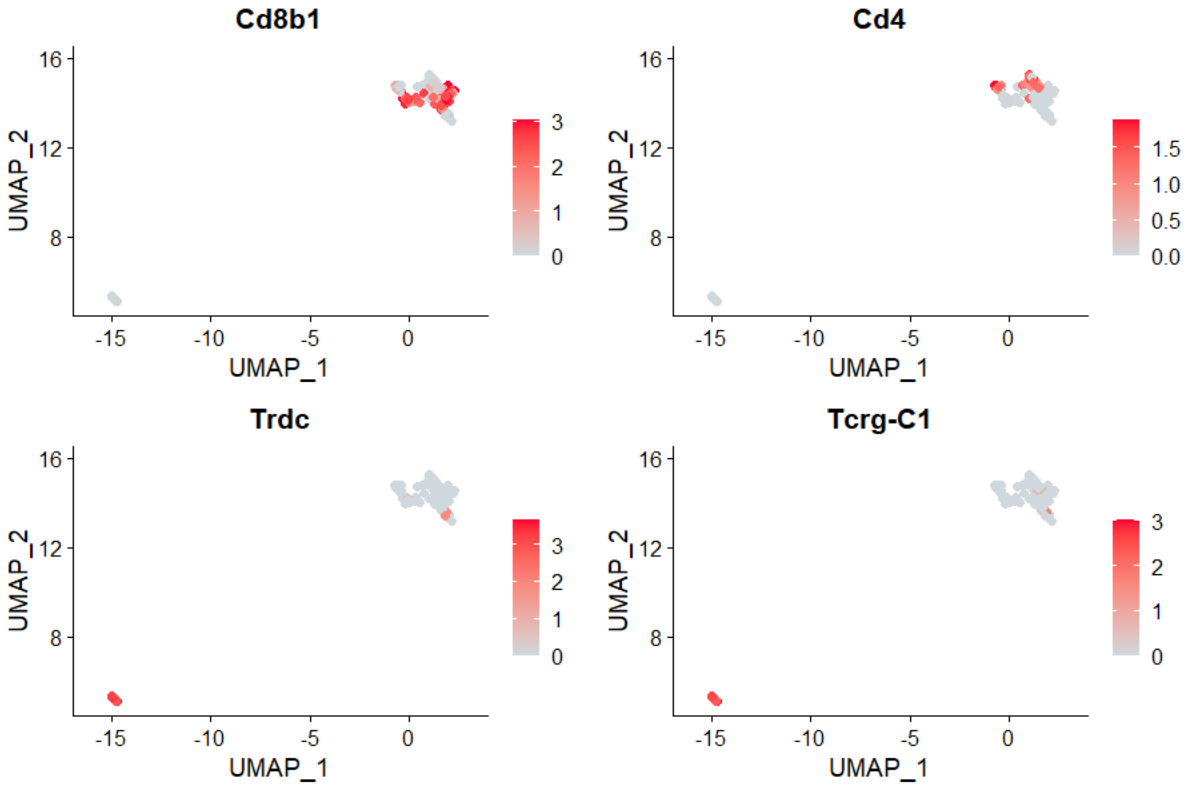

Supplementary Figure 2. UMAP showing expression of T-cell subset markers: Cd8b1, Cd4, Trdc, and Tcrg-C1. Only (Cd3+) clusters 4 and 8 are plotted.

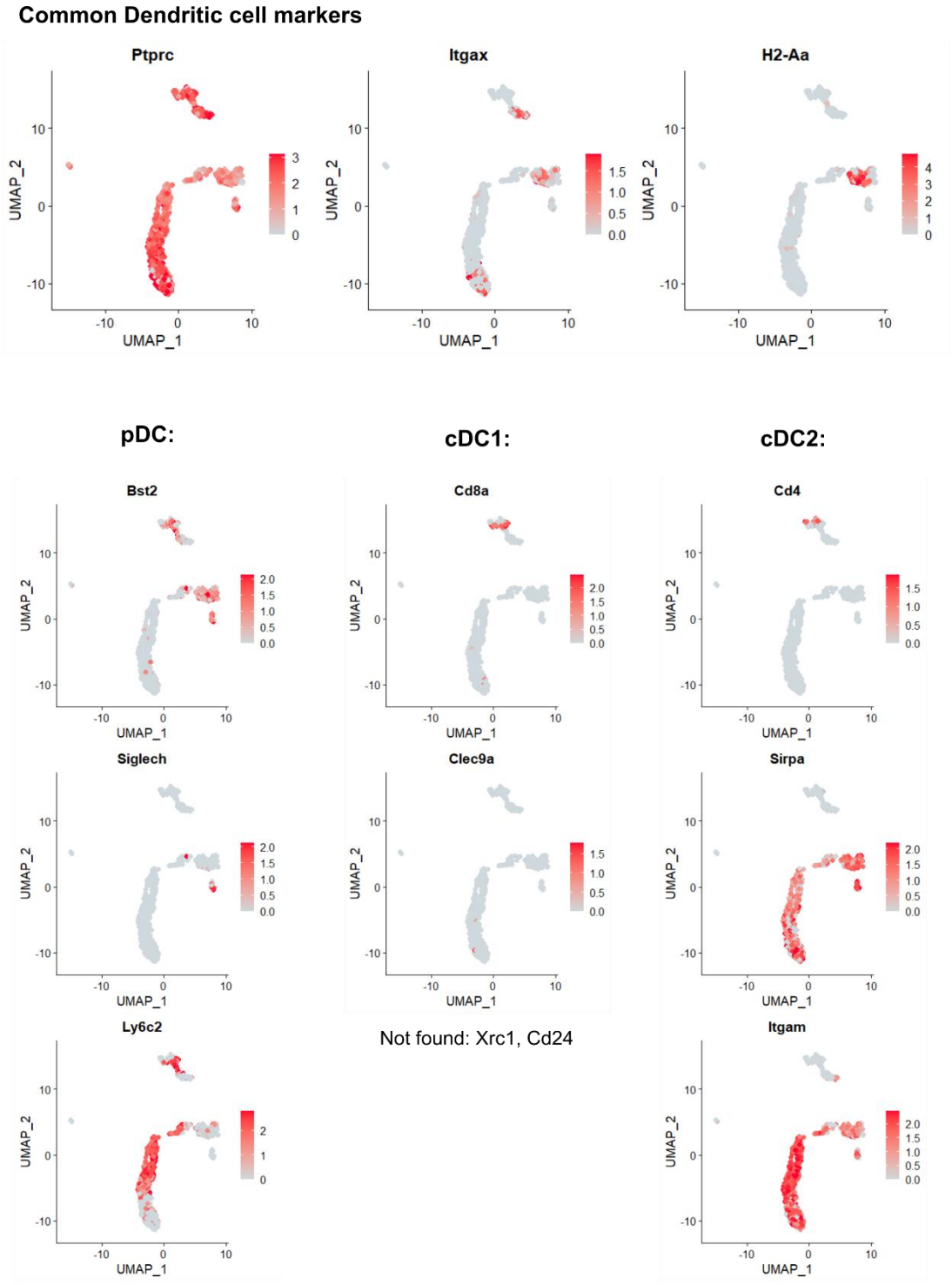

Supplementary Figure 3. UMAP showing expression of common dendritic cell (DC) markers and additional markers used to classify plasmacytoid DC (pDC), conventional DC 1 (cDC1), and conventional DC 2 (cDC2).

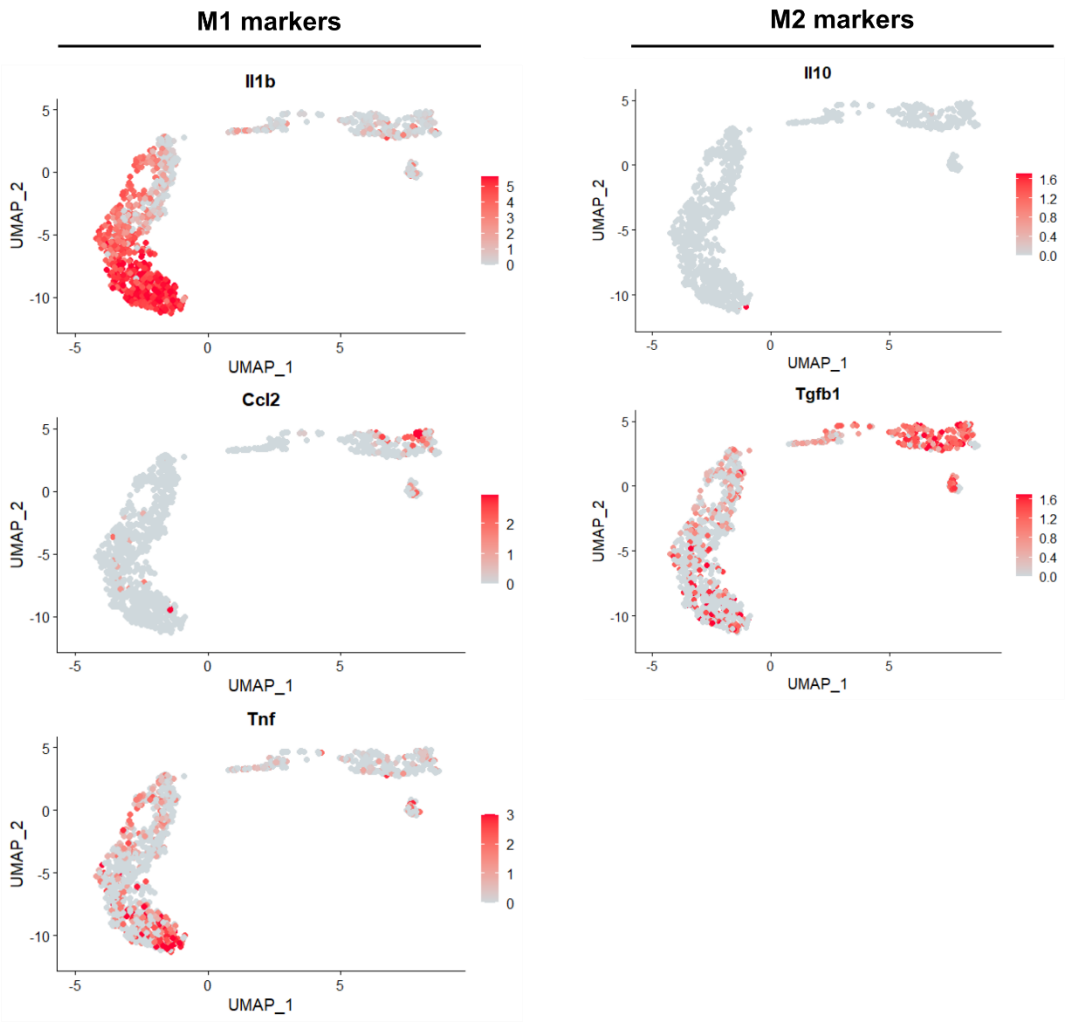

Supplementary Figure 4. UMAP showing expression of secreted M1 and M2 factors.

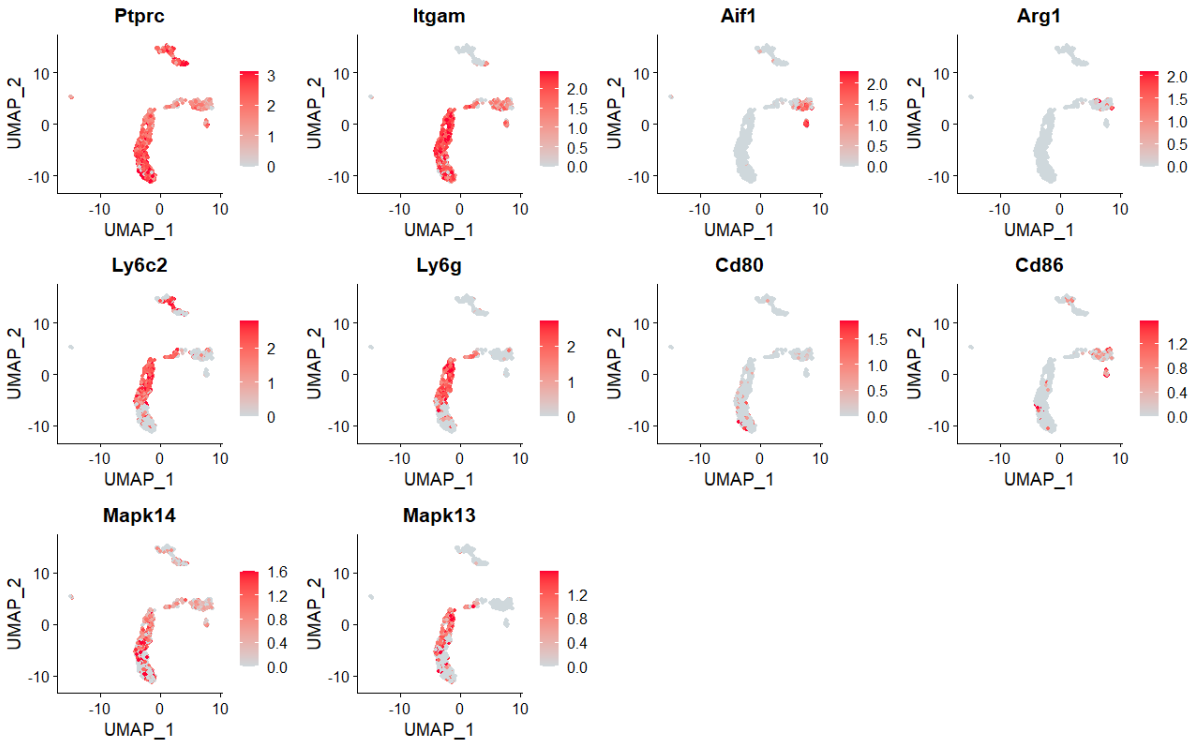

Supplementary Figure 5. UMAP showing expression of inflammation markers used throughout this thesis: Cd45 (Ptprc), Cd11b (Itgam), Iba1 (Aif1), Arg1, Ly6c (Ly6c2), Ly6g, Cd80, Cd86, p38 MAPK alpha (Mapk14), and p38 MAPK delta (Mapk13). Isoforms that showed minimal expression or were not found in the dataset are omitted from this figure.

Table S1. All proteomic hits with p<0.05.

KD			KE			KD+KE		
Protein	**Mean**	**P-value**	**Protein**	**Mean**	**P-value**	**Protein**	**Mean**	**P-value**
Aak1	0.579	0.025	Abr	-0.728	0.008	08-Sep	-0.616	0.001
Abat	0.821	0.012	Acadvl	-0.439	0.018	09-Sep	-0.345	0.023
Abhd14b	0.966	0.041	Acsl6	-0.581	0.045	A1m	-0.858	0.031
Abr	-0.669	0.014	Actb	0.438	0.028	Aarsd1	-0.280	0.008
Acads	0.492	0.022	Acy1a	0.361	0.038	Abat	-0.124	0.046
Acadvl	-0.674	0.033	Akr1a1	0.539	0.018	Abce1	-0.264	0.022
Acly	0.460	0.021	Aldh7a1	0.294	0.038	Acly	-0.259	0.024
Acox1	-0.713	0.031	Anxa4	0.405	0.002	Aco2	-0.075	0.007
Acp1	0.462	0.018	Arpc2	0.536	0.012	Actb	0.358	0.003
Actr1a	0.457	0.022	Arpc3	0.434	0.028	Actg1	0.171	0.011
Actr1b	1.007	0.006	Arrb1	0.897	0.001	Actr1a	-0.468	0.040
Acyp2	0.981	0.007	Arsb	0.977	0.023	Acyp2	0.362	0.014
Adap1	1.055	0.001	Asna1	0.859	0.031	Agl	-0.478	0.003
Adprh	-0.643	0.018	Aspa	0.686	0.006	Ahcy	-0.142	0.009
Agfg1	-0.983	0.049	Atic	0.485	0.015	Ahsg	-0.498	0.026
Ahcy	-0.387	0.043	Atl1	-0.483	0.012	Aldh9a1	-0.094	0.022
Ahcyl2	0.600	0.021	Blvra	0.340	0.001	Ampd2	-0.250	0.044
Ahsa1	0.845	0.016	Cap1	0.384	0.012	Amph	0.486	0.003
Aif1	1.292	0.039	Cbr1	0.397	0.027	Anlnl1;Anln	-0.704	0.018
Aimp1	0.885	0.002	Cct2	-0.748	0.001	Arpc1a	-0.186	0.002
Aldh3a2	-1.179	0.001	Chordc1	-0.913	0.040	Asna1	0.302	0.023
Aldoc	0.212	0.041	Ckm	-2.134	0.036	Asns	-0.252	0.000
Anp32a	-0.853	0.019	Csde1	-0.620	0.029	Aspa	0.278	0.022
Anxa7	-0.343	0.006	Ctsz	1.291	0.020	Asrgl1	-0.332	0.038
Apoe	-1.387	0.028	Cyfip1	0.323	0.029	Atl1	-0.481	0.036
Appl1	0.571	0.018	Dclk1	0.612	0.015	Atp1a1	0.595	0.005
Arhgap35	2.519	0.027	Dctn1	-0.298	0.037	Atp1a2	0.574	0.000
Arpc1a	0.647	0.018	Ddx6	0.641	0.014	Atp1a3	0.571	0.016
Arsa	0.642	0.010	Dnpep	0.433	0.006	Atp1b1	0.623	0.008
Asap2	-1.658	0.038	Dync1i1	-0.663	0.004	Atp5a1	0.839	0.005
Atp6v0d1	-1.293	0.034	Eef1d	0.446	0.042	Atp5b	0.933	0.001
Atp6v1a	0.165	0.026	Eno3	-1.908	0.032	Bcas1	0.355	0.013
Atxn2l	-0.383	0.030	Erp29	0.629	0.016	Blmh	-0.243	0.009
Bcan	0.796	0.030	Fabp5	0.618	0.014	Bzw1	0.182	0.046
Bid	-0.638	0.048	Fah	0.718	0.008	C3	-0.897	0.015
Calb1	1.037	0.028	Fkbp1a	1.030	0.025	C4	-0.304	0.014
Capg	-0.641	0.042	Fth1	0.852	0.031	Ca3	-1.792	0.015
Capn2	0.575	0.020	Ftl1	1.333	0.002	Cadps	-0.242	0.033
Capzb	-0.161	0.001	Gbe1	0.580	0.019	Calu	-0.360	0.020
Cars	0.821	0.022	Glo1	0.483	0.034	Capza1	0.483	0.044
Cbx3	-2.115	0.030	Glul	0.383	0.040	Ccdc92	-0.263	0.033
Cct8	-0.198	0.039	Gmfb	0.723	0.027	Cct2	-0.416	0.010
Ces1c	2.715	0.034	Gmpr	0.357	0.037	Cct7	-0.364	0.037
Ckap5	-0.660	0.020	Gnb2l1	0.350	0.029	Cdc37	0.297	0.042
Clpp	-0.895	0.020	Gnpda1	-1.068	0.030	Cend1	0.900	0.011
Cltb	-0.310	0.029	Gns	1.024	0.007	Chordc1	-0.477	0.023
Cndp2	-0.690	0.030	Gsr	1.255	0.004	Ckm	-1.718	0.016
Cops2	0.358	0.034	Gstp1	0.582	0.030	Ckmt1	0.389	0.015
Cops3	0.673	0.035	Hint3	0.458	0.019	Clic4	0.228	0.017
Cops5	0.647	0.014	Hmg1l1	-0.592	0.008	Cmpk1	0.250	0.028
Cpne3	0.290	0.048	Hsd17b10	0.392	0.033	Cnp	0.318	0.002
Cpne6	0.928	0.025	Hspa9	-0.332	0.025	Cntn1	-0.225	0.020
Cryab	-0.848	0.034	Ide	-0.711	0.009	Comt	0.122	0.011
Cryl1	1.342	0.001	Katnal2	1.263	0.037	Copg1	-0.481	0.018
Csrp1	1.204	0.022	Klc1	-0.346	0.001	Coro1a	-0.360	0.008
Ctps1	-0.310	0.048	Lgals3	1.075	0.040	Cpamd8	-1.198	0.026
Ctsz	-0.735	0.006	Map7d1	-0.682	0.026	Csad	0.201	0.045
Cul5	-0.629	0.029	Mapk15	0.855	0.019	Csde1	-0.631	0.045
Cyb5r2	1.108	0.030	Mapt	-0.567	0.039	Ctsb	0.453	0.000
Cyb5r3	-1.138	0.014	Mat2a	0.328	0.011	Ctsd	0.461	0.037
Cygb	1.097	0.037	Myh9	0.395	0.032	Ctsz	0.390	0.039
Dclk2	1.269	0.033	NA	-0.639	0.018	Dars	-0.372	0.033
Ddah1	-0.288	0.038	Nans	0.481	0.007	Dclk1	0.356	0.024

Ddhd2	-2.660	0.030
Dhrs7	-0.944	0.017
Dnm1	0.523	0.005
Dnpep	0.581	0.017
Dnph1	2.211	0.027
Dpysl2	0.375	0.007
Dpysl4	0.434	0.002
Dpysl5	0.417	0.049
Dynll1	0.904	0.046
Dynlrb1	1.266	0.026
Ech1	1.039	0.020
Eef1a2	0.878	0.007
Eif3a	-0.549	0.048
Eif3b	-0.469	0.043
Eif3h	-0.818	0.042
Elavl3	-0.591	0.043
Eno2	0.745	0.027
Enpp6	0.543	0.044
Epb41l2	-0.997	0.023
Epm2aip1	0.552	0.011
Eps15l1	-0.540	0.049
Faim	-1.297	0.048
Fam21	0.501	0.020
Farsb	-0.590	0.007
Fbxo2	0.746	0.004
Fkbp1a	0.716	0.008
Fn3krp	0.670	0.001
Gbe1	0.491	0.047
Gcn1	-1.109	0.008
Gcsh	0.282	0.009
Gdi1	0.635	0.015
Glo1	0.617	0.031
Glrx3	0.430	0.017
Glrx5	1.406	0.016
Glud1	0.167	0.036
Gm2a	-1.936	0.041
Gmps	0.839	0.033
Gna14	-0.570	0.015
Gnai2	-0.586	0.017
Gnpda1	-1.268	0.023
Gpi	0.436	0.004
Gpnmb	-1.324	0.044
Gripap1	-0.891	0.021
Gsk3b	0.277	0.013
H1f0	-1.516	0.010
Hadha	-0.814	0.023
Hadhb	-0.766	0.022
Hagh	1.018	0.004
Hcls1	-1.041	0.032
Hebp2	0.878	0.005
Hepacam	-1.105	0.033
Hexb	-0.913	0.025
Hint1	1.033	0.019
Hist1h1b	-1.941	0.011
Hist1h1e	-1.023	0.027
Hist1h2bl	-1.843	0.028
Hist1h3e	-3.035	0.031
Hist1h4b	-2.216	0.021
Hnrnpd	-0.774	0.005
Hnrnpf	-0.630	0.043
Hnrnph1	0.576	0.006
Hnrnpk	-0.416	0.003
Hnrnpm	-1.336	0.000
Hnrnpu	-0.908	0.010
Hsp90aa1	0.481	0.021
Hspa12a	0.612	0.000
Ncan	-0.336	0.011
Nqo1	-0.543	0.001
Nsfl1c	0.409	0.021
Ostf1	1.152	0.004
Pafah1b1	-0.340	0.040
Pccb	-0.269	0.019
Pck2	-0.491	0.004
Pcsk1n	0.882	0.034
Pdia6	0.588	0.020
Pgm1	-0.460	0.011
Ppp1ca	0.473	0.043
Psma5	0.876	0.009
Psma6	0.610	0.028
Psma7	0.636	0.001
Psmc5	-0.447	0.043
Psmd11	-0.359	0.035
Rab3a	-0.844	0.010
Ranbp1	0.318	0.003
Rnh1	0.238	0.041
Rpl18a	-0.734	0.037
Rpl3	-0.717	0.048
Rps3	-0.338	0.038
Rtn4	-0.254	0.024
S100a6	1.125	0.011
Sbds	-0.461	0.026
Sec23a	-0.569	0.001
Strap	-0.231	0.023
Suclg1	-0.571	0.024
Syn1	-0.582	0.027
Syn2	-0.499	0.026
Tpm3	-0.370	0.012
Tppp3	0.924	0.034
Tubb2a	0.347	0.016
Tubb6	-0.985	0.026
Txnl1	0.489	0.018
Vat1	0.491	0.004
Wars	0.590	0.034
Wbp2	0.600	0.008
Zyx	-0.481	0.031
Dcps	0.153	0.026
Ddah1	0.394	0.028
Ddx5	0.483	0.015
Decr1	0.315	0.026
Dlat	0.244	0.031
Dld	0.226	0.017
Dnm1	-0.166	0.028
Dstn	-0.479	0.007
Dynll1	-0.604	0.043
Echs1	-0.365	0.038
Eif3a	-0.205	0.012
Eif4a1	0.760	0.017
Eno3	-1.589	0.027
Epb41l2	0.319	0.047
Erp29	0.540	0.014
Fahd2	-0.260	0.045
Fasn	-0.256	0.014
Fgb	-0.774	0.014
Ftl1	0.305	0.020
Fuca1	-0.106	0.027
Gap43	0.627	0.002
Gars	-0.253	0.008
Gfap	0.984	0.001
Gls	0.372	0.020
GLTP	0.572	0.000
Glud1	-0.153	0.018
Gmpr	0.144	0.038
Gna14	0.627	0.014
Gstm1	0.177	0.013
Gsto1	0.431	0.004
Hagh	-0.299	0.047
Hebp2	0.468	0.023
Hist1h1e	0.239	0.014
Hist1h2bl	1.354	0.013
Hist1h3e	1.367	0.005
Hist1h4b	1.410	0.014
Hnrnpa1	0.640	0.006
Hnrnpa2b1	0.678	0.010
Hnrnpd	0.618	0.010
Hnrnpk	0.310	0.032
Hp	-1.272	0.040
Hsp90aa1	-0.145	0.016
Hsp90ab1	-0.169	0.036
Hspa8	-0.121	0.009
Hspb1	0.206	0.033
Hspd1	-0.204	0.029
Hsph1	-0.403	0.012
Huwe1	-0.442	0.018
Ide	-0.669	0.047
Idh3a	0.273	0.009
Idh3g	0.265	0.025
Impact	0.330	0.036
Ina	0.390	0.003
Itih4	-1.205	0.021
Kif1a	-0.329	0.025
Kif21a	-0.394	0.018
Klc1	-0.157	0.033
Lap3	0.156	0.047
Lasp1	0.149	0.003
Lcp1	0.192	0.007
Ldha	-0.280	0.026
Lgals3	0.704	0.021
Lyz2	0.291	0.045
Mag	0.614	0.017
Map4	-0.257	0.034
Me3	0.740	0.028

Hspa9	-0.324	0.010
Hyou1	-0.719	0.006
Idh3B	0.604	0.000
Ifi47	-0.436	0.008
Ifit3	1.591	0.047
Ighg3	2.850	0.043
Igtp	-2.012	0.018
Inpp5d	-1.040	0.026
Iqgap1	-1.130	0.001
Itgam	-1.194	0.001
Kars	-1.040	0.046
Kbtbd11	1.018	0.011
Khsrp	-0.580	0.038
Kpna3	1.293	0.029
Lancl2	-0.571	0.048
Lgmn	-0.453	0.045
Lmna	-1.670	0.021
Lrpap1	-1.021	0.016
Lypla2	0.691	0.047
Lztfl1	-0.607	0.012
Map1a	0.386	0.033
Map1b	0.636	0.012
Mapk10	0.593	0.023
Mapk15	1.242	0.005
Mapk3	0.515	0.016
Mapre2	0.505	0.033
Mapre3	0.423	0.050
Marcks	-0.741	0.029
Mdh1	0.170	0.000
Mdh2	0.624	0.006
Memo1	0.681	0.017
Mpst	0.537	0.011
Msra	0.494	0.043
Mvd	0.474	0.002
NA	1.292	0.004
Nae1	0.945	0.013
Naga	0.631	0.021
Nans	0.578	0.018
Ncdn	0.479	0.045
Ndrg1	0.630	0.019
Ndrg2	0.464	0.004
Nfu1	-0.294	0.025
Nhlrc2	0.376	0.001
Nit2	0.488	0.006
Npc2	-1.027	0.050
Nudc	0.436	0.000
Nudt2	0.786	0.000
Nudt9	-1.806	0.025
Nutf2	-1.280	0.036
Osgep	0.182	0.026
Pacsin1	0.955	0.001
Pacsin2	0.759	0.031
Pbld	0.519	0.038
Pcbp2	-0.357	0.038
Pcyt2	0.626	0.024
Pde1b	0.842	0.024
Pdia6	-0.372	0.040
Pfdn1	-0.767	0.013
Pfdn2	-0.693	0.019
Pfkl	0.225	0.018
Pfkm	0.554	0.002
Pgam1	0.542	0.007
Pgls	-0.333	0.013
Phpt1	0.322	0.003
Pin1	0.789	0.005
Pip4k2a	0.539	0.023

Mog	1.091	0.037
Mpz	-1.552	0.022
NA	-0.286	0.030
Napb	0.899	0.047
Ncan	-0.292	0.035
Nefl	0.656	0.030
Nefm	0.473	0.041
Nfasc	-0.142	0.030
Nit2	-0.409	0.047
Npepps	-0.217	0.022
Nudt3	-0.526	0.042
Ola1	0.098	0.034
Otub1	-0.240	0.034
P4hb	0.160	0.037
Pa2g4	0.288	0.030
Pacs2	0.436	0.014
Pacsin1	-0.135	0.026
Padi2	-0.438	0.045
Pafah1b1	-0.134	0.032
Pak1	-0.421	0.011
Pck2	-0.295	0.039
Pdha1	0.278	0.014
Pfkl	-0.230	0.036
Pfkp	-0.225	0.007
Phyhipl	0.183	0.025
Picalm	0.430	0.050
Pip4k2a	-0.404	0.001
Plp1	0.445	0.010
Pmp2	-1.368	0.028
Ppp2r1a	-0.173	0.005
Ppp3ca	-0.274	0.011
Ppp3cb	-0.144	0.004
Prepl	-0.214	0.002
Prkar1a	0.070	0.010
Prkar2a	-0.134	0.025
Psmc5	-0.446	0.001
Psmd3	-0.490	0.011
Ptgr2	0.265	0.012
Pygb	-0.199	0.021
Pygm	-0.394	0.023
Rab10	0.586	0.010
Rab2a	0.182	0.048
Rab5a	0.436	0.046
Renbp	-0.550	0.014
RGD1559864	0.187	0.007
Rhoa	0.432	0.031
Rpl10	-0.436	0.029
Rpl3	-0.429	0.023
Rpl4	0.285	0.016
Rufy3	-0.292	0.002
Serpina3l	-0.473	0.012
Sh3glb1	0.283	0.029
Shmt2	0.158	0.032
Slc1a2	1.062	0.001
Slc25a3	1.125	0.004
Slc25a4	1.349	0.005
Slc25a5	1.084	0.002
Slc3a2	0.561	0.011
Snx3	0.630	0.010
Snx5	-0.253	0.044
Snx6	0.211	0.008
Sod2	-0.278	0.042
Spcs2	0.836	0.013
Sptbn1	-0.389	0.007
Stip1	-0.209	0.014
Sugt1	-0.260	0.021

Pithd1	0.510	0.038
Pkm	0.153	0.013
Plbd2	1.493	0.032
Pld3	-0.959	0.048
Por	0.389	0.043
Ppa1	0.189	0.022
Ppp1r21	-1.188	0.014
Ppp2ca	0.581	0.025
Ppp4r3a	0.443	0.030
Ppp5c	0.576	0.001
Prdx2	0.485	0.039
Prdx4	-0.620	0.007
Prkca	0.528	0.045
Prkcsh	-0.824	0.044
Prune	0.493	0.010
Psap	-2.837	0.002
Psma2	0.301	0.014
Psma4	-0.463	0.045
Psmb10	-0.919	0.010
Psmb6	-0.667	0.024
Psmc2	-0.514	0.028
Psmc6	-0.680	0.040
Psme2	-0.442	0.010
Ptpn11	0.307	0.029
Ptpn6	-0.726	0.006
Purb	-0.384	0.045
Pygb	0.267	0.021
Rab5a	-0.674	0.044
Rab5b	-0.730	0.045
Rab5c	-0.597	0.033
Rabgap1	1.506	0.020
Ran	1.155	0.013
Rap1gap	0.942	0.021
Rhoa	0.597	0.038
Rnaset2	-2.036	0.001
Rpia	-1.452	0.014
Rpl10	-0.964	0.017
Rpl11	-0.773	0.030
Rpl18a	-0.854	0.021
Rpl21	-1.125	0.037
Rpl22	-1.265	0.039
Rpl24	-1.665	0.031
Rpl30	-0.925	0.007
Rpl38	-2.629	0.017
Rpl4	-0.920	0.013
Rpl6	-1.169	0.049
Rpl8	-0.666	0.031
Rplp0	-0.460	0.042
Rps11	-1.304	0.004
Rps12	-0.481	0.034
Rps15a	-0.884	0.019
Rps16	-0.867	0.015
Rps2	-0.740	0.044
Rps21	1.275	0.029
Rps28	0.681	0.035
Rps6	-0.971	0.026
Rps7	-1.942	0.007
Rpsa	-0.703	0.043
Rtcb	0.576	0.031
Rufy3	0.362	0.025
Ruvbl1	-0.669	0.006
S100a16	-0.634	0.019
S100a6	-1.092	0.041
Serpinf2	1.820	0.039
Sh3gl2	0.711	0.030
Snap25	-0.723	0.050
Synj1	-0.174	0.031
Tbcb	-0.116	0.003
Tfg	-0.157	0.013
Thop1	-0.147	0.016
Tpm3	-0.153	0.007
Tppp3	0.840	0.013
Tubal3	-0.187	0.046
Uap1l1	-0.183	0.046
Ube2m	0.597	0.028
Ugp2	-0.320	0.019
Vapb	0.409	0.029
Vat1	0.288	0.027
Vcan	0.084	0.003
Vcp	-0.145	0.022
Wdr7	0.502	0.043

Sncg	0.408	0.015		
Spcs2	-0.820	0.050		
Sri	0.776	0.025		
Sssca1	1.196	0.037		
Stat3	0.218	0.030		
Stk39	0.764	0.004		
Strn	-0.443	0.029		
Stxbp1	0.650	0.030		
Suclg1	-0.348	0.015		
Sult4a1	0.482	0.007		
Tbcb	0.390	0.025		
Tln2	0.783	0.013		
Tnr	0.851	0.009		
Tomm34	0.499	0.042		
Tpd52l2	-0.960	0.020		
Tpi1	0.201	0.045		
Tpm3	-0.549	0.032		
Trnt1	0.972	0.036		
Tsg101	-0.903	0.011		
Tuba1b	0.535	0.031		
Tuba4a	0.824	0.011		
Tubb2a	0.988	0.007		
Tubb3	0.744	0.013		
Tubb4a	0.352	0.017		
Tufm	-0.348	0.011		
Txndc12	-1.066	0.004		
Txnl1	0.642	0.016		
Ube2o	1.120	0.013		
Ubr4	-0.487	0.018		
Usp14	0.381	0.016		
Usp47	0.392	0.041		
Vdac1	0.956	0.035		
Vim	-0.850	0.010		
Vps13c	-0.472	0.049		
Vps36	-0.919	0.015		
Vwa8	-0.693	0.048		
Wdr91	-0.315	0.028		
Ywhae	0.268	0.024		
Ywhaq	0.369	0.006		